

**UNIVERSITY OF BELGRADE**  
**FACULTY OF TECHNOLOGY AND METALLURGY**

Mr Abdualnaser Muftah Almagrbi, dipl.ing.

**MATHEMATICAL MODELLING OF  
MYLTIPHASE REACTION PROCESSES  
FOR PRODUCTION OF RENEWABLE  
AND MINERAL DIESEL FUELS**

PhD thesis

Belgrade, 2013.

**UNIVERSITY OF BELGRADE**  
**FACULTY OF TECHNOLOGY AND METALLURGY**

Mr Abdualnaser Muftah Almagrbi, dipl.ing.

**MATHEMATICAL MODELLING OF  
MYLTIPHASE REACTION PROCESSES  
FOR PRODUCTION OF RENEWABLE  
AND MINERAL DIESEL FUELS**

PhD thesis

Belgrade, 2013.

**UNIVERZITET U BEOGRADU**  
**TEHNOLOŠKO-METALURŠKI FAKULTET**

Mr Abdualnaser Muftah Almagrbi, dipl.inž.

**MATEMATIČKO MODELOVANJE**  
**VIŠEFAZNIH REAKCIONIH PROCESA U**  
**PROIZVODNJI OBNOVLJIVIH I**  
**MINERALNIH DIZEL GORIVA**

Doktorska disertacija

Beograd, 2013.

*PhD Thesis evaluation committee:*

Dr **Aleksandar Orlović**, associate professor

University of Belgrade Faculty of Technology and Metallurgy

Dr **Sandra Glišić**, research associate

University of Belgrade Faculty of Technology and Metallurgy

Dr **Aleksandar Jovović**, professor

University of Belgrade Faculty of Mechanical Engineering

Defended on:

---

## Acknowledgements

First of all, I would like to acknowledge with many thanks my supervisors, **Prof. Aleksandar M. Orlovic** and **Dr. Sandra B. Glisic** for their assistance and support. Also I wish to express my deepest gratitude to them, for the patient guidance, encouragement and advice they have provided throughout my time as their student. I have been extremely lucky to have supervisors who cared so much about my work, and who responded to my questions and queries so promptly.

I wish to express my sincere thanks to **prof. Djordje Janackovic** Dean of Faculty of Technology and Metallurgy and **prof. Nenad Radovic** who was Responsible for foreign students and provided them with constant support and help.

I am extremely grateful to **all Faculty members**, for rendering their valuable help to study the Chemical Engineering and for their insidious suggestions.

I cannot fail to acknowledge financial and technical support provided by my country, Republic of Libya. Special thanks are due to **Prof. Mohammed Almeshragi** for his support and help for my PhD study.

I express my deep sense of gratitude and gratefulness and I am very thankful to my beloved **father, mother**, brothers and my sisters for their affection, full Co-operation, Prayer and Constant encouragement.

I must express my gratitude to my **dear wife**, for her continued support and encouragement. Finally, I would like to take this opportunity to thank my daughters **Esra** and **Doaa** for their constant affection and support.

I extend my immense thanks to my dearest friend **Mr. Mustafa Ohiba** for his help during the period of this study.

Lastly, but not the least, I express my sincere thanks and appreciation to the **Dean**-and the **Registrar**, University of Belgrade, for giving me an opportunity to undertake this Ph.D., Programme at this esteemed University.

***Above all, I thank GOD ALMIGHTY for his immense grace and mercy for the successful completion of my studies.***

***Abdualnaser***

## ABSTRACT

Multiphase reaction processes constitute key steps in manufacturing of diesel fuels, both renewable and mineral. In modern refineries there is a major role for the hydrotreating processes that operate under high pressure in the presence of a solid catalyst. The main role of hydrotreating within the petroleum refining is the removal of sulphur compounds, the stabilization of the product and the removal of other undesirable impurities. Hydrodesulphurization of gas oil takes place in a reactor with a fixed bed catalyst in the presence of hydrogen at elevated pressure (normally up to 60 bar) and temperature (633 K). In this thesis, a mathematical model of a deterministic type was developed and used to simulate the hydrotreating reactor operation. The model consists of differential balance equations of heat and chemical species, and the corresponding kinetic equations for the reactions of hydrodesulphurization of sulphur compounds. The system of differential equations that constitute the mathematical model was solved using the MATLAB software package.

Multiphase reactions for biodiesel synthesis were modeled and simulated for non-catalytic methanolysis and ethanolysis of triglycerides under high pressure and at elevated temperature. The vapour–liquid or vapour–liquid–liquid equilibrium and phase distribution of methanol and ethanol with triolein were investigated in order to determine the range of pressure and temperature required for high oil conversion. Simulation of phase equilibrium using RK-Aspen EOS and UniSim software were found to correlate well with the experimental data. Simulation results show the important influence of the phase equilibrium on the reaction mechanism and overall kinetics under subcritical conditions ( $T < 270\text{ }^{\circ}\text{C}$  at 200 bar) since the two liquid phases exist at the beginning of reaction, thereby limiting the contact between the reactants. In case of single reaction phase ( $T > 270\text{ }^{\circ}\text{C}$  at 200 bar) the initially high reaction rate is limited at high conversion levels due to increasing extent of reversible reaction. Mathematical model of non-catalytic biodiesel synthesis was treated as complex parallel and consecutive reversible reaction. Kinetic parameters were estimated using standard optimization methods and the best results were obtained with Genetic Algorithm procedure. The application of this method resulted in kinetic parameters with improved accuracy in predicting concentrations of important reaction intermediates, i.e.

diglycerides and monoglycerides. Activation energies of kinetic parameters obtained by the Genetic Algorithm method are in very agreement with theoretical values determined by molecular orbital calculations.

**Key words: Mathematical modeling, Multiphase reaction processes, Biodiesel, Renewable diesel, Diesel fuel, Hydrotreating**

**Scientific area:** Chemistry and chemical technology

**Specific scientific area:** Chemical Engineering

**UDK:**

## REZIME

Višefazni reakcioni procesi predstavljaju ključne stupnjeve u proizvodnji dizel goriva, obnovljivih i mineralnih. U savremenim rafinerijama proces hidrotritinga zauzima značajno mesto pri čemu se odvija u prisustvu čvrstog katalizatora. Glavni ciljevi procesa hidrotritinga u preradi nafte su uklanjanje sumpora, stabilizacija proizvoda i uklanjanje drugih neželjenih primesa. Hidrodesulfurizacija gasnog ulja se odvija u reaktoru sa nepokretnim slojem katalizatora uz prisustvo vodonika na povišenom pritisku (uobičajeno do 60 bar-a) i temperaturi (633 K). U ovoj disertaciji razvijen je deterministički matematički model reaktora za simulaciju procesa. Model čine diferencijalni bilansi toplote i hemijskih vrsta, kao i odgovarajuće kinetičke jednačine za reakcije desulfurizacije. Sistem diferencijalnih jednačina koje čine model je rešavan primenom programa napisanog u MATLAB-u.

Višefazni reakcioni proces sinteze biodizela je modelovan i simuliran za nekatalitičku etanolizu i metanolizu triglicerida na povišenom pritisku i temperaturi. Raspodela faza i ravnoteža za sistem para – tečnost i para – tečnost – tečnost metanola i etanola sa trioleinom je ispitivana sa ciljem određivanja parametara koji omogućavaju visoku konverziju ulja. Simulacija ravnoteže faza korišćenjem RK-Aspen jednačine stanja u UniSim softveru pokazala je veoma dobro slaganje sa eksperimentalnim podacima. Rezultati simulacija ukazuju na važan uticaj na reakcioni mehanizam i na ukupnu kinetiku procesa u sub-kritičnoj oblasti ( $T < 270$  °C na 200 bar-a) s obzirom da u početnoj fazi reakcije egzistiraju dve faze, što uzrokuje lošiji kontakt između reaktanata. U slučaju postojanja jedne reakcione faze ( $T > 270$  °C na 200 bar-a) inicijalno visoka brzina reakcije je limitirana na visokim konverzijama zbog porasta stepena odigravanja povratne reakcije. Matematički model nekatalitičke sinteze biodizela je tretiran kao kompleksna uzastopno – paralelna povratna reakcija. Kinetički parametri su određeni primenom standardnih optimizacionih metoda i najbolji rezultati su dobijeni primenom metode genetičkog algoritma. Primena ove metode za određivanje kinetičkih parametara rezultovala je povećanom preciznošću predviđanja koncentracija važnih intermedijera, monoglicerida i diglicerida. Energije aktivacije u izrazima za kinetičke konstante dobijene primenom metode genetičkog algoritma su u



veoma dobrom slaganju sa teoretskim vrednostima određenim metodom proračuna molekulskih orbitala.

**Ključne reči: Matematičko modelovanje, Višefazni reakcioni procesi, Biodizel, Obnovljivi dizel, Dizel gorivo, Hidrotriting**

**Naučna oblast:** Hemija i hemjska tehnologija

**Uža naučna oblast:** Hemijsko inženjerstvo

**UDK:**

## Contents

<b>ABSTRACT .....</b>	<b>5</b>
<b>REZIME .....</b>	<b>8</b>
<b>1. INTRODUCTION .....</b>	<b>1</b>
<b>1.1 Mathematical modelling importance for refinery and bio refinery design and planning .....</b>	<b>1</b>
<b>1.2. Renewable diesel fuel – biodiesel.....</b>	<b>5</b>
1.2.1. <i>Biodiesel and its properties .....</i>	6
1.2.2. <i>Biodiesel production technologies: Transesterification method .....</i>	8
1.2.2.1 <i>Catalytic biodiesel production – homogenous catalyzed transesterification .....</i>	8
1.2.2.2. <i>Heterogeneous catalytic transesterification.....</i>	12
1.2.3. <i>Non-catalytic biodiesel production - Supercritical Alcoholysis (SCA) .....</i>	14
1.2.3.1. <i>Process variables for SCA.....</i>	17
1.2.4. <i>Comparison of supercritical fluid and alkali-catalyzed methanolysis .....</i>	18
<b>1.3. Diesel fuel processing from crude oil sources .....</b>	<b>20</b>
1.3.1. <i>Drivers of ULSD production .....</i>	21
1.3.2. <i>Environmental legislation on diesel fuel specification .....</i>	21
1.3.3. <i>Hydrotreating Process.....</i>	26
1.3.3.1. <i>Hydrodesulfurization.....</i>	28
<b>2. THEORETICAL PART .....</b>	<b>51</b>
<b>2.1 Phase Equilibrium .....</b>	<b>51</b>
2.1.1 <i>Critical values .....</i>	55
2.1.2 <i>Classification of phase equilibrium .....</i>	58
2.1.3 <i>Calculation of phase equilibrium at high pressure .....</i>	60
2.1.4 <i>Equations of state used for these systems .....</i>	60
2.1.4.1. <i>Peng Robinson equation of state .....</i>	60
2.1.4.2. <i>Redlich-Kwong Aspen equation of state.....</i>	61
<b>2.2. Mathematical modelling fundamentals .....</b>	<b>62</b>
2.2.1. <i>Types of process model.....</i>	63
2.2.2. <i>Models development .....</i>	64

2.2.2.1. Problem definition.....	65
2.2.2.1. Model development .....	65
2.2.2.3. Model solving.....	66
2.2.2.4. Model verification and validation .....	67
2.2.3. Model Assumption .....	68
2.2.4. Computer Aided Process Engineering .....	68
<b>3. EXPERIMENTAL DATA USED FOR MODEL DEVELOPMENT.....</b>	<b>71</b>
<b>3.1. Multiphase system at high pressure and temperature – analysis procedure.....</b>	<b>71</b>
3.1.1. Procedure for high pressure phase equilibria simulation for biodiesel reaction system ....	71
3.1.2. Procedure for high pressure phase equilibria simulation for diesel reaction system .....	72
<b>3.2. Experimental data for kinetic modelling of biodiesel reaction .....</b>	<b>76</b>
<b>3.3. Experimental data used in the modelling of catalytic hydrotreating reactor for diesel production.....</b>	<b>78</b>
<b>4. Model Development - mathematical modelling and numerical optimisation .....</b>	<b>87</b>
<b>4.1. Model Development for non-catalytic reaction.....</b>	<b>87</b>
4.1.1. Kinetic model description of biodiesel reaction .....	87
4.1.1.1. Parameter determination by different optimization techniques .....	90
<b>4.2. Model development for catalytic reaction .....</b>	<b>92</b>
4.2.1. Mathematical mode of diesel hydrotreater.....	94
4.2.2. Reaction mechanism of benzothiophene hydrodesulphurization.....	98
4.2.2.1. Kinetic equations.....	100
4.2.3. Calculation of model parameters .....	105
4.2.3.1. Calculation of the flow rate of vapour and liquid phases .....	105
4.2.3.2. Calculation of the specific heat capacity.....	105
4.2.3.3. Catalyst wetting efficiency .....	106
4.2.3.4. Calculation of overall effectiveness in the gas phase.....	107
4.2.3.5. Calculation of overall effectiveness in the liquid phase .....	108
<b>5. RESULTS AND DISCUSSION .....</b>	<b>111</b>
<b>5.1. Multiphase system analysis for biodiesel and petroleum diesel processing .....</b>	<b>111</b>
5.1.1. Phase equilibria in non-catalytic reaction system - biodiesel production .....	111
5.1.2. Phase equilibria in catalytic reaction system - diesel production.....	118

<b>5.2. Simulation results and model validation for both catalytic and non-catalytic diesel/biodiesel production.....</b>	<b>127</b>
5.2.1. <i>Determination of kinetic parameters for complex transesterification reaction by standard optimisation methods.....</i>	127
5.2.1.1. <i>Ethanolysis of triglycerides.....</i>	136
5.2.2. <i>Simulation results of catalytic reaction system for diesel production.....</i>	140
5.2.2.1. <i>Temperature difference along the reactor – kinetic data by Froment.....</i>	144
5.2.2.2. <i>Catalyst wetting efficiency.....</i>	146
5.2.2.3. <i>The conversion of different type of sulphur compounds and aromatic components.....</i>	148
5.2.2.4. <i>Total sulphur conversion.....</i>	150
<b><u>6. CONCLUSION.....</u></b>	<b><u>152</u></b>
<b><u>7. REFERENCES.....</u></b>	<b><u>155</u></b>
<b><u>APPENDIX I.....</u></b>	<b><u>177</u></b>
<b><u>APPENDIX II.....</u></b>	<b><u>184</u></b>

## 1. INTRODUCTION

### 1.1 Mathematical modelling importance for refinery and bio refinery design and planning

Mathematical modelling in Chemical Engineering is recognised as a tool for analysing complex systems. The essence of engineering modelling is to capture the fundamental aspects of the problem which the model is intended to describe and to understand what the model's limitations as a result of the simplifications are.

Engineering models are therefore not judged by whether they are "true" or "false", but by how well they are suitable to describe the situation in question. It may therefore often be possible to devise several different models of the same physical reality and one can choose among these depending on the desired model accuracy and on their ease of analysis.

Even though in engineering applications the choice of the model can be done among the following:

1. Physical models: small-scale replica of the system or its parts (pilot plant, scale models of buildings, ships models);
2. Analog models (electronic, electric and mechanical devices);
3. Drawing and maps;
4. Mathematical models,

over the past decade there has been an increasing demand for suitable material in the area of mathematical modelling, because they represent a more convenient and economic tool to understand the factors that influence the performance of a system. Developments in computer technology and numerical solver have provided the necessary tools to increase power and sophistication which have significant implications for the use and role of mathematical modelling.

Mathematical models are of great importance in chemical engineering because they can provide information about the variations in the measurable macroscopic properties of a physical system using output from microscopic equations which cannot usually be measured in a laboratory. On the other hand, mathematical models can lead to wrong conclusions or decisions about the system under investigation if they are not validated with experimental

tests. Therefore, a complete study of a physical system should integrate modelling, simulation and experimental work.

Computer aided modelling; simulation and optimization permit a better understanding of the chemical process behaviour, saves the time and money by providing the fewer configuration of the experimental work. In addition, computer simulation and optimization can help to improve the performance and the quality of a process and represent a more flexible and cost effective approach in design and operation.

The other term which could be finding in literature is a Process system engineering (PSE) [1]. PSE is an academic and technological field related to methodologies for chemical engineering decisions. Such methodologies should be responsible for indicating how to plan, how to design, how to operate, how to control any kind of unit operation, chemical and other production process or chemical industry itself. Hence, PSE is all about the systematic and model-based solution of systems problems in chemical engineering [2]. The outreaching definition of Takamatsu (1983) [3] is emphasized by **Figure 1**, which is reprinted here from his original paper.

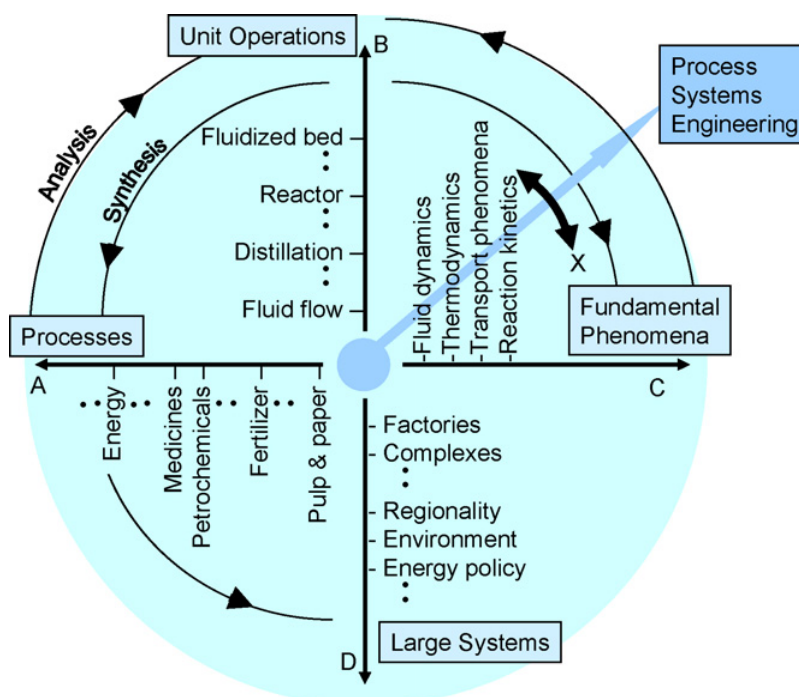


**Figure 1.** The nature of process systems engineering, reprinted from Takamatsu (1983) [3].

It already has a multi-scale flavour including physical phenomena on the mesoscale, unit operations, whole processes and the socio-economic system they are embedded in.

Furthermore, the scope is explicitly not restricted to chemical process systems but also mentions energy systems and biomedical systems, two systems problem classes which have received significant interest in recent years. The multi-scale perspective already proposed by Takamatsu (1983) [3] has been emphasized more recently by Grossmann and Westerberg (2000) [4]. They interpret the role of PSE as a set of methods and tools to support decision-making for the creation and operation of the chemical supply chain constituting of the discovery, design, manufacturing and distribution of chemical products. Hence, PSE is more than computer-aided process engineering (CAPE) since its core business is not merely the use of computers to assist problem solving – or more specifically engineering design processes – which has been the original scope of CAPE [5,6]. PSE rather addresses the inherent complexity in process systems by means of systems engineering principles and tools in a holistic approach and establishes systems thinking in the chemical engineering profession. Mathematical methods and systems engineering tools constitute the major backbone of PSE. However, it has to be mentioned that there is some terminological confusion in the scientific community, since some authors, e.g. Kraslawski (2006) [7], have used CAPE and PSE synonymously in the recent literature. The field of PSE has been rapidly developing since the 1950s reflecting the tremendous growth of the oil, gas and petrochemical industries and their increasing economical and societal impact. The appreciation of PSE as an independent scientific discipline also becomes apparent in the dedicated centres of excellence which have been established at universities and in industry. For example, the Centre for Process Systems Engineering has been established at Imperial College, London, in 1990 to promote and focus research in PSE in one central location in the United Kingdom, while the Lehrstuhl für Prozesstechnik has been founded at RWTH Aachen University in 1992 by a joint initiative of industry and academia to broaden the scientific base of this field in Germany. Many chemical companies started their own R&D activities focusing on process flow-sheeting software during the late 1970s 1980s [8] and extended their attention later to more general PSE topics. For example, a department “Systemverfahrenstechnik” (Process Systems Engineering) has been established at Bayer AG in 1992. Process modeling is an important component of process design economically, from the conceptual synthesis of the process flowsheet, to the detailed design of specialized processing equipment such as advanced reaction and separation devices, and the design of their control systems.

Refineries produce dozens of refined products (ranging from the very light, such as LPG, to the very heavy, such as residual fuel oil). They do so not only because of market demand for the various products, but also because the properties of crude oil and the capabilities of refining facilities impose constraints on the volumes of any one product that a refinery can produce. Refineries can – and do – change the operations of their refineries to respond to the continual changes in crude oil and product markets, but only within physical limits defined by the performance characteristics of their refineries and the properties of the crude oils they process. Finally, the complexity of refinery operations is such that they can be fully understood and optimized, in an economic sense, only through the use of refinery-wide mathematical models. Mathematical models of refinery operations are the only reliable means of generating achievable (i.e., feasible) and economic (i.e., optimal) responses to changes in market environment and to the introduction of new (usually more stringent) product specifications.

A demand for middle distillates and diesel fuel in particular, is constantly increasing due to current developments in diesel engine technologies. These trends are resulting in growing importance of catalytic conversion processes for the production of diesel fuel. Initiatives leading to increasing engine efficiency and decreasing CO<sub>2</sub> emissions also require increased processing of alternative feedstock to a greater extent. Among other of substantial importance are bio resources (triglycerides, biomass, algae oil etc.) and alternative petroleum streams.

Non-catalytic or heterogeneous catalysed process of biodiesel synthesis requires high pressure and temperature to achieve acceptable conversion levels of triglycerides to fatty acid (ethyl or methyl) esters. However, the process can be performed with relatively low energy consumption.

LCO is one of the existing refinery streams which can be utilized to enhance diesel fuel production in existing refineries. By blending LCO with gas oil streams a higher temperature levels can be obtained in HDS reactors thereby resulting in higher conversion of sulphur compounds and lower sulphur contents of the final product. The reactor model was developed using industrial test data and analysis of vapour – liquid equilibrium in the reactor.



## 1.2. Renewable diesel fuel – biodiesel

Increased demand for energy, increasing price of crude oil, global warming due to emission of green house gases, environmental pollution, and fast diminishing supply of fossil fuels are the major key factors leading to search for alternative sources of energy. Some of the most notable alternative sources of energy capable of replacing fossil fuels include amongst others: water, solar and wind energy, and biofuels. Currently, 86% of the energy being consumed worldwide and nearly 100% of energy desired in the transportation sector is provided by non-renewable fossil fuels [9,10]. Alternative fuels for diesel engines are becoming increasingly important due to diminishing petroleum reserves and the environmental consequences of emissions from petroleum fueled engines [11].

Biodiesel is renewable clean bioenergy as it can be produced from vegetable oils, animal fats and micro-algal oil. The property of biodiesel is almost similar to diesel fuel; thus it becomes a promising alternative to diesel fuel [11]. Biodiesel has many benefits such as it is biodegradable, non-toxic, has a low emission profile (including potential carcinogens) and is a renewable resource [12] and [13]. In addition, it does not contribute to the increase in carbon dioxide levels in the atmosphere and thus minimizes the intensity of the greenhouse effect.

Various factors contributing to the cost of biodiesel include raw material, other reactants, nature of purification, its storage, etc. However, the main factor determining the cost of biodiesel production is the feedstock, which is about 80% of the total operating cost [14]. Therefore, a great economic advantage could be achieved simply by using more economical feedstock such as waste fats and oils [13] and [15]. Biodiesel production is undergoing rapid technological reforms in industries and academia. At present, the main drawback for the commercialization of biodiesel is its higher cost than petroleum based diesel. Thus in previous years, numerous studies on the use of technologies and different methods to evaluate optimal conditions of biodiesel production technically and economically have been carried out. A number of methods are currently available and have been adopted for reduction of the viscosity of vegetables oils. Four primary ways to make biodiesel are direct use and blending of vegetable oils, micro-emulsions, thermal cracking (pyrolysis) and transesterification [16]. One of the most common methods used to reduce oil viscosity in the biodiesel industry is called transesterification which take place between a vegetable oil or

animal fat and an alcohol (methanol, ethanol, butanol) in presence of a catalyst (homogeneous, heterogeneous) or without the application of catalysts [17].

### 1.2.1. Biodiesel and its properties

Biodiesel is a renewable clean burning mono-alkyl ester (based oxygenated) fuel made derived from natural, renewable feedstock such as new/used vegetable oils, and animal fats. The resulting biodiesel is quite similar to petroleum-based diesel fuel in its main characteristics and can be blended in any proportion with petroleum diesel to create a stable biodiesel blend [18]. **Table 1** represents the parameters that must be met to achieve ASTM D6751-09 quality standards. Although at present biodiesel cannot entirely replace petroleum-based diesel fuel, this alternative fuel is becoming increasingly important due to diminishing petroleum reserves that leads to a rise in petroleum prices and the environmental consequences of exhaust gases from the petroleum-fueled engines.

**Table 1.** Biodiesel (B100) Fuel Quality Standard ASTM D6751-09.

Property	Method	Limit	Unit
Flash point (closed cup)	D93	93 min	°C
Water and sediment	D2709	0.050 max	% vol
Kinematic viscosity, 40 °C	D445	1.9–6.0	mm <sup>2</sup> /s
Sulfated ash	D874	0.02 max	% mass
Sulfur S 15 Grade	D 5453	0.0015 max (15)	% mass (ppm)
Sulfur S 500 Grade	D 5453	0.05 max (500)	% mass (ppm)
Copper strip corrosion	D130	No 3 max	
Cetane number	D613	47 min	
Cloud point	D2500	Report to Customer	°C
Carbon residue	D4530	0.05 max	% mass
Acid number	D664	0.50 max	mg KOH/g
Free glycerin	D6584	0.02	% mass
Total glycerin	D6584	0.24	% mass
Phosphorus content	D4951	10 max	ppm

Property	Method	Limit	Unit
Vacuum distillation end point	D1160	360 max	°C
Acid number	D 664	0.50 max	mg KOH/g
Cold soak filtration	Annex to D6751	360 max	s

While biodiesel is generally considered to be a substitute for all or part of petroleum-based diesel fuel, there are some key points that need to be considered when examining pure biodiesel replacing conventional diesel or when it is blended with conventional diesel that are described as follow [19] and [20]:

1. *Antifoaming*: Pure biodiesel (B100) has excellent anti-foam properties, better than petroleum diesel. This enables and ensures fast filling of vehicles, without possible foam leaks or overflows.
2. *Cetane number*: The cetane number of biodiesel is generally varying between 45 and 70, as compared to 40 and 52 for typical petroleum diesel fuels. The Cetane number of biodiesel depends on distribution of fatty acids in original oils or fat. The longer fatty acids and more saturated leads to higher Cetane number.
3. *Chemical structure*: Biodiesel is a combination of small range of molecules, typically esters of fatty acids of C12, C14, C16, C18 and C22, whereas diesel is a complex mixture of a broad range of hydrocarbons from C12 to C25, consisting of paraffins, naphthenes and aromatics, as well as a range of nitrogen and sulfur containing organic compounds. Biodiesels are predominantly straight chain hydrocarbons esters, whereas diesel contains ring structures, such as aromatic molecules.
4. *Oxygen content*: Biodiesel generally contains 11% oxygen, as the ester that leads to smoother combustion, reduces energy content and makes the biodiesel polar, through the hydroxyl (–OH) hydrogen bond. The polarity gives it properties of solvency, detergency, wet-ability (sticking to metals as a lubricant) and conductivity. Diesel fuel does not contain oxygen.
5. *Cold flow properties*: For diesel fuels, each component has its own crystallization temperature, so solidification is a gradual process, whereas B100 biodiesel tends to be a much simpler mixture containing relatively few components, so that one or two components tend to dominate, and solidification is much more rapid and difficult to control.

6. *Conductivity*: Pure biodiesel, due to its polarity has excellent conductivity, greater than 500 pico S/m, and therefore reduces the risk of static induced sparks and fires.

7. *Corrosion*: The water absorption coupled with the presence of oxygen tends to contribute to increased corrosion, but this is countered by the wet-ability that reduces oxygen transfer to metal surfaces. The copper corrosion test focuses on sulfur compounds that are aggressive to copper and yellow metals. Sulfur, and specifically the corrosive forms thereof, are absent in biodiesel, and compliance to diesel specification limits is typically easily achieved.

### ***1.2.2. Biodiesel production technologies: Transesterification method***

The transesterification reaction proceeds with catalyst or without any catalyst by using primary or secondary monohydric aliphatic alcohols having 1–8 carbon atoms [17,21]. Generally, alcohol and triglycerides (vegetable oil and animal fat) are not miscible to form a single phase of mixture. Hence, the poor surface contact between these two reactants causes transesterification reaction to proceed relatively slow. Introduction of catalysts improves the surface contact and consequently reaction rates and biodiesel yield as it is able to solve the problems of two-phase nature between triglycerides and alcohol. However, without the presence of catalysts, the reaction rate is too slow for it to produce considerable yield of biodiesel. Hence, researchers around the world have been developing numerous alternative technologies which can solve the problems facing catalytic reaction by using non-catalytic processes [22,23].

#### ***1.2.2.1 Catalytic biodiesel production – homogenous catalyzed transesterification***

Vegetable oils can be transesterified by heating them with an alcohol and a catalyst. Catalysts used in biodiesel production are divided in two general categories, homogenous and heterogeneous types. If the catalyst remains in the same (liquid) phase to that of the reactants during transesterification, it is homogeneous catalytic transesterification. On the other hand, if the catalyst remains in different phase (i.e. solid, immiscible liquid or gaseous) to that of the reactants, the process is called heterogeneous catalytic transesterification [24] and [25].

In catalytic methods, the suitable selection of the catalyst is an important parameter to lower the biodiesel production cost [26]. So, commercial biodiesel is currently produced by

transesterification using a homogenous catalyst solution. Another factor affecting the selection of catalyst type is the amount of free fatty acid (FFA) present in the oil. For oils having lower amount of FFAs, base-catalyzed reaction gives a better conversion in a relatively short time while for higher FFAs containing oils, acid-catalyzed esterification followed by transesterification is suitable [27]. It has been reported that enzymatic reactions are insensitive to FFA and water content in oil. Hence, enzymatic reactions can be used in transesterification of used cooking oil [28-30]. Various studies have been carried out using different oils as raw material, different alcohols (methanol, ethanol, butanol), as well as different catalysts, including homogeneous ones such as sodium hydroxide, potassium hydroxide, and sulfuric acid, and heterogeneous ones such as lipases, CaO and MgO [31-33].

- **Homogeneous catalytic transesterification**

Homogenous catalysts are categorized into basic and acidic catalysts. The homogenous transesterification process especially basic type requires a high purity of raw materials and post reaction separation of catalyst, by-product, and product at the end of the reaction. Both of these requirements drive up the cost of biodiesel. The general form of homogeneous catalytic transesterification process can be seen on a process flow diagram of **Figure 2**.

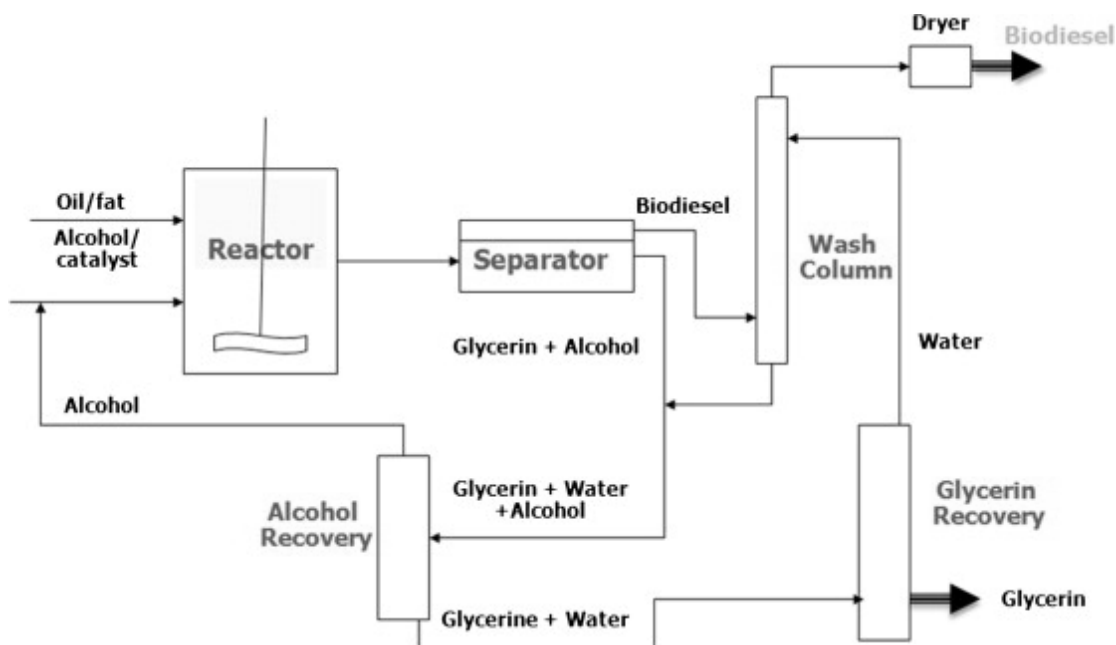


**Figure 2.** The process flowchart of homogeneous catalytic transesterification process

Currently, biodiesel is commonly produced using homogeneous base catalyst, such as an alkaline metal alkoxides and hydroxides [33-34], as well as sodium or potassium carbonates [49]. As a catalyst in the process of basic methanolysis, mostly sodium hydroxide or potassium hydroxide have been used, both in concentration from 0.4% to 2% w/w of oil. Homogeneous base catalytic catalysts are commonly used in the industries due to several reasons: (i) modest operation condition; (ii) high conversion can be achieved in a minimal time, (iii) high catalytic activity, (iv) widely available and economical [35,36]. In general, base catalytic transesterification processes are carried out at low temperatures and pressures (333–338 K and 1.4–4.2 bar) with low catalyst concentrations (0.5–2 wt.%) [37]. The limits of this process are due to the sensitivity to purity of reactants, free fatty acid content, as well as to the water concentration of the sample. When the oils contain significant amounts of free fatty acids and water content, they cannot be converted into biodiesels but to a lot of soap [34]. Free fatty acids of oil react with the basic catalyst to produce soaps that inhibit the separation of biodiesel, glycerin and wash water that cause to more wastewater from purification [38]. Because water makes the reaction partially change to saponification, the basic catalyst is consumed in producing soap and reduces catalyst efficiency. The soap causes an increase in viscosity, formation of gels which reduces ester yield and makes the separation of glycerol difficult [39]. Therefore, side reactions such as saponification and hydrolysis must be kept to a minimum.

- **Homogeneous acid catalytic transesterification**

An alternative way of processing triglycerides for biodiesel production is to use an acid catalyst. Acid catalytic transesterification of biodiesel can economically compete with base catalytic process using virgin oil, especially when the former uses low-cost feedstocks [40]. Sulfuric acid, hydrochloric acid, and sulfonic acid are usually preferred as acid catalysts. Acid-catalyzed transesterification starts by mixing the oil directly with the acidified alcohol, so that separation and transesterification occur in single step, with the alcohol acting both as a solvent and as esterification reagent [41]. The use of excess alcohol effects significant reductions in reaction time required for the homogeneous acid catalyzed reaction.

One advantage of homogeneous acid catalytic over homogeneous base catalytic transesterification is their low susceptibility to the presence of FFA in the feedstock.

However, homogeneous acid catalytic transesterification is especially sensitive to water concentration. It was reported that as little as 0.1 (wt.%) water in the reaction mixture was able to affect ester yields in transesterification of vegetable oil with methanol, with the reaction almost completely inhibited at 5 (wt.%) water concentration [41]. Disadvantages of homogeneous acid catalytic transesterification are equipment corrosion, more waste from neutralization, difficult to recycle, formation of secondary products, higher reaction temperature, long reaction times, relatively slow reaction rate, weak catalytic activity and elaborate process engineering [42,43].

In conventional industrial biodiesel processes, the methanol transesterification of vegetable oils is achieved using a homogeneous catalyst system operated in either batch or continuous mode. Different alkaline compounds are catalysts for the synthesis reaction of esters a commonly used: NaOH, KOH, Na-carbonates and alkoxides (methoxide, ethoxsid, propoksid, butoxide). The content of free fatty acids in the starting oil is one of the most important factors that determine whether it is more efficient to use the base or acid catalyst. The presence of free fatty acid with a base catalyst which leads to the formation of soap, which has a direct impact on the reduction of the concentration of catalyst in the reaction mixture and the creation of undesirable chemicals. Also, the presence of water affects the speed increase saponification (degradation by acid ester and alcohol). To prevent the creation of soap and the formation of stable emulsions starting vegetable oil must be less Alcoholysis of triglycerides in the industrial factories usually implemented at the boiling temperature of methanol (60-70 °C) at a molar ratio of methanol to oil of 6:1, which is twice the stoichiometric requirement [11]. Conversion of triglycerides into FAME of 90-98% can be achieved under these conditions for about 90 minutes, if using NaOH or Na-methoxide as catalyst (up to 5 wt% with respect to methanol). Upon reaching the desired conversion of triglycerides, by distillation from the reaction mixture to stand out excess methanol, and then, created separation separates glycerol and neutralize the catalyst. Most often these procedures, after distillation of crude product (FAME) biodiesel purity can get 99% or more with a yield that is approximately 86% [44] than 0.5% free fatty acids.

When vegetable oil has a higher content of free fatty acids is necessary to apply a two-step process of alcoholism. In the first phase, in the presence of acid catalyst ( $H_2SO_4$ ) esterification reaction of free fatty acid ester in translations, and then neutralize the acid

catalyst and remove water from the esterification reaction, to only in the second phase alcoholysis applied to the base catalyst [44].

Industrial practice shows that, regardless of the used catalyst (acid or base), the desired conversion and high triglyceride levels can only be achieved with increased methanol compared to oil. In base-catalyzed alcoholysis this ratio is usually 6:1, with NaOH as catalyst, primarily because of its lower price compared with KOH [44].

Lack of base and acid catalyzed synthesis of FAME, the purification of the final products (FAME and glycerol). During the neutralization of the catalyst (acid or base) must be applied FAME wash with warm water, and so the problem of waste water. The presence of free fatty acids and water adversely affects the base-catalyzed alcoholysis of triglycerides, and it is necessary to apply a more complex two-step procedure alcoholysis [44].

#### 1.2.2.2. Heterogeneous catalytic transesterification

In comparison with homogeneous catalysts that act in the same phase as the reaction mixture, heterogeneous catalysts act in a different phase from the reaction mixture. Being in a different phase, heterogeneous catalysts have the advantage of easy separation and reuse. The high consumption of energy and costly separation of the homogeneous catalyst from the reaction mixture, however, have called for development of heterogeneous catalyst. The use of heterogeneous catalyst does not yield soap [45]. The use of heterogeneous catalytic systems in transesterification of triglycerides implies the elimination of several steps of washing/recovery of biodiesel/catalyst, ensuring thereby higher efficiency and profitability of the process as well as lowering its production costs. There is also the possibility of being implemented in a continuous way by using a fixed bed reactor. A typical schematic diagram for heterogeneous catalytic transesterification process is shown in **Figure 3**.



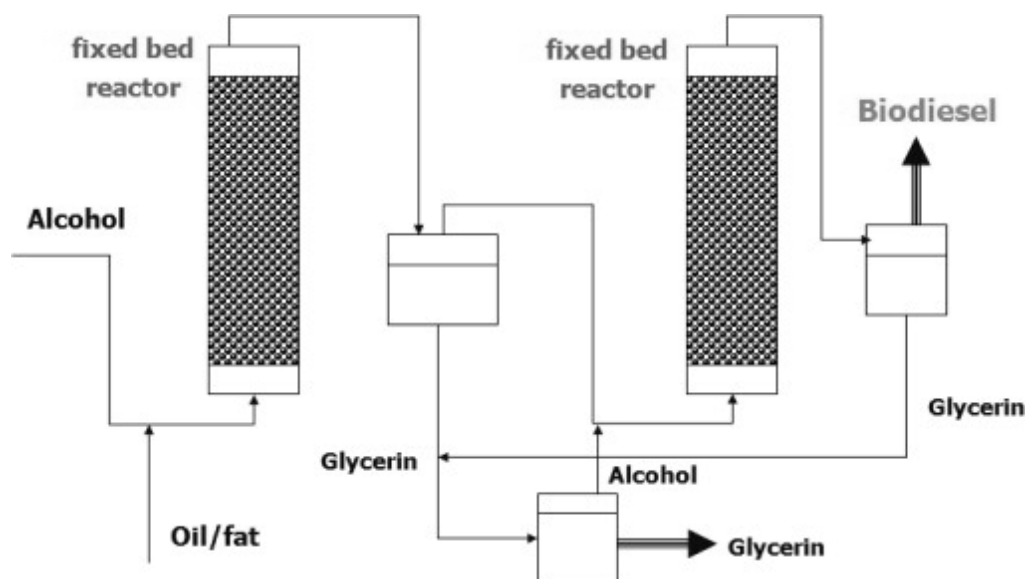


**Figure 3.** The schematic flow diagram of heterogeneous catalytic transesterification process

Compared to homogenous catalytic transesterification process, the heterogeneous catalytic transesterification process can tolerate extreme reaction conditions. The temperature could go from 70 °C to as high as 200 °C to achieve more than 95% of yield using MgO, CaO, and TiO<sub>2</sub> catalysts [46]. Kiss et al. [47] carried out a comparative assessment of cost and environmental aspects of the homogeneous and heterogeneous catalytic transesterification process in large scale biodiesel production plants. The economic assessment of heterogeneous and homogeneous processes in large scale biodiesel production plants revealed the advantages of the heterogeneous process in terms of higher yield of biodiesel and higher purity of glycerin, as well as lower cost of catalyst and maintenance. This would result in estimated US\$59 reduction in operating cost per mt of biodiesel, relative to the homogeneous process. The energy consumption and associated costs are higher in the case of heterogeneous catalyst. The analysis showed that at current market value of glycerin, prices of auxiliary material and assuming equal capital cost of heterogeneous and homogeneous production plants, the heterogeneous process would be economically competitive if the utility costs were lower than US\$85 per mt of biodiesel, or in other words, not more than threefold of the utility cost of the homogeneous catalytic transesterification process. Regarding environmental aspects, the application of the heterogeneous process would result in reduced risk associated with spillage or leakage of hazardous and flammable chemicals. Additional environmental benefits can be expected from the absence of energy intensive and waste generating glycerin purification step.

### 1.2.3. Non-catalytic biodiesel production - Supercritical Alcoholysis (SCA)

In a catalytic reaction to produce biodiesel through transesterification, several processes, such as purification of the esters, separation and recovery of unreacted reactants and catalysts, are involved. These processes render production of biodiesel through a conventional transesterification system complicated, thus giving a reason to investigate the production of biodiesel from triglycerides via non-catalytic reactions. Besides catalytic methods, there are two non-catalytic transesterification processes. These are the supercritical alcohol process and BIOX process.

- **Supercritical alcohol transesterification- Supercritical Alcoholysis (SCA)**

Supercritical alcohol methods is a non-catalytic method for biodiesel production in which instead of using catalysts, high pressure and temperature are used to carry out the transesterification reaction [23]. The reaction is fast and conversion raises 50–95% for the first 10 min but it requires temperature range of 250–400 °C. The transesterification of triglycerides by supercritical methanol, ethanol, propanol and butanol has proved to be the most promising process. The vegetable oils were transesterified 1:6–1:40 vegetable oil-alcohol molar ratios in supercritical alcohol conditions [36]. **Table 2** shows the critical temperatures, critical pressures and reaction conditions for esterification and transesterification of the various alcohols where percent conversion to fatty acid esters were shown for comparison at 10 min and 30 min reaction times at 300 °C [48].

**Table 2.** Critical states for various alcohol and yields of fatty acid esters of after 10 min esterification and 30 min transesterification.

Alcohol	Critical temperature (°C)	Critical pressure (Mpa)	Esterification yeild (10 min)%	Transesterification yeild (30 min)%
Methanol	239.2	8.09	98	98
Ethanol	243.2	6.38	79	88
1-Propanol	264.2	5.06	81	85
1-Butanol	287.2	4.9	80	75
1-Octanol	385	2.86	–	–

Instead of methanol, as the most applied in industry, can also be used other alcohols (ethanol, 1-propanol, 1-butanol and 1-octanol) but it is shown that the maximum rate of formation of esters with methanol. Methanol in supercritical condition has a high density, low viscosity and high diffusivity. Also, there is no methanol in the NIR properties of polar solvent which is a prerequisite to practice under certain conditions achieve a pseudo-homogeneous system of oil and methanol. Then the solubility of methanol in oil increased (almost complete) when such conditions have been established that alcoholysis is very fast. The disadvantages of the supercritical methods mostly are high pressure and temperature requirement [49], high methanol to oil ratios (usually 42) that renders the production expensive. Kusudiana and Saka [22,50,51] studied a non-catalyst process in which vegetable oil was transesterified with supercritical methanol and found that the amount of water in the reaction does not affect the conversion of oil into biodiesel. Conversely, the presence of certain amount of water increases the formation of methyl esters and esterification of free fatty acids takes place simultaneously in one stage. Their results showed that the reaction took only 4 min. to convert rapeseed oil into biodiesel, even though the high temperature (250–400 °C) and high pressure (35–60 MPa) were required for making methanol reach the supercritical state. Iijima et al. [52] have proposed a supercritical conditions (reaction parameters:  $T = 643\text{--}773\text{ K}$ ;  $p = 20\text{--}60\text{ MPa}$  and residence time = 4–12 min) for producing an unconventional biodiesel fuel (mainly FAME, mono- and diacylglycerol) without yielding glycerin as a by-product. Supercritical transesterification methods at high temperature and pressure conditions provide improved phase solubility, decrease mass transfer limitations, provide higher reaction rates and make easier separation and purification steps. Besides, the supercritical transesterification method is more tolerant to the presence of water and FFAs than the homogeneous base catalyst method, and hence more tolerant to various types of feedstocks. Regarding many researches that have been reported, the cost of biodiesel could certainly be lowered by using low value feedstocks. Therefore, the ability of supercritical transesterification methods in using low value feedstocks could probably reduced the share of feedstock cost in biodiesel production cost.

Although SCF technologies have enormous advantages compared to conventional catalytic reactions as discussed previously, there are several challenges and weaknesses that

need to be addressed before SCA could play a major role in biodiesel production and one of the most important is energy consumption.

**Energy consumption:** One of the weaknesses of SCF technology is the apparent high energy required to reach the supercritical conditions of the solvent. The high temperature and pressure needed in the process, depending on the type of solvents employed, consume a huge amount of energy which is unsustainable in the long term. For instance, in SCA reaction, the temperature and pressure must be above 239 °C and 8.1 MPa, respectively in order to achieve supercritical methanol state which makes SCA technologies an energy-intensive process. In addition, there are also concerns that the energy utilized in the process is more than the energy provided by biofuels obtained from SCA technology. In other words, more energy is required to yield products (biofuels) which have less energy content. Consequently, it is claimed that SCA technology is unsustainable in terms of energy consumption and subsequently not suitable for biodiesel production [53-56].

**Possible solution is: Integrated heating and cooling system:** Supercritical reaction requires huge amount of energy to carry out the reaction at elevated temperature and pressure and subsequently cool down to room temperature when the reaction is complete. The enormous energy to provide heat to the reactor and cooling effect upon reaction completion leads to claims that SCF is an energy-intensive process. Hence, it is vital to modify and improve SCF process which will minimize the amount of heat involved in heating and cooling procedures. One of the methods is to install a double tube heat exchanger before the supercritical reactor to allow pre-heating of fresh reactants by stream exiting the reactor. In this context, the integrated heat recovery system would reduce the heat duty substantially as the heating of reactants and cooling of products are carried out by a heat exchanger, instead of two independent heating and cooling mechanisms. Hence, the total energy required in SCF reaction could be diminished significantly which is vital for commercialization purposes. Recent studies have concluded that the total energy required for SCA and conventional catalytic reactions are relatively similar when integrated heating and cooling system is employed in SCA reaction [53-56]. This finding validates that SCA technology is not an energy-demanding process but instead requires comparable energy consumption to other existing processes.

### 1.2.3.1. Process variables for SCA

#### • Effect of temperature

The results showed that the highest yield was achieved at a temperature of about 40 K higher than the critical methanol (**Figure 4**). On the basis of data on the yield of FAME function of time at different temperatures, it was concluded that the reaction is fastest at 350 °C [50].

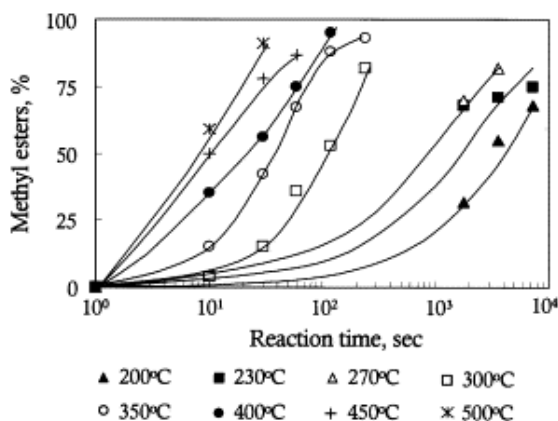


**Figure 4.** The effects of temperature on the yield of FAME [22,50,51]

Thus, at a molar ratio of methanol to oil of 42:1, at 350 °C and 200 bar achieves virtually complete conversion of triglycerides [50]. Decreasing the molar ratio decreases conversion, and when the process of triglycerides methanolysis performed at a lower temperature of 270 °C. all this confirms the conclusion in terms of achieving the necessary conditions (temperature and pressure) when triglycerides (oil) and methanol, or two nemešljive liquid at normal pressure and temperature conditions, the pseudo-homogeneous phase in which nekatalizovanareakcija between methanol and triglycerides very fast.

#### • The effect of the presence of water in oil

Only in the case of the NFA, which was carried out at a volume ratio of water: oil of 0.4 or more was observed slightly reduced yield of FAME (**Figure 5**) [51].

It is possible, on the basis of results of investigation of the presence of large quantities of water in oil, water has a positive effect on FAME formation rate when implemented methanolysis in supercritical conditions. The explanation for this effect is also playing in

these conditions of temperature and pressure side reaction of hydrolysis of triglycerides into free fatty acids where hydrolysis then esterification reaction with methanol in the reaction cross in MEFA.

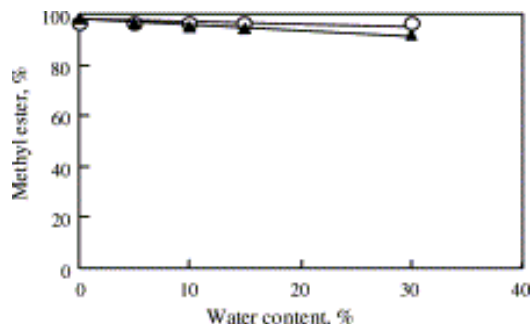


**Figure 5.** FAME yield in supercritical methanol at 350 °C in the presence of different amounts of water. The initial composition of the reaction mixture was methanol: 42:1 rapeseed oil [51].

It is possible, on the basis of results of investigation of the presence of large quantities of water in oil, water has a positive effect on FAME formation rate when implemented methanolysis in supercritical conditions. The explanation for this effect is also playing in these conditions of temperature and pressure side reaction of hydrolysis of triglycerides into free fatty acid then esterification reaction with methanol in the reaction cross in FAME.

#### ***1.2.4. Comparison of supercritical fluid and alkali-catalyzed methanolysis***

Benefits NKA compared to base-catalyzed alcoholysis of triglycerides, which are usually conducted under moderate conditions of pressure and temperature are summarized in **Table 3**. In the case of alkali-catalyzed alcoholysis reaction mixture is essential mix (intense at the beginning of the reaction) after the reaction occurs at the interface. In the case of supercritical alcoholysis, according to a recently conducted survey, it is possible to achieve a yield of FAME in much less time.

**Table 3.** Comparative analysis is performed about the effects of alkali-catalyzed (NaOH) and methanolysis under supercritical conditions

	<b>Alkaline alcoholysis (HAKA)</b>	<b>Methanolysis in supercritical conditions (high temperature and pressure,SCA)</b>
Reaction time	1-8 h	120-240 with
Conditions (P, T)	0.1 MPa, 30-65 ° C	> 8.09 MPa, 239.4 ° C
catalyst	NaOH or KOH	not required
Free fatty acids	Can react with catalyst for creating soaps	Cross in MEFA
yield	> 95%	> 98%
segregation	Methanol (surplus), the catalyst (neutralization)	Methanol (large excess)
process	complex	easy
The presence of water	undesirable	There is no impact on yield
quality FAME	good	excellent

### 1.3. Diesel fuel processing from crude oil sources

Over the past decade the environmental constraints have become increasingly more severe, impacting the quality and the upper concentration limits of sulphur in on-road and off-road commercial diesel fuels. Compression ignition engines are fuel efficient but they suffer from emissions that are harmful to the environment. Sulphur, a natural part of the crude oil is one of the primary causes of particulates or soot emissions [1-7] and the only source of sulphur oxide emissions. As a consequence, the current legislation limits the total sulphur content to 10, 15 or 50 wt. ppm in the EU, USA, and several other regions of the world. In other parts of the world the currently higher sulphur concentration limits, even up to 1000 ppm, are likely to be reduced in the near future. These global trends in legislation along with advances in compression ignition engine technology, have initiated one of the key challenges of modern refining. This challenge consists in how to produce the maximum quantity of ultra-low sulphur diesel fuel (ULSD) with the available crude oils and refinery process units [8-20].

New or revamped hydrotreating and hydrocracking units, along with novel catalytic systems, have been investigated and applied to address this challenge [8]. However, the straight run gas oil (SRGO) which is obtained by crude oil distillation, still remains the dominant feedstock for diesel fuel production. Other possible streams like light cycle oil (LCO), coker gas oil (CGO) [8] and visbreaker naphtha [21], are used only sparingly. Light cycle oil properties like low cetane number as well as the high sulphur, nitrogen and aromatic content, make LCO difficult to treat and use as a diesel blending component. Hydrotreating of LCO under a wide range of operating conditions showed that product quality improved as temperature and pressure increased and/or space velocity decreased [22]. High pressure and high hydrogen consumptions were needed in order to improve the diesel fuel final properties. Similar conclusions were drawn by studying hydrotreating of SRGO–LCO blends on commercial Co-Mo/ $\gamma$ -Al<sub>2</sub>O<sub>3</sub> catalyst. It was concluded that in order to obtain lower sulphur and nitrogen content in the final product, higher temperatures and pressures along with lower space velocities are required than for SRGO alone [23]. Furthermore, cetane numbers were always lower for hydrotreated SRGO–LCO blends than for SRGO alone. The temperature required to perform deep hydrodesulphurization (HDS) of SRGO–LCO blends was correlated to the concentration of refractory sulphur compounds and aromatic content in the feed [24]. High pressure of 5.4 MPa and high temperatures of 340–380 °C were required to bring the



total sulphur below 500 ppm, at space velocity of 2.5 h<sup>-1</sup> which is normally used in industrial hydrotreaters. A possibility to incorporate visbreaker naphtha into a diesel pool was investigated as one of the available processing options [21]. A relatively high content of normal and iso-paraffins and low aromatic content of visbreaker naphtha were found to allow an increase of 6–7% in diesel production.

Several studies were dedicated to the detailed characterization of sulphur compounds present in SRGO and LCO [25–27]. There is a general agreement that under conditions corresponding to deep HDS certain alkyldibenzothiophenes with higher boiling points exhibit the lowest reaction rates (i.e. 4-methyldibenzothiophene and 4,6-dimethyldibenzothiophene) [8,27] and therefore constitute the principal obstacle to achieve a very low sulphur content in the finished product. Also, even when found in low concentrations, nitrogen compounds can lead to strong inhibition of HDS reactions [27]. HDS reaction inhibition can also result from a high aromatic content in the feed [27, 28], which is especially critical for feeds like LCO.

### ***1.3.1. Drivers of ULSD production***

The main drivers of ULSD production in the petroleum refineries are the environmental problems and health hazards caused by exhaust emissions from the diesel powered vehicles, the strong influence of sulphur in enhancing the formation of harmful components of the emission (e.g. particulate matter (PM), NO<sub>x</sub>, SO<sub>x</sub> and CO), and the environmental legislations on diesel fuel sulphur level and air quality standard. Another important driver that encourages refiners to favour ULSD production over gasoline is the continued increase in the demand of ULSD.

### ***1.3.2. Environmental legislation on diesel fuel specification***

The linear relationship observed between sulphur level in the diesel fuel and the particulates and other harmful pollutants in the emissions are the main reasons for targeting sulphur content in diesel fuel specifications and reducing it to lower and lower levels in many countries worldwide. Studies have shown that a combination of very low sulphur fuel and particulate filters can bring about approximately 90% reductions in PM and further substantial reductions in CO and HC from existing diesel vehicles, even after 400,000 miles of operation

[4]. Significant reduction of sulfur induced corrosion and slower acidification of engine lubricating oil, which lead to longer maintenance intervals and lower maintenance costs, are additional benefits of using ultra low sulfur diesel in diesel powered vehicles. In the USA, the acceptable level of sulfur in the high way diesel was first reduced from 2000ppm to 500ppm by the Clean Air Act (CAA) amendments in the nineties, then to 350 ppm, 50ppm and 15 ppm, respectively, in the years 2000, 2005, and 2006 [29,30] (Fig. 3). In Europe, Germany introduced 10 ppm sulfur limit for diesel from January 2003. Other European Union countries and Japan introduced diesel fuel with 10ppm to the market from the year 2008 [31–34]. Similar ultra low sulfur specifications are also targeted in many other countries, and will be predominant worldwide during the next decade (Table 4) [35,36].

The specifications proposed for clean diesel by Worldwide Fuel Charter (WWFC), which reflects the view of the automobile/engine manufactures concerning the fuel qualities required for engines in use and for those yet to be developed, require increased cetane index, significant reduction of poly-nuclear aromatics (PNA), and lower T95 distillation temperature in addition to ultra low sulphur levels (Table 5). Automotive manufactures have concluded that substantial reductions in both gasoline and diesel fuel sulphur levels to quasi sulphur-free levels are essential to enable future vehicle technologies to meet the stringent vehicle emissions control requirements and reduce fuel consumption.

Similar tighter sulphur specifications have also been introduced for non-road diesel. In 2004, the US EPA issued the clean air-non-road-Tier 4 final rule which mandatds that as of 2007, fuel sulphur levels in non-road diesel fuel had to be reduced to 500ppm from its current 3000 ppm level. This included fuels used in locomotive and marine applications (except marine residual fuel used by very large engines on ocean-going vessels). In 2010, fuel sulphur levels in most non-road diesel fuel was reduced to 15 ppm, making it possible for engine manufacturers to use advanced emissions control systems that significantly reduce harmful emission, in accordance with the emission standards presented in Table 6.

**Table 4.** Sulfur standards for diesel in some countries other than USA, Japan and Europe [35,36].

Region	Country	Sulfur (wppm)	Year of implementation
South (central) America	Argentina	50	2008 <sup>a</sup>
	Brazil	500	2008 <sup>a</sup>
		50	2009 <sup>b</sup>
	Chile	350	2007
		50	2010
	Mexico	500	2005
		15	2009 <sup>a</sup>
	Peru	50	2010 <sup>a</sup>
Uruguay	50	2009	
Asia pacific	China	2000	2000
		500	2005 <sup>a</sup>
		50	2012 <sup>b</sup>
	Hong Kong	50	2007
	India	350	2005 <sup>a</sup>
		350	2010 <sup>b</sup>
		50	2010 <sup>a</sup>
	Singapore	50	2005
	Taiwan	50	2007
	Australia	500	2002
10		2009	
Middle East	Kuwait	2000	2008
		50	2010 <sup>b</sup>
	Saudi Arabia	800	2008 <sup>a</sup>
		10	2013 <sup>b</sup>
	Bahrain, Lebnon, Oman, Qatar, UAE	50	2008

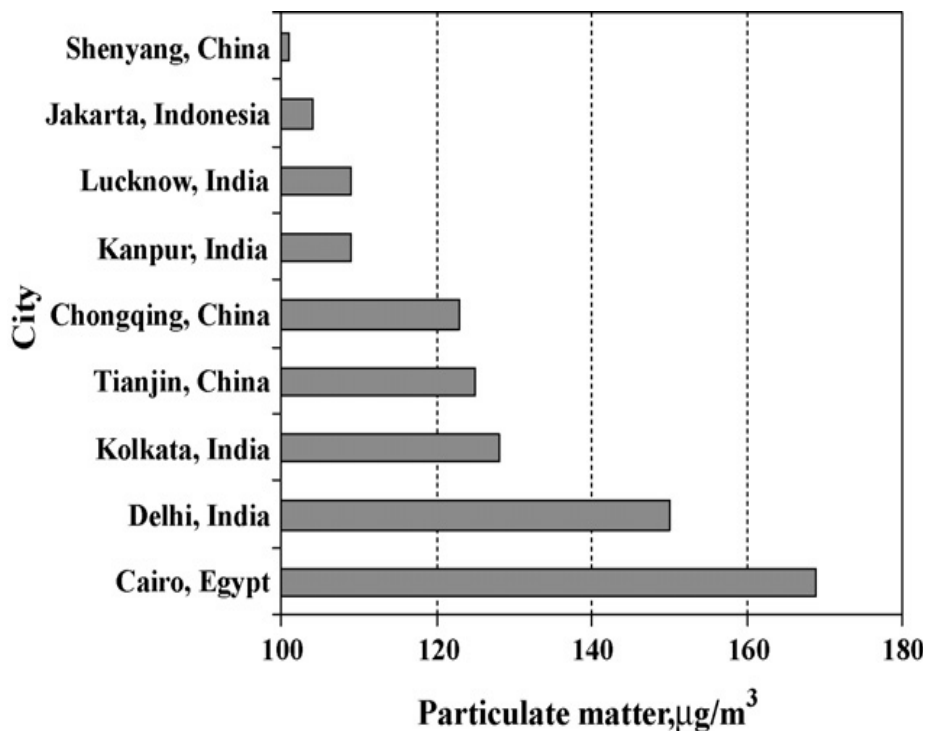
	Qatar, UAE	10	2010
	Bahrain	10	2013
	Iran	50	2008 <sup>a</sup>
	Jordon	10000	2008
		350	2012
	Russia	500	2008 <sup>a</sup>
		50	2010 <sup>b</sup>
EU	Germany, France, Denmark, Sweden	< 10	Pushing hard for Euro 5/6

**Table 5.** Worldwide fuel charter diesel fuel category 4 specifications

Source fuel specification	Worldwide fuel charter category 4
Density, max (g/cm <sup>3</sup> )	0.840
S (ppm)	5–10
Cetane index (min)	≥52
Cetane number	≥55
Aromatics	<15 vol.%
PNA	<2 vol.%
T90 (max °C)	320
T95 (max °C)	340

**Table 6.** Non-road final emission standards [37].

Rated power	First year that standards apply	Grams per horsepower hour (g/hp h)	
		PM	NO <sub>x</sub>
Hp < 25	2008	0.30	-
25 < hp < 75	2013	0.02	3.5
75 < hp < 175	2012-2013	0.01	0.3
175 < hp < 750	2011-2013	0.01	0.3
Hp > 750	2011-2014	0.075	2.6/0.50

**Figure 6.** Particulate matter present in the atmosphere of some highly populated cities [37].

To meet these emission standards, engine manufactures were required to develop and produce new engines with advanced emission control technologies similar to those already expected for on-road (highway) heavy trucks and buses. Refiners had to start producing and supplying ultra low sulphur diesel for both highway and non-highway diesel vehicles and

equipments. Many countries still do not have standards to control pollution adequately. An example of particulate matter present in the atmosphere of different cities is shown in Figure 6. The beneficial effects of switching over to more and more stringent specifications are illustrated in Figure 7 [38].

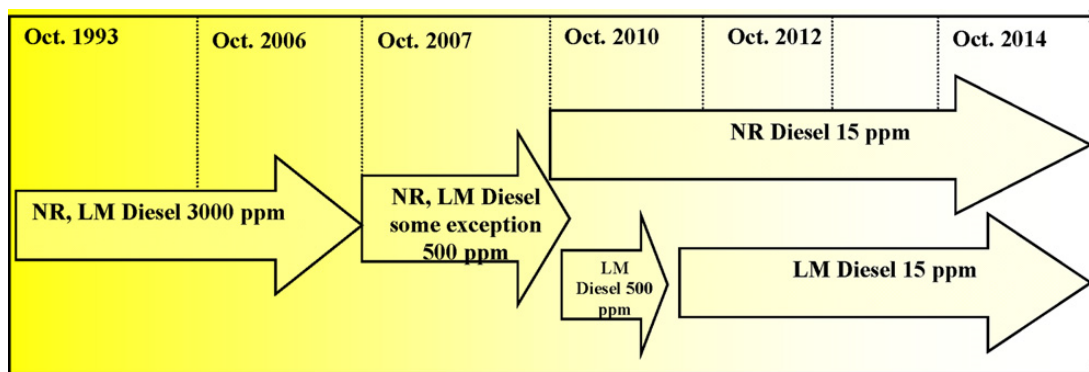


**Figure 7.** Trends in sulfur specification for non-road diesel (NR, non-road and LM, locomotive and marine diesel) [38].

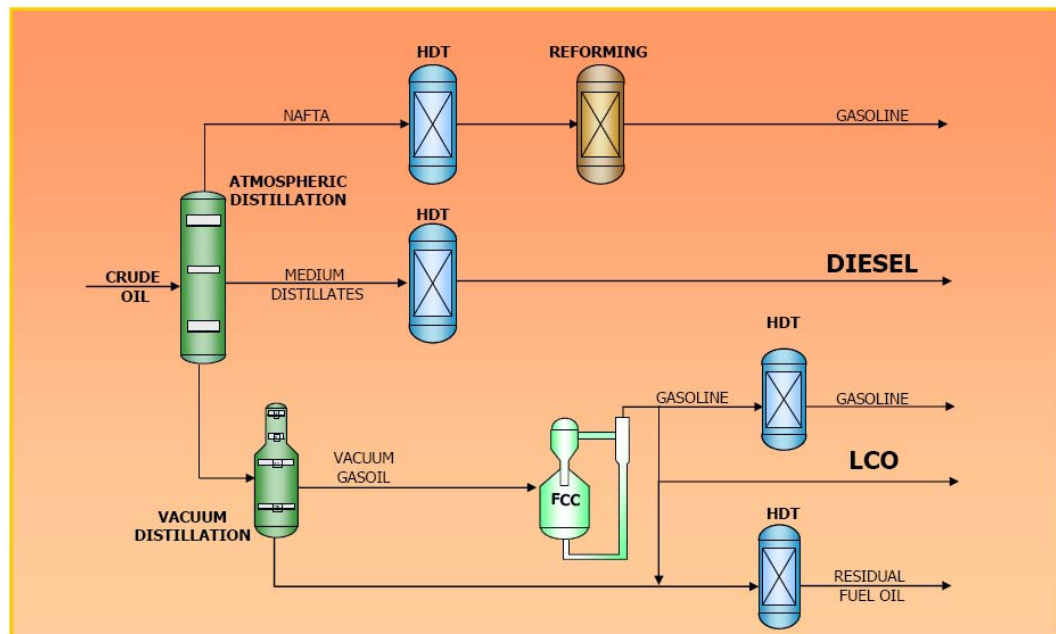
### 1.3.3. Hydrotreating Process

Hydrotreating has been part of refinery processing since the 1930's. Typical hydrotreatment reactions refer to the catalytic hydrodesulphurization (HDS), hydrodenitrogenation (HDN), hydrodeoxygenation (HDO), and hydrodearomatization (HDA) in presence of hydrogen. These reactions are typically carried out over a sulfided CoMo or NiMo catalyst at 350-450°C and 35-60 atm of hydrogen partial pressure. A summary of the hydrotreating process conditions for different feedstocks are shown in Table 7.

**Table 7.** Typical Hydrotreating Process Conditions for Different Feedstocks [38].

Feedstock	Temperature (°C)	Hydrogen partial pressure (atm)	LHSV (h <sup>-1</sup> )
Naphtha	320	10 – 20	3 – 8
Kerosene	330	20 – 30	2 – 5
Atmospheric gas oil	340	25 – 40	1.5 – 4
Vacuum gas oil	360	50 – 90	1 – 2
Atmospheric residue	370-410	80 – 130	0.2 – 0.5
Vacuum heavy gas oil	380-410	90 – 140	1 – 2
Vacuum residue	400-440	100 – 150	0.2 – 0.5

In the last two decades petroleum refining technology has significantly changed and the reactions of hydrotreating, in particular, have risen to a level of economic issue of pressing importance. Hydrotreaters now have a central position in modern refineries as shown in **Figure 8**.

**Figure 8.** Schematic of typical hydrotreating process within modern refinery (HDT).

### 1.3.3.1. Hydrodesulfurization

- **Deep HDS chemistry and kinetics**

Diesel fuels contain a complex mixture of a large variety of sulphur compounds with different reactivities. To achieve ultra deep desulphurization diesel fuels, a clear understanding of the types of sulphur compounds present in diesel feeds, their reactivity, reaction pathways, deep HDS kinetics and mechanism, and the factors that influence the reactivity of the sulphur compounds in diesel feeds including inhibition effects is very important.

- **Sulphur compounds in diesel feeds**

Recent developments in the separation and analytical techniques have facilitated the separation and quantitative analysis of individual sulphur compounds present in diesel feeds. A combination of high resolution gas chromatography and sulphur selective detectors such as flame photometric detector (FPD) and sulphur chemiluminescence detector (SCD), pulse flame photometric detector (PFPD), atomic emission detector (AED), FT-ICR-MS, etc. have been currently used for detailed analysis of different types of sulphur species present in diesel blending streams [39-46]. Fig. 8 shows the various types of sulphur containing compounds present in typical Kuwait straight-run light gas oil analyzed by GC-SCD [47]. The results clearly indicate that diesel feeds contain a large number of individual sulphur compounds which can be divided into two groups. The first group includes benzothiophenes (BTs) with alkyl substituents containing 1–7 carbon atoms, and the second class comprises dibenzothiophene (DBT) with alkyl substituents containing 1–5 carbon atoms. Distribution of the alkyl BTs and alkyl DBTs are found to be in accordance with their boiling points. C<sub>x</sub>-BTs are mainly concentrated in fractions having boiling points <300 °C and C<sub>x</sub>-DBTs in fraction boiling above 300 °C. The 300–340 °C fractions contain high concentration of C1–C2 DBTs together with C5 and C6-BTs. The same two groups of sulphur compounds are usually present in a different gas oils (SRGO, LCO, CGO), but the distribution among these compounds is somewhat different in cracked and straight-run feeds [42,48–50]. The distribution of sulfur compounds mainly depends on the origin of the petroleum. The types



and volume of different streams feeding into the diesel fuel will also have a strong influence on the concentrations of different types of sulphur compounds in the diesel feedstocks.

- **HDS reaction pathways and mechanism**

It is now well established that HDS of DBT and alkyl DBT molecules proceed mainly via two parallel routes as shown in Figure 9. The first route involves direct desulfurization (DDS) leading to the formation of biphenyl while the second route involves hydrogenation (HYD) of one of the benzene rings of the DBT producing tetrahydrodibenzothiophene in the first step which is further desulphurized to cyclohexyl benzene [27,51,52]. Model compound tests have shown that the HDS reaction of un-substituted DBT preferentially progresses via the direct sulfur extraction (DDS) route. The alkyl substituents affect the HDS of DBT in two ways: (i) they reduce their HDS reactivity and (ii) they change the ratio between rates of the two routes. The HYD route becomes dominant with the introduction of alkyl substituents in the 4 and/or, 6-positions of the DBT molecules [15,41,52,53]. It has been reported [54,55] that the partial saturation changes the spatial configuration of the molecule, making the previously sterically hindered sulphur more accessible for effective adsorption on the active site and subsequent reaction, which is of crucial importance for hydrotreating process.

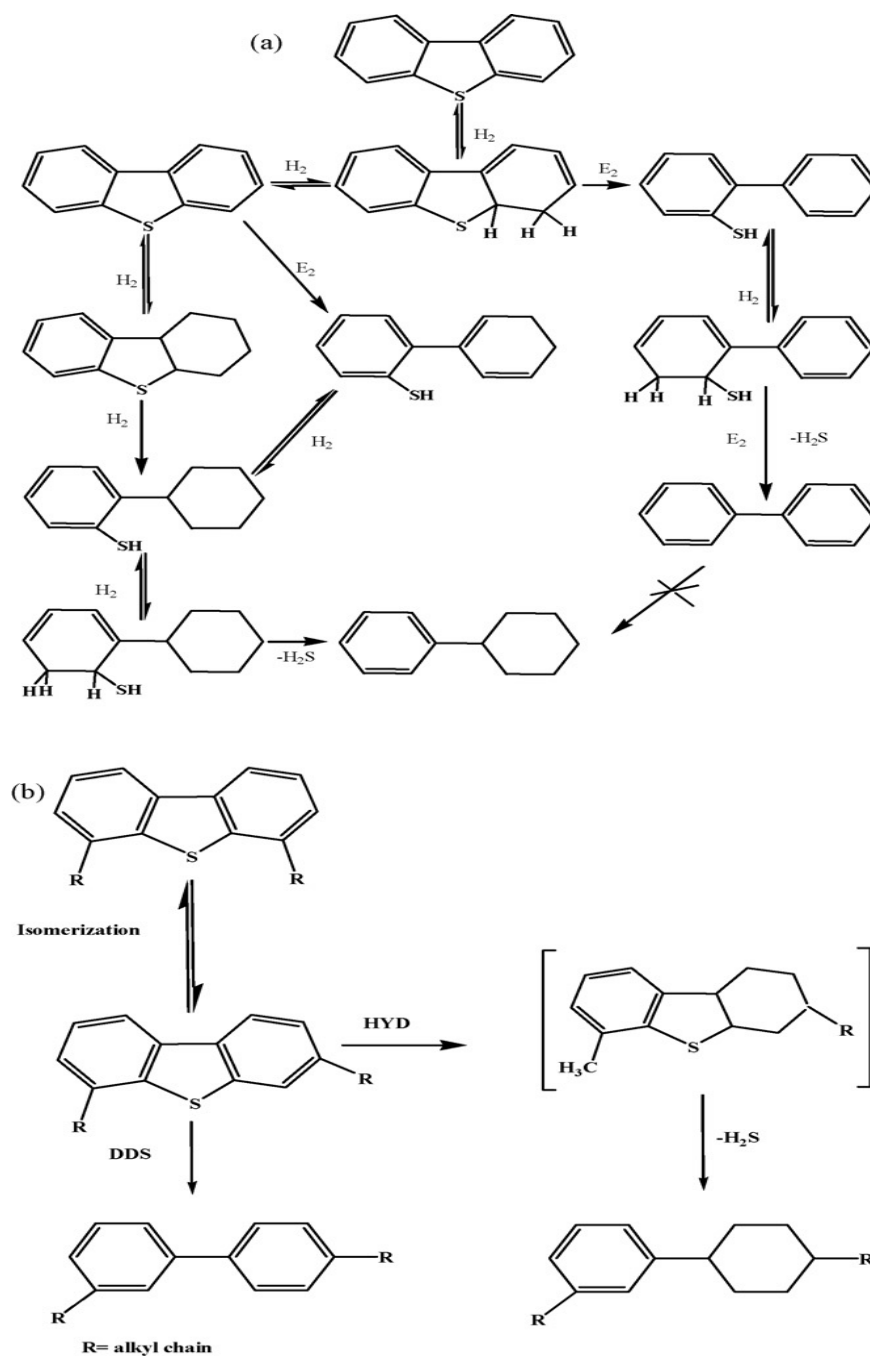


**Figure 9.** (a) The various steps of the HDS of DBT through the HYD and DDS pathways. E2: C–S bond cleavage through an elimination process involving sulphur anions as basic sites [56]. (b) Transformation of 4,6-DMDBT through isomerisation route over acid containing hydrotreating catalysts.

DDS pathway is severely inhibited while the HYD pathway is hardly affected by the presence of alkyl groups in the 4- and 6- positions of DBT. It has been suggested that the

alkyl groups in the 4,6-DMDBT do not play a significant role in the reactivity of 4,6-DMDBT along the HYD pathway, and the difference in reactivity between DBT and 4,6-DMDBT originates essentially in the selective promoting effect on the DDS pathway [56,57]. Studies on the HDS of DBT on un-promoted and cobalt promoted MoS<sub>2</sub>/Al<sub>2</sub>O<sub>3</sub> catalysts have shown that the DDS pathway is more selectively enhanced than the HYD pathway by the cobalt promoter [56]. In the case of HDS of 4,6-DMDBT, the promoting effect of Co on the DDS route is significantly small while the HYD pathway is about the same as that of DBT. A common dihydro-dibenzothiophene intermediate was suggested for the DDS and HYD reaction routes to explain these results [56]. The orientation of the reaction toward one or the other of the two possible pathways is the consequence of the difference in reactivity of the common dihydro-intermediate in further hydrogenation or in C–S bond cleavage through elimination. It was supposed that by increasing the basic character of the sulphur anions, which is in accordance with accepted theories, the promoter enhances the rate of C–S bond cleavage through the elimination (E2) mechanism. Consequently, this step which in the case of DBT is rate-limiting on MoS<sub>2</sub>/Al<sub>2</sub>O<sub>3</sub> becomes fast on promoted catalysts so that the DDS route becomes prominent. With 4,6-DMDBT, C–S bond cleavage in the common dihydro-intermediate remains relatively slow because of steric hindrance, which annihilates to a large extent the effect of the promoter on the HDS. The hindrance of the C–S bond cleavage in the partially hydrogenated intermediate could thus be the most likely reason for low reactivity of alkyl DBTs with alkyl substituent in the 4 and 6 positions.

- **Thermodynamics**

The HDS of sulfur compounds is exothermic and fundamentally irreversible under the reaction conditions employed industrially [51]. Actually, there is very little thermodynamics data available for sulfur compounds present in high boiling fractions. According to the results for dibenzothiophene HDS (51) the conversion of dibenzothiophene into biphenyl is favored at temperatures of industrial practice and is exothermic ( $\Delta H_o = -11$  kcal/mol). Those results also suggest that the HDS of higher molecular weight sulfur compounds (e.g., benzonaphthothiophenes) are also favored. Sulfur removal occurs along two parallel pathways, hydrogenolysis and hydrogenation. Since hydrogenation of the rings of sulfur compounds is equilibrium-limited at industrial HDS temperatures, the pathways concerning

previous hydrogenation of the ring can be affected by thermodynamics [51]. It was found that the equilibrium constant for hydrogenation of thiophene into tetrahydrothiophene is less than unity at temperatures above 350 °C. Thus, sulfur-removal pathways via hydrogenated sulfur intermediates may be inhibited at low pressures and high temperatures because of the low equilibrium concentrations of the latter species.

- **Reaction Kinetics**



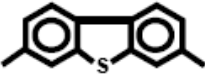
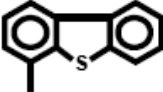
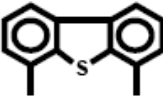
The literature on hydrodesulfurization of oil fractions and sulfur containing model compounds has been reviewed by several authors, most notably Froment and coworkers [26,57-62]. The kinetics for the decomposition of substituted benzothiophenes and dibenzothiophenes in complex mixtures has also been published by Kabe et al. [43] in the study of hydrodesulfurization of a light oil on a CoMo/Al<sub>2</sub>O<sub>3</sub> catalyst.

First-order kinetics for the removal of substituted benzothiophenes and dibenzothiophenes in complex mixtures prevails in the literature. Studies of hydrodesulfurization of a light oil (245-374°C) on a CoMo/Al<sub>2</sub>O<sub>3</sub> catalyst found that benzothiophenes with substituents in positions 2, 3, and/or 7 were less reactive than BT [43]. The most refractive methylsubstituted-BT was 2,3,7-trimethyl-BT (2,3,7-TriMeBT). Dibenzothiophenes with substituents in positions 4 and/or 6 were less reactive than other substituted dibenzothiophenes. Similar results were obtained by Ma et al. [63-65] in the HDS of substituted BT's and dibenzothiophenes in oil fractions such as diesel fuel, gasoil, and vacuum gasoil, on CoMo/Al<sub>2</sub>O<sub>3</sub> and NiMo/Al<sub>2</sub>O<sub>3</sub> catalysts. In addition, methyl substituents in positions 2, 3, and/or 7 reduce the hydrodesulfurization rate. From this it can be inferred that DBT is one of the most representative sulfur compounds comprised in higher boiling fractions of oil.

Because DBT is readily available commercially, it has been used as model compound or parent molecule for investigating the HDS of organic sulfur compounds. Vanrysselberghe and Froment (61) obtained results in a study of hydrodesulfurization of Light Cycle Oil (LCO) which indicated that benzothiophenes with substituents in positions 2, 3, and/or 7 were less reactive than benzothiophene. Dibenzothiophenes with substituents in positions 4 and/or 6 were even less reactive. Methyl groups in other positions led to hydrodesulfurization rates higher than that of dibenzothiophene. Opposite to this, Kabe et al. [43, 65] and Ma et al. [63-

65] found that methyl groups in positions 1, 2, and/or 3 had no influence on the hydrodesulfurization rate. Houalla et al. (66-69) established that the first-order rate coefficient for the HDS of DBT is almost identical with that of 2,8-DiMeDBT (dimethyldibenzothiophene) and is about 2 times larger than that of 3,7-DiMeDBT. The HDS of the reactants shown in Table 8 is described by pseudo-first order kinetics as determined by this investigator [70].

**Table 8.** Hydrogenolysis Rate Coefficients of Selected Methyl-Substituted Dibenzothiophenes (a). [67-70]

Reactant	Structure	Pseudo-first-order rate constant $\text{m}^3/(\text{kg}_{\text{cat}} \text{s})$
Dibenzothiophene (DBT)		$6.11 \times 10^{-5}$
2,8-dimethyl-dibenzothiophene (2,8-DMDBT)		$6.72 \times 10^{-5}$
3,7-dimethyl-dibenzothiophene (3,7-DMDBT)		$3.53 \times 10^{-5}$
4-methyl-dibenzothiophene (4-MDBT)		$6.64 \times 10^{-6}$
4,6-dimethyl-dibenzothiophene (4,6-DMDBT)		$4.92 \times 10^{-6}$

(a) Experimental conditions: batch reactor,  $n\text{-C}_{16}$  solvent,  $300^\circ\text{C}$ , 102 atm, CoMo/Alumina catalyst.

- **Inhibition effects**

For the production of ultra low sulphur diesel fuel (<10 ppm S) more than 99% of the sulfur compounds, including the traces of least reactive alkyl DBTs present in the feedstock should be removed during catalytic hydrotreating. The main problem in the HDS of the sterically hindered alkyl DBTs is the inhibiting effects of different poisons such as H<sub>2</sub>S, N-containing compounds and aromatic molecules on their reactivity under deep desulfurization conditions. The first route involves direct sulphur extraction while the second route involves two steps, hydrogenation of one of the aromatic rings in the first step followed by sulphur removal as H<sub>2</sub>S in the second step. The poisoning effects of the inhibitors (H<sub>2</sub>S, nitrogen compounds and aromatics) have been found to be different for the two routes in many studies [10,14,51,52,69-73,74-82]. Therefore a clear understanding of the influence of different inhibiting species on deep HDS of these substituted dibenzothiophenes is important for ULSD production. In general, the inhibition order is as follows: nitrogen compounds > organic sulfur compounds > polyaromatics≈oxygen compounds≈H<sub>2</sub>S > monoaromatics. The inhibition is not only for HDS but also between inter- and intra-molecular reactions as well as its intermediate reaction products. Individual account of different inhibitors is given in the following sections.

- a) **Effect of H<sub>2</sub>S**

The effect of hydrogen disulfide (H<sub>2</sub>S) on three different catalytic functionalities, namely, hydrogenolysis (HDS), hydrogenation (HYD) and acidity of the catalyst (isomerization and cracking function) has been investigated [10,83–86]. It is reported that these functionalities are not affected at similar magnitude with added H<sub>2</sub>S or along the trickle bed integrated reactor. Usually in such reactor the organic sulfur is converted to H<sub>2</sub>S, which generate high H<sub>2</sub>S partial pressure along the reactor [87,88] as shown in Fig. 10. Having such amount of H<sub>2</sub>S, it is expected that the coordinately unsaturated sites (CUS) (sulfur vacancy sites) in Mo are converted into saturated sites (sulfhydryl groups, –SH) [89–91]. Indeed H<sub>2</sub>S is competitively adsorbed on the active sites that decreases the total number of available CUS sites, and convert CUS into –SH. Thus, sulfided catalysts have two different kinds of sites, in

which one is CUS and other one is sulfhydryl groups, which enhance the hydrogenation activity along with the crack.

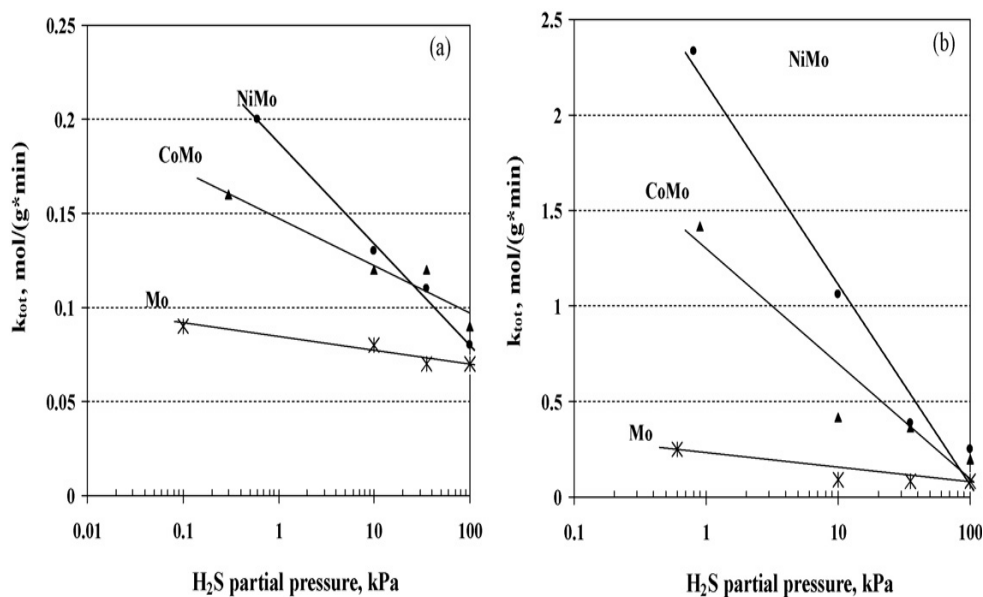


**Figure 10.** Rate constants of the total conversion of 4,6-DMDBT (a) and DBT (b) over NiMo/ $\gamma$ -Al<sub>2</sub>O<sub>3</sub>, CoMo/ $\gamma$ -Al<sub>2</sub>O<sub>3</sub> and Mo/ $\gamma$ -Al<sub>2</sub>O<sub>3</sub> catalysts as function of H<sub>2</sub>S partial pressures[71] (T = 340 °C; P = 4.8 MPa).

The inhibiting effect of H<sub>2</sub>S on the HDS of DBT and alkyl DBTs (e.g. 4,6-DMDBT) have been investigated in many studies using different types of catalysts. The important observations made in these studies are the following:

- The inhibition effect of H<sub>2</sub>S on the two main desulfurization routes of DBT type compounds is not the same. H<sub>2</sub>S is a strong inhibitor for sulfur removal via DDS route, but only has a minor effect on HYD route.
- Sensitivities to H<sub>2</sub>S poisoning are different for different types of catalysts. NiMo/Al<sub>2</sub>O<sub>3</sub> catalyst is more susceptible to H<sub>2</sub>S inhibition than CoMo/Al<sub>2</sub>O<sub>3</sub> catalyst. An example of this observation reported in a recent study by Egorova and Prins [71].
- The inhibiting effect of H<sub>2</sub>S is less pronounced in the HDS of sterically hindered alkyl DBTs such as 4,6-DMDBT than the HDS of DBT. This has been confirmed by other studies [92-94].

- H<sub>2</sub>S partial pressure has a strong influence on the sensitivities of NiMo and CoMo catalysts to H<sub>2</sub>S poisoning [95]. However, at very low partial pressure, H<sub>2</sub>S has a promotional effect on HDS [96-99].

#### **b) Effect of nitrogen compounds**

Several studies have shown that catalytic hydrodesulfurization reaction is significantly inhibited by organic nitrogen compounds [15,72,100,101,102–115]. It is generally suggested that there is competitive adsorption between nitrogen-containing compounds and sulfur containing compounds on catalyst's active sites, and nitrogen compounds inhibited HDS reactions because of their strong adsorptive strength. The extent of inhibition, however, depends on the type and concentration of organic nitrogen compounds. In straight run light gas oil feeds, typical nitrogen content is in the range 100–300 ppm. Cracked distillate feeds (e.g. LCO, CGO), usually contain higher nitrogen levels (>500 ppm). Reducing the nitrogen content of diesel feeds has been found to increase their HDS reactivity significantly [116,117].

Three types of nitrogen compounds are mainly present: non-heterocycles, heterocycles of 6 membered ring (6MR), and heterocycles of five membered rings (5MR). The non-heterocyclic nitrogen compounds such as anilines and aliphatic amines are not important as they undergo HDN quickly. Among the heterocyclic nitrogen compounds, 6MR pyridinic species (e.g. quinoline, acridine) are basic and 5MR pyrrole species (e.g. carbazole, indole) are non-basic or even acidic. Generally, the inhibiting effect of basic nitrogen compounds is the strongest [72,100,118–121]. Koltai et al. [119] compared the reaction rate of 4,6-DMDBT in the presence of acridine or carbazole on NiMo catalysts, using an autoclave. They found that the inhibiting effect on initial HDS activity by acridine was higher than by carbazole, due to its stronger adsorption.

#### **c) Effect of aromatics content**

The middle distillate petroleum fraction (diesel stream) contains large amount of aromatic hydrocarbons, condensed naphtheno-aromatics and aromatic olefins along with sulfur- and nitrogen-containing compounds. The aromatic hydrocarbons consist of mono-, di-,



and poly-nuclear aromatics. Depending on the origin of the feedstock, the total aromatics content of the diesel feed streams could vary in the range 25–75% [122]. For example, straight run gas oils usually contain 25–30% total aromatics, whereas the cracked distillates (e.g. LCO, CGO) contain significantly higher concentrations of aromatics in the range 50–75%.

The influence of aromatic compounds on the hydrodesulfurization of diesel fuel has been investigated by many researchers [49,82,122–130]. Conflicting results have been reported in the literature regarding the inhibiting effect of aromatics on HDS.

Van Looij et al. [82] studied the effects of naphthalene, tetralin, crysene and pyrene on deep HDS of diesel and found that these poly-nuclear aromatics had negligible inhibitory effect on HDS. Koltai et al. [119] found a strong inhibiting effect of polycondensed aromatics on the HDS of 4,6-DMDBT. Aromatics were found to be much stronger inhibitors than H<sub>2</sub>S in a study on the desulfurization of light gas oil (LGO) by Kabe et al. [130].

Inhibition effects of some model aromatic compounds on the HDS of 4,6-DMDBT were found to be in the following order: naphthalene > tetralin > isobutyl benzene as shown in Fig. 11. In a recent study on the influence of aromatics on deep HDS of DBT and 4,6-DMDBT over a NiMo/Al<sub>2</sub>O<sub>3</sub> catalyst, Song et al. [39] reported that aromatics with 2 or more rings were stronger inhibitors of HDS than mono-aromatics. This adverse effect was more pronounced for 4,6-DMDBT than for DBT. The competitive adsorption between the sulfur compounds and aromatics on the catalyst surface was the main reason for the decreased HDS efficiency as quantitatively verified by the heat of adsorption. Poly-nuclear aromatics showed stronger inhibition effect compared to 1-methyl naphthalene. It was reported that 10% naphthalene severely retarded the HDS of 4,6-DMDBT on NiMo catalysts. Hydrogenation of naphthalene to tetralin was preferred to HDS of 4,6-DMDBT on this catalyst.

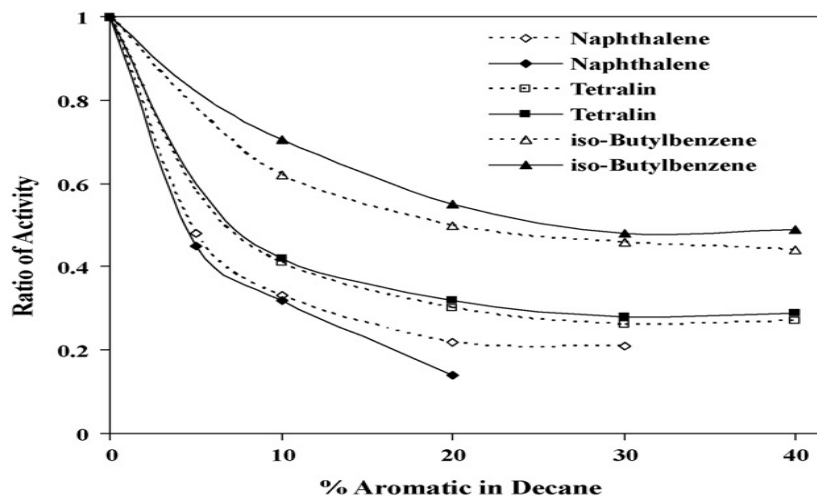


**Figure 11.** Ratio of activity for HDS of 4,6-DMDBT in decane as a function of aromatic content over NiMo (solid line) CoMo (dotted line) ( $T = 270\text{--}360\text{ }^{\circ}\text{C}$ ;  $P = 2.4\text{--}5\text{ MPa}$ )[39].

- **Feed quality effect**

Feedstock quality plays an important role on the performance of a diesel hydrotreater used for the production of ULSD. Industrial feedstocks used for diesel fuel production in different refineries are usually different in their characteristics with regard to sulphur, nitrogen, and aromatic contents which may affect the degree of desulphurization during hydrotreating. Diesel fuel feedstocks mainly consist of middle distillates in the boiling range  $220\text{--}360\text{ }^{\circ}\text{C}$  with plus or minus some front or back ends. Depending on refinery complexity, the deep HDS unit feed components may comprise a variety of distillate sources including straight-run gas oil (SRGO), coker gas oil (CGO) thermally cracked distillates, and FCC light cycle oil (LCO).

Most refiners process a wide variety of crudes and routinely adjust the operating conditions of major processing units according to the changing feeds and overall product needs. Additionally, the types and volume of streams feeding into the diesel pool may change due to seasonal swing in the product demand and changes in upstream operations. These changes in upstream operations as well as the blending of CGO and LCO with SRGO will cause the type and concentrations of sulphur and nitrogen and aromatic compounds and their distributions in the diesel feedstock to vary.

### a) Properties of diesel feeds

The properties and reactivities of diesel feeds are strongly dependent on their source [18,19,131,132]. In a recent study Marafi et al. [133] compared the total sulfur content and other characteristics of two Kuwaiti crudes and their straight run gas oils (diesel cuts). The results presented in Table 9 indicate significant differences in the key properties of the two crudes and their diesel cuts.

**Table 9.** Characteristics of various straight run gas oil (SRGO) feedstocks derived from two different Kuwait crudes [133].

Feed properties	GO-KEC	GO-LF
Density @ 15 °C (g/cm <sup>3</sup> )	0.8508	0.8962
Sulfur (wt.%)	1.52	3.22
Nitrogen (ppm)	50	187
TBN (mg/mg KOC)	0.179	0.457
Total aromatics (wt.%)	30.45	44.73
Mono aromatics (wt.%)	15.09	19.47
Polyaromatics (wt.%)	14.92	26.21
Kinematic viscosity @ 40 °C (cSt)	4.32	5.635
Cetane index	50.2	38.2
Distillation (°C)		
IBP	220	236
10 vol.%	245	261
30 vol.%	264	288
50 vol.%	305	314
70 vol.%	334	340
90 vol.%	370	366
95 vol.%	370	375

The gas oil from the heavy Lower Fars crude (GO-LF) contains substantially higher sulfur nitrogen and aromatic contents than that from light Kuwait export crude (GO-KEC).

Furthermore, the concentrations of the low-reactive sterically hindered alkyl DBTs are significantly higher in the GO-LF than in the GO-KEC (Fig. 12). Another example of the effect of crude source on diesel stream sulfur species distribution is presented in Fig. 13. It is seen that the diesel cut from North Sea crude (feed A) contains predominantly sterically hindered alkyl DBTs even though its total sulfur content is significantly low while other two feeds B (SRGO/LCO, from an Arabian crude) and C (SRGO/cracked blend derived from Nigerian crudes) with higher sulfur level contain relatively lower amount of refractory sulfur compounds [134] (**Figure 13**).

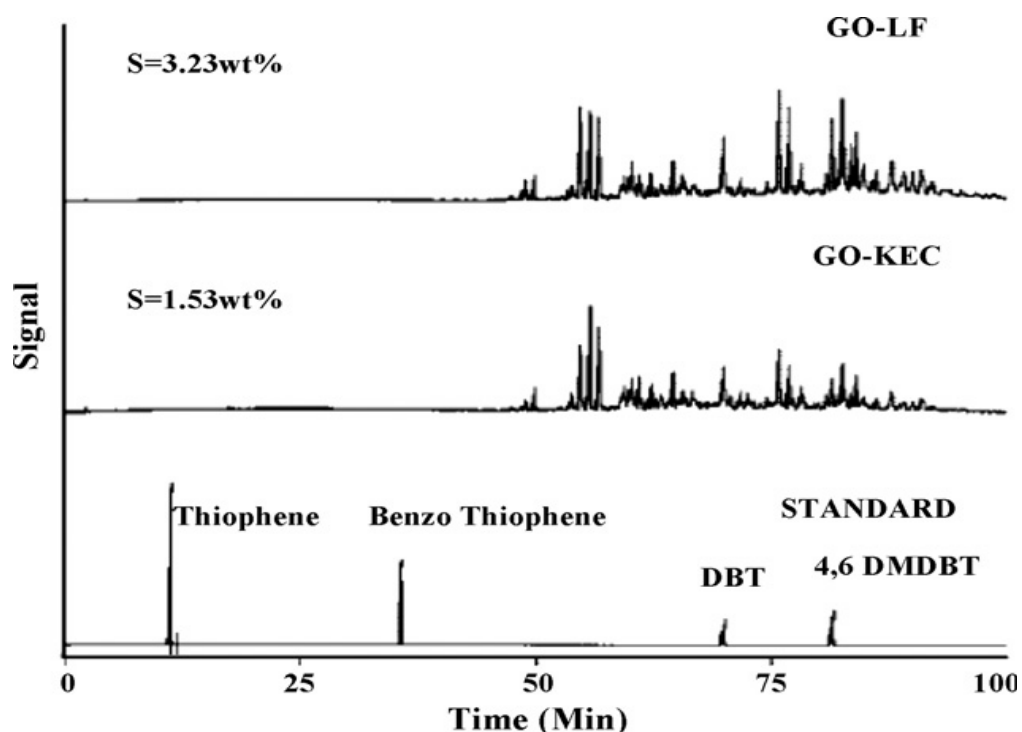


**Figure 12.** GC-FPD analysis for sulfur compounds of GO-KEC and GO-LF [133].

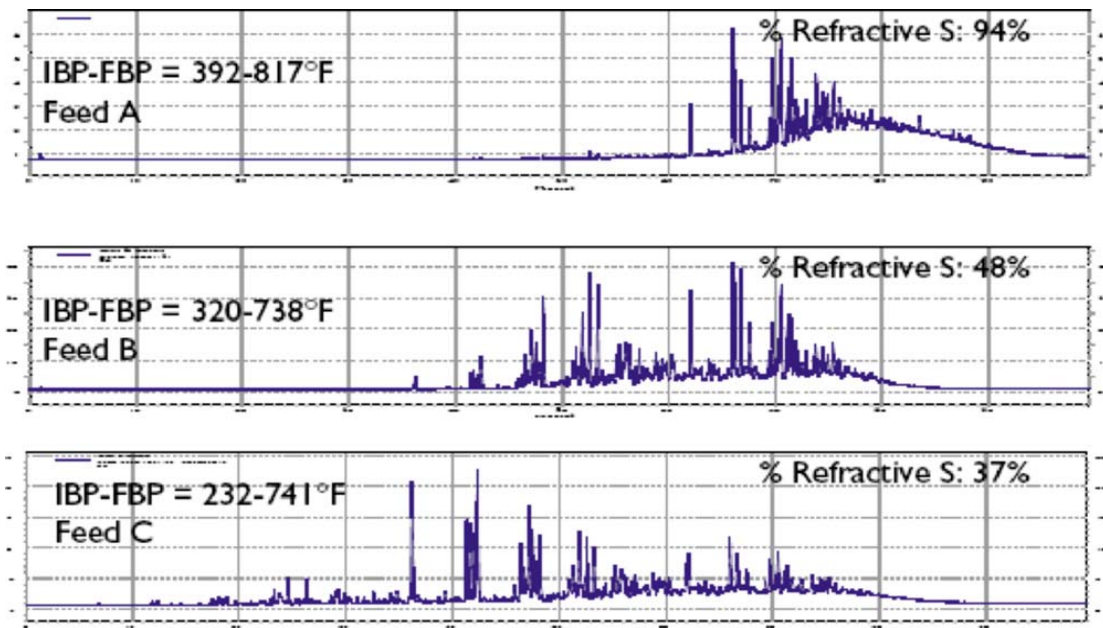


**Figure 13.** Sulfur distribution depends upon crude source and upstream processing (feed A: North Sea SRGO, S = 0.196 wt.%; feeds B: SRGO/LCO, from an Arabian crude, S = 1.29 wt.%; feed C: SRGO/cracked blend derived from Nigerian crude, S = 0.517 wt.%) [134].

**b) Feed quality effect on HDS reactivity**

In the deep desulfurization of diesel to ultra low sulfur levels, the quality of the feedstock plays a major role [18,131,133,134,135,136]. The degree of desulfurization of two diesel feeds (Table 10) derived from two different crudes was examined by Marafi et al. [133] in a recent study. Hydrotreating experiments were conducted using the feeds under identical conditions in the temperature range 320–380 °C. The results (Fig. 14a) showed that the degree of desulfurization of the diesel cut (GO-LF) from the heavy crude was remarkably lower than that of the light crude diesel cut (GOKEC). The variation in feedstock quality with distillation temperature (T90) also leads to large differences in the hydrotreating reactivity as shown in Fig. 14b, which clearly provides the relationship between the reactor temperature and product sulfur content for diesel feedstocks having different cut temperatures. Marafi et al. [133] studied the deep desulfurization of full range and low-boiling diesel streams obtained from Kuwait Lower Fars heavy crudes, and concluded that the full range diesel feed stream produced from the LF crude was very difficult to desulfurize due to its low quality caused by high aromatics content (low feed saturation) together with the presence of high concentrations of organic nitrogen compounds and sterically hindered alkyl DBTs. Similar results were also obtained by Al-Barood and Stanislaus [64] in a comparative study on the deep HDS of a full range and low-boiling straight un diesel cuts of Kuwait export crude (Fig. 15).

**Table 10.** Quality of diesel product obtained by hydrotreating of GO-KEC and GO-LF at 350 °C [133].

<b>Product properties</b>	<b>Diesel from GO-KEC</b>	<b>Diesel from GO-LF</b>
Density @ 15 °C (g/cm <sup>3</sup> )	0.8307	0.8609
Sulfur (wppm)	65	689
Nitrogen (wppm)	6	17
Total aromatics (wppm)	24.96	37.91
Monoaromatics (wppm)	20.32	29.45
Polyaromatics (wppm)	4.64	8.45
Cetane index	62	51

Light cycle oil (LCO) from fluid catalytic cracking (FCC) units and thermally processed distillates from Visbreaker, thermal cracker and coker units are generally more difficult to desulfurize. These streams contain high concentrations of aromatics and nitrogen compounds which inhibit deep HDS of the alkyl DBTs through the hydrogenation route. Studies have shown that LCO is typically 2–4 times harder to desulfurize than the average straight run feed [19]. These low reactive diesel feed streams are usually blended with straight run gas oils (diesel cuts) in order to improve the feedstock quality (Fig.16).

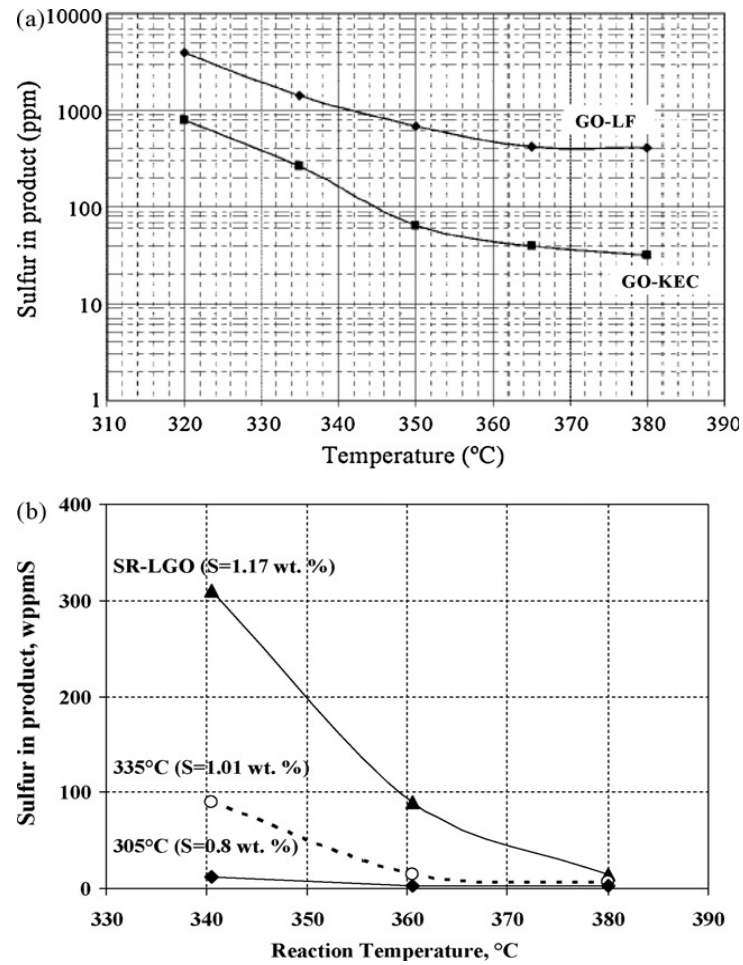


**Figure 14.** (a) Temperature effect on desulfurization of diesel cuts derived from two different crudes (GO-LF and GO-KEC) [133]. (Catalyst: CoMo/Al<sub>2</sub>O<sub>3</sub>; P=4MPa; LHSV = 1.3 h<sup>-1</sup>; H<sub>2</sub>/HC = 200 mL/mL.) (b) Effect of feedstock cut temperature as a function of reaction temperature on product sulfur content. (P=5MPa; LHSV=2h<sup>-1</sup>.)



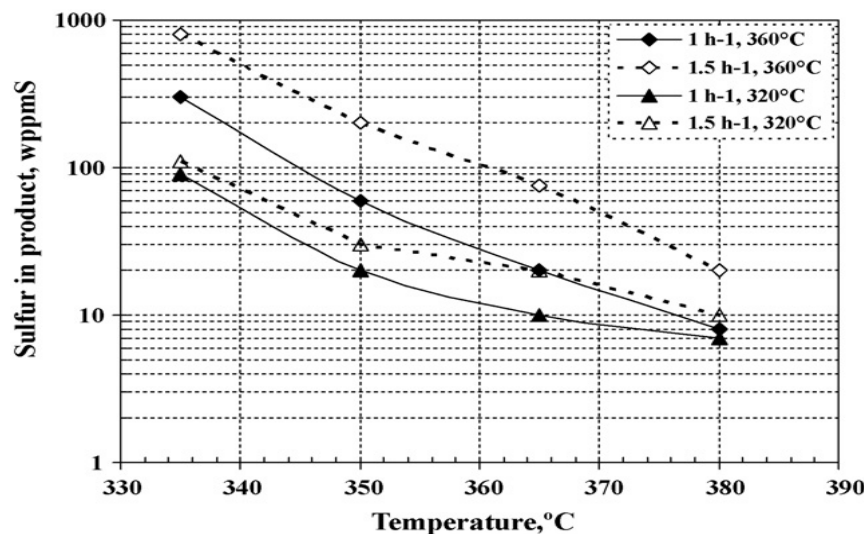


**Figure 15.** Effect of lowering T95 (320 °C and 360 °C) of SRGO on deep HDS as a function of reaction temperature and with variation liquid hour space velocity (1 h<sup>-1</sup> and 1.5 h<sup>-1</sup>) [48]. (Catalyst: CoMo/Al<sub>2</sub>O<sub>3</sub>; P = 5MPa; H<sub>2</sub>/HC = 200 mL/mL.)

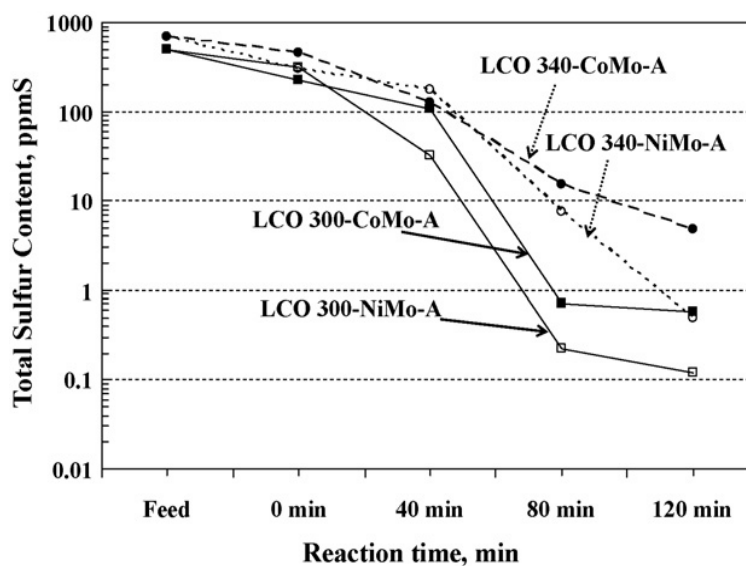


**Figure 16.** Remaining amount of sulfur in HDS product from LCO 300- and 340-over CoMo-A and NiMo-A [49]. (T = 340 °C; P = 7MPa; LHSV = 1.3 h<sup>-1</sup>; H<sub>2</sub>/HC = 200 mL/mL.)

### c) Correlation between feedstock properties and HDS reactivity

To obtain a better understanding of feedstock effects on hydrodesulphurization of middle distillates, it is important to develop some form of correlations to relate feed property to reactivity. A number of such correlations are available in the open literature. A simple empirical correlation was developed by Shih et al. [131] to describe the temperature required for desulfurization of distillates to 0.05 wt.% sulfur. A total of eight feedstock components were employed in the correlation, covering straight-run gas oil (GO), coker gas oil (CGO), and FCC light cycle oil (LCO). The temperature required to achieve 500 wppm product sulfur (T<sub>500</sub>) was found to be correlated with the concentration of 600 °F (315.5 °C) sulfur and total nitrogen in the feed, but independent of the feedstock source. The reactivity, T<sub>500</sub>, was expressed as a function of S<sub>600F+</sub> (sulfur content in wt % of the 600 °F+ (315.5 °C) fraction of the feed) and N<sub>f</sub> (feed nitrogen content) as,

$$T_{500} = (454^{\circ}\text{F}) + (31^{\circ}\text{F}) \exp(S_{600^{\circ}\text{F}}) + (25^{\circ}\text{F}) \ln(N_f) \quad (1)$$

However, the correlation does not include the overall feed quality such as the API gravity. This property–reactivity correlation was later modified in the form of HDS reactivity. The T<sub>500</sub> reactivity data was resealed through an Arrhenius expression of

$$RHDS = 0.0008 \exp(5398 / T_{500})$$

Where T<sub>500</sub> was now in K instead of °F. And the modified correlation became:

$$RHDS = (S_{600^{\circ}\text{F}})^{-0.33} (N_f)^{-0.2} \quad (2)$$

The property–reactivity correlation was formulated in the following expression:

$$RHDS_{\text{activity}}, RHDS = (^{\circ}\text{API})^{2.18} (\text{DBTs})^{-0.31} + (N_f)^{-0.2} \quad (3)$$

The corresponding correlation was expressed as,

$$R_{\text{HDS}} = k_{\text{HDS}} (1 - \lambda K_N N_f) \quad (4)$$

where  $\lambda$  is a dimensionless parameter which characterizes the extent of HDN reaction, and  $K_N$  is the adsorption constant of feed nitrogen.

In a recent study, Choudary et al. [132] demonstrated that for heavy gas oil feeds the desulfurization chemistry is essentially controlled by the strong inhibitory effect of large 3+ ring aromatic hydrocarbon content as shown in the following correlation.

$$S_{\text{Product}} = [S^f \exp\left(\frac{-kP_{H_2} \lambda}{(K)(R+3)LHSV}\right)] \quad (5)$$

Where  $S^f$  = feed sulfur,  $K$  = 3+ ring, aromatic inhibition constant = 0.0663,  $3+R$  = 3+ ring core aromatic content,  $\alpha$  = pressure dependence term,  $LHSV$  = liquid hourly space velocity,  $K_{\text{group}(x)} = A_{\text{group}(x)} \exp(-E_{\text{group}(x)}/RT)$ ,  $k$  = rate constant,  $A$  = pre-exponential factor = 84,370 1/h, and  $E$  = activation energy = 56.5 kJ/mol. An excellent correlation was observed between the sulfur conversion (644K and 6.9 MPa) for the eight different heavy oil feeds and 3 + ring aromatic content (Fig. 17).

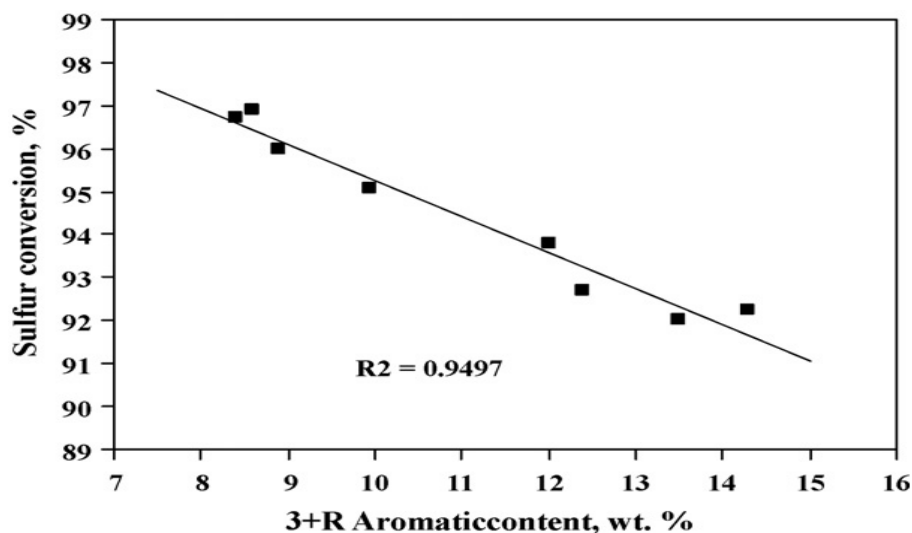


**Figure 17.** Relationship between three + ring aromatic content of eight heavy oils and the corresponding sulfur conversion (reaction conditions: temperature = 644 K;  $LHSV=1 \text{ h}^{-1}$ ; pressure = 6.9 MPa;  $H_2/HO$  ratio =  $356 \text{ m}^3/\text{m}^3$ ) [132].

- **Effect of process variables and thermodynamic limitation**

The performances of gas oil hydrotreaters is affected by operating conditions such as reactor temperature, liquid hourly space velocity (LHSV), hydrogen partial pressure and recycle gas to oil ratio. Kinetics studies [14] have shown that the rate of HDS can be increased and the sulfur content can be reduced to lower levels with increase of temperature, increase of hydrogen partial pressure and decrease of space velocity (Fig. 18). Similar results have also been reported in many other studies [9,14-16,41,137,138]. The use of higher operating severity for lowering sulfur levels to ultra low levels in conventional diesel hydrotreaters have practical limitations related to cycle length, throughput, design pressure, hydrogen availability, thermodynamic equilibrium, etc. The optimum operating conditions for the ultra low sulfur hydrotreater operations will vary depending on the feedstock quality, catalyst type, and thermodynamic limitations.

Since most of the sterically hindered refractory sulfur molecules are present as polyaromatic sulfur compounds, thermodynamic constraint can easily play a role in ultra deep desulfurization of diesel. The increase in reactor temperature does not result in the HDS rate increase expected on the basis of the traditional activation energy. Actually, the removal of sulfur itself is not limited by thermodynamics, but the pre-hydrogenation of one of the aromatic rings before sulfur removal will be strongly influenced by thermodynamics. Aromatics hydrogenation reactions are highly exothermic and reversible. Hydrogenation is promoted by a decrease in temperature and by an increase in hydrogen pressure [125,136,139,140]. At lower hydrogen pressure, increasing reactor temperature to very high levels will have a negative effect on the desulfurization of the polyaromatic sulfur containing compounds (e.g. DBT and alkyl DBT) (Fig. 47). This limitation will be particularly problematic at temperatures close to the end-of the run temperature and in the downstream zone of a commercial hydrotreater where hydrogen partial pressure is low. Farag et al. [141] studied the effect of temperature on the HDS of 4,6-DMDBT at 2.9MPa hydrogen pressure over two CoMo catalysts, one supported on Al<sub>2</sub>O<sub>3</sub> and the other supported on carbon. The results are presented in Fig. 47b, which shows the effect of temperature (as Arrhenius plots) on the rates of direct desulfurization (DDS) and hydrogenation (HYD) reactions of 4,6-DMDBT over the two catalysts. It is seen that at low temperatures [T < 340 °C (613 K)], the HYD route is predominant while at higher temperatures [e.g. 380 °C (653 K)], the DDS route

becomes significant. For both catalysts, the HYD route passes through a maximum as the reactor temperature is increased from 300 °C (573 K) to 380 °C (653 K) and becomes unflavored at higher temperatures. This could be attributed to the thermodynamic limitation of the hydrogenation of 4,6-DMDBT to 4,6-dimethyl tetrahydrodibenzothiophene (H4-4,6-DMDBT). In another related study, Whitehurst et al. [142] experimentally demonstrated that the preferred mode of sulfur removal from 4,6-DMDBT was about 90% by the hydrogenation (HYD) route at 300 °C while at 380 °C the preferred route was about 90% by the direct desulfurization (DDS) route. This dramatic shift in reaction pathway in this temperature range was due to a marked shift in the thermodynamic equilibrium limit imposed on the tetrahydro-4,6-DMDBT (THDMDBT) intermediate at the higher temperature.

At higher pressures the thermodynamic equilibrium limitation for polyaromatics saturation is reduced and pure kinetic plays a major role in deep HDS. In addition to deep HDS, cetane improvement by aromatics hydrogenation will also be favored at lower temperatures and higher pressures. Hydrotreating of middle distillates is very complex technology which brings together: reactor/reaction engineering, catalysis, petroleum refining, chemistry of complex petroleum mixtures and other aspects of chemical engineering. It would be an overwhelming task to try discussing all these aspects, or even mention them shortly, but the interested reader can find plenty of relevant data in the referenced literature [143-198].

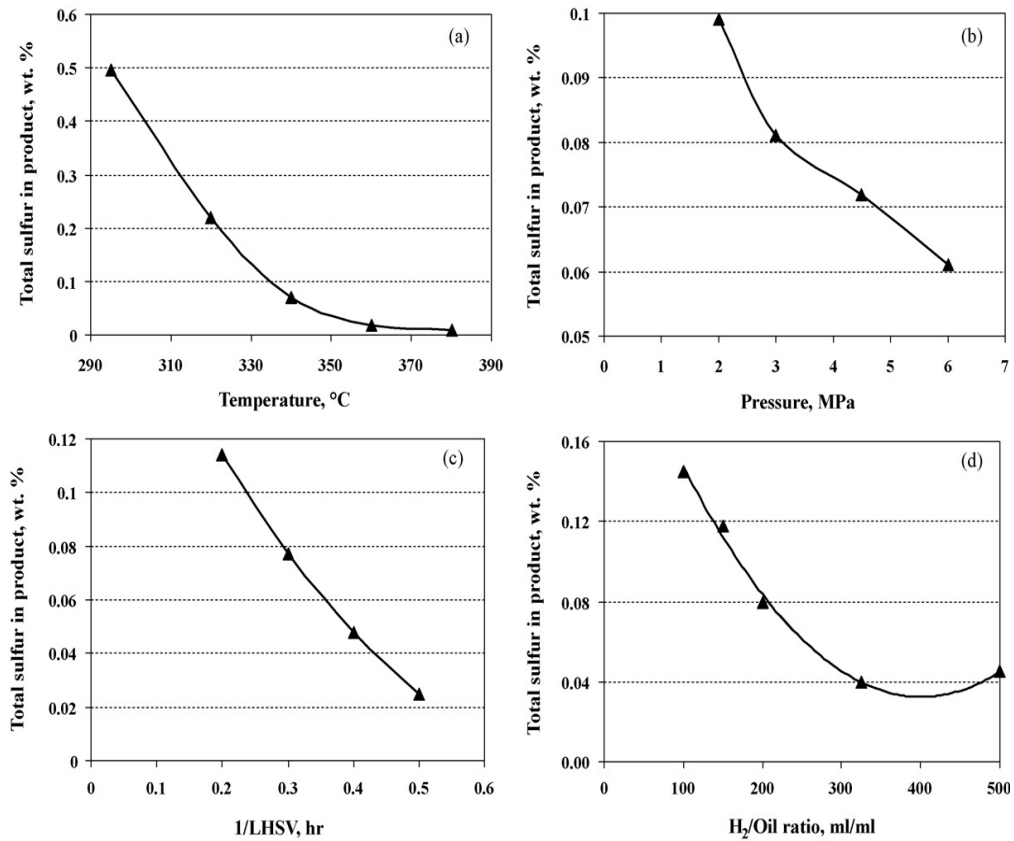


**Figure 18.** Effect of temperature (a), pressure (b), LHSV (c) and H<sub>2</sub>/HC ratio (d) on the total sulfur removal from gas oil [14]. (Catalyst: CoMo/Al<sub>2</sub>O<sub>3</sub> ; for temperature effect: P = 3 MPa; H<sub>2</sub>/HC = 200 mL/mL; LHSV=4h<sup>-1</sup>; for pressure effect: T = 340 °C; H<sub>2</sub>/HC = 200 mL/mL; LHSV=4h<sup>-1</sup>; for LHSV effect: T = 340 °C; P = 3MPa; H<sub>2</sub>/HC = 200 mL/mL; for H<sub>2</sub>/HC effect: T = 340 °C; P=3MPa; LHSV=4h<sup>-1</sup>.)

## 2. THEORETICAL PART

### 2.1 Phase Equilibrium

The equilibrium phase is defined by changing the Gibbs energy. According to the second law of thermodynamics, the total Gibbs energy of a closed system at constant pressure and temperature is lowest when the system is in equilibrium. If you meet this condition together with the condition that the total number of moles of the components in a closed system is constant [199]:

$$\sum_i n_i^\alpha = \text{Const} \quad (6)$$

Where:

$n_i$  is the number of moles of the components and the phase  $\alpha$ .

So that the equilibrium conditions for phase  $\pi$  and N components

$$\mu_1^\alpha = \mu_1^\beta = \dots = \mu_1^\pi \quad (7)$$

Chemical potential of component in phase  $\alpha$  is defined by the equation:

$$\mu_1^\alpha = \left[ \frac{d(\sum_i n_i^\alpha g_i^\alpha)}{dn_1^\alpha} \right]_{P, T, n_{j \neq 1}} = g_1^\alpha \quad (8)$$

Where:

$g$ , the molar Gibbs energy

$\mu_1^\alpha$ , as a function of pressure, temperature, and (N-1) mole fractions (based on conditions  $\sum_i X_i^\alpha = 1$  it can be concluded that the mole fraction dependent variable) from the system

of equation (7) We have  $N(\pi - 1)$  equation and  $2 + \pi(N - 1)$  variables, so the number of degrees of freedom equal to  $F$ :

$$F = 2 + \pi(N - 1) - N(\pi - 1) = 2 - \pi + N \quad (9)$$

Equation (9) is Gibbs phase rule. Under this rule, a system of  $N$  components and  $\pi$  is well defined phases, if selected promenljih  $F$ , such that ensures that the molar Gibbs energy of each phase depending on pressure, temperature and composition is known. At thermodynamic equilibrium analysis phase are used Fugacity and activity components [199].

$$d\mu_i \equiv RT \ln f_i \quad (10)$$

, at a constant temperature and applies to:

$$\lim_{P \rightarrow 0} \frac{\hat{f}_i}{P_i} = 1 \quad (11)$$

From the last equation it follows that the partial pressure Fugacity equal when it comes to the ideal gas. Fugacity coefficient defined by equation (11):

$$\phi_i = \frac{\hat{f}_i}{P_i} \quad (12)$$

a measure of the deviation from ideal gas behaviour. Fugacity coefficient can be calculated based on the equation of state for one of the following expressions

$$RT \ln \phi_i = \int_0^P \left( V_i - \frac{RT}{P} \right) dp \quad (13)$$

$$RT \ln \phi_i = \int_{\infty}^V \left( \left[ \frac{dp}{dn_i} \right]_{V,T,n_{i \neq j}} - \frac{RT}{V} \right) dV + RT \left[ \frac{\sum_i n_i RT}{PV} \right] \quad (14)$$



In accordance with equation (10) is an equilibrium relationship (2) can be shown by equation (14)

$$f_i^{\alpha} = f_i^{\beta} = \dots \dots \dots = f_i^{\kappa} \quad (15)$$

Activity is defined as the ratio  $f_i$  fugacity and standard components  $i$  at the same P and T

$$a_i = \frac{\hat{f}_i(P,T,X)}{\hat{f}_i^{\circ}(P,T,X^{\circ})} \quad (16)$$

In an ideal solution the activity is defined by the equation:

$$a_i^{id} \equiv X_i \quad (17)$$

Activity coefficient of component  $i$ ,  $\gamma_i$  a measure of the deviation from ideal behaviour of the solution:

$$\gamma_i = \frac{a_i}{X_i} \quad (18)$$

On the basis of equations (11-13) the activity of a component of the solution (solid or liquid) can be defined by determining the appropriate fugacity:

$$f_i^L = X_i \gamma_i f_i^{\circ} \quad (19)$$

Activity coefficient  $\gamma_i$  can be calculated based on the values of excess molar enthalpies energy  $g^E$

$$RT \ln \gamma_i = \left[ \frac{d[\sum_i n_i g^E]}{dn_i} \right]_{P,T,n_{i \neq j}} = g_i^{-E} \quad (20)$$

It is standard Fugacity liquid or solid components, Fugacity and components in clean condition and is associated with the sublimation pressure  $P_{i\text{sub}}$  and vapour  $P_{i\text{sat}}$

$$f_i^S(P_{i\text{sub}}, T) = f_i^V(P_{i\text{sub}}, T) = \phi_i^V(P_{i\text{sub}}, T) P_{i\text{sub}} \quad (21)$$

Respectively

$$f_i^S(P, T) = f_i^S(P_{i\text{sub}}, T) \exp \left[ \int_{P_{i\text{sub}}}^P \frac{d\mu_i^S}{RT} \right] = f_i^S(P_{i\text{sub}}, T) \exp \left[ \int_{P_{i\text{sub}}}^P \frac{V_i^S}{RT} dp \right] \quad (22)$$

Where  $V_i^S$  molar volume of pure solid components i. From equations (15) and (16) we get

$$f_i^S(P, T) = \phi_i^S(P_{i\text{sub}}, T) P_{i\text{sub}} \left[ \int_{P_{i\text{sub}}}^P \frac{V_i^S}{RT} dp \right] \quad (23)$$

In a similar way, we can get that

$$f_i^L(P, T) = \phi_i^V(P_{i\text{sat}}, T) P_{i\text{sat}} \left[ \int_{P_{i\text{sub}}}^P \frac{V_i^L}{RT} dp \right] \quad (24)$$

At low pressure fugacity coefficients and exponential equations members (23 and 24) are equal to 1 and it follows that

$$f_i^S \approx P_{i\text{sub}} \quad \text{and} \quad f_i^L \approx P_{i\text{sat}} \quad (25)$$

### 2.1.1 Critical values

Two phases could appear in one in critical conditions of temperature and pressure. Critical values can be calculated by solving the two equations defined by Gibbs. For a system of N equations of the two components are [199].

$$(D_{SP})_T = \begin{vmatrix} \frac{d^2 a}{dv^2} & \frac{d^2 a}{dv dv_1} & \frac{d^2 a}{dv dv_2} & \dots & \frac{d^2 a}{dv dv_{N-1}} \\ \frac{d^2 a}{dv dv_1} & \frac{d^2 a}{dv_1^2} & \frac{d^2 a}{dv_1 dv_2} & \dots & \frac{d^2 a}{dv_1 dv_{N-1}} \\ \frac{d^2 a}{dv dv_2} & \frac{d^2 a}{dv_1 dv_2} & \frac{d^2 a}{dv_2^2} & \dots & \frac{d^2 a}{dv_2 dv_{N-1}} \\ \vdots & \vdots & \vdots & \ddots & \vdots \\ \frac{d^2 a}{dv dv_{N-1}} & \frac{d^2 a}{dv_1 dv_{N-1}} & \frac{d^2 a}{dv_2 dv_{N-1}} & \dots & \frac{d^2 a}{dv_{N-1}^2} \end{vmatrix} = 0 \quad (26)$$

$$(D_C)_T = \begin{vmatrix} \frac{\partial D_{SP}}{\partial v} & \frac{\partial D_{SP}}{\partial x_1} & \frac{\partial D_{SP}}{\partial x_2} & \dots & \frac{\partial D_{SP}}{\partial x_{N-1}} \\ \frac{\partial^2 a}{\partial v \partial x_1} & \frac{\partial^2 a}{\partial x_1^2} & \frac{\partial^2 a}{\partial x_1 \partial x_2} & \dots & \frac{\partial^2 a}{\partial x_1 \partial x_{N-1}} \\ \frac{\partial^2 a}{\partial v \partial x_2} & \frac{\partial^2 a}{\partial x_1 \partial x_2} & \frac{\partial^2 a}{\partial x_2^2} & \dots & \frac{\partial^2 a}{\partial x_2 \partial x_{N-1}} \\ \vdots & \vdots & \vdots & \ddots & \vdots \\ \frac{\partial^2 a}{\partial v \partial x_{N-1}} & \frac{\partial^2 a}{\partial x_1 \partial x_{N-1}} & \frac{\partial^2 a}{\partial x_2 \partial x_{N-1}} & \dots & \frac{\partial^2 a}{\partial x_{N-1}^2} \end{vmatrix} = 0 \quad (27)$$

Where  $a$  is the molar Helmholtz energy

The molar Helmholtz energy is obtained from the equation of state and statements as defined in relation  $\left(\frac{\partial a}{\partial v}\right)_{T,x} = -P$  all excerpts from the two determinants can be obtained on the basis of the corresponding equation of state. For pure components in these determinants remain only the elements (1.1), and get familiar conditions for the critical values of temperature and pressure

$$\left(\frac{\partial p}{\partial v}\right)_T = 0 \quad \text{and} \quad \left(\frac{\partial^2 p}{\partial v^2}\right)_T = 0 \quad (28)$$

According to the equation (22) isothermal compressibility  $K_T$  tends to infinity at the critical value, it is

$$K_T = -\frac{1}{v} \left(\frac{\partial v}{\partial p}\right)_T \quad (29)$$

And modern physics experiments have shown that all classical, analytical equations of state, such as a cubic equation of state, are ineffective in trying to explain how divergent  $K_T$  and other thermodynamic quantities. The reason for this is that they are based on the mean-field theory, which neglects higher density fluctuations near the critical value. If the deviation from the critical value defined by the equations:

$$\Delta P^* = \frac{P - P_c}{P_c}, \quad \Delta T^* = \frac{T - T_c}{T_c}, \quad \Delta \rho^* = \frac{\rho - \rho_c}{\rho_c} \quad (30)$$

Then the thermodynamic quantities diverge in the way set out in **Table 11**.

**Table 11.** Laws, paths, critical exponents and their relations

Parameter	law	Path
isothermal compressibility	$K_T \propto  \Delta T^* ^{-\gamma}$	critical izohora
isochoric heat capacity	$C_V \propto  \Delta T^* ^{-\alpha}$	critical izohora
density difference	$(\rho - \rho_c) \propto  \Delta T^* ^{\beta}$	two phases
pressure	$\Delta \rho^* \propto  \Delta T^* ^{\delta}$	critical isotherm

The values of the exponent  $\alpha$ ,  $\beta$ ,  $\gamma$  and  $\delta$  are universal and are given in **Table 12**.

**Table 12.** The values of critical exponents

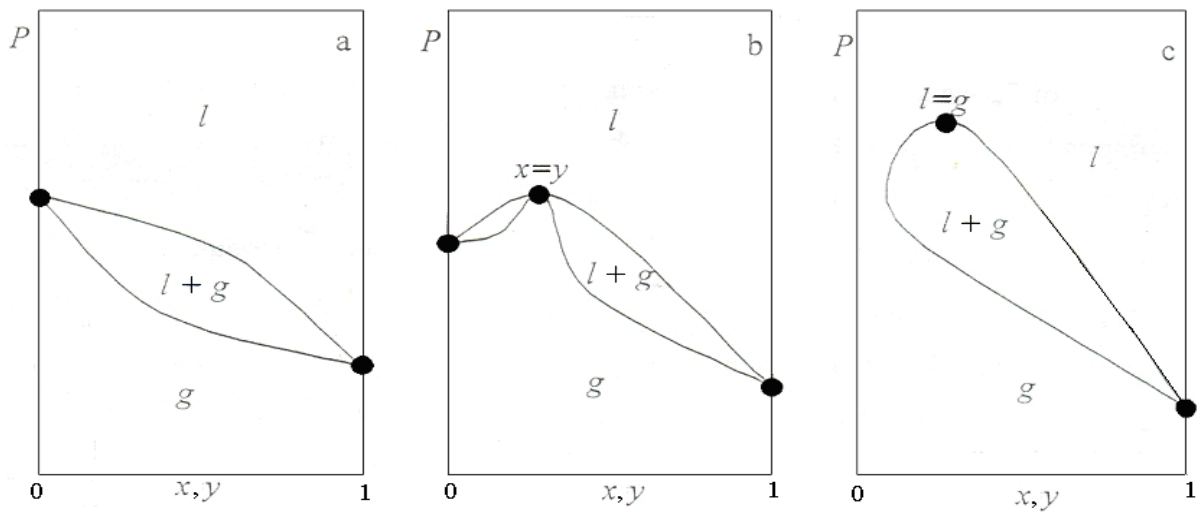
Superscript	Real fluid	Ideal fluid
$\alpha$	0	0.110
$\beta$	0.5	0.326
$\gamma$	1	1.239
$\delta$	3	4.80

Expressions given in Table 12 and the values of the critical exponents given in Table 11 can be accurately determined thermodynamic behavior of pure components in the vicinity of the critical point, while for values that are not close to the critical need to apply mean-field theory. The theory that could give accurate values of thermodynamic parameters around a critical value, and when they are not close to the so-called cross-over theory (cross-over theory). But this theory is very complex and can be implemented only if the critical values are known.

### 2.1.2 Classification of phase equilibrium

For two components ( $N = 2$ ) phase rule  $F = 2 - \pi + N$  is reduced to  $F = 4 - \pi$ . According to this equation up to four phases can be in equilibrium in the binary system ( $F = 0$ ) and the largest number of degrees of freedom needed to describe the system is 3 ( $\pi = 1$ ). This means that the overall equilibrium phase may present a three-dimensional  $P, T, x$  diagram. For a system in equilibrium is a characteristic that all have the same  $P$  and  $T$ , but different compositions  $x$ . In  $P, T, x$  diagram of the equilibrium phase four with four data points ( $F = 0$ ), the three phases of the three curves ( $F = 1$ ), the two phases of the two surfaces ( $F = 2$ ) and a phase of District ( $F = 3$ ). Azeotrope critical condition and curves are presented [199].

If one of the variables considered as a constant, we get  $P - x - y, t - x - y, P, T$  diagrams. **Figure 19** presented three different binary gas equilibrium (g) and liquid (l). The balance of these phases is represented by the so-called binodal curves. When the pressure for a given composition is between binodal curves, the mixture separates into two phases whose composition is determined curves. Mixtures that are outside of this area will be a single-phase (liquid or gas). Binodal curve may have common points of the components were cleaned, and the isotropic critical point [199].



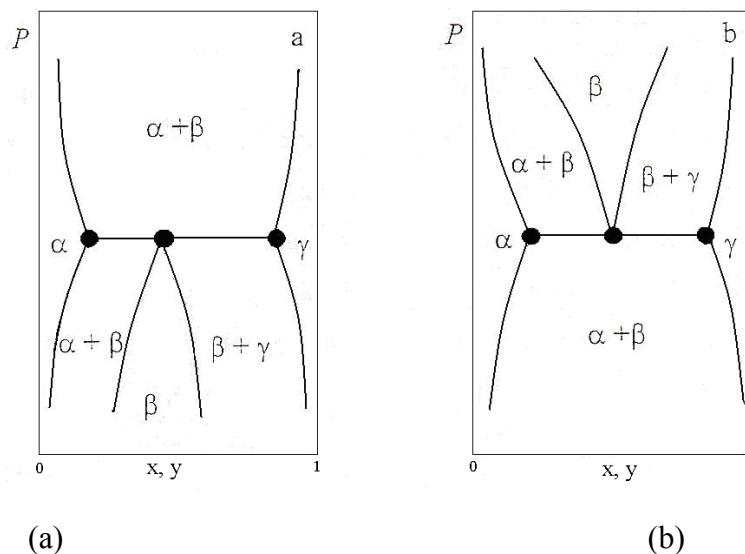
(a)

(b)

(c)

**Figure 19.** The balance of two stages - three cases analyzes of two phases are equal: a) The boiling point of pure component b) Azeotropic point c) critical point

The balance of the three phases of the  $P - x - y$  -  $t - x - y$  diagram is represented by three points. All of the mixture composition corresponding to that point will be divided into three phases. **Figure 20** presented three-phase equilibrium in  $P - x - y$  diagram. Around three-phase equilibrium, there are three two-phase and three-phase field area. According to the theory of phase transformation two-phase and single-phase field must be arranged as shown in Figure 2.2a and 2.2b [199].



(a)

(b)

**Figure 20.** Possible positions of single and two-phase equilibrium phase equilibrium around the  $P - x - y$  diagram [199]

### 2.1.3 Calculation of phase equilibrium at high pressure

The purpose of phase equilibrium calculations to predict thermodynamic properties of mixtures, without the use of an experiment, or that the existing data are extrapolated to other temperatures and pressures. To develop any thermodynamic calculation it is necessary to adopt an appropriate model and know the parameters required for this model. In the case of phase equilibrium at high pressure equation of state is used, which can describe the properties of both phases [199].

General starting equation is the equality of fugacity of each component in each phase

$$f_i^L = (T, P, X_i) = f_i^V = (T, P, y_i) \quad (31)$$

$$\text{Or introducing a fugacity coefficient } \phi_i^V = \frac{f_i^V}{P y_i} \text{ and } \phi_i^L = \frac{f_i^L}{P x_i} \quad (32)$$

$$\phi_i^V y_i = \phi_i^L x_i \quad i=1,2,\dots,N \quad (33)$$

Fugacity coefficients of components are calculated using the appropriate equation of state based on the following equation (the equation is written for the gas phase, but the same can be written for the liquid phase):

$$\ln \frac{f_i^V(T, P, y_i)}{y_i P} = \ln \phi_i^V = \frac{1}{RT} \int_{\infty}^V \left[ \frac{RT}{V} - n \left[ \frac{\partial P}{\partial n_i} \right]_{T, P, n_{j \neq i}} \right] dV - \ln \frac{PV}{RT} \quad (34)$$

The equilibrium phase can be represented in different ways. In this paper we will use the P-x-y diagrams. This requires draw liquid and gas phases at given temperatures and pressures.

### 2.1.4 Equations of state used for these systems

#### 2.1.4.1. Peng Robinson equation of state

The Peng-Robinson EOS has become the most popular equation of state for natural gas systems in the petroleum industry. During the decade of the 1970's, D. Peng was a PhD student of Prof. D.B. Robinson at the University of Alberta (Edmonton, Canada). The Canadian Energy Board sponsored them to develop an EOS specifically focused on natural



gas systems. When you compare the performance of the PR EOS and the SRK EOS, they are pretty close to a tie; they are “neck to neck,” except for a slightly better behaviour by the PR EOS at the critical point. A slightly better performance around critical conditions makes the PR EOS somewhat better suited to gas/condensate systems [200].

Moreover for a system consisting of a mixture of hydrogen - hydrocarbons for a description of vapor-liquid equilibrium using the Peng-Robinson equation of state with quadratic mixing rule:

$$P = \frac{RT}{V-B} - \frac{a(T)}{V^2 + 2bV - b^2} \quad (35)$$

Where  $a_i$  and  $b_i$  parametric equation of state for pure components:

$$a_i(T) = 0.45724 \frac{R^2 T_c^2}{P_c} \left[ 1 + (0.37464 + 1.54226\omega - 0.26992\omega^2)(1 - \sqrt{T_r}) \right]^2 \quad (36)$$

$$b_i = 0.0778 \frac{RT_c}{P_c} \quad (37)$$

#### 2.1.4.2. Redlich-Kwong Aspen equation of state

$$P = \frac{RT}{V-b} - \frac{a(T)}{V^2 + bV} \quad (38)$$

Where  $a_i$  and  $b_i$  parametric equation of state for pure components [201].

$$a_i = f(T, T_{ct}, P_{ct}, \omega_i, \eta_i) \quad (39)$$

$$b_i = f(T_{ct}, P_{ct}) \quad (40)$$

For polarity factor  $\eta$  is taken zero for compounds, methanol and triolein.

#### Van der Waals

[201]

$$a = \sum_{i=1}^N \sum_{j=1}^N x_i x_j a_{ij} \quad (41)$$

$$b = \sum_{i=1}^N \sum_{j=1}^N x_i x_j b_{ij} \quad (42)$$

$$a_{ij} = \sqrt{a_i a_j} (1 - K_{ij}) \quad \text{Where} \quad K_{ij} = K_{ji} \quad (43)$$

$$b_{ij} = \frac{b_i + b_j}{2} (1 - l_{ij}) \quad \text{Where } l_{ij} = l_{ji} \quad (44)$$

Moderate deviations for both phases are calculated based on the relative deviation of secondary roots (relative root-mean-square deviations, RMSDr) defined by the equation:

$$RMSDr = 100. \sqrt{\frac{1}{n} \left( \frac{\tau_i^{exp} - \tau_i^{cal}}{\tau_i^{exp}} \right)^2} [\%] \quad (45)$$

Where  $\tau$  is the mole fraction of component  $i$  in vapor or liquid phase.

## 2.2. Mathematical modelling fundamentals

Process model is combination of different system (reactor system, separation system, control and safety system and so on) of a process plant (**Figure 21**). Process modelling is not a new concept to chemical engineer. Due to advancement of computer base mathematical and process modelling software modelling played an important role in design and operation by simulation and optimisation study. It arises from the traditional disciplines such as transport phenomena, chemical kinetics, reaction design and thermodynamics. The variety of products made by processes of chemical technology is overwhelming; it comprises inorganic and organic basic chemicals. The equipment (apparatus, machines, pipelines, automation and safety systems, etc.) has to be chosen so that the investments made in them yield the maximum economy. The plant must be reliable and sufficiently flexible. The computer aided process modelling permit the chemical process to be interpreted in a computer base software package to understand the chemical process behaviour quickly.

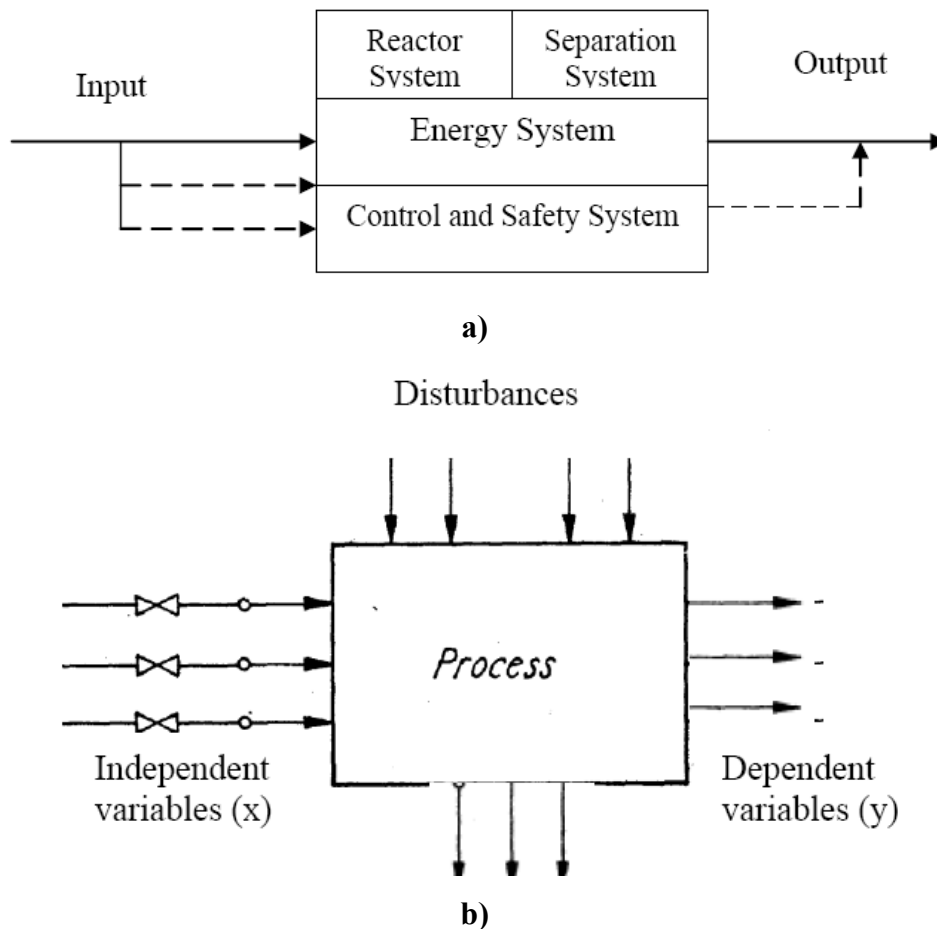


**Figure 21.** Basic chemical process model a) and process model b)

### 2.2.1. Types of process model

The conceptual representation of a real physical system can be translated in mathematical terms adopting the usual types of models and their combinations:

1. **Deterministic models:** the relationships between different quantities of different engineering system are given via the continuum equations describing the conservation of mass, momentum and energy and the relevant constitutive equations. The appropriate differential equations are solved for a set or system of process variables and parameters;
2. **Statistical-Stochastic models:** the principle of uncertainty is introduced instead of the possibility of assigning defined values to each dependant variable for a set of values of

independent ones. Being the input-output relationships and the structure of elements not precisely known, the use of statistical tools is implemented;

3. **Empirical models:** they are directly connected to the functional relationships between variables and parameters by fitting empirical data, without assigning any physical meaning and consequently any cause to their relationships. Examples of empirical models are those based on polynomials used to fit empirical data by the “least square” method,

or using more recent tools such as neural network and fuzzy logic techniques or fractal theory.

Two types of process (steady state and dynamic) are prominent in chemical engineering. A steady state model ignores the changes in process variables with time whereas the dynamic model considers dynamic characteristics. The dynamic models are useful to understand the start-up and shutdown characteristics of the process. According to the modelling complexity (see Figure 1) different modelling techniques should have be chosen:

- Empirical Models or Regression Model/Statistical Model
- Black Box Model
- First Principle Models
- Reduced model (Linearization) Transfer Function

### **2.2.2. Models development**

Specific task is demonstrating how, through the use of information coming from experimental investigations and simulation, it is possible checking the validity of the assumptions made and fine tuning the predictive mathematical model capability.

The possibility of analysing and quantifying the role played by each step of the process is examined in order to define the relevant mathematical expressions. The latter allows getting useful indications about the impact of different operating conditions on the role of each step discussing the improvements in operation (efficiency of the process) brought about by simulation.

The general strategy of analysis of real systems consists of the following steps:

### *2.2.2.1. Problem definition*

Preliminary it is necessary to pick up the essential information related to the case study/project; establish the objectives and related priority; state what is given and what is required. Then, it should be analysed the entire process and the system in which it develops to fix the independent and dependent variables. When the process and/or the system is so complex that it is difficult either understand and describe it as a whole, it can be break down into subsystems. They do not necessary have to correspond to any physical parts of the real process; they can be hypothetical elements which are isolated for detailed considerations. After the process has been split up into the elements and each part has been analysed, relationships existing among the subsystems have to be defined and assembled in order to describe the entire process. Through the analysis of the variables and their relationships, it is possible to define a simple and consistent set which is satisfactory for the scope. While doing this, we can simplify the problem by introducing some assumptions so that the mathematical model can be easy to manipulate. These simplifications had to be later evaluated to have assurance of representing the real process with reasonable degree of confidence.

### *2.2.2.1. Model development*

Defining the problem means that it should be translated into mathematical terms. Models based on transport phenomena principles, the first category of mathematical models mentioned above, are the common type models used in chemical engineering. The various mathematical levels (molecular, microscopic, multiple gradient, maximum gradient and macroscopic) used to represent the real processes are chosen according to the complexity of the internal detail included in the process description. For engineering purposes, molecular representation is not of much direct use. Microscopic and multiple-gradient models, give a detailed description of processes but they are often excessively complex for practical applications. Maximum-gradient model level may be considered a multiple-gradient model in which the dispersion terms are deleted and only the largest component of the gradient of the dependent variable is considered in each balance. These models are more easy to deal with and generally satisfactory for describing chemical systems Then, macroscopic scale is used to represent a process ignoring spatial variations and considering properties and variables homogeneous throughout the entire system. In this way no spatial gradients are involved in

equations and time remains the only differential independent variable in the balances. Mathematical description results greatly simplified, but there is a significant loss of information regarding the behaviour of the systems.

The development of a mathematical model requires not only to formulate the differential or algebraic equations but as well to select appropriate initial and/or boundary conditions. In order to determine the value of the constants which are introduced in the solution of differential equations, it is necessary to fix a set of  $n$  boundary conditions for each  $n$ th order derivative with respect to the space variable or with respect to time. In particular, boundary conditions can influence the selection of a coordinate system used to formulate the equations in microscopic and multiple-gradient models.

After setting up the model, the model parameters should be evaluated. In the microscopic models, the required parameters are transport properties. Various methods of estimating values for pure components and for mixtures are available in literature. The “effective” parameters, introduced in mathematical models to describe transport phenomena in homogeneous or multiphase systems, are clearly empirical and must be determined for the particular system of interest. In literature predicting relationships only for traditional systems may be available.

If deterministic models cannot be satisfactory applied in developing a model, stochastic or empirical models can be used. These model-building techniques have more limited applications as a consequence of that a lot of the limitations of deterministic models apply also to stochastic and empirical ones. Moreover, the empirical models show additional limitations due to the fact that they are valid only for the process for which data were collected.

Whatever is the model-building technique adopted, as more complex is the mathematical description of the process, as more difficult is its solution. Therefore the process description shall be a compromise among the required details, the available information on model parameters and the limitations of the available mathematical tools.

#### *2.2.2.3. Model solving*

The goal of this step is to obtain the analytical solution (if this is possible) and/or, failing that, the numerical solution of the model equations, which may include algebraic equations, differential equations and inequalities. For many complex chemical processes the

model result is set of nonlinear equation requiring numerical solution. The most common way to deal with this is to use modelling software such as gPROMS, COMSOL, Aspen Custom Builder or other software such as Matlab.

#### 2.2.2.4. Model verification and validation

These actions are essential part of the model building process. Verification concerns with building the model right. In this step a comparison between the chosen conceptual representation and the outcome of the model is carried out to evaluate its suitability to describe the conception. Verification is achieved through tests performed to ensure that the model has been implemented properly and that the input parameters and logical structure of the model have been correctly represented.

Validation concerns with building the right model. This step grants that the model is in line with the intended requirements with reference to the methods adopted and outcome. Validation is achieved through an interactive process of comparing prediction data to experimental ones and using discrepancies between the values and information coming from comparison to improve the model. This procedure is repeated as many times as desired model accuracy is achieved.

A mathematics routes to solving engineering problems are summarised on **Figure 22**.

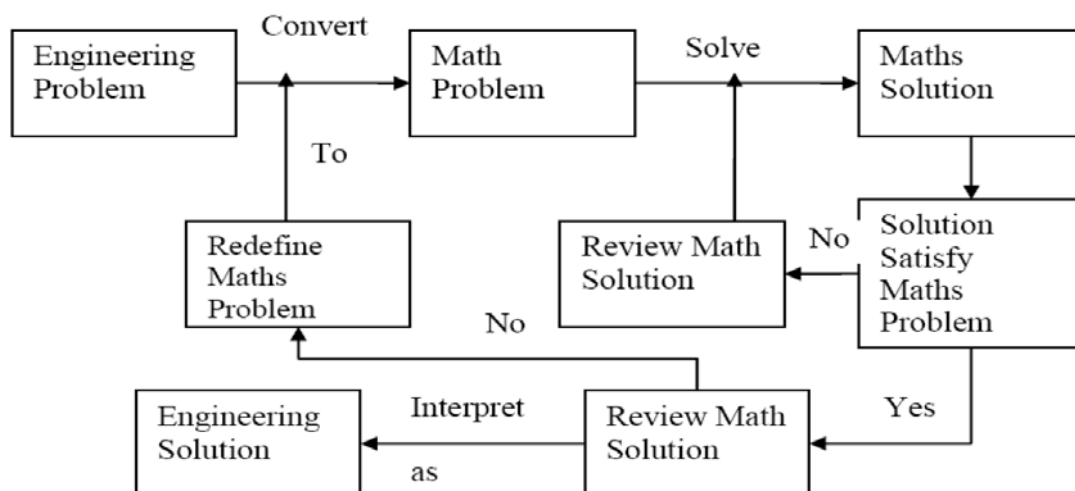


**Figure 22.** A mathematics routes to solving engineering problems

### 2.2.3. Model Assumption

The complexity of model depends on the types of assumption considered the mathematical and computational difficulties occurring in solving the model equations (computing time, store location) are reasons for the model simplifications required in the majority of cases. It also leads to appropriate type of modelling techniques. Key to a good model lies in what and how simplification is introduced; it is very important to understand what aspects of the system the model is intended to describe, and what are the model's limitations as a result of the simplification. Some of common assumptions in chemical reactor modelling are presented on **Figure 23**.

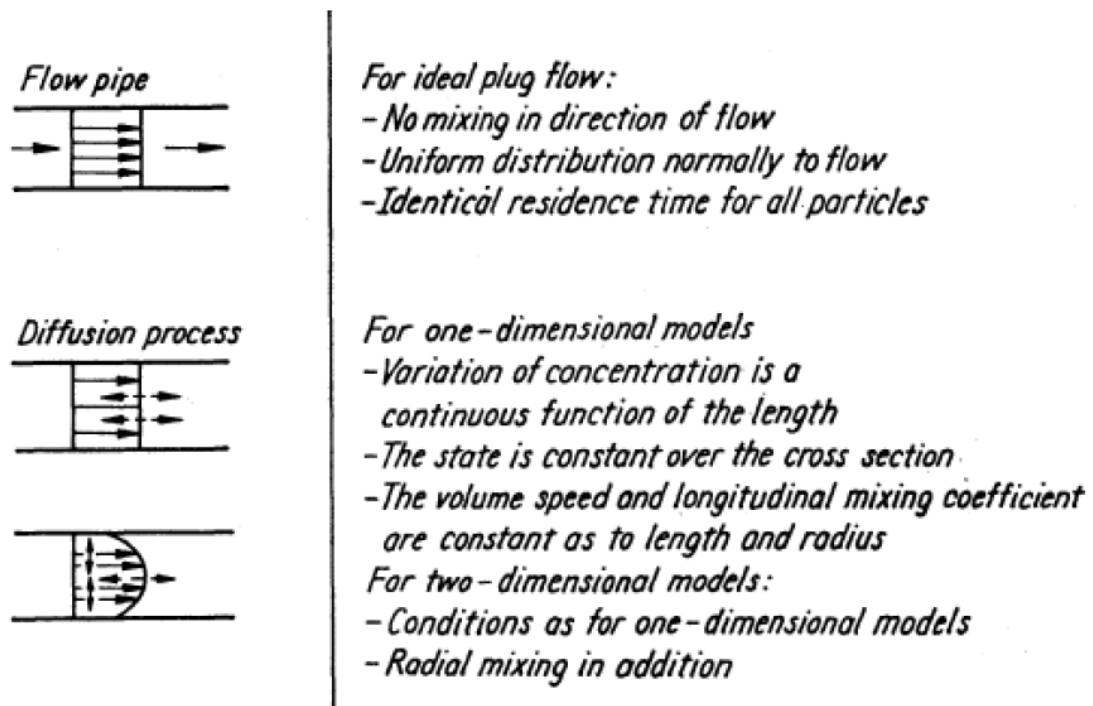


**Figure 23.** Some of common assumptions in chemical reactor modelling

### 2.2.4. Computer Aided Process Engineering

Over the past decade there has been an increasing demand for suitable material in the area of mathematical modeling as applied to science, engineering, business and management. Recent developments in computer technology and related software have provided the



necessary tools of increasing power and sophistication which have significant implications for the use and role of mathematical modeling in the above disciplines. In the past, traditional methods have relied heavily on expensive experimentation and the building of scaled models, but now a more flexible and cost effective approach is available through greater use of mathematical modeling and computer simulation. Due to the advancement of the microcomputers, the models are now directly connected to the plant operation to carry out the plant performance calculations, generate management information and also to perform limited alarm diagnostic. With the improvement of the microcomputers and availability of the cheaper microcomputers, process modeling using the microcomputers has become cost effective.

Any experimental work is expensive and the real plant operation is an expensive and time consuming. Computer aided modeling, simulation and optimization saves the time and money by providing the fewer configuration of the experimental work. In addition, computer simulation, optimization saves the money in design and operation. The long-term performance and reliability of individual plant vary from plant to plant and day to day for various reasons such as operating conditions, scaling and fouling of heat transfer surfaces in boilers and different desalination units. Therefore, better operations of the existing plant depend on the better understanding of the different parameters of the plant. Simulation helps to visualize the ultimate picture and trends of various conditions of existing plant as well as those of a new situation of the plant.

The typical modelling approach (**Figure 24**) in recent years for simulation and optimisation uses numerical solvers. The numerical solvers may involve SQP based methods or any other non-gradient based optimiser such as GA, SA algorithm and in simulation the solver may involve Newton-Raphson method, etc.

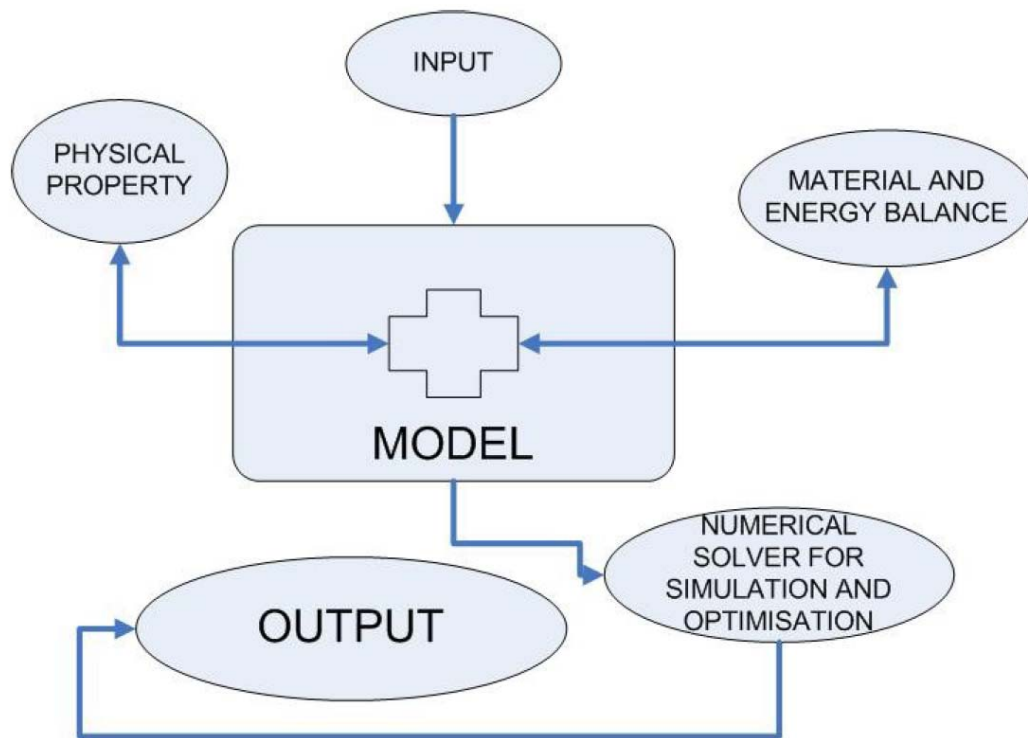


**Figure 24.** Typical simulation and optimization architecture

Here is a list of related commercial commonly used software for modelling, simulation and optimisation in chemical industries:

1. GAMS
2. ASPEN HySys
3. gPROMS
4. Simulink / MATLAB
5. Berkeley Madonna and others

Process mathematical model is a collection of (set) of equations that describe some aspect of the chemical system under investigation. For many complex chemical processes the model result is set of nonlinear equation requiring numerical solution. The most common way to deal with this is to program the equations using the modelling software such as gPROMS, Aspen Custom Builder or other engineering Software such as Matlab.

### 3. EXPERIMENTAL DATA USED FOR MODEL DEVELOPMENT

#### 3.1. Multiphase system at high pressure and temperature – analysis procedure

The simulation of phase equilibrium was performed using UniSim® software (Honeywell Canada). The procedure used for equilibrium simulation was performed by defining the components, followed by calculation of the critical thermodynamic parameters and applying appropriate EOS.

##### *3.1.1. Procedure for high pressure phase equilibria simulation for biodiesel reaction system*

Since oleic acid is one of the most abundant fatty acids in majority of vegetable oils (canola, rapeseed, soybean and sunflower oil) and since it is the component with well defined thermodynamic properties, glycerol tri-oleate was chosen as the key component in the simulation (triolein), as well as glycerol mono- and di-oleate for partially converted trioleins. RK-Aspen thermodynamic model was used as it was previously determined to be the best one for the similar system containing triolein and methanol at near critical conditions [202,203]. The rigorous flash option for VLL equilibria was also used in the simulation. The Constantinou–Gani group contribution method was used for estimation of thermodynamic properties [204-217]. The method was applied to the following physical and thermodynamic properties of pure compounds: the normal boiling point, the critical pressure, the critical temperature, the critical volume, the standard enthalpy of vaporization at 298 K, the standard Gibbs energy, the standard enthalpy of formation at 298 K, the acentric factor and liquid molar volume at 298 K. The physical and thermodynamic parameters are presented in **Table 13**.

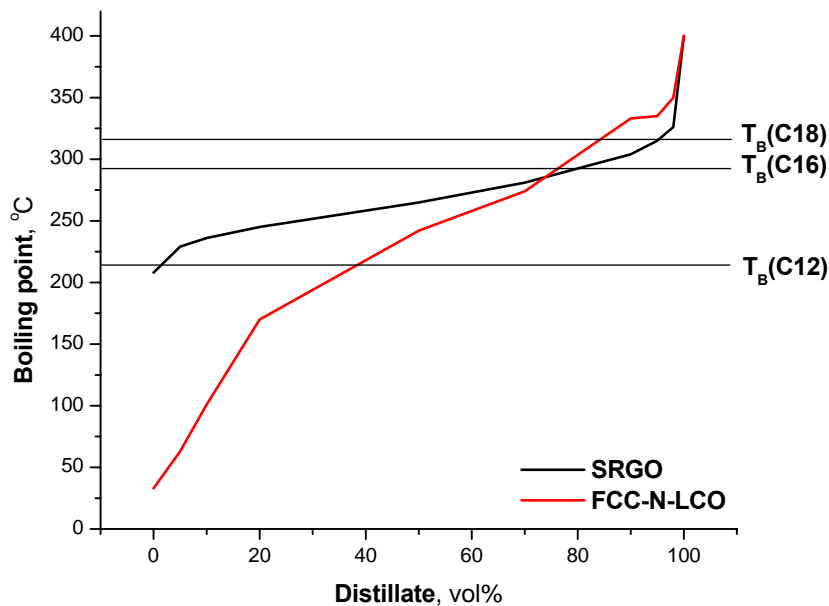
**Table 13.** The physical and thermodynamic parameters of tri-, di-, mono-olein, methyl oleate, ethyl oleate

Parameter	Triolein	Dirolein	Monoolein	Methyl oleate	Ethyl oleate
<b>M</b> , g/mol	885.45	621.00	356.55	296.49	310.51
<b>T<sub>B</sub></b> , K	827.40	765.03	674.82	595.93	617.00
<b>V<sub>B</sub></b> , m <sup>3</sup> /kmol	2.708	1.106	0.533	0.489	0.489
<b>V<sub>1</sub></b> (298K), m <sup>3</sup> /kmol	0.958	0.623	0.360	0.341	0.341
<b>T<sub>C</sub></b> , K	977.88	920.20	835.06	721.02	764.00
<b>P<sub>C</sub></b> , bar	3.34	5.05	10.56	11.03	12.80
<b>V<sub>C</sub></b> , m <sup>3</sup> /kmol	3.250	2.830	1.254	1.108	1.060
<b>ω</b>	1.9782	1.7632	1.5324	1.0494	1.0494
<b>ΔG<sub>f</sub></b> (298K), kJ/kmol	-1.8E+05	-3.00E+05	-3.23E+05	-1.20E+05	-1.17E+06
<b>ΔH<sub>f</sub></b> (298K), kJ/kmol	1.97E+05	8.08E+05	5.69E+05	-6.40E+05	-6.26E+05
<b>ΔH<sub>v</sub></b> (298K), kJ/kmol	3.02E+05	2.19E+05	9.01E+04	6.36E+04	6.36E+04

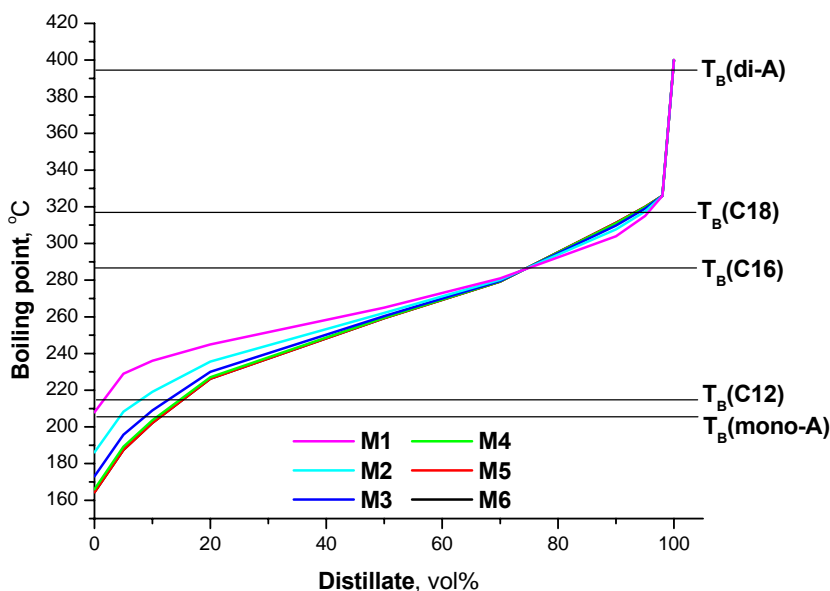
M, g/mol – molecular weight; T<sub>B</sub>, K- normal boiling point; V<sub>B</sub>, m<sup>3</sup>/kmol – liquid volume at T<sub>B</sub>; V<sub>1</sub> (298K), m<sup>3</sup>/kmol - liquid molar volume at 298 K; T<sub>C</sub>, K – critical temperature; P<sub>C</sub>, bar - critical pressure; V<sub>C</sub>, m<sup>3</sup>/kmol - liquid molar volume at critical point; ω - acentric factor; ΔG<sub>f</sub> (298K), kJ/kmol - standard Gibbs energy at 298 K; ΔH<sub>f</sub> (298K), kJ/kmol - standard enthalpy of formation at 298 K; ΔH<sub>v</sub> (298K), kJ/kmol - standard enthalpy of vaporization at 298 K

### 3.1.2. Procedure for high pressure phase equilibria simulation for diesel reaction system

The reaction mixture which entering the HDS unit has four components: hydrogen (H<sub>2</sub>), methane (CH<sub>4</sub>), straight run gas oil (SRGO) and in some inputs FCC naphtha and light cycle oil LCO (in further text FCC N–LCO). The distillation curves for both SRGO and FCC N-LCO are presented on **Figure 25a**. Since the diesel stream is mixture of SRGO and FCC N-LCO, the six characteristic input points, mixtures (M1-M6) were analyzed and their distillation curves are shown on **Figure 25b**.



a)



b)

**Figure 25.** The distillation curves for **a)** SRGO and FCC N-LCO and **b)** the six characteristic input mixtures M1-M6: M1-pure SRGO, M2 – 87.5vol% SRGO and 12.5vol% FCC N-LCO, M3 - 80vol% SRGO and 20vol% FCC N-LCO, M4 - 76vol% SRGO and 24vol% FCC N-LCO, M5 and M6 - 75vol% SRGO and 25vol% FCC N-LCO

As could be seen from **Figure 25b**, each mixture can be approximated with C12 to C18 hydrocarbons (n-dodecane, n-hexadecane and n-octadecane) and/or some mono- and di-aromatic compounds (tetraline and phenantrene). The impact of number of components which approximated the diesel mixture, on simulation results was analysed in this paper. The

mixture of SRGO and FCC N-LCO was approximated with two components (n-dodecane and n-octadecane), three (n-dodecane, n-hexadecane and n-octadecane) and five components (three hydrocarbons: n-dodecane, n-hexadecane, n-octadecane and one monoaromate: tetraline and one diaromate: phenantrene). In **Table 14** was summarised all composition for each input mixture if the two, three or five components approximation is applied. The sulfur distribution is accepted from our previously published paper [218].

**Table 14.** The compositions of input mixtures depending on number of components used for their approximation

<b>Input data</b>							
<b>Input streams</b>		<b>Gas + M1</b>	<b>Gas + M2</b>	<b>Gas + M3</b>	<b>Gas + M4</b>	<b>Gas + M5</b>	<b>Gas + M6</b>
T <sub>input</sub>	<b>K</b>	<b>606.0</b>	<b>605.0</b>	<b>602.0</b>	<b>602.0</b>	<b>601.0</b>	<b>600.0</b>
T <sub>output</sub>	<b>K</b>	<b>617.5</b>	<b>616.5</b>	<b>609.7</b>	<b>609.3</b>	<b>606.1</b>	<b>604.1</b>
Sulfur conversion	<b>mol%</b>	<b>99.49</b>	<b>99.26</b>	<b>99.41</b>	<b>99.37</b>	<b>99.23</b>	<b>99.27</b>
<b>Input stream composition</b>	<b>approx. compound</b>	<b>mol%</b>					
<b>Approximation of diesel fraction with two compounds</b>							
Hydrogen	H <sub>2</sub>	0.709562	0.709590	0.710063	0.711973	0.715502	0.721490
Methane	CH <sub>4</sub>	0.211896	0.211904	0.212045	0.212615	0.213669	0.215458
BT	C12	0.006374	0.007160	0.005717	0.005986	0.005215	0.004564
DBT1	C18	0.000620	0.000697	0.000556	0.000582	0.000507	0.000444
DBT2	C18	0.000779	0.000875	0.000699	0.000732	0.000637	0.000558
DBT3	C18	0.000757	0.000850	0.000679	0.000711	0.000619	0.000542
non-sulfur light fraction	C12	0.013739	0.013194	0.014222	0.012769	0.011301	0.008029
non-sulfur heavy fraction	C18	0.029239	0.028691	0.029538	0.029097	0.03679	0.036577
Diaromatics	C18	0.007477	0.007477	0.007582	0.007443	0.001993	0.001949
Monoaromatics	C12	0.019561	0.019562	0.018899	0.018093	0.013767	0.010389
<b>Approximation of diesel fraction with three (five) compounds</b>							
Hydrogen	H <sub>2</sub>	0.709562	0.709590	0.710063	0.711973	0.715502	0.721490
Methane	CH <sub>4</sub>	0.211896	0.211904	0.212045	0.212615	0.213669	0.215458
BT	C12	0.006374	0.007160	0.005717	0.005986	0.005215	0.004564
DBT1	C18	0.000620	0.000697	0.000556	0.000582	0.000507	0.000444
DBT2	C18	0.000779	0.000875	0.000699	0.000732	0.000637	0.000558
DBT3	C18	0.000757	0.000850	0.000679	0.000711	0.000619	0.000542
non-sulfur light fraction	C12	0.013739	0.013194	0.014222	0.012769	0.011301	0.008029
non-sulfur mid fraction	C16	0.029196	0.028691	0.029538	0.029097	0.032702	0.033678
non-sulfur heavy fraction	C18	0.000043	0.000000	0.000000	0.000000	0.004088	0.002899
Diaromatics	C18 (di-A)	0.007477	0.007477	0.007582	0.007443	0.001993	0.001949
Monoaromatics	C16 (mono-A)	0.019561	0.019562	0.018899	0.018093	0.013767	0.010389

The physical and thermodynamic parameters of normal alkanes, n-dodecane, n-hexadecane and n-octadecane, and mono- and di-aromatic compounds, tetraline and

phenantrene, are presented in **Table 15** and are obtained from the database of Unisim software based on DIPPR data.

**Table 15.** The physical and thermodynamic parameters of normal alkanes and mono and di-aromatic compound

Parameter	H <sub>2</sub>	CH <sub>4</sub>	C <sub>12</sub> H <sub>24</sub>	C <sub>16</sub> H <sub>32</sub>	C <sub>18</sub> H <sub>36</sub>	tetraline	phenantrene
M, g/mol	2.02	16.04	170.34	226.45	254.50	132.21	202.26
T <sub>B</sub> , °C	-252.76	-161.49	216.323	286.864	316.71	207.62	394.8
V <sub>B</sub> , m <sup>3</sup> /kmol	0.029	0.038	0.287	0.397	0.454	0.161	0.230
V <sub>1</sub> (298K), m <sup>3</sup> /kmol	0.054	0.054	0.227	0.292	0.325	0.136	0.185
T <sub>C</sub> , °C	-239.96	-82.586	384.85	449.85	473.85	446.85	662.85
P <sub>C</sub> , bar	13.13	45.99	18.2	14	12.7	36.5	26.1
V <sub>C</sub> , m <sup>3</sup> /kmol	0.064	0.099	0.716	0.944	1.060	0.408	0.660
ω	-0.216	0.012	0.576	0.717	0.811	0.335	0.507
ΔG <sub>f</sub> (298K), J/kmol	-	-	-	-	-	-	-
	-	5.05E+07	4.98E+07	8.22E+07	9.91E+07	1.67E+08	3.27E+08
ΔH <sub>f</sub> (298K), J/kmol	-	-	-	-	-	-	-
	-	7.45E+07	2.91E+08	3.74E+08	4.15E+08	2.66E+07	2.25E+08
ΔH <sub>v</sub> (298K), J/kmol	8.97E+05	8.17E+06	4.44E+07	5.14E+07	5.50E+07	4.24E+07	6.07E+07

M, g/mol – molecular weight; T<sub>B</sub>, K- normal boiling point; V<sub>B</sub>, m<sup>3</sup>/kmol – liquid volume at T<sub>B</sub>; V<sub>1</sub> (298K), m<sup>3</sup>/kmol - liquid molar volume at 298 K; T<sub>C</sub>, K – critical temperature; P<sub>C</sub>, bar - critical pressure; V<sub>C</sub>, m<sup>3</sup>/kmol - liquid molar volume at critical point; ω - acentric factor; ΔG<sub>f</sub> (298K), kJ/kmol - standard Gibbs energy at 298 K; ΔH<sub>f</sub> (298K), kJ/kmol - standard enthalpy of formation at 298 K; ΔH<sub>v</sub> (298K), kJ/kmol - standard enthalpy of vaporization at 298 K

### 3.2. Experimental data for kinetic modelling of biodiesel reaction

The experimental data for kinetic modelling are taken from the previously published data [219]. The experiments eas conducted in the high pressure batch reactor, volume of 2 dm<sup>3</sup>, mechanically agitated at 300 ppm at 150 and 210 °C and 1.0 and 4.5 MPa. The specified amounts of methanol and sunflower oil corresponding to molar ratio 42 to 1 were used. Detailed description of the experimental procedure can be found in the literature [203,219]. The composition profile during reaction for both analysed conditions is shown in **Table 16**.



**Table 16.** The reaction mixture composition profile during methanolysis of sunflower oil at 150 °C and 1.0 MPa, and at 210 °C and 4.5 MPa.

Time, min	Concentration, kmol/dm <sup>3</sup>					
	Experiment 1 (150 °C and 1.1 MPa)					
	MeOH	TG	DG	MG	FAME	Glycerol
0	2.833	6.84E-02	0.00	0.00	0.00	0.00
256	2.807	4.75E-02	1.51E-02	3.71E-03	2.60E-02	8.18E-04
613	2.795	3.92E-02	1.98E-02	5.83E-03	3.83E-02	1.60E-03
1228	2.772	2.95E-02	2.83E-02	9.78E-03	6.07E-02	2.30E-03
1433	2.762	2.40E-02	3.13E-02	1.49E-02	7.08E-02	4.48E-03
1633	2.747	1.74E-02	2.02E-02	2.16E-02	8.57E-02	6.23E-03
1933	2.715	1.03E-02	9.10E-03	2.83E-02	1.18E-01	6.97E-03
2623	2.699	7.49E-03	7.87E-03	2.34E-02	1.34E-01	9.83E-03
3028	2.676	3.04E-03	6.56E-03	1.58E-02	1.57E-01	1.68E-02
9000	2.639	0.00	0.00	0.00	1.94E-01	6.06E-02
Time, min	Experiment 2 (210 °C and 4.5 MPa)					
0	2.835	6.78E-02	0.00	0.00	0.00	0.00
130	2.806	3.56E-02	1.96E-02	1.92E-02	3.35E-02	0.00
160	2.755	3.42E-02	1.49E-02	2.54E-02	4.17E-02	0.00
190	2.735	2.92E-02	1.38E-02	2.83E-02	5.67E-02	0.00
220	2.715	2.20E-02	1.40E-02	2.80E-02	7.97E-02	4.37E-03
250	2.698	1.70E-02	7.89E-03	3.12E-02	1.05E-01	1.24E-02
280	2.675	1.29E-02	5.45E-03	2.78E-02	1.28E-01	2.23E-02
340	2.659	7.02E-03	5.90E-03	1.56E-02	1.58E-01	3.99E-02
400	2.648	3.65E-03	5.13E-03	7.92E-03	1.75E-01	5.17E-02
460	2.641	2.66E-03	5.04E-03	4.64E-03	1.79E-01	5.61E-02
520	2.637	1.49E-03	3.57E-03	2.48E-03	1.86E-01	6.09E-02
580	2.633	3.35E-04	4.96E-04	1.84E-03	1.95E-01	6.58E-02
640	2.632	2.49E-04	2.40E-04	1.44E-03	1.98E-01	6.65E-02
700	2.630	2.31E-04	2.90E-05	1.28E-03	2.00E-01	6.69E-02
760	2.630	0.00	0.00	7.61E-04	2.02E-01	6.77E-02

### 3.3. Experimental data used in the modelling of catalytic hydrotreating reactor for diesel production

The experimental results for the modelling of the catalytic reaction of diesel production were taken from the previously published data [218]. Industrial catalytic reactor used for model development and multiphase hydrotreating reaction simulation, was adiabatic tubular reactor of conventional design with fixed bed of catalyst and trickling flow of reacting fluids. The catalyst bed was divided into two separate layers with flow re-distribution between the layers. Catalyst pellets were packed in conventional manner i.e. dense catalyst loading techniques were not employed in the reactor. A total of 19 m<sup>3</sup> of commercial catalyst was present in both catalyst layers within the tubular vessel with internal diameter of 2.135 m.

Straight run gas oil (SRGO) stream was fed into the catalytic reactor from the atmospheric distillation unit of Refinery Pancevo. Fluid Catalytic Cracking (FCC) naphtha and Light Cycle Oil (LCO) streams were taken from the FCC unit and co-fed with SRGO into the catalytic reactor of hydrotreating process unit. The FCC stream containing naphtha and gas oil fractions was within the 33–335 °C distillation range (in further text FCC N–LCO). Hydrotreating test run was performed over conventional Co-Mo/ $\gamma$ -Al<sub>2</sub>O<sub>3</sub> catalyst with properties shown in **Table 17**.

**Table 17.** Properties of commercial Co-Mo/ $\gamma$ -Al<sub>2</sub>O<sub>3</sub> hydrotreating catalyst used during the test run.

Property	Value
MoO <sub>3</sub> content, %wt.	16.2
CoO content, %wt.	5.0
Na <sub>2</sub> O content, %wt.	0.05
SO <sub>4</sub> content, %wt.	0.3
Compacted bed bulk density, kg/m <sup>3</sup>	737
Surface area, m <sup>2</sup> /g	230
Pore volume (H <sub>2</sub> O), cm <sup>3</sup> /g	0.52

The industrial test run was performed using middle distillates hydrotreating unit at NIS GAZPROM NEFT Refinery Pancevo. The data collected was used for model development and subsequent simulation. Total test run recorded time was 108 h while the 6 hours periods prior to the run and upon the test completion were used to stabilize the process unit. The initial feed into the catalytic reactor was SRGO while FCC N-LCO stream was added to the feed gradually over the testing period. The initial flow rate of SRGO was 20 m<sup>3</sup>/h while flow rate of FCC N-LCO stream was gradually increased from 0 to 5 m<sup>3</sup>/h. After reaching FCC N-LCO flow rates of 2, 4 and 5 m<sup>3</sup>/h the unit parameters were kept constant for certain period of time. In order to evaluate the influence of the inlet temperature on the hydrotreater performance, the feed temperature was also gradually increased during the run.

Reactor pressure during the test run was 40 bar and the overall flow rate of hydrogen stream, consisting of recycle and make-up streams, was 22700 Nm<sup>3</sup>/h. Hydrogen content of the hydrogen stream was 76 – 78 mole %.

Characterization of the inlet and outlet streams was performed using standard characterization methods shown in **Table 18**. Characterization results are shown in **Table 19** for the sample collected at run time of 108 h.

**Table 18.** Methods used for characterization of feed streams and hydrotreated product

Property	Method
Density at 15 °C, g/cm <sup>3</sup>	ASTM D 4052
Kinematic viscosity at 40 °C, mm <sup>2</sup> /s	ASTM D 445
Flash point, °C	EN ISO 2719 :2002
Cold Filter Plugging Point, °C	EN 116
Cloud point, °C	ISO 3015:1992
Cetane index	ASTM D 4737
Distillation	EN ISO 3405:2000
Sulphur content, % wt.	ISO 8754:2003
Sulphur content, mg/kg	ASTM D 5453
Thiol/mercaptan sulphur, %wt.	UOP 163
Paraffin and naphthenic content, % vol.	UOP 501
Olefins content, % vol.	UOP 501
Aromatics content, % vol.	UOP 501
Mono-aromatic content, % wt.	EN 12916:2006
Di-aromatic content, % wt.	EN 12916:2006
Tri+aromatic content, % wt.	EN 12916:2006
Total nitrogen content, % wt.	ASTM D 4629
Basic nitrogen content, % wt.	UOP 269

**Table 19.** Characterisation of straight-run gas oil (SRGO), FCC naphtha and light cycle oil (FCC N-LCO), and hydrotreated gas oil (HGO) streams sampled at 108 h of the test run.

Property	SRGO	FCC N-LCO	HGO
Density at 15 °C, g/cm <sup>3</sup>	0.8504	0.8540	0.8401
Kinematic viscosity at 40 °C, mm <sup>2</sup> /s	2.07		2.59
Flash point, °C	77		60
Cold Filter Plugging Point, °C	-22		-22
Cloud point, °C	-20		-21
Cetane index	47.5		49.7
Distillation, °C			
IBP	208	33	196
5 %vol.	229	63	223
10 %vol.	236	101	231
20 %vol.	245	170	241
50 %vol.	265	242	259
70 %vol.	281	274	275
90 %vol.	304	333	294
95 %vol.	315		302
FBP	326 / 98%	335 / 91%	321 / 98%
Sulphur content, % wt.	0.7305	1.1400	
Sulphur content, mg/kg			37
Thiol/mercaptan sulphur, %wt.	0.0162	0.0271	0
Paraffin and naphthenic content, % vol.	68.7	32.1	73.0
Olefins content, % vol.	5.2	16.9	0
Aromatics content, % vol.	26.1	51.0	27.0
Mono-aromatic content, % wt.	19.4		27.4
Di-aromatic content, % wt.	11.5		4.6
Tri+aromatic content, % wt.	1.41		0.70
Total nitrogen content, % wt.	0.0103		0.0022
Basic nitrogen content, % wt.	0.0032		0.0009

A gradual increase of FCC N–LCO stream fed to the reactor increased the temperature difference across the reactor since sulphur and aromatic contents of this stream were considerably higher than in SRGO. In order to reach sulphur contents in the hydrotreated gas oil (HGO) below target value of 50 ppm the inlet temperature of the mixed feed was gradually increased from 327 °C to 334 °C. The uppermost value of the inlet temperature was limited by other elements of the process unit, mostly by the furnace and pre-heater capacity.

The increased values of the temperature difference within the catalytic reactor resulted from the increased inlet concentrations of sulphur compounds, higher inlet temperature and higher concentrations of unsaturated compounds. The strategy to increase conversion in adiabatic trickle-bed catalytic reactors by increasing the inlet temperature and temperature difference in the catalytic bed is well known and it has been observed and reported for hydrotreating of various petroleum fractions. Considerable gains in terms of conversion can be achieved especially when light fractions are being hydrogenated or hydrotreated. Elevated pressures and temperatures, along with the high hydrogen to hydrocarbon flow ratios, can lead to a shift in vapour–liquid equilibrium and dry out locations in the catalyst bed. In those locations the catalyst bed is in contact with reactants in the gas phase, leading to a much higher reaction rate in dry catalyst pellets. This type of reactor operation strategy was applied during this test run with the aim to reduce sulphur levels below 50 ppm. As can be seen from the temperature difference data shown in **Figure 26**, the addition of FCC N–LCO stream to the reactor inlet and the gradual increase of inlet stream temperature resulted in the reactor  $\Delta T$  increase from 4 to 12 °C.

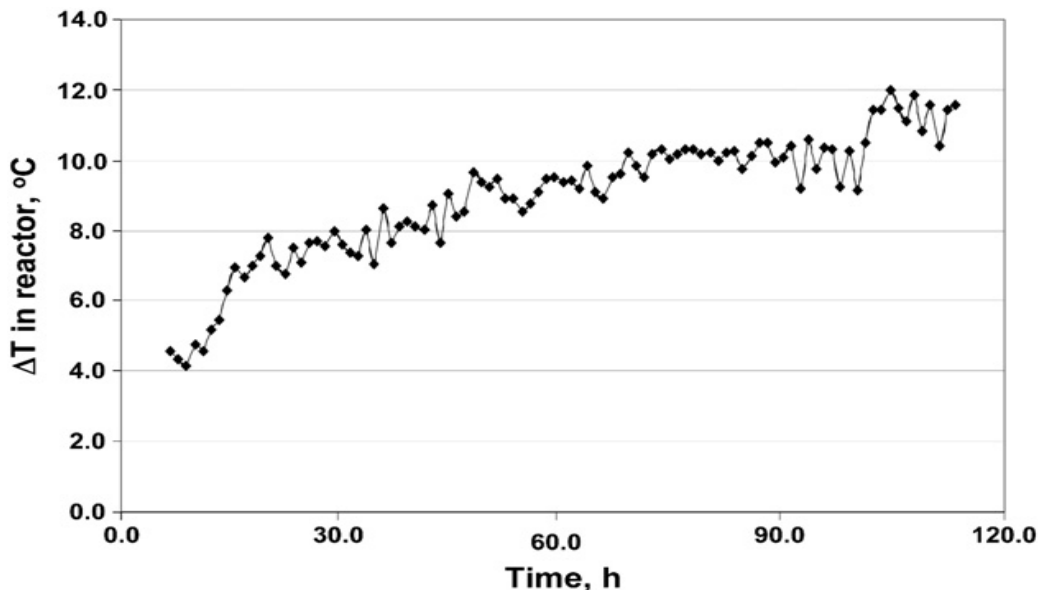


**Figure 26.** Temperature difference across the catalytic reactor during the test run

These data point to the fact that exothermic hydrodesulphurization and hydrogenation reactions have proceeded to a much larger extent and that the overall conversion of sulphur compounds was higher when FCC N–LCO stream was added to the reactor inlet. Part of the reason for higher energy release and resulting higher conversion is due to the increased concentrations of sulphur and unsaturated compounds. Additional reason most probably lies in the fact that increased temperatures in the reactor and the presence of volatile fraction like FCC naphtha resulted in the partial dry out of the catalyst bed and thus in higher reaction rates and improved sulphur conversion.

The total sulphur contents of the reactor feed, including SRGO and FCC N–LCO, are shown in **Figure 27** for the whole testing period, as well as the resulting outlet sulphur concentrations. It can be observed that variations of the sulphur inlet concentrations were detected but they remained within the 6500–8200 ppm range. The sulphur concentrations at the reactor outlet were within the 35–72 ppm range over the entire testing period and the averaged sulphur content in the product over the whole testing period was 49 ppm. The results of sulphur conversion indicate a very deep desulphurisation of the feed even at conditions when flow rate of FCC N–LCO stream was at 5 m<sup>3</sup>/h, or 20%vol of the total reactor inlet flow.

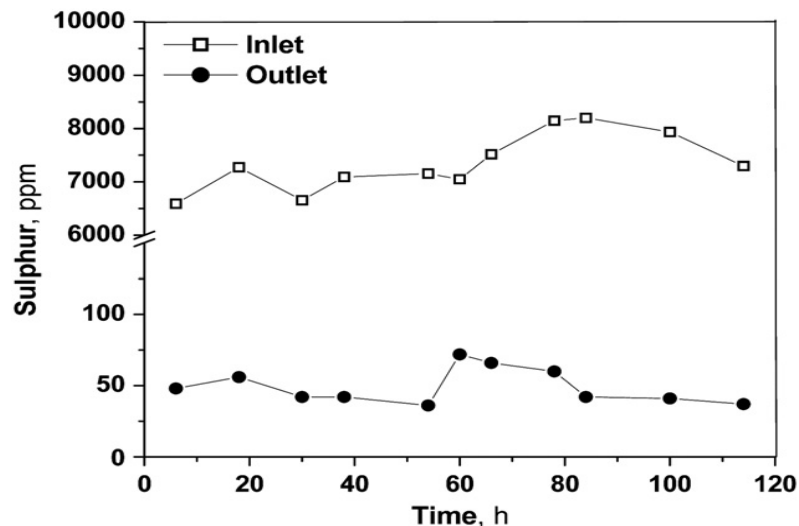


**Figure 27.** Values of total sulphur content for the inlet and outlet streams of the catalytic reactor

The distribution of sulphur compounds between different classes for the petroleum fractions used in the test run was analysed by GC–MS method and obtained corresponding peaks are presented in **Figure 28** [218]. Thiophenic compounds typically present in middle distillate fractions can be classified into sub-families according to the parent molecule and the type and number of alkyl substituents. For these fractions parent molecules are: benzothiophene (BT), dibenzothiophene (DBT) and naphthothiophene (NT). These molecules usually have up to 4 C atoms in the substituent groups (C1 to C4) which could be: methyl, ethyl and propyl. However, smaller alkyl substituent groups, like methyl, are more abundant. It can be observed that a high percentage of sulphur was present in the alkyl derivatives of benzothiophene, which is known to react more easily than certain derivatives of dibenzothiophene, especially 4,6-dimethyldibenzothiophene (C2-DBT).



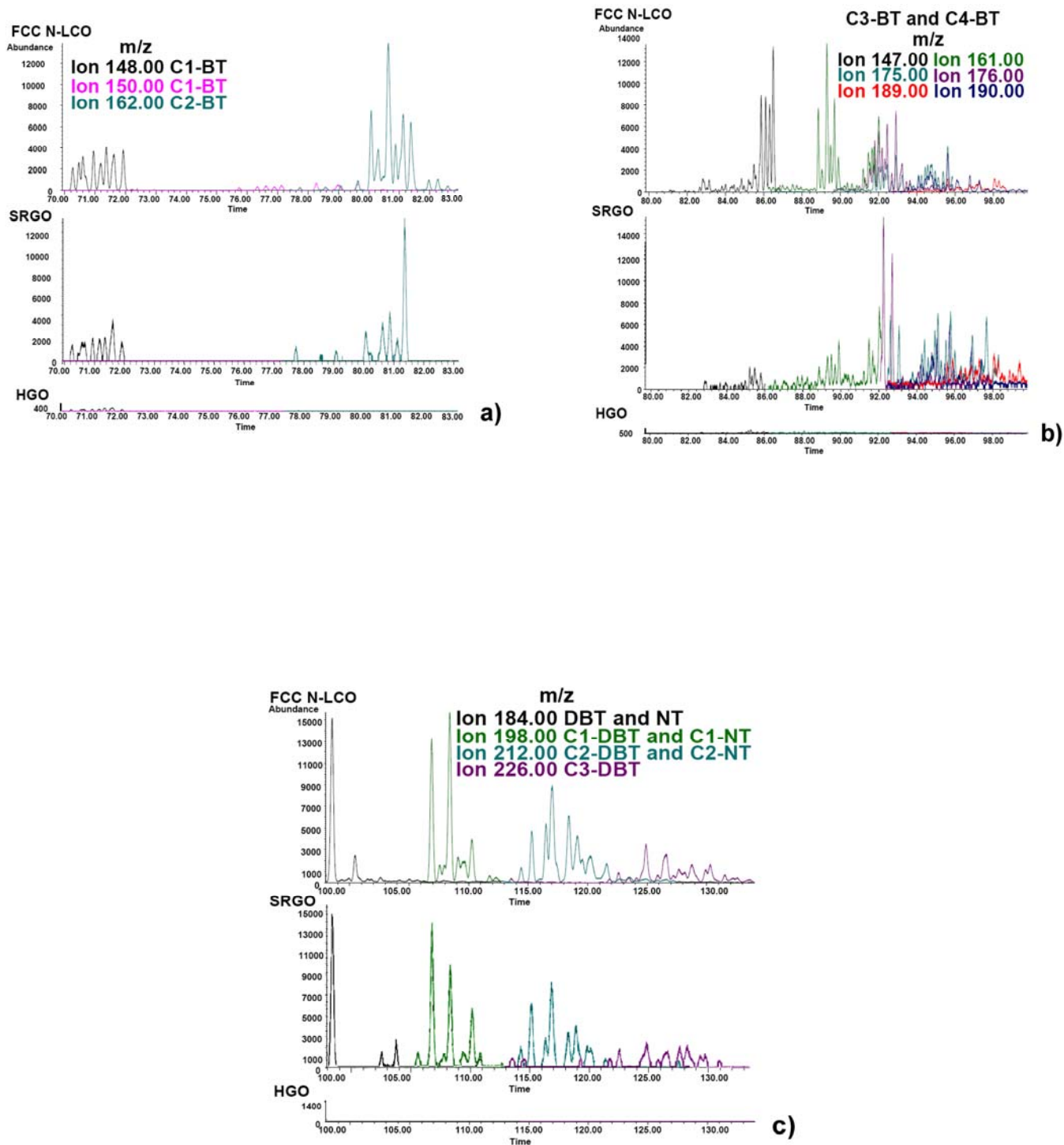


**Figure 28.** GC-MS analysis showing characteristic  $m/z$  chromatograms of SRGO, FCC N-LCO and HGO samples taken at 108 h of run duration: a) C1 and C2 BT; b) C3 and C4 BT; and c) DT, NT, C1 DBT and C1 NT, C2 DBT and C2 NT, and C3 DBT.

Data shown in **Figure 29** confirm that sulphur was mostly concentrated in derivatives of benzothiophene and that less than 1000 ppm of the inlet sulphur was in C2-DBT, which is difficult to hydrogenate. As stated previously, this could be the additional reason for high sulphur conversion during the test run, along with the high reactor temperature and the low space velocity [218].

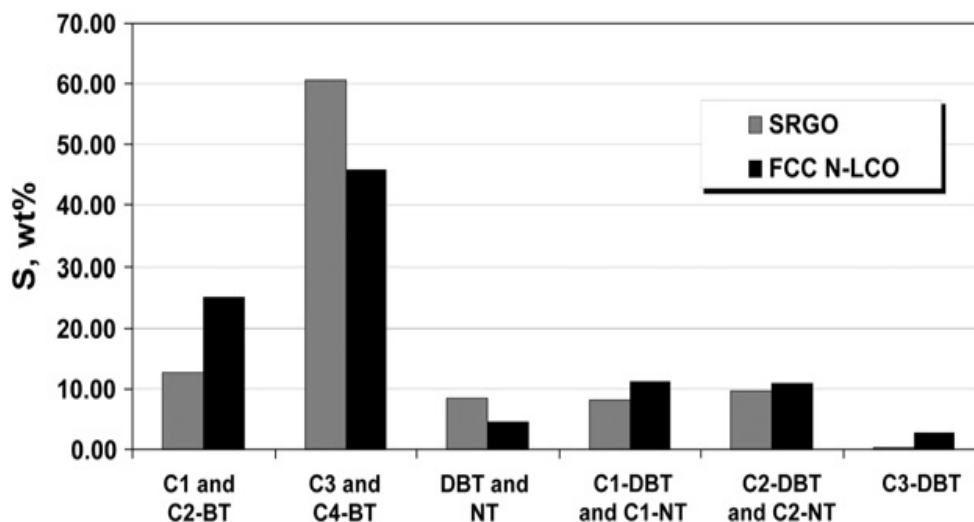


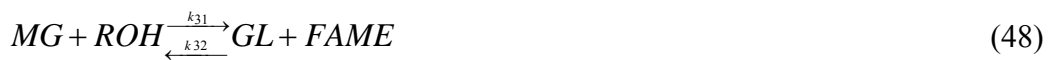
**Figure 29.** Distribution of sulphur over different classes of sulphur containing compounds for SRGO and FCC N–LCO streams

## 4. Model Development - mathematical modelling and numerical optimisation

### 4.1. Model Development for non-catalytic reaction

#### 4.1.1. Kinetic model description of biodiesel reaction

Transesterification or FAME synthesis under subcritical conditions is a catalyst-free chemical reaction between triglycerides (the major component in vegetable oils, animal fats, and used vegetable oils) with a low molecular weight alcohol, usually methanol, at a temperature and pressure under the critical point of triglyceride-alcohol mixture. The overall reaction occurs as a sequence of three steps, parallel with respect to alcohol and consecutive with respect to triglyceride [220-222]. Triglyceride (TG) reacts with an alcohol (ROH) in the first reaction and forms diglyceride (DG) and fatty acid methyl ester (FAME). Monoglycerides (MG) and fatty acid methyl esters (FAME) are formed in the second reaction from diglyceride (DG) and methanol. The final products, appearing as products of the third reaction, are glycerol (GL) and again fatty acid methyl esters (FAME). The reaction scheme is shown below (Eq.46-48):



It is important to point out that the reversible reactions of DG, MG and GL with FAME control the maximum/equilibrium conversion of triglycerides. The reaction rate for each component in the system (constant volume batch system) can be represented by the following set of equations where each reaction step is assumed to be second order in both directions and therefore dependent on concentration of reacting components (Eq. 49-54):

$$r_{TG} = \frac{dC_{TG}}{dt} = -k_{11}C_{TG}C_{ROH} + k_{12}C_{DG}C_{FAME} \quad (49)$$

$$r_{DG} = \frac{dC_{DG}}{dt} = k_{11}C_{TG}C_{ROH} - k_{12}C_{DG}C_{FAME} - k_{21}C_{DG}C_{ROH} + k_{22}C_{MG}C_{FAME} \quad (50)$$

$$r_{MG} = \frac{dC_{MG}}{dt} = k_{21}C_{DG}C_{ROH} - k_{22}C_{MG}C_{FAME} - k_{31}C_{MG}C_{ROH} + k_{32}C_{GL}C_{FAME} \quad (51)$$

$$r_{GL} = \frac{dC_{GL}}{dt} = k_{31}C_{MG}C_{ROH} - k_{32}C_{GL}C_{FAME} \quad (52)$$

$$r_{FAME} = \frac{dC_{FAME}}{dt} = -3 \cdot \left( \frac{dC_{TG}}{dt} \right) - 2 \cdot \left( \frac{dC_{DG}}{dt} \right) - \left( \frac{dC_{MG}}{dt} \right) \quad (53)$$

$$r_{ROH} = \frac{dC_{ROH}}{dt} = -\frac{dC_{FAME}}{dt} \quad (54)$$

If the reaction scheme is represented by the above equations the concentrations of reacting species are assumed to be numbers of moles divided by the overall reaction volume, regardless of the existence of multiple phases. Each reaction is characterized by its reaction rate constant (both forward and reverse reactions). The slowest forward reaction rate controls the overall reaction rate along with reaction equilibrium constant for each of the reversible reactions shown above [219].

Batch reaction system containing triglycerides and methanol at investigated pressure and temperature is characterised by the equilibrium between two liquid phases at the beginning of reaction. During methanolysis of triglycerides, the phase distribution is changing according to the actual composition of reaction mixture, temperature and pressure, for a given time of reaction. Distribution of methanol between the oil phase, the methyl esters phase, and the glycerol rich phase strongly depends on operating conditions [203].

The rate of triglycerides methanolysis depends also on the phase equilibrium and on the methanol distribution in the oil-rich phase. Up to 150 °C and 1.1 MPa the oil is present only in one liquid phase together with a smaller amount of dissolved methanol [203,219]. The methanol to oil molar ratio is 1:1, three times less than required by stoichiometry, thereby causing very low reaction rate (complete conversion could be achieved after approximately 150 h). At 210 °C and 4.5 MPa the methanol to oil molar ratio in the oil phase is changing from 6:1 to 10:1 through the course of reaction, thus increasing the rate of reaction and resulting in complete conversion of triglycerides in approximately 10h. The methyl esters being produced form the third liquid phase which contains almost all diglycerides, monoglycerides and glycerol, together with certain amount of methanol. This is also the

period when probability for reverse reaction between glycerol and FAME is much higher than probability of reaction between glycerides (present in low concentrations) and methanol. At the end of reaction (at 210 °C and 4.5 MPa) one liquid phase contains methanol, FAME and glycerol, as well as certain small amount of monoglycerides and diglycerides [203,219].

The sigmoid shape of the conversion curves during FAME synthesis points out to a complex reaction mechanism. Initially slow reaction rate increases with conversion and in its final stage the FAME yield curve reaches a plateau. At the beginning of reaction, the interfacial area between the phases containing reactants is dependent on the agitation intensity and mass transfer controls the overall reaction rate ( $k_{\text{kinetic}} \gg k_{\text{mass transfer}}$ ). This is more pronounced at conditions corresponding to low methanol solubility in the oil phase, e.g. under lower pressure and temperature. Therefore, the kinetic constant for the forward reaction of triglycerides conversion could be corrected with following equation, introducing the mass transfer effects [219]:

$$k_{11}' = k_{mt} + k_{11} \cdot (C_{DG} + C_{MG}) / C_{TGo} \quad (55)$$

where the  $k_{mt}$  represents the mass transfer controlled kinetic constant in the initial phase of the reaction. Increasing conversion followed by changing phase distribution, increasing concentrations of intermediates (mono and diglycerides) and the enhancement of interfacial area will result in the increase of overall kinetic constant [219]. Based on the calculation of mass transfer coefficient in mechanically stirred system the numerical value of  $k_{mt}$  for the first and second experiment was determined as  $9.2 \times 10^{-7}$  and  $1.5 \times 10^{-6}$   $\text{dm}^3/\text{kmol}\cdot\text{min}$  respectively [219]. Intense agitation provides sufficiently high values of mass transfer coefficient to accommodate for methanol consumed by the reaction in oil phase, while the extent of reaction in methanol rich phase can be neglected due to very low concentrations of glycerides in that phase [219]. Hence, the calculation of apparent values for kinetic parameters using the overall reaction volume can be applied with the incorporation of mass transfer effects at the beginning of reaction.

#### 4.1.1.1. Parameter determination by different optimization techniques

The proposed kinetic model for biodiesel synthesis is nonlinear implying that finding the best set of values for kinetic parameters requires the use of optimization techniques and/or their combinations. In general, the techniques used for parameters estimation can be divided into two groups: the short cut methods and the global optimization techniques that do not require initial guesses [223-228].

Due to the fact that most of the methods for parameters estimation require good initial guess to find the optimal set of results, finding the initial values of unknown parameters is essential for successful parameters estimation. In this study model parameters, or reaction constants, were determined using Simulated Annealing (SA), lsqcurvefit (LM), and Genetic Algorithm (GA) methods (as defined functions in MATLAB). In order to make a comparison among these optimization methods the following objective function was defined for all of them (Eq.56):

$$\text{Objective function} = \sum_{i=1}^6 \sum_{j=1}^n \left( \frac{C_{i,j}^{Exp} - C_{i,j}^{Model}}{C_{i,max}^{Exp}} \right)^2 \quad (56)$$

Where i refers to the component (TG, DG, MG, GL, FAME, ROH), and j refers to the experimental data for each component.  $C_{i,max}^{Exp}$  is the maximum concentration of component i within the experimental data set.

The default parameters were defined as the parameters predetermined by MATLAB (MathWorks 7.1). The only deviation from this was the applied algorithm for solving optimization by lsqcurvefit which was changed from trust-region-reflective (default) to Levenberg-Marquardt.

- **Simulated annealing (SA)**

Simulated annealing is a probabilistic global search method [229,230]. SA is stochastic search techniques and it is used when the structure of a space is not well understood

or is not smooth. In particular, these techniques are frequently used to solve combinatorial optimization problems, such as the travelling salesman problem. The goal is to find a point in the space at which a real valued energy function (or cost function) is minimized. Simulated annealing is a minimization technique which has given good results in avoiding local minima; it is based on the idea of taking a random walk through the space at successively lower temperatures, where the probability of taking a step is given by a Boltzmann distribution [229,230].

- **The lsqcurvefit with Levenberg–Marquardt algorithm (LM)**

The lsqcurvefit solves nonlinear data-fitting problems. The lsqcurvefit requires a user-defined function to compute the vector-valued function  $F(x, xdata)$ . The size of the vector returned by the user-defined function must be the same as the size of  $ydata$  [231,232].

The Levenberg–Marquardt algorithm (LMA), also known as the damped least-squares (DLS) method, is an iterative technique which provides a numerical solution to the problem of minimizing a function, generally nonlinear, over a space of parameters of the function. These minimization problems arise especially in least squares curve fitting and nonlinear programming. It has become a standard technique for non-linear least-squares problems, widely adopted in a broad spectrum of disciplines [231,232].

The LMA interpolates between the Gauss–Newton algorithm (GNA) and the method of gradient descent. When the current solution is far from the correct one, the algorithm behaves like a steepest descent method (slow but certain convergence). When the current solution is close to the correct solution, it becomes a Gauss-Newton method [231,232]. The LMA is a very popular curve-fitting algorithm used in many software applications for solving generic curve-fitting problems. However, the LMA finds only a local minimum, not a global minimum [231,232].

The first, initial guess required for these two techniques (LM and SA) was found by applying combination of two short cut methods. This approach combines differential method of analysis [233] and method for kinetics parameters estimation proposed by Glowinski and Stocki [234]. In order to reveal the dependency of the optimum solution to the initial guess, three guesses were considered for each experiment. The first guess is  $0.1 \times x_0$ , the second guess

is  $x_0$ , and the last one is  $10 \times x_0$ , where  $x_0$  is the vector containing the obtained values of reaction constants by linear technique.

- **Global optimization technique - Genetic Algorithm**

Nowadays this technique is widely used. Commonly, genetic algorithm optimization technique is used to estimate initial values of parameters, because this approach does not require any initial assumption of parameters value. The method compares experimental data of species concentration with values predicted by the model. Due to the fact that concentration of species values differ from each other by several orders of magnitude and sum of squares of deviation between experimental and modelled values are summarized in one objective function, the values should be brought to the same numeric interval. There are several techniques to achieve this: i) minimize square of relative error between experimental and model predicted values of concentration, and ii) involve variances of experimental measurements. The drawback of using square of relative error is that error of each experimental measurement has significant impact on objective function. On the other side using variance of experimental measurements are more convenient, since error of measurements is averaged which results in lower impact of individual measurement error on objective function. If values of variances of experimental values are not available, they can be optimized together with unknown rate reaction parameters. The drawback of this technique is that it increases number of parameters to be optimized [235-240].

The genetic algorithm technique makes use of the Darwinian survival of the fittest procedure. These are search procedures based on mechanics of natural genetics and natural selection [235]. Five GA operators are used in the DNA-GA to enhance the searching ability of the GA [236]. In particular, the “mutation step” helps in avoiding getting trapped in local minima during the search procedure [236]. The parameters were searched within non-negative numbers.

#### **4.2. Model development for catalytic reaction**

The developed model is a heterogeneous one-dimensional model and consists of differential equations of mass and heat balance and kinetics equations for the main reactions



occurring in the hydrotreating process. Kinetic parameters were established by Froment et al. (1994). Equations were solved using software package MATLAB 7.1.

Industrial test run was performed under pressure of 40 bar in the catalytic reactor with two layers of conventional Co-Mo/ $\gamma$ -Al<sub>2</sub>O<sub>3</sub> catalyst. Due to the complex physical-chemical phenomena taking place in trickle bed reactors, their mathematical description leads to a large number of equations and mathematical problems.

Balance equations for the TBR components can be derived from the mass balance equations of tube fixed bed reactor with catalyst (Figure 30).

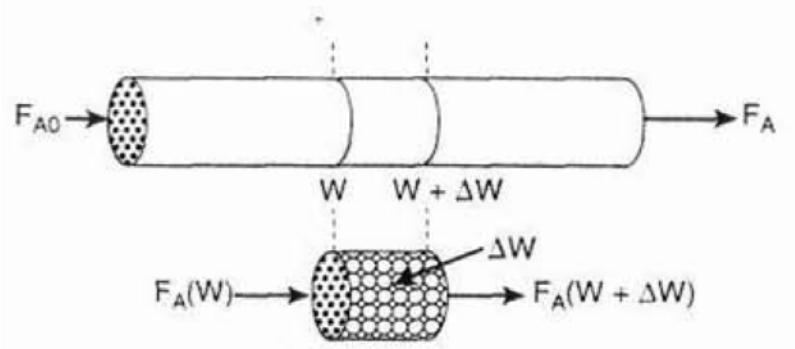


**Figure 30.** Schematic view of tube fixed bed reactor with catalyst

Input - Output + Generation = 0

$$F_{A(W)} - F_{A(W+\Delta W)} + r_A \cdot \Delta W = 0 \quad (57)$$

$$r_A \cdot \Delta W \equiv \frac{\text{molA}}{\text{time} \cdot \text{mass} - \text{catalyst}} \cdot \text{mass} - \text{catalyst} \equiv \frac{\text{molA}}{\text{time}}$$

or the by differential balance

$$\frac{dF_A}{dW} = r_A$$

#### ***4.2.1. Mathematical mode of diesel hydrotreater***

The process of hydrodesulphurization of straight run gas oil mixture (SRGO) and light cycle oil (LCO) in TBR reactor can be described mathematically in different ways. In this study a deterministic model approach is applied based on the assumptions shown below. These assumptions have been adopted on the basis of known properties TBR reactor and the reactor on the basis of data for gas oil HDS Series S2400 in Pancevo Oil Refinery (NIS – Gazprom Neft) and its process parameters.

The model is defined and formed the basis of the following assumptions:

1. Mixture of SRGO, FCC-N and LCO flows from the top down through the fixed bed of catalyst consisting of two layers. The basis of the model consists of differential equations of material balance of sulphur compounds of interest and the overall reactor energy balance.
2. The effects of axial dispersion of vapour and liquid phases flow in the reactor are negligible.
3. The model assumes that the reaction occurs in two phases, vapour and liquid. Reaction rate of any chemical species in a given phase is treated as catalytic heterogeneous reaction with rate equations of Hougen-Watson type.
4. Fraction of the catalyst bed where the reaction occurs in the vapour or liquid phase is defined on the basis of the effective catalyst bed wetting for the observed flow conditions and the vapour-liquid equilibrium.
5. Effectiveness factors for catalytic reactions in vapour and liquid phase are dependent on concentrations of reacting species, temperature, mass transfer effects, and are calculated separately for each of the phases.
6. In front of each segment of the reactor (Figure 31) a new distribution of the components in the vapour and liquid phase is defined, in accordance with the phase equilibrium of the system at a given temperature.
7. Outlet temperature from the previous segment is the inlet temperature of the following segment, and it constitutes a basis for new phase equilibrium calculation.

8. Mass transfer resistance of hydrogen from vapour to liquid phase is assumed to be negligible, as confirmed by the calculation of mass transfer coefficients.
9. The pressure drop in the reactor is negligible in terms of impact on the reaction rate, which was confirmed by plant DCS data collected during the test run. Data on measured pressure drop were used to calculate the catalyst bed wetting.
10. The influence of pressure on the values of the specific heat capacity of n-alkanes, hydrogen, and methane is negligible.

The influence of vapour-liquid equilibrium on the conversion of sulphur compounds was calculated by the model for the reactor divided into sub-segments.

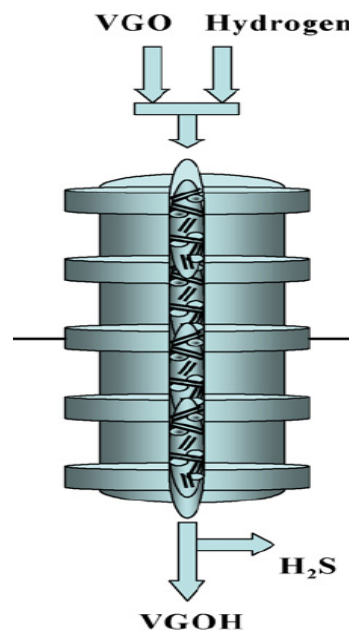


**Figure 31.** Schematic view of the reactor divided into segments [11]

Distribution of the components in the gas or vapour and liquid phase along the reactor is calculated at the inlet of every segment of the reactor using polynomial dependence of equilibrium constant  $K$  on temperature, which calculated using FLASH calculations and Peng-Robinson equation of state.

Total length of the reactor is divided into 4 equal segments. Distribution of components in both phases along the reactor is calculated for every segment of the reactor where each segment stands for 1800 kg of the catalyst.

Total mole fraction of component  $i$  in mixture is calculated for segment  $n$  as shown in Eq. (58).

$$z_{i,n+1} = \frac{F_{i,n}^L + F_{i,n}^V}{F_{tot}} \quad (58)$$

Mole fraction of component  $i$  in liquid phase is calculated in Eq. (17), and in vapour phase in Eq. (59).

$$x_{i,n+1} = \frac{z_{i,n+1} * (1 + \frac{F^L}{F^V})}{K_{i,n+1} + \frac{F^L}{F^V}} \quad (59)$$

$$y_{i,n+1} = K_{i,n+1} * x_{i,n+1} \quad (60)$$

Equilibrium constant is calculated as shown in Eq. (61).

$$K_i = \frac{y_i}{x_i} \quad (61)$$

### Mass balance equations

Balance equations for trickle bed reactor are derived using material balance equations of an ideal tubular packed bed reactor.

Mass balance equations for components involved in hydrodesulfurization (BT, DBT1, DBT2, DBT3) in the gas phase and in the liquid phase are expressed by Eqs (62, 63).

$$-\frac{dF_i^V}{dw} = (1-f) \cdot \Omega_i^V \cdot r_{i,HDS} \quad (62)$$

$$-\frac{dF_i^L}{dw} = f \cdot \Omega_i^L \cdot r_{i,HDS} \quad (63)$$

Mass balance equations for components involved in process of hydrodearomatization (A1, A2) in gas phase and in liquid phase (Eqs (64-66)):

$$-\frac{dF_i^V}{dw} = \frac{(1-f) \cdot \Omega_i^V \cdot r_{i,ARM}}{\rho_p \cdot (1-\varepsilon_p)} \quad (64)$$

$$-\frac{dF_i^L}{dw} = \frac{f \cdot \Omega_i^L \cdot r_{i,ARM}}{\rho_p \cdot (1-\varepsilon_p)} \quad (65)$$

$$\frac{dF_i^V}{dw} = \frac{(1-f) \cdot \Omega_i^V \cdot r_{i,ARM}}{\rho_p \cdot (1-\varepsilon_p)} \quad (66)$$

$$\frac{dF_i^L}{dw} = \frac{f \cdot \Omega_i^L \cdot r_{i,ARM}}{\rho_p \cdot (1-\varepsilon_p)} \quad (67)$$

Mass balance equations for hydrogen in the gas phase and in the liquid phase:

$$-\frac{dF_{H_2}^V}{dw} = -\frac{dF_{BT}^V}{dw} + \left(-\frac{dF_{dBT1}^V}{dw}\right) + \left(-\frac{dF_{dBT2}^V}{dw}\right) + \left(-\frac{dF_{dBT3}^V}{dw}\right) + \left(-\frac{dF_{A1}^V}{dw}\right) \quad (68)$$

$$-\frac{dF_{H_2}^L}{dw} = 0 \quad (69)$$

Mass balance equations for hydrogen sulfide in the gas phase and in the liquid phase:

$$\frac{dF_{H_2S}^V}{dw} = -\frac{dF_{BT}^V}{dw} + \left(-\frac{dF_{dBT1}^V}{dw}\right) + \left(-\frac{dF_{dBT2}^V}{dw}\right) + \left(-\frac{dF_{dBT3}^V}{dw}\right) \quad (70)$$

$$\frac{dF_{H_2S}^L}{dw} = -\frac{dF_{BT}^L}{dw} + \left(-\frac{dF_{dBT1}^L}{dw}\right) + \left(-\frac{dF_{dBT2}^L}{dw}\right) + \left(-\frac{dF_{dBT3}^L}{dw}\right) \quad (71)$$

**Energy balance equation**

Enthalpy change of the components involved in the process of hydrodesulfurization:

$$\Delta E_{HDS} = \sum_1^i F_i^V \cdot (1-f) \cdot \Omega_i^V \cdot r_{i,HDS} \cdot \Delta H_{HDS} + \sum_1^i F_i^L \cdot f \cdot \Omega_i^L \cdot r_{i,HDS} \cdot \Delta H_{HDS} \quad (72)$$

Enthalpy change of the components involved in the process of hydrodearomatization:

$$\Delta E_{ARM} = \sum_1^j F_j^V \cdot (1-f) \cdot \Omega_j^V \cdot r_{j,ARM} \cdot \Delta H_{ARM} + \sum_1^j F_j^L \cdot f \cdot \Omega_j^L \cdot r_{j,ARM} \cdot \Delta H_{ARM} \quad (73)$$

Total energy balance is shown in equation (32):

$$\frac{dT}{dw} = \frac{\Delta E_{HDS} + \Delta E_{ARM}}{\sum_i F_i^V \cdot Cp_i + \sum_i F_i^L \cdot Cp_i} \quad (74)$$

**4.2.2. Reaction mechanism of benzothiophene hydrodesulphurization**

Previous research on HDS of benzothiophene and substituted derivatives with Co-Mo/Al<sub>2</sub>O<sub>3</sub> catalyst, indicate the existence of the equilibrium level of the first phase HDS processes, and rapid reaction between BT and 2,3-dihydro-benzothiophene (Figure 32):

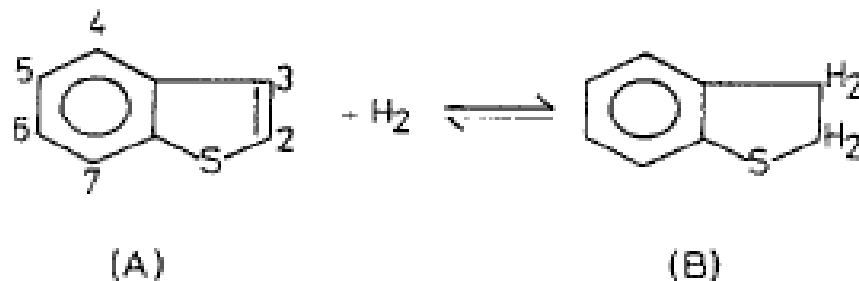
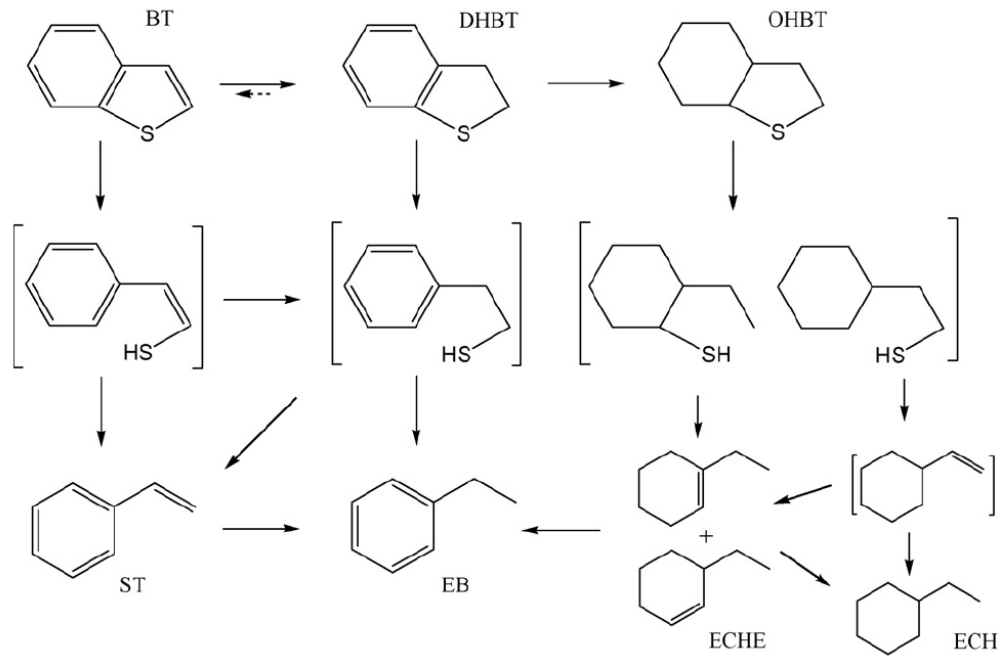


**Figure 32.** The degree of equilibrium between benzothiophene (A) and 2,3-dihydro-benzothiophene

The reaction scheme of benzothiophene and dibenzothiophene hydrodesulphurization are summarised and shown in **Figure 33**.

**benzothiophene:**



**dibenzothiophene:**

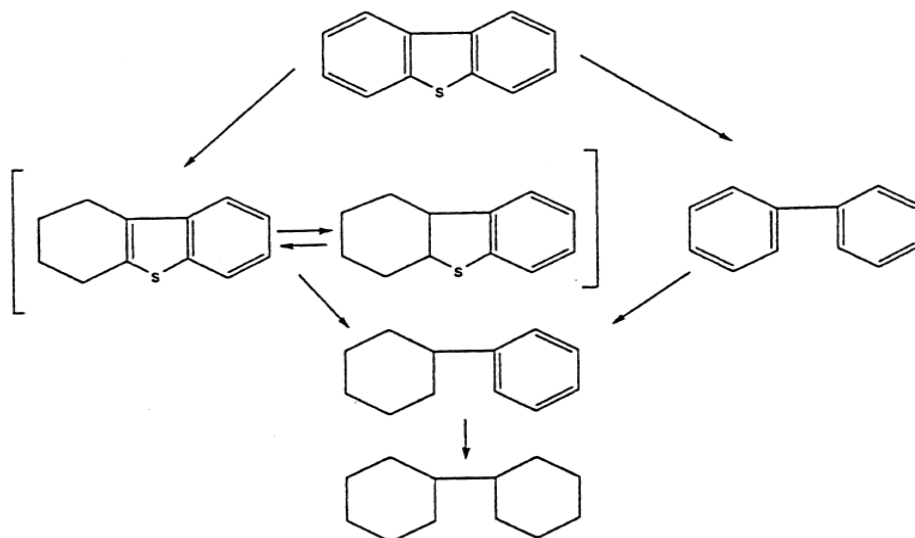
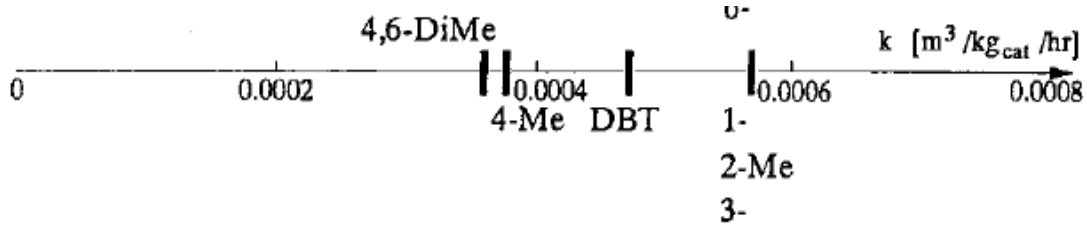


**Figure 33.** Benzothiophene and dibenzothiophene hydrodesulphurization reaction scheme [6]

Relative HDS reaction rate ratio for benzothiophene and methyl-substituted derivatives were measured and could be summarised as:

Benzothiophene (1) > 2-methyl-BT (0.4) > 3-methyl-BT (0.2) > 2,3-dimethyl-BT



#### 4.2.2.1. Kinetic equations

Kinetic parameters were taken from the literature [Froment]. Extensive studies of the kinetic modelling and simulation of the hydrotreatment reactions have been made by Van Parys and Froment (1986), Van Parys et al. (1986), Froment et al. (1994, and 1997) and Vanrysselberghe and Froment (1996, and 1998b). Rate equations for all reactions in the network for the HDS of DBT were developed on a commercial CoMo/Al<sub>2</sub>O<sub>3</sub> catalyst under operating conditions significant to industrial applications (Vanrysselberghe and Froment 1996). Rate equations of the Hougen-Watson type were developed for the HDS of 4-Me-DBT and 4,6-DiMeDBT using the same catalyst and operating conditions (Vanrysselberghe et al. 1998a).

The reaction rate equations for hydrodesulfurization of benzothiophene in vapour and in liquid phase are shown in Eqs. (75, 76) [2].

$$r_{BT}^V = C_{BT}^V \cdot C_{H_2}^V \cdot \left[ \frac{k_{BT,\sigma} K_{BT,\sigma} \cdot K_{H,\sigma}}{DEN_\sigma^V} + \frac{k_{BT,\tau} K_{BT,\tau} \cdot K_{H,\tau}}{DEN_\tau^V} \right] \quad (75)$$

$$r_{BT}^L = C_{BT}^L \cdot C_{H_2}^L \cdot \left[ \frac{k_{BT,\sigma} K_{BT,\sigma} \cdot K_{H,\sigma}}{DEN_\sigma^L} + \frac{k_{BT,\tau} K_{BT,\tau} \cdot K_{H,\tau}}{DEN_\tau^L} \right] \quad (76)$$

where:

$$DEN_\sigma^V = \left[ 1 + \sum_j K_{j,\sigma} \cdot C_j^V + \sqrt{K_{H,\sigma} \cdot C_{H_2}^V} \right]^3 \quad (77)$$



$$DEN_{\sigma}^L = \left[ 1 + \sum_j K_{j,\sigma} \cdot C_j^L + \sqrt{K_{H,\sigma} \cdot C_{H_2}^L} \right]^3 \quad (78)$$

$$DEN_{\tau}^V = \left[ 1 + \sum_j K_{j,\tau} \cdot C_j^V + \sqrt{K_{H,\tau} \cdot C_{H_2}^V} \right]^3 \quad (79)$$

$$DEN_{\tau}^L = \left[ 1 + \sum_j K_{j,\tau} \cdot C_j^L + \sqrt{K_{H,\tau} \cdot C_{H_2}^L} \right]^3 \quad (80)$$

and the reaction rate constant and the adsorption equilibrium constants are given by:

$$k_{BT,\sigma} K_{BT,\sigma} = 1.54237 \cdot 10^{17} \cdot \exp \left[ \frac{-150297}{R_{gas} \cdot T} \right] \quad (81)$$

$$k_{BT,\tau} K_{BT,\tau} = 1.35198 \cdot 10^{21} \cdot \exp \left[ \frac{-207325}{R_{gas} \cdot T} \right] \quad (82)$$

$$K_{H,\sigma} = 3.36312 \cdot 10^{-11} \cdot \exp \left[ \frac{113.232 \cdot 10^3}{R_{gas} \cdot T} \right] \quad (83)$$

$$K_{H,\tau} = 1.40255 \cdot 10^{-15} \cdot \exp \left[ \frac{142.693 \cdot 10^3}{R_{gas} \cdot T} \right] \quad (84)$$

$$K_{H_2S,\sigma} = 1.47118 \cdot 10^{-8} \cdot \exp \left[ \frac{105670}{R_{gas} \cdot T} \right] \quad (85)$$

The reaction rate equations for hydrodesulfurization of 4-dimethyldibenzothiophene (DBT1) in vapour and in liquid phase were determined as [3].

$$r_{DBT_1}^V = C_{DBT_1}^V \cdot C_{H_2}^V \cdot \left[ \frac{k_{DBT_1,\sigma} K_{DBT_1,\sigma} \cdot K_{H,\sigma}}{DEN_{\sigma}^V} + \frac{k_{DBT_1,\tau} K_{DBT_1,\tau} \cdot (k_{1DBT_1,\tau} + k_{2DBT_2,\tau})}{DEN_{\tau}^V} \right] \quad (86)$$

$$r_{DBT_1}^L = C_{DBT_1}^L \cdot C_{H_2}^L \cdot \left[ \frac{k_{DBT_1,\sigma} K_{DBT_1,\sigma} \cdot K_{H,\sigma}}{DEN_\sigma^L} + \frac{k_{DBT_1,\tau} K_{DBT_1,\tau} \cdot (k_{1DBT_1,\tau} + k_{2DBT_2,\tau})}{DEN_\tau^L} \right] \quad (87)$$

Where:

$$r_{DBT_1} = r_{DBT_1,\sigma} + r_{1DBT_1,\tau} + r_{2DBT_2,\tau} \quad (88)$$

$$K_{DBT_1,\sigma} = 2.34677 \cdot 10 \quad (89)$$

$$K_{DBT_1,\tau} = 6.03699 \cdot 10^{-8} \cdot \exp \left[ \frac{83802}{R_{gas} \cdot T} \right] \quad (90)$$

$$k_{DBT_1,\sigma} = 1.31506 \cdot 10^{11} \cdot \exp \left[ \frac{-133302}{R_{gas} \cdot T} \right] \quad (91)$$

$$k_{1DBT_1,\tau} = 4.25112 \cdot 10^{24} \cdot \exp \left[ \frac{-269460}{R_{gas} \cdot T} \right] \quad (92)$$

The reaction rate equations for hydrodesulfurization of 4,6-dimethyldibenzothiophene (DBT2) were determined as [4].

$$r_{DBT_2}^V = C_{DBT_2}^V \cdot C_{H_2}^V \cdot \left[ \frac{k_{DBT_2,\sigma} K_{DBT_2,\sigma} \cdot K_{H,\sigma}}{DEN_\sigma^V} + \frac{k_{DBT_2,\tau} K_{DBT_2,\tau} \cdot K_{H,\tau}}{DEN_\tau^V} \right] \quad (93)$$

$$r_{DBT_2}^L = C_{DBT_2}^L \cdot C_{H_2}^L \cdot \left[ \frac{k_{DBT_2,\sigma} K_{DBT_2,\sigma} \cdot K_{H,\sigma}}{DEN_\sigma^L} + \frac{k_{DBT_2,\tau} K_{DBT_2,\tau} \cdot K_{H,\tau}}{DEN_\tau^L} \right] \quad (94)$$

where:

$$r_{DBT_2} = r_{DBT_2,\sigma} + r_{DBT_2,\tau} \quad (95)$$

$$K_{DBT_2,\sigma} = 1.80397 \cdot 10 \quad (96)$$

$$K_{DBT_2,\tau} = 1.58733 \cdot 10^{-8} \cdot \exp\left[\frac{90485}{R_{gas} \cdot T}\right] \quad (97)$$

$$k_{DBT_2,\sigma} = 6.4456 \cdot 10^7 \cdot \exp\left[\frac{-106223}{R_{gas} \cdot T}\right] \quad (98)$$

$$k_{DBT_2,\tau} = 3.68208 \cdot 10^{27} \cdot \exp\left[\frac{-299042}{R_{gas} \cdot T}\right] \quad (99)$$

Rate equations for hydrodesulfurization of trimethylbenzothiophenes (DBT3) in vapour and in liquid phase were available at [4].

$$r_{DBT_3}^V = C_{DBT_3}^V \cdot C_{H_2}^V \cdot \left[ \frac{k_{DBT_3,\sigma} K_{DBT_3,\sigma} \cdot K_{H,\sigma}}{DEN_{\sigma}^V} + \frac{k_{DBT_3,\tau} K_{DBT_3,\tau} \cdot K_{H,\tau}}{DEN_{\tau}^V} \right] \quad (100)$$

$$r_{DBT_3}^L = C_{DBT_3}^L \cdot C_{H_2}^L \cdot \left[ \frac{k_{DBT_3,\sigma} K_{DBT_3,\sigma} \cdot K_{H,\sigma}}{DEN_{\sigma}^L} + \frac{k_{DBT_3,\tau} K_{DBT_3,\tau} \cdot K_{H,\tau}}{DEN_{\tau}^L} \right] \quad (101)$$

where:

$$r_{DBT_3} = r_{DBT_3,\sigma} + r_{DBT_3,\tau} \quad (102)$$

$$K_{DBT_3,\sigma} = 7.56868 \cdot 10 \quad (103)$$

$$K_{DBT_3,\tau} = 2.50395 \cdot 10^{-7} \cdot \exp\left[\frac{76840}{R_{gas} \cdot T}\right] \quad (104)$$

$$k_{DBT_3,\tau} = 2.86757 \cdot 10^{16} \cdot \exp\left[\frac{-186190}{R_{gas} \cdot T}\right]$$

(105)

$$k_{DBT_3, \sigma} = 2.44336 \cdot 10^{10} \cdot \exp\left[\frac{-122770}{R_{gas} \cdot T}\right] \quad (106)$$

Rate equations for aromatics hydrogenation is [5]:

$$(-r_{A1}) = \frac{-k_H^E}{K_I} \cdot C_{A1} + \frac{k_D^E}{K_I} \cdot C_{A2} \quad (107)$$

Where:

$$k_H^E = k_H \cdot P_{H_2}^{1.5} \cdot \exp\left[-\left(\frac{E}{R}\right) \cdot \left(\frac{1}{T} - \frac{1}{T_o}\right)\right] \quad (108)$$

$$k_D^E = \frac{k_H}{K_p \cdot P_{H_2}^{0.5}} \cdot \exp\left[-\left(\frac{E - \Delta H_A}{R}\right) \cdot \left(\frac{1}{T} - \frac{1}{T_o}\right)\right] \quad (109)$$

where:

$$K_I = 1 + K_{H_2S} \cdot P_{H_2S}$$

$$k_H = 9 \cdot 10^{-3} s^{-1}$$

$$K_p = 1.4 \cdot 10^{-2}$$

$$K_{H_2S} = 2.8$$

$$T_o = 623K$$

$$E = 667.4 \frac{kJ}{mol}$$

$$\Delta H_A = 140.68 \frac{kJ}{mol}$$

### 4.2.3. Calculation of model parameters

#### 4.2.3.1. Calculation of the flow rate of vapour and liquid phases

Volumetric flow rates of vapour and liquid phases were calculated using the following equation:

$$v^V = \frac{(F_{cet}^V + F_{H_2}^V + F_{CH_4}^V)}{\rho^V} \quad (110)$$

$$v^L = \frac{(F_{cet}^L + F_{H_2}^L + F_{CH_4}^L)}{\rho^L} \quad (111)$$

#### 4.2.3.2. Calculation of the specific heat capacity

Calculation for heat capacity of hydrogen is shown in Eq. (5) [1].

$$C_{p_{H_2}} = 33.066178 - 11.363417 \frac{T}{1000} + 11.432816 \left( \frac{T}{1000} \right)^2 - 2.772874 \left( \frac{T}{1000} \right)^3 - \frac{0.158558}{\left( \frac{T}{1000} \right)^2} \quad (112)$$

Heat capacities for liquid methane and methane in gas phase are calculated by Eqs. (6) and (7) [2].

$$C_{p_{CH_4}}^V = 33.01 + 0.010035T - 1.052310^{-4} \cdot T^2 + 3.3947 \cdot 10^{-7} \cdot T^3 \quad (113)$$

$$C_{p_{CH_4}}^L = 17.254 + 1.43031T - 0.015053T^2 + 5.2134 \cdot 10^{-5} \cdot T^3 \quad (114)$$

Heat capacity for octadecane is defined by Eq. (8)[3]:

$$Cp_{C_{18}}^V = 30.1528 + 1.57802T - 0.00087171T^2 + 1.8669 \cdot 10^{-7} \cdot T^3 \quad (114)$$

$$Cp_{C_{18}}^L = 600 \quad (115)$$

Properties of hexadecane [4]:

$$Cp_{C_{16}}^V = -11.656 + 1.52384T - 0.0008466T^2 + 1.79 \cdot 10^{-7} \cdot T^3 \quad (116)$$

$$Cp_{C_{16}}^L = 20.16$$

Heat capacity equation for dodecane in the gas phase is shown in Eq. (11) [5], and for dodecane in the liquid phase in equation (12) [6].

$$Cp_{C_{12}}^V = -8.02 + 1.14384T - 0.000629T^2 + 1.31 \cdot 10^{-7} \cdot T^3 \quad (117)$$

$$Cp_{C_{12}}^L = 2.273845 - 4.55977910^{-3} \cdot T + 1.84353710^{-5} \cdot T^2 - 1.30652110^{-8} \cdot T^3 \quad (118)$$

#### 4.2.3.3. Catalyst wetting efficiency

Catalyst wetting efficiency in trickle bed reactors can be predicted as a function of operating conditions. In trickle flow regime the catalyst pellets are usually incompletely wetted. The following correlation (Eqs. 13-15) was developed by Al-Dahhan-a and Duduković [1]:

$$f = 1.104 \cdot \text{Re}_L \cdot \left[ \frac{1 + \left[ \frac{\Delta P}{Z} \right]}{\rho_L \cdot g} \right]^{1/9} \cdot \left[ \frac{1}{Ga_L} \right] \quad (119)$$

$$\text{Re}_L = \frac{U_L \cdot \rho_L \cdot d_p}{\mu_L \cdot (1 - \varepsilon_p)} \quad (120)$$

$$Ga_L = \frac{d_p^3 \cdot \rho_L^2 \cdot g \cdot \varepsilon_p^3}{\mu_L^2 \cdot (1 - \varepsilon_p)^3} \quad (121)$$

Catalyst wetting efficiency depends on reactor design, catalyst shape and size but mostly it depends on liquid velocity.

#### 4.2.3.4. Calculation of overall effectiveness in the gas phase

Diffusivity for component i is given in the following equations where the parameter was calculated for each component.

$$D_{AB,i} = a_i * 10^{-11} * T^{1.75} \quad (122)$$

$$D_{eff,i} = \frac{1}{\frac{1}{D_{AB,i}} + \frac{1}{D_{k,i}}} \quad (123)$$

$$D_{k,i} = 2.056 * 10^{-7} * \sqrt{\frac{T}{M_i}} \quad (124)$$

$$C_{H_2}^V = \frac{y_{H_2} * P}{R * T} \quad (125)$$

Thiele modulus was calculated was each of the reacting species:

$$\phi_i^V = d_p * \frac{K_{i,uk} * C_{H_2}^V}{D_{eff,i}} \quad (126)$$

And so was the internal effectiveness factor:

$$\eta_i^V = \frac{3}{\phi_i^2} * (\phi_i * \frac{e^{\phi_i} + e^{-\phi_i}}{e^{\phi_i} - e^{-\phi_i}} - 1) \quad (127)$$

Overall effectiveness factor for reactions in the gas phase was calculated using following equations:

$$\Omega_i^V = \frac{\eta_i^V}{1 + \frac{\eta_i^V * K_{i,uk} * C_{H_2}^V}{k_{gi} * a}} \quad (128)$$

$$a = \frac{6 * (1 - \xi_b)}{d_p} \quad (129)$$

$$k_{gi} = \frac{D_{AB}^i * (1 - \xi_b)}{d_p * \xi_b} * \bar{R}_{eg}^{1/2} * S_{cg}^{1/3} \quad (130)$$

$$\bar{R}_{eg} = \frac{R_{eg}}{1 - \xi_b} \quad (131)$$

$$R_{eg} = \frac{\rho_g * u_g * d_p}{\mu_g} \quad (132)$$

$$S_{cg} = \frac{v_g}{D_{AB}^i} \quad (133)$$

#### 4.2.3.5. Calculation of overall effectiveness in the liquid phase

Diffusivity for component i is given in the following equations where the parameter was calculated for each component.

$$D_{AB,i}^L = a_i^L * 10^{-11} * T \quad (134)$$

$$D_{k,i} = 2.056 * 10^{-7} * \sqrt{\frac{T}{M_i}} \quad (135)$$

$$D_{eff,i} = \frac{1}{\frac{1}{D_{AB,i}^L} + \frac{1}{D_{k,i}}} \quad (136)$$



$$C_{H_2}^L = \frac{F_{H_2}^L}{V^L} \quad (137)$$

Thiele modulus was calculated was each of the reacting species in the liquid phase:

$$\Phi_i^2 = \frac{k_{iAPP}^I \cdot R^2 \cdot C_i^L}{D_{eff,i}^L} \quad (138)$$

Internal effectiveness factor was calculated using Thiele modulus value:

$$\eta_i^L = \frac{3}{\Phi_i^2} * (\Phi_i * \frac{e^{\Phi_i} + e^{-\Phi_i}}{e^{\Phi_i} - e^{-\Phi_i}} - 1) \quad (139)$$

Overall effectiveness factor in the liquid phase was calculated using equations shown below:

$$\Omega_i^L = \frac{\eta_i^L}{1 + \frac{K_{i,uk} * C_{H_2}^L}{k_{l,i} * a}} \quad (140)$$

$$k_{l,i} \cdot a = \frac{D_{eff,i}^L}{d_k^2} \cdot 0.091 \cdot \left[ X_G^{1/4} \cdot Re_L^{1/5} \cdot We_L^{1/5} \cdot Sc_L^{3/10} \cdot \left( \frac{a_v \cdot d_k}{1 - \varepsilon_b} \right)^{1/4} \right]^{3.8} \quad (141)$$

$$d_k = d_p * \sqrt[3]{\frac{16 \cdot \varepsilon_b^2}{9 \cdot \pi \cdot (1 - \varepsilon_b)^2}} \quad (142)$$

$$Re_L = \frac{\rho_L \cdot u_L \cdot d_p}{\mu_L \cdot (1 - \varepsilon_b)} \quad (143)$$

$$X_G = \frac{u_G \cdot \sqrt{\rho_G}}{u_L \cdot \sqrt{\rho_L}} \quad (144)$$

$$We_L = \frac{\rho_L \cdot u_L^2 \cdot d_p}{\delta_L} \quad (145)$$

$$We_L = \frac{\rho_L \cdot u_L^2 \cdot d_p}{\delta_L} \quad (146)$$

$$Sc_L = \frac{v_L}{D_{eff,i}} \quad (147)$$

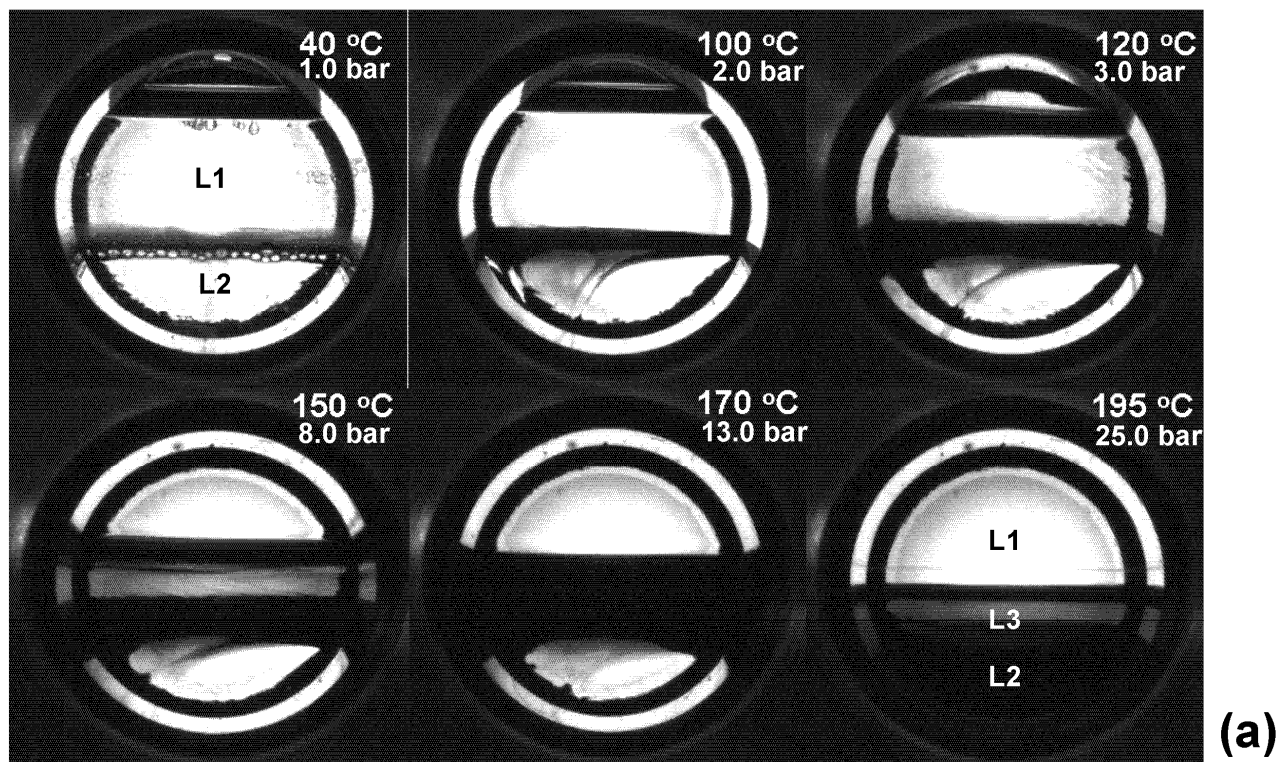
$$a_V = \frac{6 \cdot (1 - \varepsilon_b)}{d_p} \quad (148)$$

## 5. RESULTS AND DISCUSSION

### 5.1. Multiphase system analysis for biodiesel and petroleum diesel processing

#### 5.1.1. Phase equilibria in non-catalytic reaction system - biodiesel production

The analysis of phase equilibrium and composition during formation of ethyl esters of fatty acids (FAEE) at high pressure and temperature is very important for describing an applicable and useful kinetic model which might be used for reactor design. Formation of di- and mono-glycerides during ethanolysis of triglycerides, together with FAEE and glycerol, which are the final products of reaction, makes this system very complex and difficult for simulation. In this study, the phase equilibrium of the triolein and ethanol mixture (1:40 and 1:26 molar ratio of triolein to ethanol) was monitored in a view cell in order to determine the phase transition during heating of mixture up to 195 °C (corresponding pressures were 24 and 25 bar). The phase transition during heating of the investigated reactive mixture is shown in **Figure 34**.



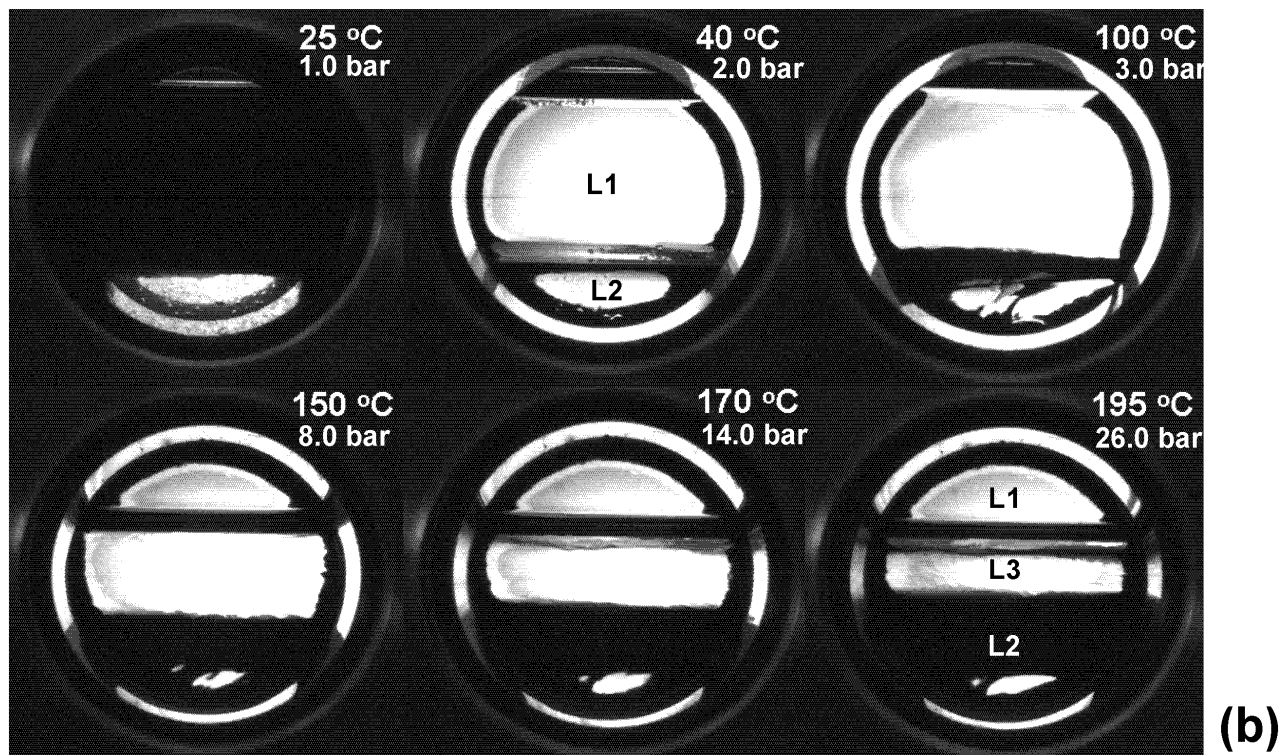


**Figure 34.** The phase transition during the heating of mixture of vegetable oil and ethanol up to 195 °C and 26 bars with ethanol to oil molar ratio of 1:26 (a) and 1:40 (b).

The initially present intermediate phase containing ethanol and triglycerides gradually disappears since the existence of this phase is the consequence of addition of components to the system and emulsion like behaviour of ethanol and triglycerides (first images in **Figure 34a** and **34b**). Upon heating, the amount of ethanol rich phase (L1) increases while at the same time the volume of vegetable oil-ethanol phase (the second stable phase L2) only slightly increases due to dissolution of ethanol in vegetable oil. After heating of up to 195 °C (corresponding pressures were 25 bar and 26 bar), a small amount of FAEE was formed, around 3 mass% in reaction mixture (**Table 20**).

With relatively small quantities of mono- and di-glycerides, FAEE was mainly concentrated in intermediate L3 phase (ethanol-FAEE phase initially appearing at 100 °C). At 195 °C and 25 or 26 bar, three liquid phases: ethanol rich phase (L1), TG-ethanol (L2) and ethanol-FAEE (L3) were in equilibrium (LLL). Two samples were taken from the view cell, the top phase (L1) and bottom phase (L2). The intermediate phase (L3) sample was collected from the reactor system (Ernst Haage 2 dm<sup>3</sup>) using sampling tube. In order to minimize the

experimental error samples of L1 and L2 were taken from the 2 dm<sup>3</sup> reactor as well. Measured compositions of L1, L2 and L3 are shown in **Table 20**.

The L1 phase consisted of almost pure ethanol (>99 mass%, **Table 20**) while the bottom phase (L2) contained certain amount of ethanol dissolved in oil (21-26 mass%), depending on the initial ethanol to oil molar ratio. The third liquid phase (L3, the intermediate phase) consisted mainly of ethanol, in which some amount of ethyl esters (FAEE) were dissolved together with traces of glycerol and monoglycerides. The latter were also generated by the transesterification reaction. As indicated in **Table 20** the composition of phases was almost independent of the ethanol to oil molar ratio. For molar ratio of ethanol to oil of 40 (**Figure 34b**, frame taken at 195 °C), the intermediate phase (L3) increases in volume but low quantity of FAEE is dissolved in this phase under specified conditions (5.90 mass% of L3). The FAEE distribution between the L2 and L3 phases is different when 26:1 molar ratio of ethanol to oil was used.

**Table 20.** The chemical composition of the existing phases at 195 °C

Ethanol to oil molar ratio	Phases	Mass% of phase	The mass% of component in the phase					
			Glycerol	EtOH	FAEE	MG	DG	TG
<b>Experimental data</b>								
<b>1:26</b> <b>25 bar</b>	Liquid 1	51.49	0.02	99.48	0.50	0	0	0
	Liquid 2	36.50	0.20	20.51	4.37	1.67	0.60	72.66
	Liquid 3	12.01	0.64	83.02	11.36	5.04	0.45	0
<b>1:40</b> <b>26 bar</b>	Liquid 1	32.62	0.03	99.37	0.60	0	0	0
	Liquid 2	38.54	0.19	23.17	1.80	0.41	1.17	73.27
	Liquid 3	28.84	0.76	89.51	5.90	3.82	0.01	0
<b>Simulation data</b>								
<b>1:26</b> <b>25 bar</b>	Liquid 1	50.79	0.09	99.81	0.14	0	0	0
	Liquid 2	37.48	0.13	20.38	3.36	1.04	1.49	73.60
	Liquid 3	11.73	1.88	75.89	14.39	7.74	0.09	0,01
<b>1:40</b> <b>26 bar</b>	Liquid 1	32.39	0.03	99.91	0.05	0	0	0
	Liquid 2	37.89	0.05	22.21	1.60	0.50	1.10	74.54
	Liquid 3	29.72	0.83	88.92	6.62	3.59	0.04	0

Simulation results for phase equilibrium and phase composition obtained using Aspen software correspond well to those detected experimentally (**Table 20**), with the standard deviation of 1.38%, 2.39% and 2.62% for ethanol rich phase (L1), ethanol-ethyl esters phase (L3), and oil-ethanol phase (L2) respectively, when the 26:1 molar ratio of ethanol to oil was used. The standard deviation was 0.52%, 1.19% and 2.78% for L1, L2 and L3 phases when the 40:1 molar ratio of ethanol to oil was used. The average deviation between experimental and calculated values of phase composition was around 0.5% for the ethanol phase and 1.5-3.0 % for ethanol-ethyl esters phase and oil-ethanol phase.

The Aspen simulation, with the appropriate physical and thermodynamic parameters, correlates accurately the phase distribution as well as a component distribution for such complex mixture [203]. RK-Aspen EOS and data for triolein as vegetable oil pseudo-component were used to obtain the  $P$ - $x$ - $y$  diagram of the investigated system for a temperature range from 100 to 400 °C (**Figure 35**).

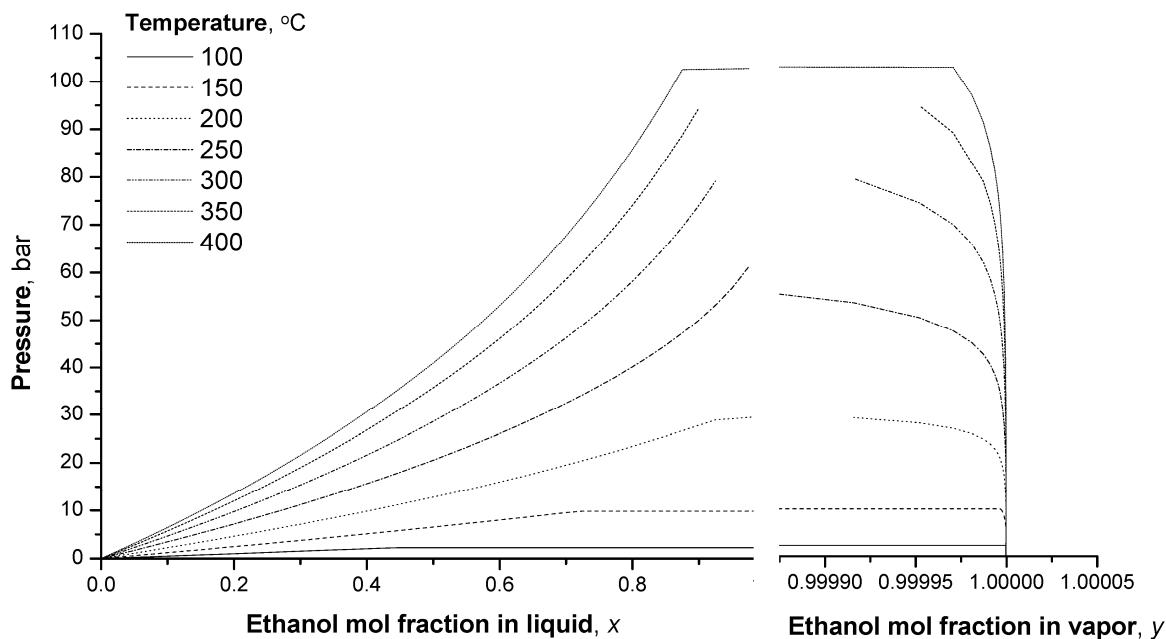


**Figure 35.** The  $P$ - $x$ - $y$  diagram for triolein and ethanol in temperature interval 100-400 °C

With the aim to understand the kinetics of subcritical and supercritical ethanolysis and in order to be able to explain the difference in obtained yields at these conditions, it is also necessary to determine the phase equilibria of the oil and ethanol over the broader range of elevated pressure and temperature. The phase equilibria of the triolein and ethanol mixture at 200 bars and for different temperature from 200 to 400 °C were calculated using the flash separation procedure of UniSim<sup>®</sup> software. The flash type VLL equilibria system was analyzed with RK-Aspen EOS already established as the most appropriate thermodynamic model in the case of triolein alcoholysis [203].

The results obtained by this simulation show that below 270 °C, the system consists of the two phases in equilibrium (**Figure 36**) and only one supercritical or dense phase is present at higher temperatures. The similar phase equilibrium was observed for methanol and triolein as shown in **Figure 36** [203]. Ethanol is the main constituent of vapour phase (more than 99.9

mol %) and content of ethanol in the liquid phase i.e. in triolein, increases with temperature. The similar data was obtained for methanol and triolein system (40:1 methanol to triolein molar ratio) at the same temperature and pressure (**Figure 36**) However, the content of ethanol in oil phase (liquid phase) and oil in ethanol (vapour phase) are both lower than in case of methanol – triolein system at the same temperature and pressure.

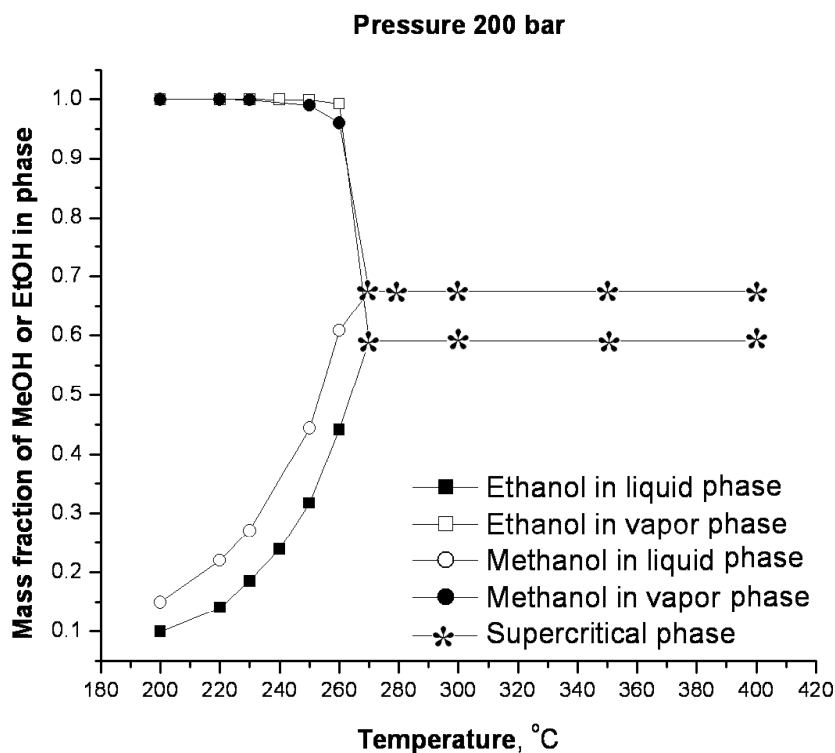


**Figure 36.** VLE at different temperature and content of ethanol in vapour, liquid and supercritical phase at 200 bars (molar ratio of methanol and triolein of 42:1)

The distribution of vapour and liquid phases during the temperature increase from 200 to 400 °C under the constant pressure of 200 bars is presented in **Figure 37**.



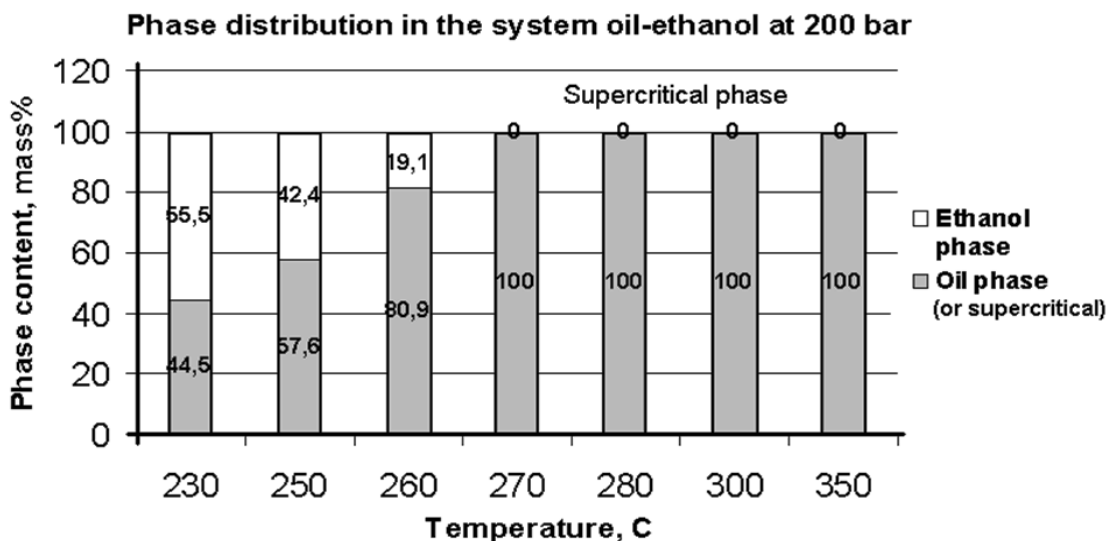


**Figure 37.** The phase distribution in mass% at different temperature

This is an idealized situation which might be expected if triolein and ethanol do not react. However, since ethanolysis will occur under investigated conditions one can expect that formation of different compounds during ethanolysis will change the mass ratio between phases, as well as their composition [203]. The calculated values of densities for vapour, liquid and supercritical phase are presented in **Figure 38**. The densities of methanol and oil mixture, for both liquid and vapour phase, are by approximately 10-20% higher than densities of ethanol and oil mixture (vapour and liquid phase), for 40:1 molar ratio of alcohol and triolein.

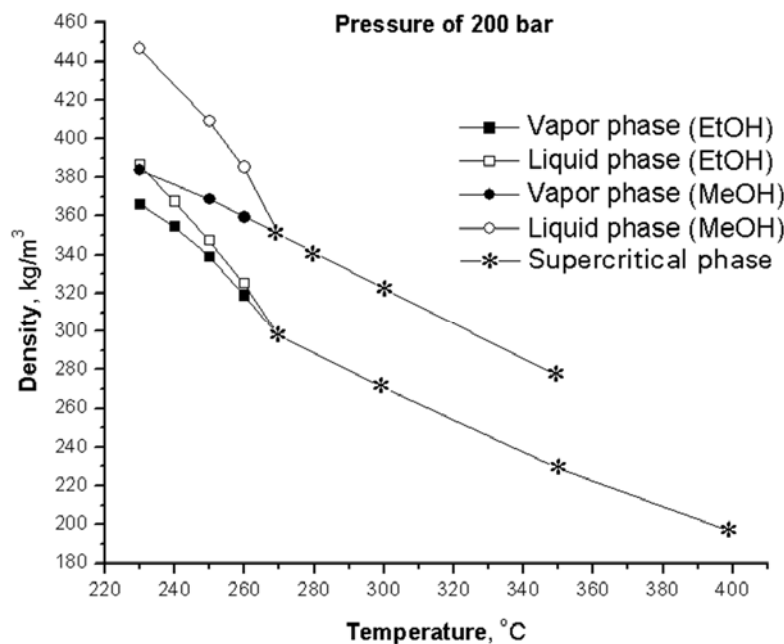


**Figure 38.** The temperature dependence of density at 200 bar

### 5.1.2. Phase equilibria in catalytic reaction system - diesel production

The high pressure and temperature equilibria of multiphase system of diesel production was analysed by Unisim software. The impact of different approximations of number of components which representing the reaction mixture was analysed too. The obtained results are shown in **Figure 39** where could be seen that liquid fraction in reaction mixture could significantly be different depending on the number of pseudo components used in the simulation. Namely, if the reaction mixture is approximated only with two normal alkanes (dodecane and octadecane) the reaction mixture has a small amount of liquid almost throughout the entire length of the reactor. The reaction mixture approximated with three alkanes (dodecane, hexadecane and octadecane) shows only the vapour phase throughout the reactor length. Such results depend highly on the distillation curves where the whole mixture should be approximated with 2, 3 or 5 components but with the requirement to be consistent with the distillation boiling point trend.

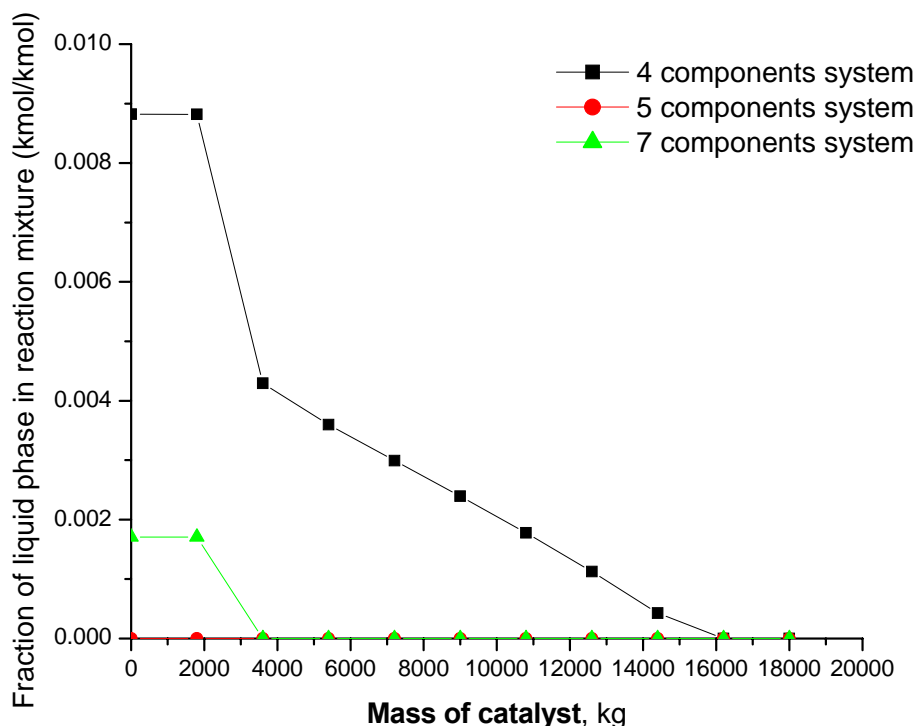


**Figure 39.** The fraction of liquid phase in reaction mixture along the length of reactor for different approximation of reaction mixture

The influence of different approximations and number of pseudo components of reaction mixture on the obtained results are summarised in **Figures 40** and **41**. From both Figures it could be seen that there is no difference, or the difference is insignificant, on sulphur conversion results for all approximations. From the other side, the approximation of reaction mixture with only two alkanes gave significant lower temperature difference in the reactor when compared with two other approximations and experimental results.

Based on this analysis it could be concluded that the best approximation for such system could be the seven component system: three hydrocarbons: n-dodecane, n-hexadecane, n-octadecane and one mono-aromatic compound: tetraline and one di-aromatic compound: phenantrene, with the addition of hydrogen and methane.

This composition was used in further evaluation and validation of proposed mathematic model for diesel production.

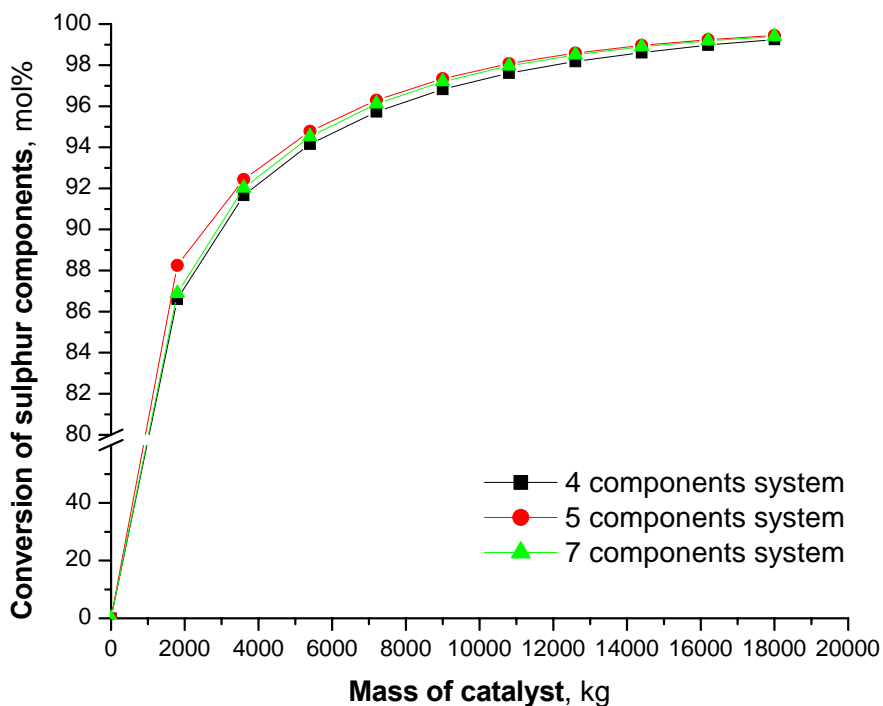


Figure 40. The sulphur conversion and impact of approximation of reaction mixture

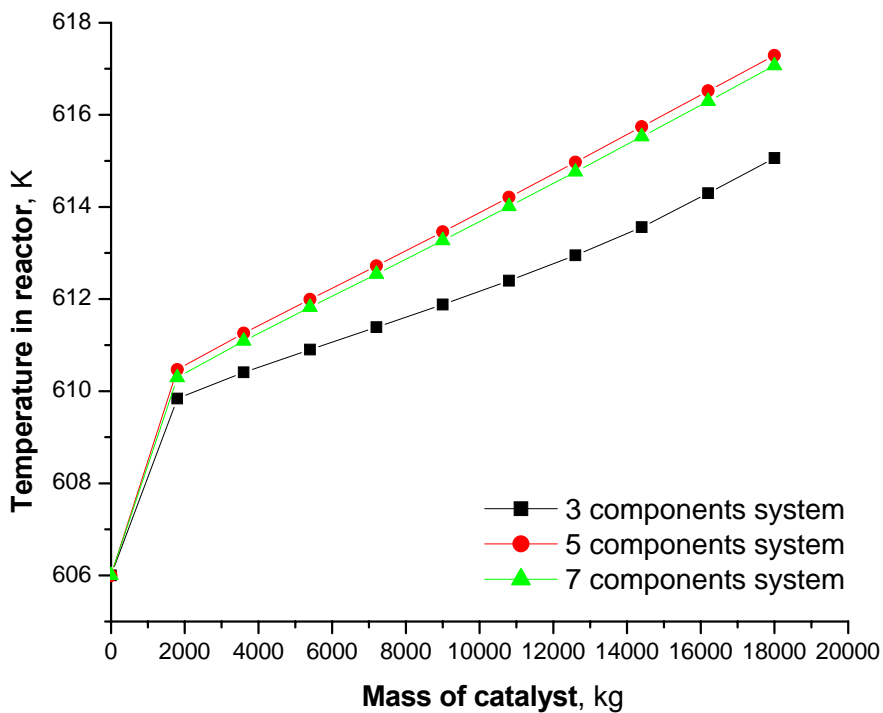


Figure 41. The temperature in reactor and impact of approximation of reaction mixture

Using those phase equilibria simulations, the necessary data for mathematical model (density, phase equilibrium constant and the ratio of total flow of liquid and vapor phases) were obtained. Density, phase equilibrium constant and the ratio of total flow of liquid and vapor phases were obtained by fitting the data using polynomial equations as a function of temperature. Data on the equilibrium distribution of components were obtained by using the Peng-Robinson equation of state and Unisim software (**Tables 21,22, 23 and 24**).

$$\rho^V = A + B \cdot T$$

**Table 21.** Vapor mixture density

$\rho^V$	M1	M2	M3	M4	M5	M6
<i>Four-component system</i>						
A	1.60539	1.59621	1.56971	1.56808	1.60671	1.60774
B	-0.00136	-0.00134	-0.00135	-0.00135	-0.00136	-0.00136
<i>Five - component system</i>						
A	3.29029	2.53461	2.53461	3.2035	3.21157	2.59147
B	-0.00717	-0.00454	-0.00454	-0.00688	-0.00689	-0.00472
C	5.01774*10 <sup>-6</sup>	9.9531*10 <sup>-6</sup>	9.9531*10 <sup>-6</sup>	4.7619*10 <sup>-6</sup>	4.7619*10 <sup>-6</sup>	2.85714*10 <sup>-6</sup>
<i>Seven - component system</i>						
A	2.37066	2.37079	2.37298	2.38194	2.56378	2.55286
B	-0.00396	-0.00396	-0.00397	-0.004	-0.00464	-0.00459
C	2.21351*10 <sup>-6</sup>	2.21351*10 <sup>-6</sup>	2.21961*10 <sup>-6</sup>	2.24367*10 <sup>-6</sup>	2.806*10 <sup>-6</sup>	2.764*10 <sup>-6</sup>

$$\rho^L = A + B \cdot T$$

**Table 22.** Liquid mixture density

$\rho^L$	M1	M2	M3	M4	M5	M6
<i>Four-component system</i>						
A	4.95037	4.91849	4.9114	4.90166	4.88102	4.79002
B	-0.00428	-0.00424	-0.0042	-0.00421	-0.00419	-0.00409
<i>Five - component system</i>						
A	5.52357	8.61223	8.61223	0.57143	5.25071	5.12943
B	-0.00564	-0.001628	-0.001628	0.01164	-0.0471	-0.00451
C	7.9381*10 <sup>-7</sup>	9.9531*10 <sup>-6</sup>	9.9531*10 <sup>-6</sup>	-1.42857*10 <sup>-5</sup>	-1.1294*10 <sup>-17</sup>	1.33665*10 <sup>-17</sup>
<i>Seven - component system</i>						
A	69.73895	69.11362	68.07401	69.53556	58.10043	71.89132
B	-0.23674	-0.23465	-0.23124	-0.23675	-0.19098	-0.2403
C	2.10789*10 <sup>-6</sup>	2.09051*10 <sup>-4</sup>	2.06266*10 <sup>-4</sup>	2.11424*10 <sup>-4</sup>	-1.6488*10 <sup>-4</sup>	2.0889*10 <sup>-4</sup>

$$K_i = A + B \cdot T + C \cdot T^2 + D \cdot T^3$$

Table 23. Distribution coefficient

Ki	M1	M2	M3	M4	M5	M6
<i>Four-component system</i>						
<i>i=C<sub>12</sub></i>						
A	4.31254	4.12213	4.11317	4.92711	-64.89526	2.81899
B	0.02386	-0.2288	-0.02279	-0.02684	0.33039	-0.01556
C	4.01714*10 <sup>-5</sup>	3.85047*10 <sup>-5</sup>	3.82888*10 <sup>-5</sup>	4.50522*10 <sup>-5</sup>	-5.63905*10 <sup>-4</sup>	2.52416*10 <sup>-5</sup>
D	1.79722*10 <sup>-8</sup>	-1.70254*10 <sup>-8</sup>	-1.68809*10 <sup>-8</sup>	-2.06474*10 <sup>-8</sup>	3.25227*10 <sup>-7</sup>	-9.18535*10 <sup>-9</sup>
<i>i=C<sub>18</sub></i>						
A	-6.77251	-6.94142	-6.93469	-6.84698	-23.54032	-6.72686
B	0.03762	0.03848	0.03844	0.3799	0.12312	0.03732
C	7.0244*10 <sup>-5</sup>	-7.17118*10 <sup>-5</sup>	-7.16343*10 <sup>-5</sup>	-7.08497*10 <sup>-5</sup>	-2.15814*10 <sup>-4</sup>	-6.95819*10 <sup>-5</sup>
D	4.144*10 <sup>-8</sup>	4.49764*10 <sup>-8</sup>	4.49246*10 <sup>-8</sup>	4.44*10 <sup>-8</sup>	1.26726*10 <sup>-7</sup>	4.3657*10 <sup>-8</sup>
<i>i=H<sub>2</sub></i>						
A	79.75	76.2677	77.50073	93.81811	881.22029	75.7698
B	-0.23555	-0.21766	-0.22312	-0.30474	-4.32488	-0.20344
C	3.04124*10 <sup>-4</sup>	2.73547*10 <sup>-4</sup>	2.81734*10 <sup>-4</sup>	4.18092*10 <sup>-4</sup>	0.00726	-1.58912*10 <sup>-5</sup>
D	-1.72418*10 <sup>-7</sup>	-1.55077*10 <sup>-7</sup>	-1.59132*10 <sup>-7</sup>	-2.35141*10 <sup>-7</sup>	-4.11625*10 <sup>-6</sup>	-2.53881*10 <sup>-8</sup>
<i>i=CH<sub>4</sub></i>						
A	3.50108	2.3622	2.5877	10.1888	267.47133	-0.04195
B	0.0061	0.01197	0.01115	-0.02692	-1.34002	0.02905
C	2.99433*10 <sup>-5</sup>	1.9855*10 <sup>-5</sup>	2.08183*10 <sup>-5</sup>	8.44483*10 <sup>-5</sup>	0.00232	-1.58912*10 <sup>-5</sup>
D	-5.47765*10 <sup>-8</sup>	-4.90092*10 <sup>-8</sup>	-4.93373*10 <sup>-8</sup>	-8.48088*10 <sup>-8</sup>	-1.35164*10 <sup>-6</sup>	-2.53881*10 <sup>-8</sup>

Ki	M1	M2	M3	M4	M5	M6
<b>Five -component system</b>						
$i=C_{12}$						
A	-9.19669	-9.35361	-9.35361	-9.49316	-10.11304	-10.73439
B	0.05398	0.05485	0.05485	0.05566	0.05899	0.0624
C	$-1.07819 \times 10^{-4}$	$-1.09462 \times 10^{-4}$	$-1.09462 \times 10^{-4}$	$-1.10982 \times 10^{-4}$	$-1.16934 \times 10^{-4}$	$-1.23077 \times 10^{-4}$
D	$7.36687 \times 10^{-8}$	$7.47062 \times 10^{-8}$	$7.47062 \times 10^{-8}$	$7.56302 \times 10^{-8}$	$7.91422 \times 10^{-8}$	$8.27646 \times 10^{-8}$
$i=C_{16}$						
	-6.44882	-6.40833	-6.40833	-6.40833	-6.14062	-5.57742
	0.03717	0.03695	0.03695	0.03695	0.03554	0.03187
	$-7.21333 \times 10^{-5}$	$-7.17387 \times 10^{-5}$	$-7.17387 \times 10^{-5}$	$-7.17387 \times 10^{-5}$	$-6.92612 \times 10^{-5}$	$-6.1171 \times 10^{-5}$
	$4.72003 \times 10^{-8}$	$4.69627 \times 10^{-8}$	$4.69627 \times 10^{-8}$	$4.69627 \times 10^{-8}$	$4.55091 \times 10^{-8}$	$3.94946 \times 10^{-8}$
$i=C_{18}$						
A	-6.23719	-6.20825	-6.20825	-5.88779	-5.87115	-5.87115
B	0.03532	0.03516	0.03516	0.03349	0.0334	0.0334
C	$-6.72043 \times 10^{-5}$	$-6.69158 \times 10^{-5}$	$-6.69158 \times 10^{-5}$	$-6.39962 \times 10^{-5}$	$-6.38453 \times 10^{-5}$	$-6.38453 \times 10^{-5}$
D	$4.30222 \times 10^{-8}$	$4.28461 \times 10^{-8}$	$4.28461 \times 10^{-8}$	$4.11491 \times 10^{-8}$	$4.10564 \times 10^{-8}$	$4.10564 \times 10^{-8}$
$i=H_2$						
A	82.71474	81.06351	81.06351	81.13466	79.75671	74.73516
B	-0.2339	-0.22535	-0.22535	-0.22527	-0.21753	-0.19029
C	$2.77798 \times 10^{-4}$	$2.62902 \times 10^{-4}$	$2.62902 \times 10^{-4}$	$2.62274 \times 10^{-4}$	$2.48321 \times 10^{-4}$	$2.00125 \times 10^{-4}$
D	$-1.48637 \times 10^{-7}$	$-1.39913 \times 10^{-7}$	$-1.39913 \times 10^{-7}$	$-1.39389 \times 10^{-7}$	$-1.31167 \times 10^{-6}$	$-1.03095 \times 10^{-7}$
$i=CH_4$						
A	1.80998	0.78804	0.78804	0.06505	-1.68752	-1.78366
B	0.01464	0.02004	0.02004	0.02391	0.03312	0.03368
C	$1.33206 \times 10^{-5}$	$3.77446 \times 10^{-6}$	$3.77446 \times 10^{-6}$	$-3.10691 \times 10^{-6}$	$-1.92147 \times 10^{-5}$	$-2.03066 \times 10^{-5}$
D	$-4.45542 \times 10^{-8}$	$-3.89037 \times 10^{-8}$	$-3.89037 \times 10^{-8}$	$-3.48371 \times 10^{-8}$	$-2.54238 \times 10^{-8}$	$-2.4691 \times 10^{-8}$



Ki	M1	M2	M3	M4	M5	M6
<b>Seven -component system</b>						
$i=C_{12}$						
A	-59.2551	-58.29258	-58.00928	-59.40887	2.70667	2.61079
B	0.31754	0.31253	0.31158	0.31906	-0.01167	-0.01124
C	$-5.70193*10^{-4}$	$-5.61515*10^{-4}$	$-5.60752*10^{-4}$	$5.74101*10^{-4}$	$1.26909*10^{-5}$	$2.764*10^{-5}$
D	$3.43822*10^{-7}$	$3.3883*10^{-7}$	$3.3888*10^{-7}$	$3.46824*10^{-7}$	-	-
$i=C_{16}$						
A	-46.71842	-46.44286	-45.97876	-46.81743	2.21256	2.21816
B	0.24892	0.24757	0.24526	0.24982	-0.00853	-0.00854
C	$-4.43432*10^{-4}$	$-4.41233*10^{-5}$	$-4.37399*10^{-4}$	$-4.45669*10^{-4}$	$8.259802*10^{-6}$	$8.29694*10^{-6}$
D	$2.6432*10^{-7}$	$2.6136*10^{-7}$	$2.61026*10^{-7}$	$2.66014*10^{-7}$	-	-
$i=C_{18}$						
A	-39.25229	-39.06325	-38.74454	-39.34248	1.74286	1.74362
B	0.20865	0.20773	0.20613	0.2094	-0.00664	-0.00663
C	$-3.70626*10^{-4}$	$-3.69172*10^{-4}$	$-3.66492*10^{-4}$	$-3.72453*10^{-7}$	$6.36606*10^{-6}$	$6.35145*10^{-6}$
D	$2.20167*10^{-7}$	$2.19403*10^{-7}$	$2.17913*10^{-7}$	$2.21522*10^{-7}$	-	-
$i=H_2$						
A	3815.726	3947.1963	4161.50448	4236.57925	471.82557	595.51867
B	-18.28825	-18.96829	-20.07161	-20.45035	-1.56368	-2.00174
C	0.02909	0.03027	0.03216	0.03279	0.00133	0.00172
D	$-1.52643*10^{-5}$	$1.59356*10^{-5}$	$-1.70153*10^{-5}$	$-1.73592*10^{-5}$	-	-
$i=CH_4$						
A	1262.07646	1310.16277	1382.34379	1406.03789	163.40972	210.6305
B	-6.01547	-6.26438	-6.63639	-6.7562	-0.54345	-0.711
C	0.00951	0.00994	0.01057	0.017077	$9.3524*10^{-7}$	$6.20065*10^{-4}$
D	$-4.93375*10^{-6}$	$-5.17986*10^{-6}$	$-5.54434*10^{-6}$	$-5.65307*10^{-6}$	-	-
$i=A_I$						
A	-26.49013	-26.63872	-26.99391	-27.68327	-0.33341	-1.09304
B	0.13555	0.13638	0.13825	0.14192	$-5.65451*10^{-4}$	0.00214

C	$2.17165 \cdot 10^{-5}$	$-2.3468 \cdot 10^{-4}$	$-2.37971 \cdot 10^{-4}$	$-2.44476 \cdot 10^{-4}$	$2.55814 \cdot 10^{-6}$	$1.5128 \cdot 10^{-7}$
D	$1.24303 \cdot 10^{-8}$	$1.36704 \cdot 10^{-7}$	$1.38621 \cdot 10^{-7}$	$1.4244 \cdot 10^{-7}$	-	-
$i=A_2$						
A	2.54164	-2.61577	-2.73884	-2.78788	0.17098	-0.03204
B	0.01281	0.0132	0.01384	0.0141	$-8.1533 \cdot 10^{-4}$	$-9.62507 \cdot 10^{-5}$
C	$-2.17165 \cdot 10^{-5}$	$-2.2393 \cdot 10^{-5}$	$-2.3492 \cdot 10^{-5}$	$-2.39388 \cdot 10^{-5}$	$9.3524 \cdot 10^{-6}$	$2.9817 \cdot 10^{-7}$
D	$1.24303 \cdot 10^{-8}$	$1.28225 \cdot 10^{-8}$	$1.34528 \cdot 10^{-8}$	$1.37075 \cdot 10^{-8}$	-	-

$$\frac{F^L}{F^V} = A + B \cdot T + C \cdot T^2 + D \cdot T^3$$

Table 24. Molar flow rate ratio

	M1	M2	M3	M4	M5	M6
<b>Four - component system</b>						
A	-2.28097	-2.34576	-2.34559	-2.32509	-2.6606	-2.27099
B	0.00872	0.00894	0.00894	0.00886	0.00998	0.00862
C	$-8.15402 \cdot 10^{-6}$	$-8.34217 \cdot 10^{-6}$	$-8.33667 \cdot 10^{-6}$	$-8.26352 \cdot 10^{-6}$	$-9.20426 \cdot 10^{-6}$	$-8.0314 \cdot 10^{-6}$
<b>Five - component system</b>						
A	-2.26429	-2.24768	-2.24768	-2.1532	-2.16432	-2.09995
B	0.00907	0.00901	0.00901	0.00866	0.00868	0.00841
C	$-8.83995 \cdot 10^{-6}$	$-8.77894 \cdot 10^{-6}$	$-8.77894 \cdot 10^{-6}$	$-8.4742 \cdot 10^{-6}$	$-8.47695 \cdot 10^{-6}$	$-8.22506 \cdot 10^{-6}$
<b>Seven - component system</b>						
A	1.88313	1.87275	1.86654	1.82707	0.32929	0.69563
B	-0.00575	-0.00572	-0.0057	-0.00559	$-2.06704 \cdot 10^{-4}$	-0.00154
C	$4.36526 \cdot 10^{-6}$	$4.34262 \cdot 10^{-6}$	$4.32828 \cdot 10^{-6}$	$4.25331 \cdot 10^{-6}$	$-6.0027 \cdot 10^{-7}$	$6.0848 \cdot 10^{-7}$

## **5.2. Simulation results and model validation for both catalytic and non-catalytic diesel/biodiesel production**

### ***5.2.1. Determination of kinetic parameters for complex transesterification reaction by standard optimisation methods***

The kinetic model of biodiesel synthesis as defined by *Eq. 4-9*, including modification of  $k_{11}$  rate constant as shown by *Eq. 10*, was applied to the experimental data of transesterification reaction performed under subcritical conditions (150 °C and 1.1 MPa and 210 °C and 4.5 MPa). Six kinetic parameters for forward and reverse reactions were obtained by different approaches using numerical methods (**Tables 25, 26, 27**).

**Table 25.** Kinetic constants ( $\text{dm}^3/\text{kmol min}$ ) obtained by SA method

	Exp. 1		Exp. 1 with modified k11		Exp. 2		Exp. 2 with modified k11	
	Initial guess	Optimum	Initial guess	Optimum	Initial guess	Optimum	Initial guess	Optimum
k11	7.58E-07	5.83E-06	7.58E-07	1.95E-05	3.70E-06	5.73E-05	3.70E-06	2.32E-04
k12	0.00E+00	7.40E-06	0.00E+00	3.75E-05	0.00E+00	3.12E-03	0.00E+00	8.58E-06
k21	2.20E-07	6.38E-06	2.20E-07	8.45E-06	7.83E-06	6.32E-05	7.83E-06	1.13E-04
k22	0.00E+00	0.00E+00	0.00E+00	4.60E-06	0.00E+00	1.17E-04	0.00E+00	8.15E-04
k31	2.15E-07	3.20E-05	2.15E-07	8.37E-05	6.18E-06	2.37E-03	6.18E-06	7.98E-04
k32	0.00E+00	2.98E-05	0.00E+00	1.28E-04	0.00E+00	2.85E-03	0.00E+00	6.32E-05
<b>Error</b>		<b>3.286</b>		<b>3.741</b>		<b>6.129</b>		<b>5.359</b>
k11	7.58E-06	1.67E-05	7.58E-06	2.80E-05	3.70E-05	3.70E-05	3.70E-05	2.63E-04
k12	0.00E+00	4.45E-06	0.00E+00	1.58E-05	0.00E+00	0.00E+00	0.00E+00	3.62E-04
k21	2.20E-06	5.03E-06	2.20E-06	1.25E-05	7.83E-05	7.83E-05	7.83E-05	1.30E-04
k22	0.00E+00	0.00E+00	0.00E+00	2.13E-05	0.00E+00	0.00E+00	0.00E+00	7.35E-04
k31	2.15E-06	4.82E-06	2.15E-06	5.20E-06	6.18E-05	6.18E-05	6.18E-05	9.30E-04
k32	0.00E+00	0.00E+00	0.00E+00	1.78E-05	0.00E+00	0.00E+00	0.00E+00	1.20E-03
<b>Error</b>		<b>2.678</b>		<b>2.656</b>		<b>1.552</b>		<b>4.999</b>
k11	7.58E-05	1.83E-05	7.58E-05	4.45E-05	3.70E-04	4.78E-05	3.70E-04	3.30E-04
k12	0.00E+00	5.80E-04	0.00E+00	1.73E-04	0.00E+00	9.85E-04	0.00E+00	5.50E-04
k21	2.20E-05	1.08E-05	2.20E-05	1.47E-05	7.83E-04	6.17E-04	7.83E-04	2.05E-04
k22	0.00E+00	2.15E-04	0.00E+00	3.88E-04	0.00E+00	5.40E-03	0.00E+00	2.53E-03
k31	2.15E-05	4.23E-05	2.15E-05	6.73E-05	6.18E-04	1.92E-03	6.18E-04	1.27E-03
k32	0.00E+00	1.16E-03	0.00E+00	3.72E-04	0.00E+00	1.10E-02	0.00E+00	2.75E-03
<b>Error</b>		<b>2.996</b>		<b>3.642</b>		<b>7.237</b>		<b>5.738</b>

The results obtained by SA method are presented in **Table 25**. The initial guess was obtained using linear technique. In order to reveal the dependency of the optimum solution on the initial guess, three guesses were considered for each experiment. The first guess is  $0.1 \times x_0$ , the second guess is  $x_0$ , and the last one is  $10 \times x_0$ , where  $x_0$  is the vector containing the obtained values of reactions' constants by linear technique. The optimum values of the kinetic constants depended significantly on the initial guess, and the second initial guess was found to result in the minimum error (*Eq. 11*).

The results obtained by LM method are shown in **Table 26**. The same initial guesses as in the case of SA were used. The results have indicated that the optimum value is practically insensitive and independent on the initial guess, and therefore only one set of results is shown in **Table 26**. Also, error values are considerably lower than in the case of SA method. In order to check whether the results obtained by LM are a local optimum or the global one, the LM program was performed with various initial guesses. For generating logical and different initial guess values and to avoid trapping into a local minimum, the initial guesses were determined using GA with sufficient population size (the default population size was changed from 20 to 500). In this way the time required for running the GA program increased significantly, but it has been confirmed that correct initial guess values have been obtained. The results showed that the data presented in **Table 26** are really the global optimum.

**Table 26.** Kinetic constants ( $\text{dm}^3/\text{kmol}\cdot\text{min}$ ) obtained by LM method

	Exp. 1	Exp. 1 with modified k11	Exp. 2	Exp. 2 with modified k11
k11	5.92E-06	2.77E-05	4.25E-05	2.30E-04
k12	7.15E-05	3.92E-04	3.72E-19	1.57E-03
k21	5.42E-06	5.80E-06	8.38E-05	1.43E-04
k22	3.70E-20	3.70E-20	3.72E-19	2.12E-04
k31	3.42E-06	3.52E-06	4.28E-05	4.68E-05
k32	3.70E-20	3.70E-20	3.72E-19	3.70E-19
<b>Error</b>	0.582	0.683	1.167	0.892

The kinetic parameters obtained by GA method are shown in **Table 27**. The error values are slightly higher than in the case of LM method. By comparing results shown in **Tables 26-27** it can be observed that LM method results in lower minimum error than SA method and even lower than GA method.

**Table 27.** Kinetic constants ( $\text{dm}^3/\text{kmol min}$ ) obtained by GA method

	<b>Exp. 1</b>	<b>Exp. 1 with modified <math>k_{11}</math></b>	<b>Exp. 2</b>	<b>Exp. 2 with modified <math>k_{11}</math></b>
<b><math>k_{11}</math></b>	5.03E-06	1.60E-05	4.25E-05	2.10E-04
<b><math>k_{12}</math></b>	3.82E-06	1.19E-05	1.40E-05	1.37E-04
<b><math>k_{21}</math></b>	5.93E-06	8.03E-06	8.53E-05	1.54E-04
<b><math>k_{22}</math></b>	1.04E-07	5.17E-06	1.39E-05	1.41E-04
<b><math>k_{31}</math></b>	3.60E-06	4.62E-06	4.35E-05	5.12E-05
<b><math>k_{32}</math></b>	5.43E-09	6.62E-07	1.78E-06	1.19E-06
<b>Error</b>	0.629	0.999	1.182	1.040

Model equations *Eq. 4-9* were solved using kinetic parameters obtained by LM and GA methods. The resulting composition profiles for each component, at analysed temperatures and pressures, are shown in **Figure 42** for LM method and **Figure 43** for GA method.

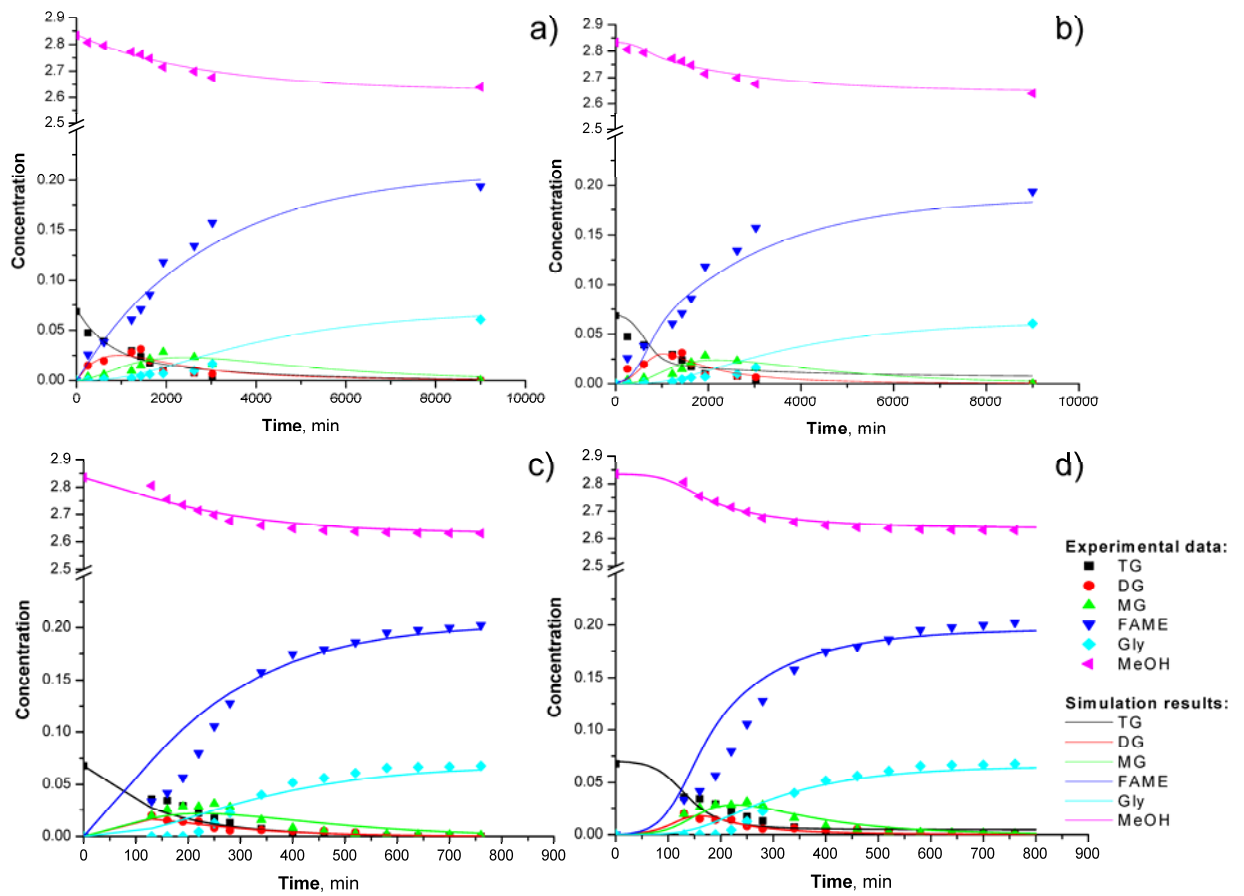


**Figure 42.** The comparison of model simulation results (kinetic constants obtained by LM method) and experimental results: a) Exp. 1; b) Exp.1 with modified  $k_{11}$ ; c) Exp. 2; d) Exp.2 with modified  $k_{11}$

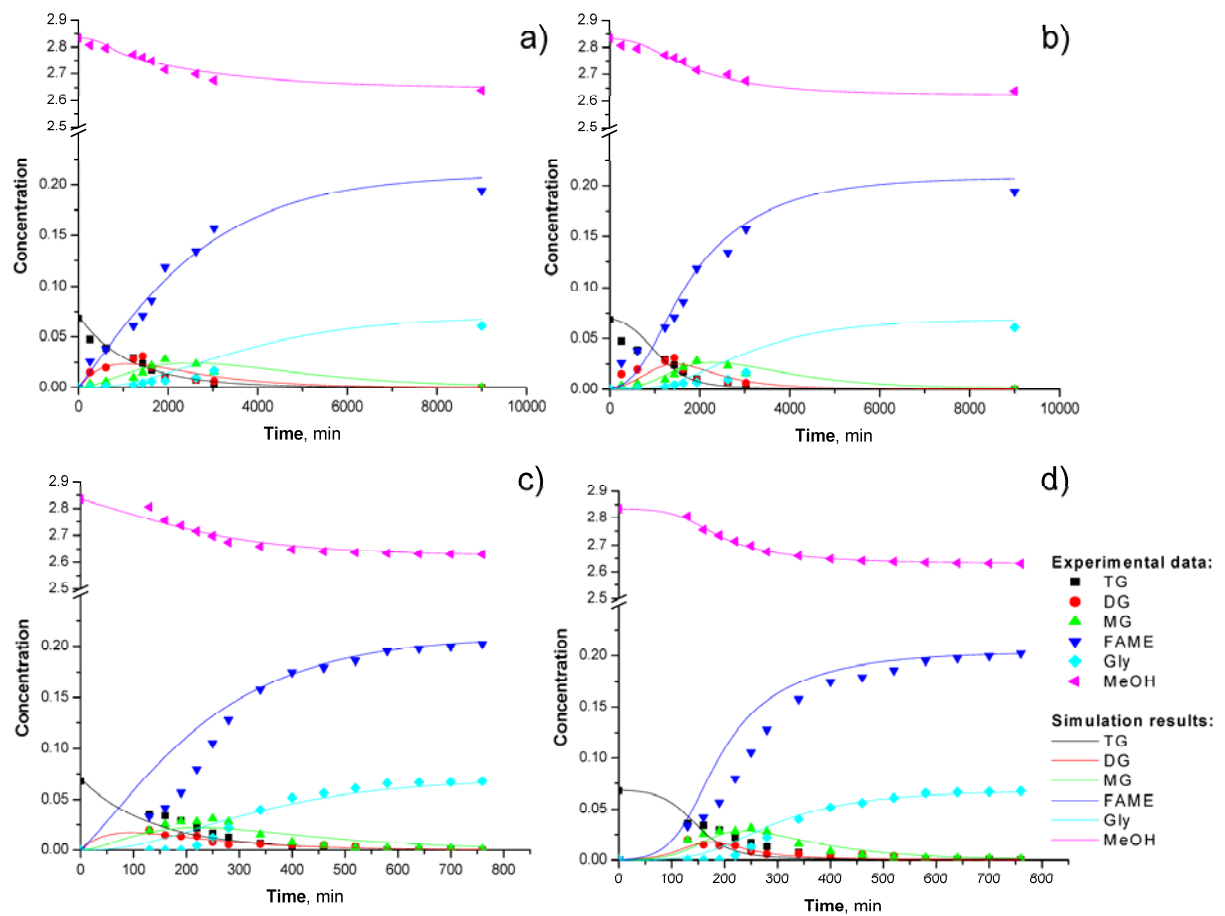


**Figure 43.** The comparison of model simulation results (kinetic constants obtained by GA method) and experimental results: a) Exp. 1; b) Exp.1 with modified  $k_{11}$ ; c) Exp. 2; d) Exp.2 with modified  $k_{11}$

The obtained results indicate that kinetic parameters determined by LM and GA are in good agreement with experimental data obtained at 150 °C and 1.1 MPa (Exp.1) with (Fig.42a and 1b) or without (Fig.43a and 2b) mass transfer limitations included in the expression for kinetic constant  $k_{11}$ . However, kinetic parameters deviate considerably from the experimental results at 210 °C and 4.5 MPa if the mass transfer limitations are not included in the kinetic constant  $k_{11}$  (Fig.42c and Fig.43c). Introducing the mass transfer modification of  $k_{11}$  kinetic constant improves accuracy but still doesn't lead to excellent correlation of experimental data. This is especially the case for concentration profile of FAME. Judging by FAME concentration profile it would seem that kinetic parameters obtained by numerical



optimisation methods correlate experimental data slightly worse than the parameters obtained by simplified kinetic procedure (**Fig.6b** in reference [219]).

Error values were thus calculated (using *Eq. 11*) for the procedure based only on triglycerides conversion and these were found to be 3.899 and 3.459 for the Exp.1 and Exp.2, respectively. Obviously these values are considerably higher than for LM and GA methods. Concentration profiles of intermediate species (diglycerides and monoglycerides) for these three methods are shown in **Figure 44**.

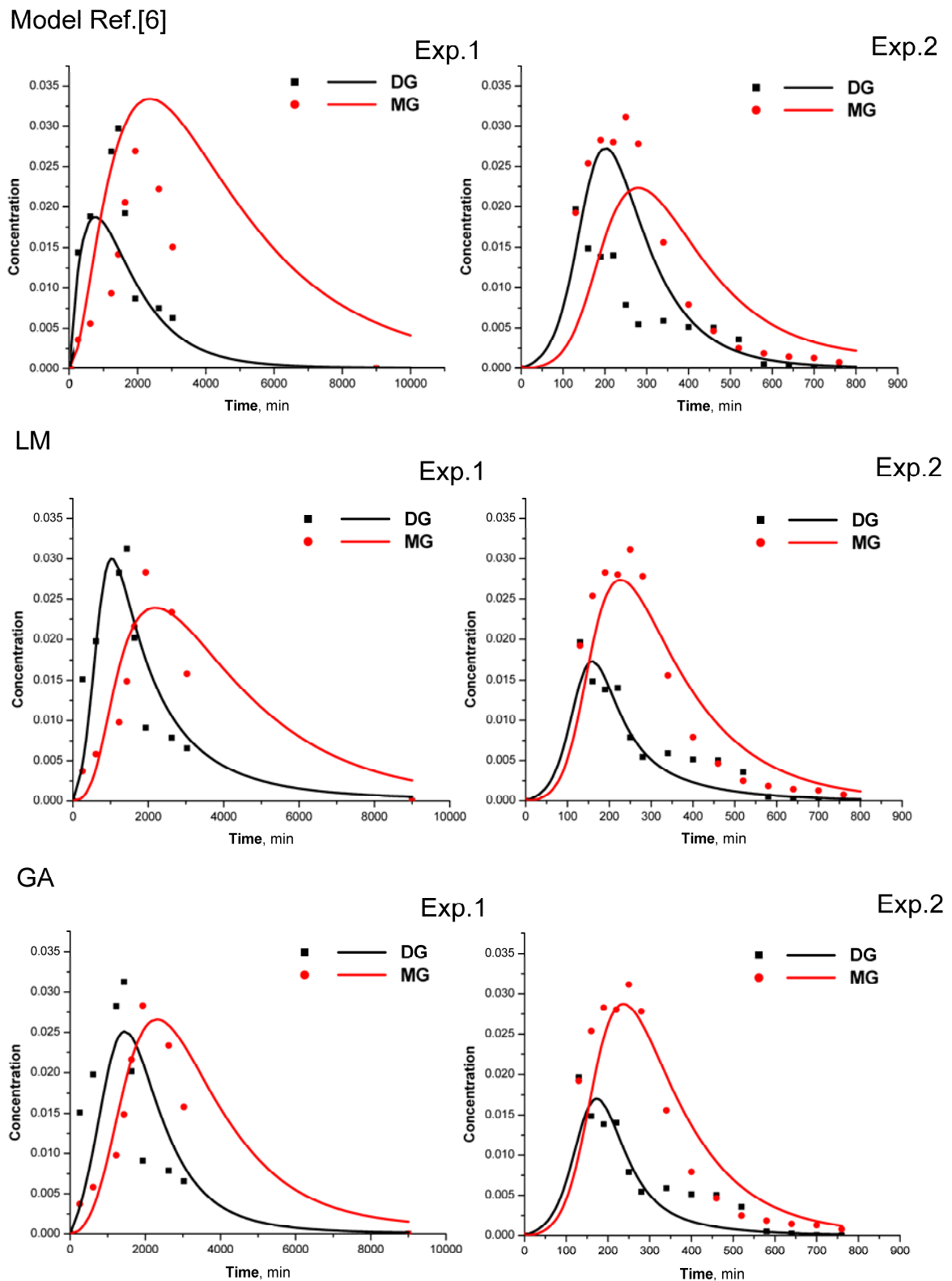


**Figure 44.** Comparison of the experimental and simulated data using kinetic constants obtained with the GA and LM optimisation methods and the simplified procedure [219].

It is clear that kinetic parameters obtained by optimisation methods are superior in predicting concentration profiles of diglycerides and monoglycerides, and this is especially the case for GA method. The ability to predict accurately concentrations of intermediates could be of crucial importance for proper design of reactor system for FAME synthesis. This is in fact critical parameter for FAME biodiesel quality due to limitations imposed by pertaining technical standards.

As stated previously the error values of LM method are slightly better than for GA method. However, careful inspection of values for kinetic parameters  $k_{11} - k_{32}$  in **Table 26** shows that kinetic constant for the first reverse reaction  $k_{12}$  is higher than forward reaction. However, this type of behaviour shouldn't be seen in this type of reactive system [249]. Also, values of  $k_{22}$  at 150 and 210 °C indicate that activation energy for  $k_{22}$  should be equal to 1026.2 kJ/mol which is hardly possible when compared to the values obtained in theoretical study using molecular orbital calculations [250,251].

**Table 28.** The comparison of  $E_a$  for forward reactions based on molecular orbital calculations [251] and values obtained in this study by the GA method.

	$E_a$ taken from [251], kJ/mol	$E_a$ by GA method, kJ/mol
for $k_{11}$	79.4	72.8
for $k_{21}$	71.1	83.5
for $k_{31}$	83.6	68.0

Kinetic constants obtained by the GA method (**Table 27**) indicate that equilibrium constants are always above 1 and also that equilibrium constants decrease with increasing temperature, which is in accordance with theoretical calculations of phase and chemical equilibrium [249]. Furthermore, the values of activation energies for forward reactions (in  $k_{11}$ ,  $k_{21}$  and  $k_{31}$ ) are in very good agreement with the values obtained through theoretical calculations based on molecular orbital calculations for synthesis under acidic conditions [250-252]. Values for route (c) from [251] have been used to make comparison and this is shown in **Table 28**.

### 5.2.1.1. *Ethanolysis of triglycerides*

Ethanol has a slightly higher critical temperature but almost 20 bars lower critical pressure than methanol. Since the molecular structures of ethanol and methanol differ only by one methyl group, there is no substantial difference between the chemical and physical properties of these alcohols. Lower alcohols have been investigated as the source of alcohol for production of biodiesel under supercritical conditions [253-256] and it was found that the reactivity of alcohol decreases when ethanol is used. By using ethanol in the reaction of vegetable oil alcoholysis, it is possible to obtain the FAEE yield higher than 90 mass%, but the necessary time for this level of conversion is three times longer than in the case of methanol. It is obvious that much lower reaction rates are obtained at subcritical conditions of alcohol [255, Fig. 2 and 11, Fig.3] while the reaction rate could be gradually increased as either pressure or temperature rises. Moreover the increase of reaction temperature and pressure, especially to and above critical values for methanol or ethanol, results in a favourable influence on the yield of ester [255,256]. The effect of various process parameters on the yield of FAEE was studied by several researchers [257,258,255-261]. The process parameters studied, are shown in **Table 29**. The yield of FAEE or conversion of vegetable oil during methanolysis or ethanolysis of vegetable oil depends also on the type of vegetable oil. The application of saturated vegetable oils resulted in the higher yield of ester product. The optimum process conditions for ethanolysis of vegetable oils producing FAEE, with 90-95 mass% yields, were determined as: temperature in the vicinity of 300 °C, reaction time of approximately 30 min and high molar ratio of ethanol to oil (40:1), as can be seen in **Table 29**.

**Table 29.** Review of process parameters used for ethanolysis of vegetable oil under supercritical conditions and production of FAEE

References	Type of oil	Optimum reaction conditions				Yield. mass%
		Pressure bar	Temperature °C	Time min	EtOH:oil molar ratio	
Warabi et al. 2004 [257]	Rapeseed	165*	300	45	42	99.0
Madras et al., 2004 [259]	Sunflower	200	350	40	40	99.0
Varma and Madras. 2005 [260]	Linseed	200	300	100	40	99.0
	Castor	200	300	100	40	96.0
Vieitez et al., 2008 [261]	Soybean	200	350	42	40	77.5
Demirbas. 2008 [255]	Cottonseed	200	250	8	41	85.0
Demirbas. 2009 [256]	Linseed	200	250	8	41	88.0
Gui et al., 2009 [257]	Palm	295*	349	30	33	79.2
Valle et al., 2010 [262]	Fodder radish	-	319	22	39	97.5

\* Calculated by the vapour pressure

The observed differences in reaction rates of triglycerides methanolysis and ethanolysis could be explained by the values of solubility parameters, defined as the square root of the cohesive energy density. Solubility parameters for ethanol, methanol and vegetable oils are available in standard handbooks [263]. Since the solubility parameter for methanol ( $29.7 \text{ MPa}^{1/2}$ ) is higher than for ethanol ( $26.2 \text{ MPa}^{1/2}$ ) and more similar to solubility parameter of oil ( $37.4 \text{ MPa}^{1/2}$ ), the mutual solubility of oil in methanol and consequently conversions in methanol, are higher compared to those obtained in ethanol. Contact of reactants for the system alcohol – triglyceride certainly plays a crucial role in increasing reaction rate and it can be more quantitatively described by phase equilibrium at investigated pressures and temperatures.

Ethanolysis reaction proceeds in three consecutive steps and each of the steps is reversible reaction. Initial phase of the overall reaction is mainly resulting from the first step in which triglycerides are converted to diglycerides and fatty acid ethyl esters (FAEE). In the

intermediate phase diglycerides, unconverted triglycerides and small amount of monoglycerides are being converted to mainly monoglycerides, small amount of glycerol and FAEE. In the final stage, the remaining monoglycerides are converted to FAEE and glycerol. Based on the analogy with methanolysis of triglycerides [203] it can be concluded that pressure and temperature levels will influence different phase distribution scenarios with increasing conversion during reaction. Existence of vapour – liquid equilibrium or coexistence of one vapour and two liquid phases at certain p,T conditions will influence the reaction rate through local single phase concentrations, mass transfer of reactive species between the phases and reaction equilibrium (the magnitude of reversible reaction). Simplified kinetic analysis of the published experimental data shown in **Table 29** [257,258,255-261] was performed, assuming the first or second order reaction kinetics for overall reaction. The kinetic analysis for the first and second order irreversible reaction, conducted in a batch reactor, is shown in **Figure 45** for several temperatures of interest for high pressure non-catalytic ethanolysis (200 – 400 °C).

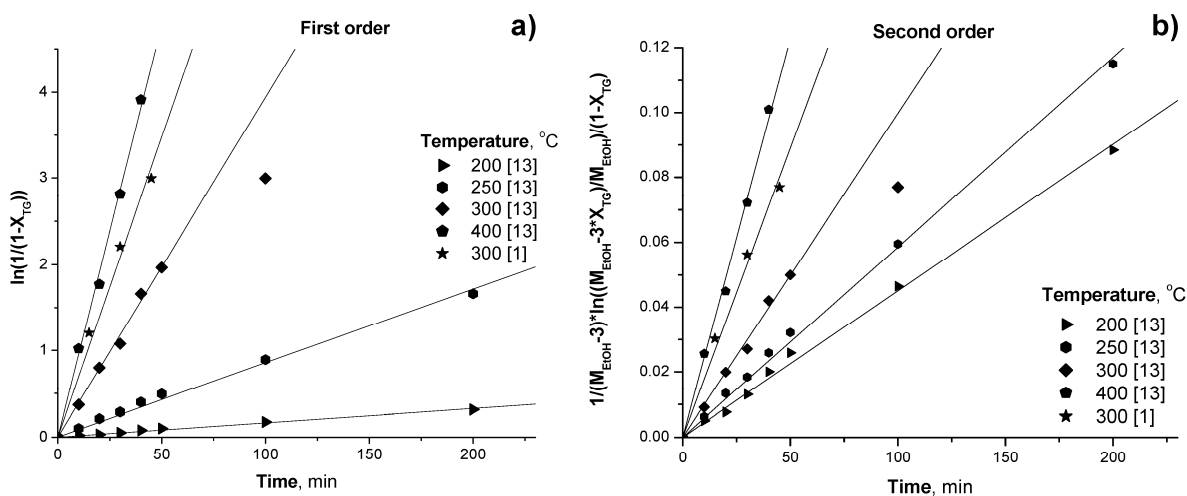


**Figure 45.** Analysis of the experimental data [257,260] using the pseudo first order (a) and second order (b) kinetic models

In **Figure 45a** the kinetic data are tested for irreversible first order kinetics in a batch reactor and in **Figure 45b** the same is shown for irreversible second order kinetics. In the initial phase of reaction at subcritical conditions of ethanol (200 °C at 200 bar), the mass transfer of reacting species plays a significant role in limitation of the overall reaction rate so the expected second order reaction kinetics turns into first order kinetics (first order kinetics at

200 °C in **Figure 45a** better fits the experimental data than second order kinetics shown in **Figure 45b**). This fact is confirmed by the molar ratio of oil to ethanol in oil rich phase (L2 in which the reaction takes place), which has a value of 1:2 at 200 °C (liquid phase composition data is shown in **Figure 34**). This excess of ethanol is less than required by the reaction stoichiometry and mass transfer of ethanol into L2 phase limits the overall reaction resulting in apparent first order kinetics. At 250 °C the oil to ethanol ratio in L2 phase is 1:16 (data shown in **Figure 34**) which provides sufficient excess of ethanol for the reaction. Consequently the first order kinetics can describe the experimental data due to more than fivefold excess of ethanol in L2. The second order kinetics are also in good agreement with experimental data at 250 °C since the mole balance equation used for second order kinetics contains local L2 ethanol to oil molar ratio –  $M_{\text{EtOH}}$ . At conditions of supercritical ethanol – triglycerides mixture (above 270 °C at 200 bar as predicted by the phase equilibrium model calculations, **Figures 34** and **36**), corresponding to the single reaction phase and the absence of mass transfer limitations, the pseudo first order reaction kinetic model is in better agreement with experimental data than second order kinetic model. This is the consequence of high ethanol to oil molar ratio at the beginning of reaction.

Due to relatively high ethanol to oil ratio used in the analysed kinetic experiments and increasing concentration of FAEE in the system, formation of a single fluid phase could be expected at higher triglycerides conversions [203]. Moreover, the increasing amount of monoglycerides, diglycerides and glycerol at higher conversions trigger the reversible reaction and the assumed model (irreversible first or second order) can not fit well the experimental data (data at 300 °C for 100 min in **Figure 45**). This trend occurs after 70% of total triglycerides conversion and corresponds to the appearance of the initial amount of glycerol in the system (**Figure 45a** and **Figure 45b**, and [203]). Similar deviations could have been observed at other temperatures if the higher conversion levels had been obtained in the analysed experiments (200 °C and 250 °C). This simplified kinetic analysis shows that it is not possible to describe such complex system by simple kinetic models and that the phase distribution and the phase composition play an important role in the overall reaction kinetics.

### 5.2.2. Simulation results of catalytic reaction system for diesel production

The complete results of all simulation performed with MatLab program based on developed mathematical model are summarised in following **Tables**.

**Table 30.** *Four component system: H<sub>2</sub>, CH<sub>4</sub>, C<sub>12</sub>, C<sub>18</sub>*

#### Kinetic data taken from Froment

composition	1	2	3	4	5	6
time	114(108)	78(72)	38(32)	30(24)	18(12)	6(0)
To, K	606	605	602	602	601	600
x (BT), %	100	100	100	100	100	100
x (DBT1), %	99.65	99.52	99.32	99.49	99.37	99.29
x (DBT2), %	84.09	83.75	93.45	95.22	92.21	89.56
x (DBT3), %	100	100	100	100	100	100
x (A1), %	33.66	28.63	9.69	9.57	8.68	8.13
x (S), %	98.52	98.48	99.35	99.53	99.24	98.99
dT	9	8.9	5.2	5.5	4	3.7

#### Kinetic data taken from Froment – linear increase of reaction rate by 50%

composition	1	2	3	4	5	6
time	114(108)	78(72)	38(32)	30(24)	18(12)	6(0)
To, K	606	605	602	602	601	600
x (BT), %	100	100	100	100	100	100
x (DBT1), %	99.66	99.48	99.32	99.49	99.37	99.29
x (DBT2), %	92.29	91.80	95.76	96.98	95.18	93.67
x (DBT3), %	100	100	100	100	100	100
x (A1), %	33.80	27.23	9.71	9.59	8.69	8.15
x (S), %	99.27	99.21	99.56	99.69	99.51	99.37
dT	9.1	8.8	5.3	5.6	4	3.70



**Table 31.** *Five component system: H<sub>2</sub>, CH<sub>4</sub>, C<sub>12</sub>, C<sub>16</sub>, C<sub>18</sub>***Kinetic data taken from Froment**

composition	1	2	3	4	5	6
time	114(108)	78(72)	38(32)	30(24)	18(12)	6(0)
To, K	606	605	602	602	601	600
x (BT), %	100	100	100	100	100	100
x (DBT1), %	99.89	99.85	99.76	99.76	99.74	99.73
x (DBT2), %	84.68	83.84	81.19	81.31	80.43	79.93
x (DBT3), %	100	100	100	100	100	100
x (A1), %	46.55	41.93	24.47	25.02	17.99	15.41
x (S), %	98.59	98.51	98.27	98.28	98.19	98.15
dT	11	11	7.6	7.9	4.7	4.4

**Kinetic data taken from Froment – linear increase of reaction rate by 50%**

composition	1	2	3	4	5	6
time	114(108)	78(72)	38(32)	30(24)	18(12)	6(0)
To, K	606	605	602	602	601	600
x (BT), %	100	100	100	100	100	100
x (DBT1), %	99.89	99.85	99.77	99.76	99.74	99.73
x (DBT2), %	94.03	93.54	91.87	91.95	91.37	91.03
x (DBT3), %	100	100	100	100	100	100
x (A1), %	46.68	42.08	24.54	25.11	18.04	15.45
x (S), %	99.45	99.40	99.24	99.25	99.19	99.16
dT	11.1	11.1	7.6	7.9	4.8	4.4

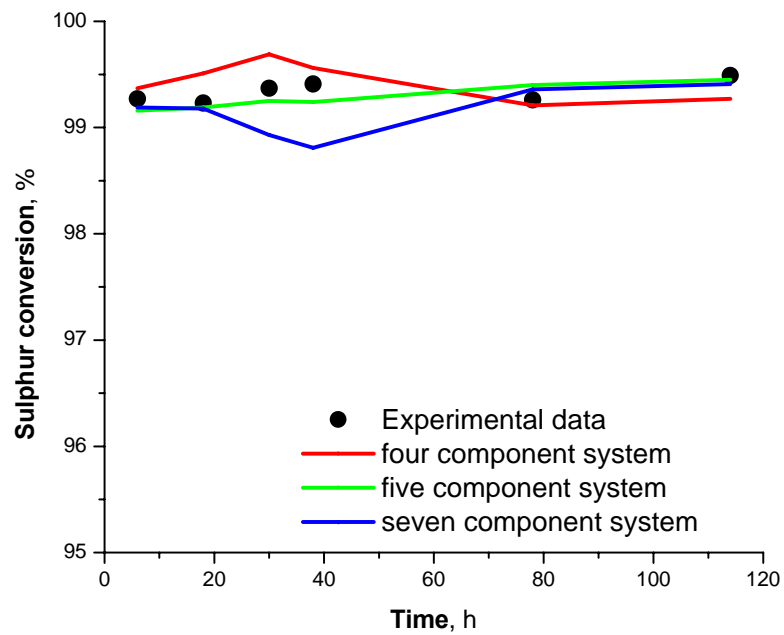
**Table 32.** *Seven component system: H<sub>2</sub>, CH<sub>4</sub>, C<sub>12</sub>, C<sub>16</sub>, C<sub>18</sub>, A<sub>1</sub>, A<sub>2</sub>***Kinetic data taken from Froment**

composition	1	2	3	4	5	6
time	114(108)	78(72)	38(32)	30(24)	18(12)	6(0)
To, K	606	605	602	602	601	600
x (BT), %	100	100	100	100	100	100
x (DBT1), %	99.86	99.81	99.15	99.30	99.72	99.75
x (DBT2), %	84.07	83.30	76.71	77.21	80.24	80.36
x (DBT3), %	100	100	100	100	100	100
x (A1), %	44.93	40.43	18.20	19.79	17.91	15.49
x (S), %	98.54	98.46	97.81	97.87	98.18	98.19
dT	10.8	10.9	6.8	7.3	4.7	4.4

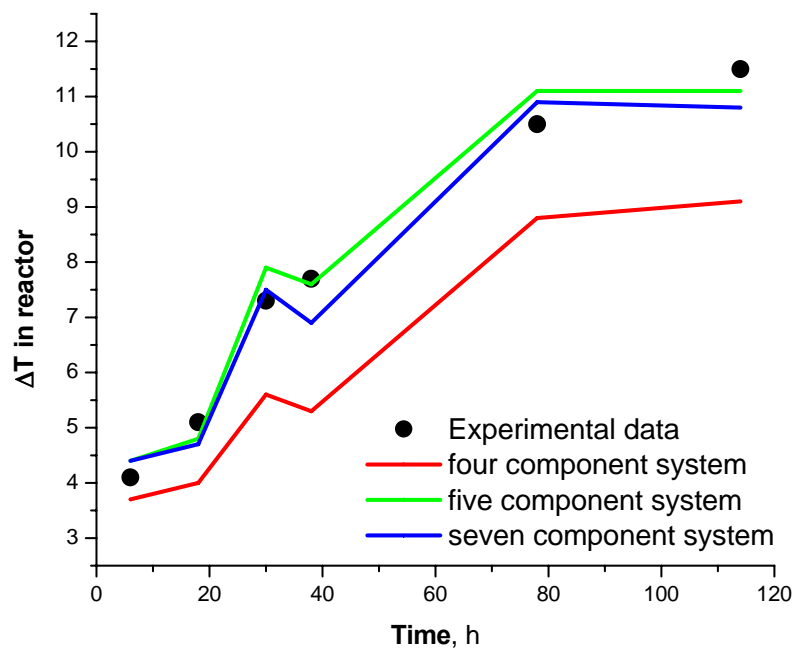
**Kinetic data taken from Froment – linear increase of reaction rate by 50%**

composition	1	2	3	4	5	6
time	114(108)	78(72)	38(32)	30(24)	18(12)	6(0)
To, K	606	605	602	602	601	600
x (BT), %	100	100	99.99999	100	100	100
x (DBT1), %	99.87	99.82	99.16	99.36	99.73	99.75
x (DBT2), %	93.60	93.14	87.67	88.74	91.24	91.32
x (DBT3), %	100	100	100	100	100	100
x (A1), %	45.05	40.58	18.29	20.24	17.96	15.53
x (S), %	99.41	99.36	98.81	98.93	99.18	99.19
dT	10.8	10.9	6.9	7.5	4.7	4.4

Model results were compared to data obtained during industrial test run performed in Refinery Pancevo. As explained previously the test was performed in industrial hydrotreating reactor. As shown in **Figure 46 a)** the agreement of model results and experimental conversion data is very good in all cases. It is important to stress that kinetic constant had to be increased by 50 % in order to achieve this very good correlation. This can attributed to higher inherent activity of the catalyst used in the test run than the activity of the catalyst used to develop kinetic equations. The best agreement was achieved when using five component system, or three components to describe middle distillates. Temperature rise in the reactor is shown in **Figure 46 b)** and it shows that five component system and seven component system agree well with measured data. Results obtained with four component system are predicting temperature rise with far worse accuracy.



a)



b)

**Figure 46.** Validation of model results

## 5.2.2.1. Temperature difference along the reactor – kinetic data by Froment

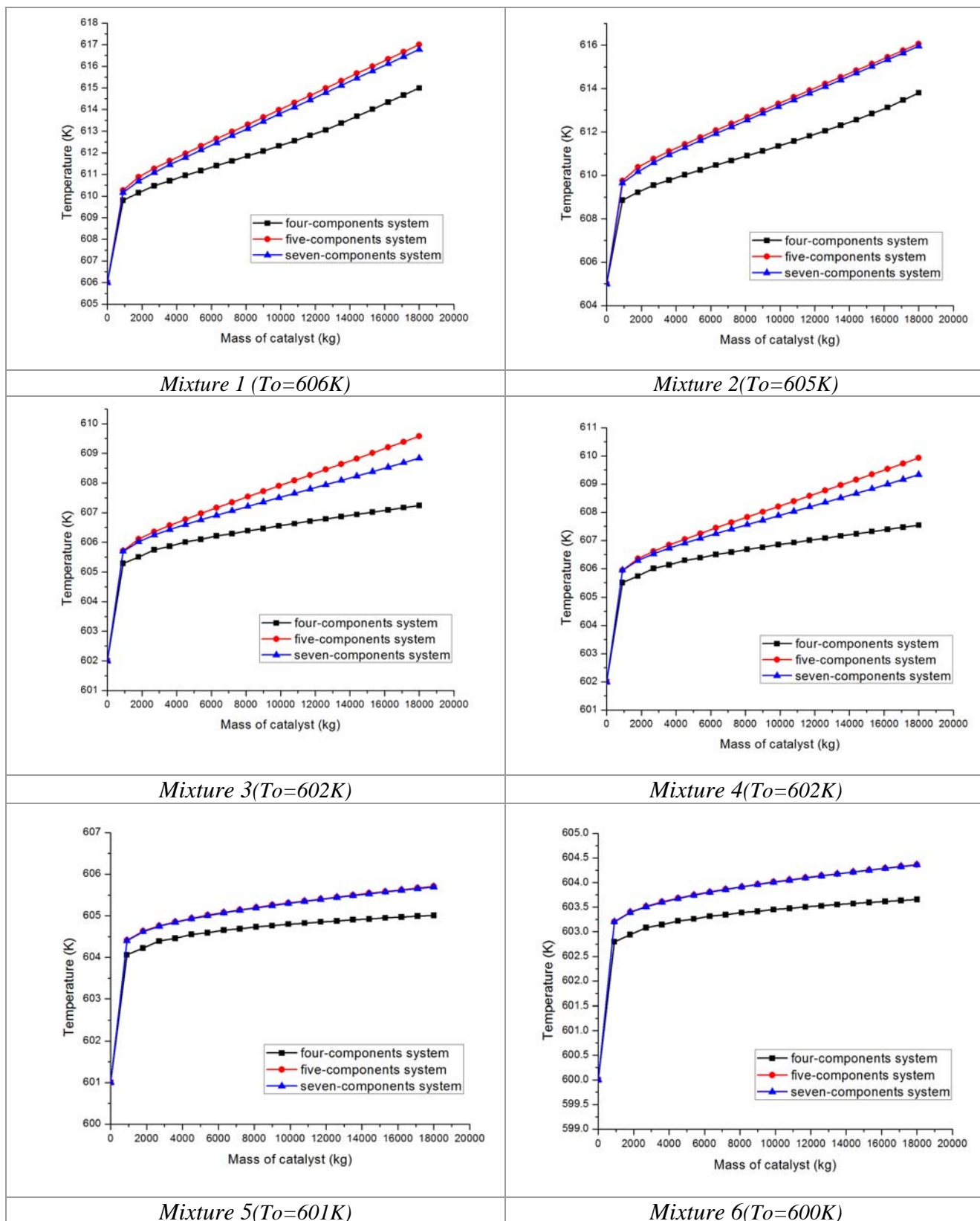


Figure 47. Temperature along the reactor catalyst bed

Temperature distribution in the reactor catalyst bed is shown in **Figure 47**. It can be observed that temperature raises abruptly in the entry sections of the reactor. This is less pronounced for higher inlet temperatures which correspond to higher inlet fraction of Light Cycle Oil during the run. This type of behaviour is expected since higher fraction of LCO means that inlet concentrations of diaromatic compounds are higher which leads to higher conversion of diaromatics and higher heat generation (due to exothermic reaction).

5.2.2.2. Catalyst wetting efficiency

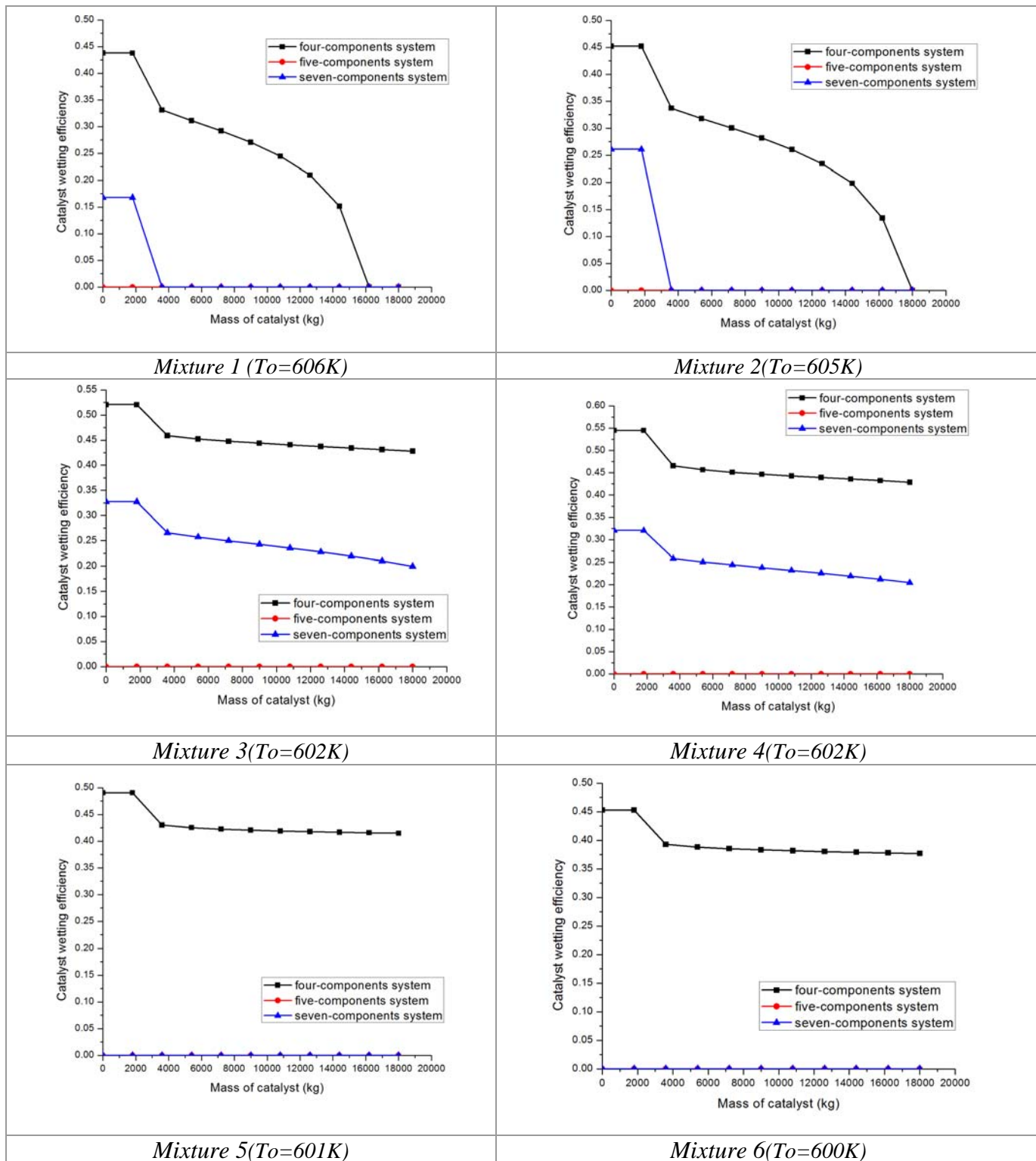
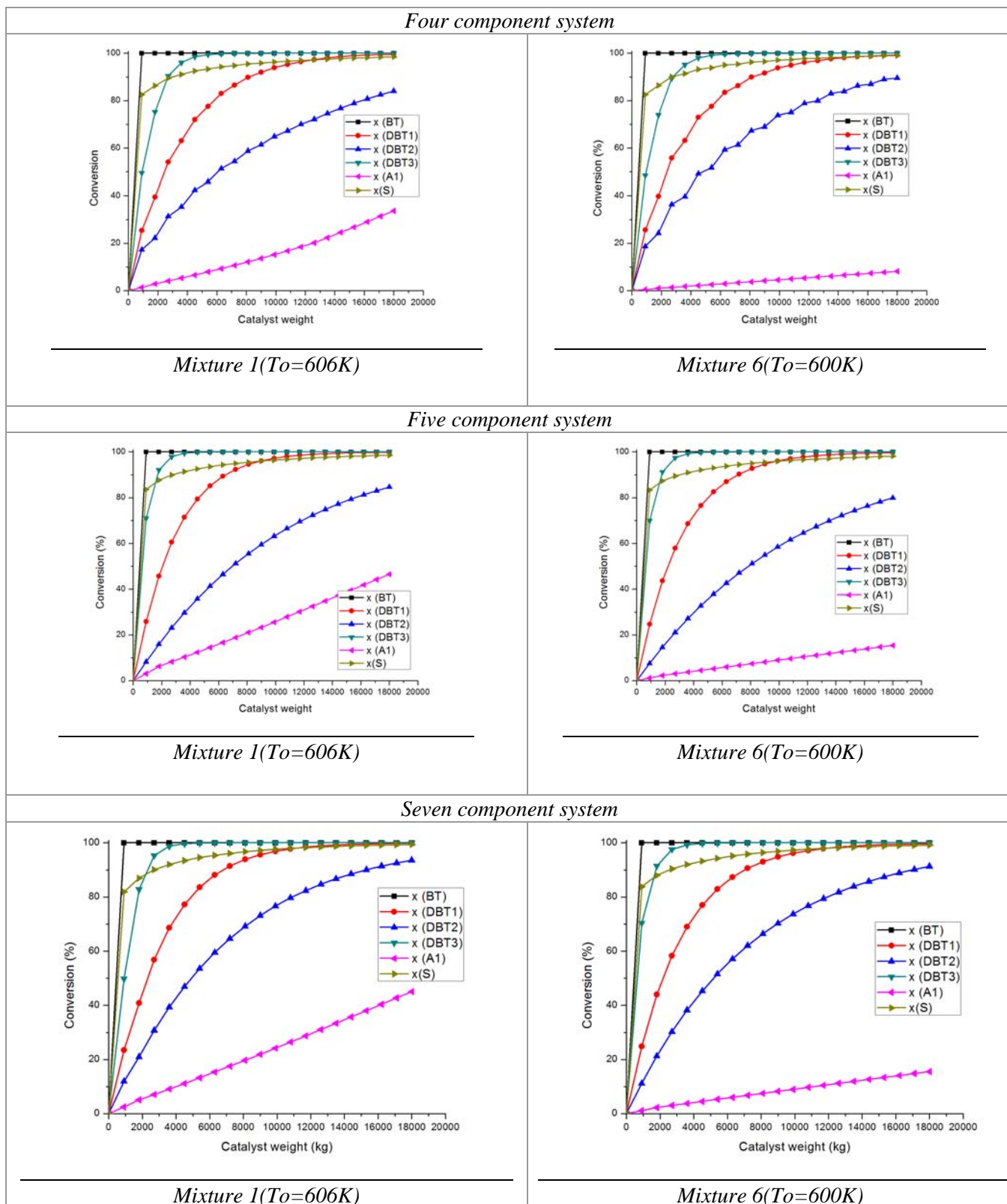


Figure 48. Catalyst wetting efficiency along the reactor catalyst bed

Distribution of the catalyst wetting efficiency in the reactor catalyst bed is shown in Figure 48. It can be observed that lower inlet temperature results in the absence of catalyst wetting due to evaporation of middle distillates. This is the case for five and seven component systems, while in the case of four component system a considerable fraction of the catalyst is wetted (around 40 %). Increasing inlet temperatures appear to increase wetting for seven component system. Although this seems contrary to the expectations it is consistent with the type of pseudo component used in seven component system. Those additional two components are aromatics with higher boiling points and they enter the reactor at higher inlet temperatures (they are not present at inlet temperatures of 600 and 601 K). This can be seen in **Table 14** on page 87 where one can observe twofold increase of monoaromatics quantity and threefold increase of diaromatics quantity. There is certain small influence of this type of behaviour of seven component system on the conversion since inlet temperatures of 602 K seem to underestimate the overall conversion (**Figure 46 a**).

## 5.2.2.3. The conversion of different type of sulphur compounds and aromatic components

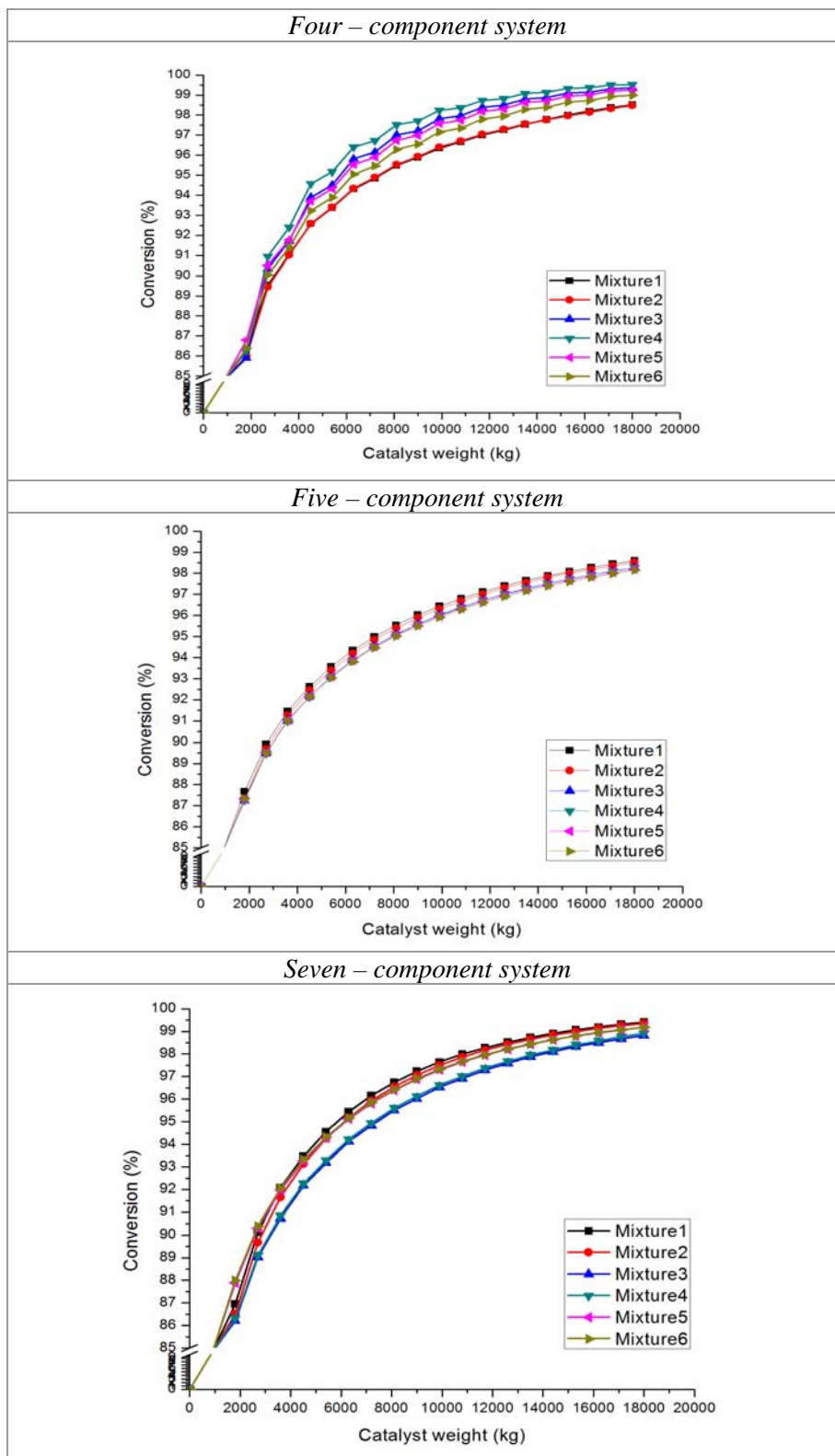


**Figure 49.** Conversion of different classes of sulphur compounds and aromatic compounds along the reactor catalyst bed



Conversion results shown in **Figure 49** indicate that all sulphur compounds react readily, except DBT2 which is known to be difficult to desulphurise. This is of course expected since kinetic equations should lead to this result. Small differences can be seen when different number of pseudo components have been used. This is particularly the case for DBT2 and diaromatic compounds.

## 5.2.2.4. Total sulphur conversion

**Figure 50.** Overall sulphur conversion along the reactor catalyst bed

Conversion results shown in **Figure 50** are expected and they indicate slightly lower conversion for mixture 3 in case of seven component system. This is similar to the observation shown previously and is probably the consequence of small deviations in inlet stream composition and maybe measurement of sulphur concentrations.

## 6. CONCLUSION

Multiphase non-catalytic and catalytic reaction processes are key elements for production of renewable and mineral diesel fuels. Although there are numerous theoretical investigations of multiphase reaction processes in the literature, this thesis is one of the few attempts to develop accurate and theoretically correct mathematical models of these processes, which could serve for reliable engineering analysis and optimization of diesel fuel production. The mathematical models presented here are deterministic models mainly because they can enable reliable extrapolation of analysis to a broader range of process operating conditions. By doing so, the user can perform reliable simulations and different technological scenarios of relevance for diesel production and processing.

Renewable diesel (fatty acid methyl ester, known as FAME biodiesel) production, or FAME biodiesel synthesis, can be performed using catalytic and non-catalytic process. In this thesis mathematical modeling was performed on non-catalytic process under elevated pressure and temperature. The model was developed on the starting hypothesis, which was previously observed experimentally, that the complex parallel – consecutive reversible reaction proceeds in the system which is essentially consisted of several phases. Phase equilibrium data were previously obtained using a high pressure view cell followed by GC analysis of the collected samples. The simulation of phase distribution using RK-Aspen equation of state correlated well the experimental data of a phase and component distribution for the investigated complex system. The results also indicate that the phase equilibrium of the system plays an important role in the reaction mechanism and kinetics of the non-catalytic synthesis of biodiesel under conditions of high pressure and temperature. Simulation of phase distribution results confirm that the rate of triglycerides transesterification, or overall reaction rate, depends strongly on the oil to ethanol or methanol ratio in the oil rich phase (corresponding to the two phase system below 270 °C at 200 bar). The reversible reaction extent increases if one phase system exists at the end of reaction, thereby decreasing the overall reaction rate.

The parameter estimation procedures were applied to the determination of kinetic parameters of non-catalytic fatty acids methyl esters (FAME) synthesis under elevated pressure. Experimental data used for modeling and parameter estimation were obtained

previously using mechanically agitated batch reactor of constant volume at 150 °C and 1.1 MPa and 210 °C and 4.5 MPa. The kinetic model used in this study consisted of three consecutive and parallel reversible reactions of second order. The kinetic constants for forward and reverse reaction steps were obtained by three different types of numerical optimisation methods: Simulated Annealing (SA), lsqcurvefit with Levenberg–Marquardt algorithm (LM) and Genetic Algorithm (GA). The proposed kinetic model and kinetic parameters determined by the GA method, with the inclusion of mass transfer limitations, fitted well the experimental data. Predictions of triglycerides conversion and FAME yield were very good as well as the predicted concentrations of intermediates (mono- and diglycerides). The activation energies of forward reactions are in very good agreement with values obtained by molecular orbital calculations.

Processing of petroleum middle distillate fractions is very important aspect of refineries processing crude oil. Several processes are used to produce diesel fuel and one of those is middle distillates hydrotreating. This reaction process proceeds in three phase system, reactants are present in liquid and vapour phase and the reaction takes place on the surface of solid catalyst. The model developed in this thesis focuses on phase equilibrium of reacting phases and the influence of phase compositions on the overall process performance. The developed model is a heterogeneous one-dimensional model and consists of differential equations of mass and heat balance and kinetics equations for the main reactions occurring in the hydrotreating process. Kinetic parameters were established by Froment et al. (1994) and model equations were solved using software package MATLAB 7.1. Effects of mass transfer were also incorporated in this model through catalyst effectiveness and effective catalyst wetting. Model validation was performed using data from industrial test run conducted under pressure of 40 bar in the catalytic reactor with two layers of conventional Co-Mo/ $\gamma$ -Al<sub>2</sub>O<sub>3</sub> catalyst. Due to the complex physical-chemical phenomena taking place in trickle bed reactors, their mathematical description leads to a system of differential equations.

The deterministic model developed in this thesis showed very good agreement with measured data during industrial test run. Temperature difference in the adiabatic reactor was predicted with high accuracy. Overall sulphur conversion results have shown slight underestimate of the achieved conversions and this can be attributed to difference in catalytic material between the test run catalyst and the one used to develop kinetic equations. The best agreement with experimental data was achieved when middle distillates were represented with

three or five pseudo – components. Only two pseudo components were found to be insufficient for accurate predictions. Vapor – liquid equilibrium in the catalyst bed was found to play important role in establishing overall reaction conditions due to partial wetting of the catalyst bed.

## 7. REFERENCES

- [1]. K.U. Klatt, W. Marquardt, Perspectives for process systems engineering - Personal views from academia and industry, *Computers and Chemical Engineering* 33 (2009) 536–550.
- [2]. J. Ponton, Process systems engineering: Halfway through the first century. *Chem. Eng. Sci.*, 50(24)(1995) 4045–4059.
- [3]. T.Takamatsu, The nature and role of process systems engineering. *Comput. Chem. Engg.*, 7 (1983) 203–218.
- [4]. I.E. Grossmann, A.W. Westerberg, Research challenges in process systems engineering. *AIChE J.*, 46 (2000)1700–1703.
- [5]. R. L. Motard, Integrated computer-aided process engineering. *Comput. Chem. Engng.*, 13 (1989) 1199–1206.
- [6]. P. Winter, Perspectives on computer-aided process engineering. *Chem. Eng. Res. Des.*, 68 (1990) 403–406.
- [7]. P. Winter, Perspectives on computer-aided process engineering. *Chem. Eng. Res. Des.*, 68 (1990) 403–406.
- [8]. W. Marquardt, From process simulation to lifecycle modeling. *Chem. Ing. Tech.*, 71 (1999) 1119–1137.
- [9]. L.C Thiam, B.Subhash, Catalytic processes towards the production of biofuels in a palm oil and oil palm biomass-based bio-refinery. *Bioresour Technol* 2008;99:7911–22.
- [10]. Atadashi IM, Aroua MK, Abdul Aziz A. Biodiesel separation and purification: a review. *Renew Energy* 2011;36:437–43.
- [11]. Fukuda H, Kondo A, Noda H. Biodiesel fuel production by transesterification of oils. *J Biosci Bioeng* 2001;92:405–16.
- [12]. Khan AK. Research into biodiesel kinetics and catalyst development. MSc thesis, University of Queensland; 2002.
- [13]. Ma F, Hanna MA. Biodiesel production: a review. *Bioresour Technol* 1999;70:1–15.
- [14]. Demirbas A. Importance of biodiesel as transportation fuel. *Energy Policy* 2007;35:4661–70.

## REFERENCES

---

- [15]. Haas MJ, McAloon AJ, Yee WC, Foglia TA. A process model to estimate biodiesel production costs. *Bioresour Technol* 2006;97:671–8.
- [16]. Fangrui M, Hana Milford A. Biodiesel production: a review. *Bioresour Technol* 1999;70:1–15.
- [17]. Demirbas A. Biodiesel from waste cooking oil via base-catalytic and supercritical methanol transesterification. *Energy Convers Manage* 2009;50:923–7.
- [18]. Agarwal AK. Biofuels (alcohols and biodiesel) applications as fuels for internal combustion engines. *Prog Energy Combust Sci* 2007;33:233–71.
- [19]. Openshaw M. Specific biodiesel issues for the additive industry, ATC fuel additive group. <[www.atc-europe.org](http://www.atc-europe.org)>.
- [20]. Waynick JA. Characterization of biodiesel oxidation and oxidation products. CRC Project No. AVFL-2b; task 1 results; SwRI\_ Project No. 08-10721; Prepared for: the coordinating research council, national renewable energy laboratory, US Department of Energy; 2005.
- [21]. Demirbas A. Biodiesel production from vegetable oils via catalytic and noncatalytic supercritical methanol transesterification methods. *Prog Energy Combust Sci* 2005;31:466–87.
- [22]. Saka S, Kusdiana D. Biodiesel fuel from rapeseed oil as prepared in supercritical methanol. *Fuel* 2001;80:225–31.
- [23]. Tan KT, Lee KT, Mohamed AR. Production of FAME by palm oil transesterification via supercritical methanol technology. *Biomass Bioenergy* 2009;33:1096–9.
- [24]. Helwani Z, Othman MR, Aziz N, Kim J, Fernando WJN. Solid heterogeneous catalysts for transesterification of triglycerides with methanol: a review. *Appl Catal A: Gen* 2009;363:1–10.
- [25]. Zabeti M, Wan M, Wan M, Wan D. Activity of solid catalysts for biodiesel production: a review. *Fuel Process Technol* 2009;90:770–7.
- [26]. Sherma YC, Singh B, Upadhyay SN. Advancements in development and characterization of biodiesel: a review. *Fuel* 2008;87:2355–73.
- [27]. Schuchardt U, Serchelia R, Vargas RM. Transesterification of vegetable oils: a review. *J Brazil Chem Soc* 1998;9:199–210.
- [28]. Kulkarni MG, Dalai AK. Waste cooking oil-an economical source for biodiesel: a review. *Ind Eng Chem Res* 2006;45:2901–13.



## REFERENCES

---

- [29]. Wu WH, Foglia TA, Marmer WN, Phillips JG. Optimizing production of ethyl esters of grease using 95% ethanol by response surface methodology. *J Am Oil Chem Soc* 1999;76(4):571–621.
- [30]. Hsu A, Jones KC, Marmer WN. Production of alkyl esters from tallow and grease using lipase immobilized in pylosilicate sol–gel. *J Am Oil Chem Soc* 2001;78(6):585–8.
- [31]. Marchetti JM, Miguel VU, Errazu AF. Possible methods for biodiesel production. *Renew Sust Energy Rev* 2007;11:1300–11.
- [32]. Granados ML, Poves MDZ, Alonso DM, Mariscal R, Galisteo FC, Tost RM. Biodiesel from sunflower oil by using activated calcium oxide. *Appl Catal B, Environ* 2007;73:317–26.
- [33]. Dossin TF, Reyniers MF, Berger RJ, Marin GB. Simulation of heterogeneously MgO-catalyzed transesterification for fine-chemical and biodiesel industrial production. *Appl Catal B, Environ* 2006;67:136–48.
- [34]. Freedman B, Butterfield RO, Pryde EH. Transesterification kinetics of soybean oil. *J Am Oil Chem Soc* 1986;63(10):1375–80.
- [35]. Meher LC, Kulkarni MG, Dalai AK, Naik SN. Transesterification of karanja (*Pongamia pinnata*) oil by solid basic catalysts. *Eur J Lipid Sci Technol* 2006;108:389–97.
- [36]. Kawashima A, Matsubara K, Honda K. Acceleration of catalytic activity of calcium oxide for biodiesel production. *Bioresour Technol* 2009;100:696–700.
- [37]. Lotero E, Liu Y, Lopez DE, Suwannakarn K, Bruce DA, Goodwin Jr JG. Synthesis of biodiesel via acid catalysis. *Ind Eng Chem Res* 2005;44:5353–63.
- [38]. Lotero E, Goodwin JG, Bruce DA, Suwannakarn K, Liu Y, Lopez DE. The catalysis of biodiesel synthesis. *Catalysis* 2006;19:41–83.
- [39]. Enweremadu CC, Mbarawa MM. Technical aspects of production and analysis of biodiesel from used cooking oil – a review. *Renew Sust Energy Rev* 2009;13:2205–24.
- [40]. Canakci M, Van Gerpen J. Biodiesel production via acid catalysis. *Transactions on ASAE* 1999;42:1203–10.
- [41]. Cerveró PJM, Coca J, Luque S. Production of biodiesel from vegetable oils. *Grasasy Aceites* 2008;59(1):76–83.

## REFERENCES

---

- [42]. Goff MJ, Bauer NS, Lopes S, Sutterlin WR, Suppes GJ. Acid-catalyzed alcoholysis of soybean oil. *J Am Oil Chem Soc* 2004;81:415–20.
- [43]. Di Serio M, Cozzolino M, Tesser R, Patrono P, Pinzari F, Bonelli B. Vanadyl phosphate catalysts in biodiesel production. *Appl Catal A: Gen* 2007;320:1–7.
- [44]. Y. Zhang, M.A. Dube, D.D. McLean, M. Kates, Biodiesel production from waste cooking oil: 1. Process design and technology assessment, *Bioresour. Technol.* 89 (2003) 1–16.
- [45]. Wang LY, Yang JC. Transesterification of soybean oil with nano-MgO or not in supercritical and subcritical methanol. *Fuel* 2007;86(3):328–33.
- [46]. Singh AK, Fernando SD. Reaction kinetics of soybean oil transesterification using heterogeneous metal oxide catalysts. *Chem Eng Tech* 2007;30(12):1–6.
- [47]. Kiss FE, Jovanovic M, Boškovic GC. Economic and ecological aspects of biodiesel production over homogeneous and heterogeneous catalysts. *Fuel Process Technol* 2010;91:1316–20.
- [48]. Drapcho CM, Nhuan NP, Walker TH. *Biofuels engineering process technology*. The McGraw-Hill Companies; 2008.
- [49]. Balat M, Balat H. A critical review of biodiesel as a vehicular fuel. *Energy Convers Manage* 2008;49(10):2727–41.
- [50]. Kusudiana D, Saka S. Kinetics of transesterification in rapeseed oil to biodiesel fuel as treated in supercritical methanol. *Fuel* 2001;80:693–8.
- [51]. Kusudiana D, Saka S. Effect of water on biodiesel fuel production by supercritical methanol treatment. *Bioresour Technol* 2004;91:289–95.
- [52]. Iijimia W, Kobayashi Y, Taniwaki K. Process for non-catalytically producing biodiesel fuel without yielding by-product, 2006 US Pat Appl.
- [53]. Sandra Glišić, Dejan Skala, *Biodiesel Production: The Problems in Software Design at Supercritical and Subcritical Conditions*’, chapter in ‘‘Supercritical fluids’’, Nova Science Publishers, Hauppauge, NY, United States (2009).
- [54]. Sandra Glišić, Dejan Skala, The problems in design and detailed analyses of energy consumption for biodiesel synthesis at supercritical conditions, *The Journal of Supercritical Fluids*, 49 (2) (2009) 293-301.

## REFERENCES

---

- [55]. Sandra Glišić, Ivana Lukic, Dejan Skala, Biodiesel Synthesis at High Pressure and Temperature: Analysis of energy consumption on industrial scale, *Bioresource Technology* 100 (2009) 6347–63
- [56]. Sandra Glišić, Dejan Skala, Design and Optimization of Purification Procedure for Biodiesel Washing, *CI&CIQ* 15 (3) 2009, 159-169.
- [57]. “U.S. Highway Fuel Demand: Trends and Prospects,” American Petroleum Institute Research Study No. 084, November 1996.
- [58]. S. Phirun, M. Lu, K. Tim, F. Liang, K.S. Jai, The effect of diesel fuel sulfur content on particulate matter emission for a non-road diesel generator, *J. Air Waste Manage. Assoc.* 55 (2005) 993.
- [59]. A. Sydbom, A. Blomberg, S. Parnia, N. Stenfors, T. Sandstrom, S.-E. Dahlen, Health effects of diesel exhaust emissions, *Eur. Respir. J.* 17 (2001) 733.
- [60]. (a) Diesel Emission Control – Sulfur Effects (DECSE) Program, Final Report: Diesel Oxidation Catalysts and Lean-NO<sub>x</sub> Catalysts, 2001, The US Department of Energy, Engine Manufacturers Association.; (b) Phase I Interim Data Report No. 3, Diesel Fuel Effects on Particulate Matter Emissions, November 1999.
- [61]. G. Corro, Sulfur impact on diesel emission control—a review, *React. Kinet. Catal. Lett.* 75 (2002) 89.
- [62]. J. Zhang, K. He, Y. Ge, X. Shi, Influence of fuel sulfur on the characterization of PM<sub>10</sub> from a diesel engine, *Fuel* 88 (2009) 504-510.
- [63]. M.M. Mariq, R.E. Chase, N. Xu, P.M. Laing, The effects of the catalytic converter and fuel sulfur level on motor vehicle particulate matter emissions: light duty diesel vehicles, *Environ. Sci. Technol.* 36 (2002) 283-289.
- [64]. A. Stanislaus, A. Marafi, A.S. Rana, Recent advances in the science and technology of ultra low sulfur diesel (ULSD) production, *Catal. Today* 153 (2010) 1-68.
- [65]. B.H. Cooper, K.G. Knudsen, Ultra deep desulfurization of diesel: how an understanding of the underlying kinetics can reduce investment costs, in: *Book Chapter-10 in, Practical Advances in Petroleum Processing*, 2006, p. 297.
- [66]. M. Breyse, G. Djega-Mariadassou, S. Pessayre, C. Geantet, M. Vrinat, G. Perot, M. Lemaire, Deep desulfurization: reactions, catalysts and technological challenges, *Catal. Today* 84 (2003) 129.

## REFERENCES

---

- [67]. C. Song, An overview of new approaches to deep desulfurization for ultra-clean gasoline, diesel fuel and jet fuel, *Catal. Today* 86 (2003)211–263;
- [68]. C. Song, X. Ma, New design approaches to ultra-clean diesel fuels by deep desulfurization and deep dearomatization, *Appl. Catal. B: Environ.* 41 (2003) 207.
- [69]. H. Topsøe, B. Hinnemann, J.K. Nørskov, J.V. Lauritsen, F. Besenbacher, P.L.Hansen, G. Hytoft, R.G. Egeberg, K.G. Knudsen, The role of reaction pathways and support interactions in the development of high activity hydrotreating catalysts, *Catal. Today* 107–108 (2005) 12.
- [70]. M. Andari, F. Abuseedo, A. Stanislaus, H. Qabazard, Kinetics of individual sulfur compounds in deep desulfurization of Kuwait diesel oil, *Fuel* 75 (1996) 1664–1670.
- [71]. K.G. Knudsen, B.H. Cooper, H. Topsoe, Catalyst and process technologies for ultra low sulfur diesel, *Appl. Catal. A: Gen.* 189 (1999) 205–215.
- [72]. R.R. Bharvani, R.S. Henderson, Revamp your hydrotreater for deep desulfurization: clean fuels, *Hydrocarb. Process.* 81 (2002) 61–64.
- [73]. A. Marafi, A. Al-Hindi, A. Stanislaus, Deep desulfurization of full range and low boiling diesel streams from Kuwait Lower Fars heavy crude, *Fuel Process. Technol.* 88 (2007) 905–911.
- [74]. T.C. Ho, Property–reactivity correlation for HDS of middle distillates, *Appl. Catal. A: Gen.* 244 (2003) 115–128.
- [75]. S. Torrisi, P.M. Gunter, Fundamentals of ultra-low sulfur diesel production: the 4 C's, in: NPRA Annual Meeting, March 21–23, San Antonio, TX, AM-04-27, 2004 (*Petroleum Technology Quarterly*, Summer 2004).
- [76]. T.C. Ho, Deep HDS of diesel fuel: chemistry, *Catal. Today* 98 (2004) 3–18.
- [77]. G.C. Laredo, J.L. Cano, C.R. Lopez, R. Saint Martin, M.C. Martinez, J.O. Marroquin, Alternate use of heavy hydrotreatment and visbreaker naphths by incorporation into diesel, *Fuel Proc. Technol.*, 88 (2007) 897-903.
- [78]. W.J. Danaher, L.D. Palmer, Chemical changes and ignition quality improvement resulting from hydrotreating light cycle oil, *Fuel*, 67 (1988) 1441-1445.
- [79]. J. Ancheyta-Juarez, E. Aguilar-Rodriguez, D. Salazar-Sotelo, G. Betancourt-Rivera, M. Leiva-Nuncio, Hydrotreating of straight run gas oil-light cycle oil blends, *Appl. Catal. A:General*, 180 (1999) 195-205.

## REFERENCES

---

- [80]. G.C. Laredo, R. Saint-Martin, M.C. Martinez, J. Castillo, J.L. Cano, High quality diesel by hydrotreating of atmospheric gas oil/light cycle oil blends, *Fuel*, 83 (2004) 1381-1389.
- [81]. T. Kabe, A. Ishihara, H. Tajima, Hydrodesulfurization of sulfur-containing polyaromatic compounds in light oil, *Ind. Eng. Chem. Res.*, 31 (1992) 1577-1580.
- [82]. G.A. Depauw, G.F. Froment, Molecular analysis of the sulphur components in a light cycle oil of a catalytic cracking unit by gas chromatography with mass spectrometric and atomic emission detection, *J. Chromatogr. A*, 761 (1997) 231-247.
- [83]. R. Shafi, G.J. Hutchings, Hydrodesulfurization of hindered dibenzothiophenes: an overview, *Catal. Today*, 59 (2000) 423-442.
- [84]. T. Koltai, M. Macaud, A. Guevara, E. Schultz, M. Lemaire, R. Bacaud, M. Vrinat, Comparative inhibiting effect of polycondensed aromatics and nitrogen compounds on the hydrodesulfurization of alkylidibenzothiophenes, *Appl. Catal. A: General*, 231 (2002) 253-261.
- [85]. Z.C. Mester, Trends in diesel fuel sulfur regulations, in: *Meeting Sulfur Specifications for 2000 and Beyond*, March 26–29, San Francisco, 2000.
- [86]. Ultra Low-sulfur Diesel Regulations Take Effect in US. *Green Car Congress: Ultra Low-sulfur Diesel Regulations*, 2006.
- [87]. F.L. Plantenga, R.G. Leliveld, Sulfur in fuels: more stringent sulfur specifications for fuels are driving innovation, *Appl. Catal. A: Gen.* 248 (2003) 1–7.
- [88]. F. Daniel, *Global Clean Fuels and the Middle East*, Refining, PTQ Autumn, 2002.
- [89]. European Union. Fuel Regulations, *Fuels* (<http://www.dieselnet.com/standards/eu/fuel.php>).
- [90]. Japan: Diesel Fuel, Fuel Regulations, <http://www.dieselnet.com/standards/jp/fuel.php>.
- [91]. Fuel Regulations, [www.dieselnet.com/standards/fuels.html](http://www.dieselnet.com/standards/fuels.html).
- [92]. Middle East Fuel Quality – Overview, Hart Energy Consulting, Presented to UNEP Jordan, National post lead workshop, July 24, 2008, Amman, Jordan, <http://www.unep.org/pcfv/PDF/JordanWrkshp-MiddleEastFuelQuality.pdf>.
- [93]. Clean Air Nonroad Diesel Rule, Energy Information Administration, Official Energy Statistics from the US Government, [http://www.eia.doe.gov/oiaf/aeo/otheranalysis/aeo\\_2005analysispapers/candr.html](http://www.eia.doe.gov/oiaf/aeo/otheranalysis/aeo_2005analysispapers/candr.html).

## REFERENCES

---

- [94]. European Emission Standards ([http://en.wikipedia.org/wiki/European emission standards](http://en.wikipedia.org/wiki/European_emission_standards)).
- [95]. C. Song, Introduction to chemistry of diesel fuel, in: C. Song, S. Hsu, I. Mochida (Eds.), *Chemistry of Diesel Fuels*, Taylor & Francis, New York, 2000 (Chapter 1);
- [96]. S. Torrisi, R. Street, T. Remans, J. Swain, *The Challenging Chemistry of Ultra-low-sulfur Diesel, Catalysis, Process Technology*, World Refining January/ February 2003.
- [97]. M.V. Landau, Deep hydrotreating of middle distillates from crude and shale oils, *Catal. Today* 36 (1997) 393–429.
- [98]. A. Amorelli, Y.D. Amos, C.P. Halsing, J.J. Kosman, R.J. Jonker, M. de Wind, J. Vrieling, Characterization of sulfur compounds in middle distillates and deeply hydrotreated products, *Hydrocarb. Process.* (June) (1992) 93–101.
- [99]. T. Kabe, H. Tajima, Deep desulfurization of methyl-substituted benziothiophenes and dibenzothiophenes in light gas oil, *J. Jpn. Petrol. Inst.* 36 (1992) 467–471.
- [100]. B.D. Quimby, V. Giarrocco, K.A. McCleary, Fast analysis of oxygen and sulfur compounds in gasoline by GC–AED, *J. High Resol. Chromatogr.* 15 (2005) 705–709.
- [101]. C. Lopez Garcia, M. Becchi, M.F. Grenier-Loustalot, O. Paisse, R. Szymanski, Analysis of aromatic sulfur compounds in gas oils using GC with sulfur chemiluminescence detection and high-resolution MS, *Anal. Chem.* 74 (2002) 3857.
- [102]. F. Adam, F. Bertoncini, N. Brodusch, E. Durand, D. Thiebaut, D. Espinat, M.- C. Hennion, New benchmark for basic and neutral nitrogen compounds speciation in middle distillates using comprehensive two-dimensional gas chromatography, *J. Chromatogr. A* 1148 (2007) 55–64.
- [103]. H. Qabazard, F. Abu-Seedo, A. Stanislaus, M. Andari, M. Absi-Halabi, Comparison between the performance of conventional and high-metal Co–Mo and Ni–Mo catalysts in deep desulfurization of Kuwait atmospheric gas oil, *Fuel Sci. Technol. Int.* 13 (1995) 1135–1151.
- [104]. A. Al-Barood, A. Stanislaus, Ultra-deep desulfurization of coker and straightrun gas oils: effect of lowering feedstock 95% boiling point, *Fuel Process. Technol.* 88 (2007) 309–315.
- [105]. K.H. Choi, Y. Sano, Y. Korai, I. Mochida, An approach to the deep hydrodesulfurization of light cycle oil, *Appl. Catal. B: Environ.* 53 (2004) 275–283.

## REFERENCES

---

- [106]. T.G. Kaufmann, A. Kaldor, G.F. Stuntz, M.C. Kerby, L.L. Ansell, Catalysis science and technology for cleaner transportation fuels, *Catal. Today* 62 (2000) 77–90.
- [107]. M.J. Girgis, B.C. Gates, Reactivities, reaction networks and kinetics in high pressure catalytic hydroprocessing, *Ind. Eng. Chem. Res.* 30 (1991) 2021–2058.
- [108]. B.C. Gates, H. Topsoe, Reactivities in deep catalytic hydrodesulfurization: challenges, opportunities, and the importance of 4-methyldibenzothiophene and 4,6-dimethyldibenzothiophene, *Polyhedron* 16 (1997) 3213–3217.
- [109]. H. Topsoe, B.S. Clausen, F.E. Massoth, in: J.R. Anderson, M. Boudart (Eds.), *Hydrotreating Catalysis-science and Technology*, vol. 11, Springer Verlag, Berlin, 1996.
- [110]. M.S. Rana, B.N. Srinivas, S.K. Maity, G. Murali Dhar, T.S.R. Prasada Rao, Origin of cracking functionality of sulfided (Ni) CoMo/SiO<sub>2</sub>–ZrO<sub>2</sub> catalysts, *J. Catal.* 195 (2000) 31–37.
- [111]. D.H. Broderick, B.C. Gates, Hydrogenolysis and hydrogenation of dibenzothiophene catalyzed by sulfided Co–Mo/Al<sub>2</sub>O<sub>3</sub>: the reaction kinetics, *AIChE J.* 27 (1981) 663–673.
- [112]. G. Perot, Hydrotreating catalysts containing zeolites and related materials mechanism aspects related to deep desulfurization, *Catal. Today* 86 (2003) 111–128
- [113]. F. Bataille, J.L. Leniberton, P. Michanct, G. Perot, M. Vrinai, M. Lemaire, E. Schulz, M. Breysse, S. Kaszlelan, Alkyldibenzothiophenes hydrodesulfurization-promoter effect, reactivity, and reaction mechanism, *J. Catal.* 191 (2000) 409–422.
- [114]. G.F. Froment, G.A. Depauw, V. Vanrysselberghe, Kinetic modeling and reactor simulation in hydrodesulfurization of oil fractions, *Ind. Eng. Chem. Res.*, **33**(12) (1994) 2975-2988
- [115]. V. Vanrysselberghe, G.F. Froment, Hydrodesulfurization of dibenzothiophene on a CoMo/Al<sub>2</sub>O<sub>3</sub> catalyst: Reaction network and kinetics, *Ind. Eng. Chem. Res.*, **35**(10) (1996) 3311-3318
- [116]. G.F. Froment, G.A. Depauw, V. Vanrysselberghe, Kinetics of the catalytic removal of the sulphur from the light cycle oil of a catalytic cracking unit, *Stud. Surf. Sci. Catal.*, **106** (1997) 83-96
- [117]. V. Vanrysselberghe, G.F. Froment, Kinetic modeling of hydrodesulfurization of oil fractions: Light cycle oil, *Ind. Eng. Chem. Res.*, **37**(11) (1998) 4231-4240

## REFERENCES

---

- [118]. V. Vanrysselberghe, R.L. Gall, G.F. Froment, Hydrodesulfurization of 4-Methyldibenzothiophene and 4,6-Dimethyldibenzothiophene on a CoMo/Al<sub>2</sub>O<sub>3</sub> catalyst: Reaction network and kinetics, *Ind. Eng. Chem. Res.*, **37**(4) (1998) 1235-1242
- [119]. I. Mochida, K. Sakanishi, X. Ma, S. Nagao, T. Isoda, Deep hydrodesulfurization of diesel fuel: design of reaction process and catalysts, *Catal. Today* 29 (1996) 185–189.
- [120]. X.L. Ma, K. Sakanishi, I. Mochida, Hydrodesulfurization reactivities of narrow cut fractions in a gas oil, *Ind. Eng. Chem. Res.* 34 (1995) 748–754.
- [121]. X.L. Ma, K. Sakanishi, I. Mochida, Hydrodesulfurization reactivities of various sulfur compounds in vacuum gas oil, *Ind. Eng. Chem. Res.* 35 (1996) 2487–2494.
- [122]. T. Kabe, K. Akamatsu, A. Ishihara, S. Otsuki, M. Godo, Q. Zhang, W. Qian, Deep hydrodesulfurization of light gas oil. 1. Kinetics and mechanisms of dibenzothiophene hydrodesulfurization, *Ind. Eng. Chem. Res.* 36 (1997) 5146–5152.
- [123]. M. Houalla, D. Broderick, V.H.J. de Beer, B.C. Gates, H. Kwart, Hydrodesulfurization of dibenzothiophene and related compounds catalyzed by sulfide CoO–MoO<sub>3</sub>/–Al<sub>2</sub>O<sub>3</sub>: effects of reactant structure on reactivity, *Am. Chem. Soc. Prep. Div. Petrol. Chem.* 22 (1977) 941.
- [124]. M. Houalla, N.K. Nag, A.V. Sapre, D.H. Broderick, B.C. Gates, Hydrodesulfurization of dibenzothiophene catalyzed by sulfided CoO–MoO<sub>3</sub>/–Al<sub>2</sub>O<sub>3</sub>: the reaction network, *AIChE J.* 24 (1978) 1015–1021.
- [125]. M. Houalla, D.H. Broderick, A.V. Sapre, N.K. Nag, V.H.J. De Beer, B.C. Gates, H. Kwart, Hydrodesulfurization of methyl-substituted dibenzothiophenes catalyzed by sulfided Co–Mo/–Al<sub>2</sub>O<sub>3</sub>, *J. Catal.* 61 (1980) 523–527
- [126]. N.K. Nag, A.V. Sapre, D.H. Broderick, B.C. Gates, Hydrodesulfurization of polycyclic aromatics catalyzed by sulfided CoO–MoO<sub>3</sub>/–Al<sub>2</sub>O<sub>3</sub>: the relative reactivities, *J. Catal.* 57 (1979) 509–512.
- [127]. M. Egorova, R. Prins, Hydrodesulfurization of dibenzothiophene and 4,6-dimethyldibenzothiophene over sulfided NiMo/–Al<sub>2</sub>O<sub>3</sub>, CoMo/–Al<sub>2</sub>O<sub>3</sub>, and Mo/–Al<sub>2</sub>O<sub>3</sub> catalysts, *J. Catal.* 225 (2004) 417–427.
- [128]. P. Zeuthen, K.G. Knudsen, D.D. Whitehurst, Organic nitrogen compounds in gas–oil blends and their importance to hydrotreatment, *Catal. Today.* 65 (2001) 307–314.



- [129]. F. Bataille, J.L. Leniberton, P. Michanct, G. Perot, M. Vrinai, M. Lemaire, E. Schulz, M. Breysse, S. Kaszlelan, Alkyldibenzothiophenes hydrodesulfurization-promoter effect, reactivity, and reaction mechanism, *J. Catal.* 191 (2000) 409–422.
- [130]. A.V. Sapre, D.H. Broderick, D. Fraenkel, B.C. Gates, N.K. Nag, Hydrodesulfurization of benzo(b)naphtho(2,3-d)thiophene catalyzed by sulfide CoO–MoO<sub>3</sub>/-Al<sub>2</sub>O<sub>3</sub>: the reaction network, *AIChE J.* 26 (1980) 690–694.
- [131]. A. Logadottir, P.G. Moses, B. Hinnemann, -N.Yu. Topsøe, K.G. Knudsen, H. Topsøe, J.K. Nørskov, A density functional study of inhibition of the HDS hydrogenation pathway by pyridine, benzene, and H<sub>2</sub>S on MoS<sub>2</sub>-based catalysts, *Catal. Today* 111 (2006) 44–51.
- [132]. F. Besenbacher, M. Brorson, B.S. Clausen, S. Helveg, B. Hinnemann, J. Kibsgaard, J.V. Lauritsen, P.G. Moses, J.K. Nørskov, H. Topsøe, Recent STM, DFT and HAADF-STEM studies of sulfide-based hydrotreating catalysts: insight into mechanistic, structural and particle size effects, *Catal. Today* 130 (2008) 86–96.
- [133]. E.J.M. Hensen, V.H.J. de Beer, J.A.R. van Veen, R.A. van Santen, On the sulfur tolerance of supported Ni(Co)Mo sulfide hydrotreating catalysts, *J. Catal.* 215 (2003) 353–357.
- [134]. M. Egorova, R. Prins, Mutual influence of the HDS of dibenzothiophene and HDN of 2-methylpyridine, *J. Catal.* 221 (2004) 11–19.
- [135]. H. Wang, R. Prins, Hydrodesulfurization of dibenzothiophene, 4,6-dimethyldibenzothiophene, and their hydrogenated intermediates over Ni–MoS<sub>2</sub>/-Al<sub>2</sub>O<sub>3</sub>, *J. Catal.* 264 (2009) 31–43.
- [136]. T. Kabe, A. Ishihara, W. Qian, Hydrodesulfurization and Hydrogenation, *Chemistry and Engineering*, Wiley-CH, Kodansha, Tokyo, New York, 1999.
- [137]. H. Farag, K. Sakanishi, Investigation of 4,6-dimethyldibenzothiophene hydrodesulfurization over a highly active bulk MoS<sub>2</sub> catalyst, *J. Catal.* 225 (2004) 531–535.
- [138]. F. van Looij, P. van der Laan, W.H.J. Stork, D.J. DiCamillo, J. Swain, Key parameters in deep hydrodesulfurization of diesel fuel, *Appl. Catal. A: Gen.* 170 (1998) 1–12.
- [139]. M.S. Rana, R. Navarro, J. Leglise, Competitive effects of nitrogen and sulfur content on activity of hydrotreating CoMo/Al<sub>2</sub>O<sub>3</sub> catalysts: a batch reactor study, *Catal. Today* 98 (2004) 67–74.

- [140]. E.A. Blekkan, A. Virnovskaia, H. Bergen, P. Steiner, Hydrodesulfurization of DBT over a NiMo catalyst: inhibition by sulfur and aromatic compounds, *ACS Fuel Chem. Div. Prep.* 48 (2003) 37–39.
- [141]. J. van Gestel, J. Leglise, J.-C. Duchet, Effect of hydrogen sulphide on the reaction of 2,6-dimethylaniline over sulphided hydrotreating catalysts, *Appl. Catal. A: Gen.* 92 (1992) 143–154.
- [142]. L.S. Byskov, J.K. Nørskov, B.S. Clausen, H. Topsøe, DFT calculations of unpromoted and promoted MoS<sub>2</sub>-based hydrodesulfurization catalysts, *J. Catal.* 187 (1999) 109–122.
- [143]. W.H.J. Stork, Molecules, catalysts and reactors in hydroprocessing of oil fractions *Stud. Surf. Sci. Catal.* 106 (1997) 41–67; (a) R. Krishna, S.T. Sie, Strategies for multiphase reactor selection, *Chem. Eng. Sci.* 49 (24) (1994) 4029–4065.
- [144]. J.F. Le Page, J. Cosyns, P. Courty, E. Freund, J.P. Franck, Y.J. Jscquin, B.C. Marcilly, G. Martino, J. Miquel, R. Montarnal, A. Sugier, H. van Landeghem, *Applied Heterogeneous Catalysis, Design, Manufacture. Use of Solid Catalyst*, Technip, Paris, 1987.
- [145]. N.-Y. Topsøe, H. Topsøe, FTIR studies of Mo/Al<sub>2</sub>O<sub>3</sub>-based catalysts. II. Evidence for the presence of SH groups and their role in acidity and activity, *J. Catal.* 139 (1993) 641–651.
- [146]. M.S. Rana, S.K. Maity, J. Ancheyta, G. Murali Dhar, T.S.R. Prasada Rao, Cumene cracking functionalities on sulfided Co(Ni)Mo/TiO<sub>2</sub>-SiO<sub>2</sub> catalysts, *Appl. Catal. A: Gen.* 258 (2004) 215–225.
- [147]. M.S. Rana, B.N. Srinivas, S.K. Maity, G. Murali Dhar, T.S.R. Prasada Rao, Origin of cracking functionality of sulfided (Ni) CoMo/SiO<sub>2</sub>-ZrO<sub>2</sub> catalysts, *J. Catal.* 195 (2000) 31–37.
- [148]. K. Sakanishi, T. Nagamatsu, I. Mochida, D.D. Whitehurst, Hydrodesulfurization kinetics and mechanism of 4,6-dimethyldibenzothiophene over NiMo catalyst supported on carbon, *J. Mol. Catal. A: Chem.* 155 (2000) 101–109.
- [149]. V. Meille, E. Schulz, M. Lemaire, M. Vrinat, Effect of experimental parameters on the relative reactivity of dibenzothiophene and 4-methyldibenzothiophene, *Appl. Catal. A: Gen.* 131 (1995) 143–157.

- [150]. H. Farag, I. Mochida, K. Sakanishi, Fundamental comparison studies on hydrodesulfurization of dibenzothiophenes over CoMo-based carbon and alumina catalysts, *Appl. Catal. A: Gen.* 194–195 (2000) 147–157.
- [151]. T. Kabe, Y. Aoyama, D. Wang, A. Ishihara, W. Qian, M. Hosoya, Q. Zhang, Effects of H<sub>2</sub>S on hydrodesulfurization of dibenzothiophene and 4,6-dimethyldibenzothiophene on alumina-supported NiMo and NiW catalysts, *Appl. Catal. A: Gen.* 209 (2001) 237–247.
- [152]. J. Leglise, L. Finot, J.N.M. van Gestel, J.C. Duchet, Conversion of model sulfur compounds to characterize hydrodesulfurization CoMo/Al<sub>2</sub>O<sub>3</sub> catalysts, *Stud. Surf. Sci. Catal.* 127 (1999) 51–65.
- [153]. H. Farag, K. Sakanishi, T. Sakae, Autocatalysis-like behavior of hydrogen sulfide on hydrodesulfurization of polyaromatic thiophenes over a synthesized molybdenum sulfide catalyst, *Appl. Catal. A: Gen.* 314 (2006) 114–122;
- [154]. N. Guernalec, C. Geantet, P. Raybaud, T. Cseri, M. Aouine, M. Vrinat, Dual effect of H<sub>2</sub>S on volcano curves in hydrotreating sulfide catalysis, *Oil Gas Sci. Technol.* 61 (4) (2006) 515–525;
- [155]. E. Olguin Orozco, M. Vrinat, Kinetics of dibenzothiophene hydrodesulfurization over MoS<sub>2</sub> supported catalysts: modelization of the H<sub>2</sub>S partial pressure effect, *Appl. Catal. A: Gen.* 170 (1998) 195–206.
- [156]. U.T. Turaga, X.L. Ma, C.S. Song, Influence of nitrogen compounds on deep hydrodesulfurization of 4,6-dimethyldibenzothiophene over Al<sub>2</sub>O<sub>3</sub>- and MCM-41 supported Co–Mo sulfide catalysts, *Catal. Today* 86 (2003) 265.
- [157]. V. Rabarihoela-Rakotovao, F. Diehl, S. Brunet, Deep HDS of diesel fuel: inhibiting effect of nitrogen compounds on the transformation of the refractory 4,6-dimethyldibenzothiophene over a NiMoP/Al<sub>2</sub>O<sub>3</sub> catalyst, *Catal. Lett.* 129 (2009) 50–56.
- [158]. S. Li, J.S. Lee, T. Hyeon, K.S. Suslick, Catalytic hydrodenitrogenation of indole over molybdenum nitride and carbides with different structures, *Appl. Catal. A: Gen.* 184 (1999) 1–9.
- [159]. F.E. Massoth, S.C. Kim, Polymer formation during the HDN of indole, *Catal. Lett.* 57 (1999) 129–134.

- [160]. K. Miga, K. Stanczyk, C. Sayag, D. Brodzki, G. Djéga-Mariadassou, Bifunctional behavior of bulk MoOxNy and nitrided supported NiMo catalyst in hydrodenitrogenation of indole, *J. Catal.* 183 (1999) 63–68.
- [161]. S.C. Kim, F.E. Massoth, Hydrodenitrogenation activities of methyl-substituted indoles, *J. Catal.* 189 (2000) 70–78.
- [162]. S.C. Kim, F.E. Massoth, Kinetics of the hydrodenitrogenation of indole, *Ind. Eng. Chem. Res.* 39 (2000) 1705–1712.
- [163]. A. Bunch, L. Zhang, G. Karakas, U.S. Ozkan, Reaction network of indole hydrodenitrogenation over NiMoS/-Al<sub>2</sub>O<sub>3</sub> catalysts, *Appl. Catal. A: Gen.* 190 (2000) 51–60.
- [164]. H. Farag, A.-N.A. El-Hendawy, K. Sakanishi, M. Kishida, I. Mochida, Catalytic activity of synthesized nanosized molybdenum disulfide for the hydrodesulfurization of dibenzothiophene: effect of H<sub>2</sub>S partial pressure, *Appl. Catal. B: Environ.* 91 (2009) 189–197.
- [165]. Y.K. Lee, Y. Shu, S. Ted Oyama, Active phase of a nickel phosphide (Ni<sub>2</sub>P) catalyst supported on KUSY zeolite for the hydrodesulfurization of 4,6-DMDBT, *Appl. Catal. A: Gen.* 322 (2007) 191–204.
- [166]. T.C. Ho, D. Nguyen, Poisoning effect of ethylcarbazole on hydrodesulfurization of 4,6-diethyldibenzothiophene, *J. Catal.* 222 (2004) 450–460.
- [167]. H. Yang, J. Chen, Y. Briker, R. Szynekarczuk, Z. Ring, Effect of nitrogen removal from light cycle oil on the hydrodesulphurization of dibenzothiophene, 4-methyldibenzothiophene and 4,6-dimethyldibenzothiophene, *Catal. Today* 109 (2005) 16–23.
- [168]. J. Chen, Z. Ring, HDS reactivities of dibenzothiophenic compounds in a LC-finer LGO and H<sub>2</sub>S/NH<sub>3</sub> inhibition effect, *Fuel* 83 (2004) 305–313.
- [169]. G.C. Laredo, A. Montesinos, J.A. De los Reyes, Inhibition effects observed between dibenzothiophene and carbazole during the hydrotreating process, *Appl. Catal. A: Gen.* 265 (2004) 171–183.
- [170]. F. S.-Minero, J. Ramirez, A. G.-Alejandre, C. F.-Vargas, P. T.-Mancera, R. C.-Garcia, Analysis of the HDS of 4,6-DMDBT in the presence of naphthalene and carbazole over NiMo/Al<sub>2</sub>O<sub>3</sub>-SiO<sub>2</sub>(x) catalysts, *Catal. Today* 133–135 (2008) 267–276.

## REFERENCES

---

- [171]. E. Furimsky, F.E. Massoth, Hydrodenitrogenation of petroleum, *Catal. Rev.* 47 (2005) 297–489.
- [172]. H. Yang, J.W. Chen, C. Fairbridge, Y. Briker, Y.J. Zhu, Z. Ring, Inhibition of nitrogen compounds on the hydrodesulfurization of substituted dibenzothiophenes in light cycle oil, *Fuel Process. Technol.* 85 (2004) 1415–1429.
- [173]. M. Macaud, M. Sevignon, A. Favre-Reguillon, M. Lemaire, E. Schulz, M. Vrinat, Novel methodology toward deep desulfurization of diesel feed based on the selective elimination of nitrogen compounds, *Ind. Eng. Chem. Res.* 43 (2004) 7843–7849.
- [174]. G.C. Laredo, J. Antonio De los Reyes, J. Luis Cano, J.J. Castillo, Inhibition effects of nitrogen compounds on the hydrodesulfurization of dibenzothiophene, *Appl. Catal. A: Gen.* 207 (2001) 103–112.
- [175]. T. Koltai, M. Macaud, A. Guevara, E. Schulz, M. Lemaire, R. Bacaud, M. Vrinat, Comparative inhibiting effect of polycondensed aromatics and nitrogen compounds on the hydrodesulfurization of alkyldibenzothiophenes, *Appl. Catal. A: Gen.* 231 (2002) 253–261.
- [176]. S.D. Sumbogo Murti, H. Yang, K.-H. Choi, Y. Korai, I. Mochida, Influences of nitrogen species on the hydrodesulfurization reactivity of a gas oil over sulfide catalysts of variable activity, *Appl. Catal. A: Gen.* 252 (2003) 331–346. N. Kagami, B.M. Vogelaar, A.D. van Langeveld, J.A. Moulijn, Reaction pathways on NiMo/Al<sub>2</sub>O<sub>3</sub> catalysts for hydrodesulfurization of diesel fuel, *Appl. Catal. A: Gen.* 293 (2005) 11–23.
- [177]. N. Kagami, B.M. Vogelaar, A.D. van Langeveld, J.A. Moulijn, Reaction pathways on NiMo/Al<sub>2</sub>O<sub>3</sub> catalysts for hydrodesulfurization of diesel fuel, *Appl. Catal. A: Gen.* 293 (2005) 11–23.
- [178]. Z. Liu, Q. Zhang, Y. Zheng, J. Chen, Effects of nitrogen and aromatics on hydrodesulfurization of light cycle oil predicted by a system dynamics model, *Energy Fuels* 22 (2008) 860–866.
- [179]. P. Steiner, Doctorate Thesis, Kinetics and deactivation studies of hydrodesulfurization catalysts, The Norwegian University of Science and Technology, Department of Chem. Eng., 2002.

## REFERENCES

---

- [180]. H. Farag, K. Sakanishi, I. Mochida, D.D. Whitehurst, Kinetic analyses and inhibition by naphthalene and H<sub>2</sub>S in hydrodesulfurization of 4,6- dimethyldibenzothiophene (4,6-DMDBT) over CoMo-based carbon catalyst, *Energy Fuels* 13 (1999) 449–453.
- [181]. A. Stanislaus, B.H. Cooper, Aromatic hydrogenation catalysis: a review, *Catal. Rev.: Sci. Eng.* 36 (1994) 75–123.
- [182]. K.H. Choi, N. Kunisada, Y. Korai, I. Mochida, K. Nakano, Facile ultra-deep desulfurization of gas oil through two-stage or -layer catalyst bed, *Catal. Today* 86 (2003) 277–286.
- [183]. J.H. Kim, X. Ma, C. Song, Kinetic study of effects of aromatic compounds on deep hydrodesulfurization of 4,6-dimethyldibenzothiophene, *Prep. Pap.-Am. Chem. Soc., Div. Fuel Chem.* 48 (2003) 553–1553.
- [184]. T. Isoda, S. Nagao, X. Ma, Y. Korai, I. Mochida, Catalytic activities of NiMo and CoMo/Al<sub>2</sub>O<sub>3</sub> of variable Ni and Co contents for the hydrodesulfurization of 4,6-dimethyldibenzothiophene in the presence of naphthalene, *Appl. Catal. A: Gen.* 150 (1997) 1–11.
- [185]. E. Lecrenay, I. Mochida, Catalytic hydrodesulfurization of petroleum middle distillate and model sulfur compounds over a series of catalysts activity and scheme, *Stud. Surf. Sci. Catal.* 106 (1997) 333–342.
- [186]. T. Kabe, A. Ishihara, M. Nomura, T. Itoh, P. Qi, Effects of solvents in deep desulfurization of benzothiophene and dibenzothiophene, *Chem. Lett.* 20 (12) (1991) 2233.
- [187]. S.S. Shih, S. Mizrahi, L.A. Green, M.S. Sarli, Deep desulfurization of distillates, *Ind. Eng. Chem. Res.* 31 (1992) 1232–1235.
- [188]. T.V. Choudhary, S. Parrott, B. Johnson, Unraveling heavy oil desulfurization chemistry—targeting clean fuels, *Environ. Sci. and Tech.* 42 (2008) 1944–1947.
- [189]. A. Marafi, A. Al-Hendi, A. Al-Mutawa, A. Stanislaus, Studies on hydrotreating of diesel streams from different kuwait crudes for ultralow sulfur diesel production, *Energy Fuels* 21 (2007) 3401–3405.
- [190]. S. Torrisi, The challenging chemistry of ultra-low sulfur diesel. *Process Technology, Catalysis, WorldRefining*, December, 2002 ([http://www.shell.com/static/criterion-gb/downloads/pdf/trade pub reprints/wr 1201reprint torrisi ulsd.pdf](http://www.shell.com/static/criterion-gb/downloads/pdf/trade%20pub%20reprints/wr%201201reprint%20torrisi%20ulsd.pdf)).

## REFERENCES

---

- [191]. A. Stanislaus, A. Al-Barood, H. Qabazard, Effect of feed quality on deep desulfurization of diesel, *Prep. Am. Chem. Div. Fuel Chem.* 48 (2003) 655–656.
- [192]. R. Ohmes, S. Sayles, ULSD Best Practices, *Hydrocarb. Eng.* (September) (2006).
- [193]. Z. Varga, J. Hancsok, Deep hydrodesulphurization of gas oils, *Petrol. Coal.* 45 (3–4) (2003) 135–141.
- [194]. T. Tippet, K.G. Knudsen, B.H. Cooper, Ultra Low Sulfur Diesel: Catalyst and Process Conditions, NPRA Annual Meeting, March 1999, AM-99-06.
- [195]. S. Torrisi, R. Street, T. Remans, J. Swain, The Challenging Chemistry of Ultra-low-sulfur Diesel, *Catalysis, Process Technology*, World Refining January/ February 2003.
- [196]. S. Torrisi, D. Krenzke, Distillate Catalyst Technology, NPRA Clean Fuel Challenge, Houston, August, 2003.
- [197]. H. Farag, D.D. Whitehurst, K. Sakanishi, I. Mochida, Carbon versus alumina as a support for Co–Mo catalysts reactivity towards HDS of dibenzothiophenes and diesel fuel, *Catal. Today* 50 (1999) 9–17.
- [198]. D.D. Whitehurst, H. Farag, T. Nagamatsu, K. Sakanishi, I. Mochida, Assessment of limitations and potentials for improvement in deep desulfurization through detailed kinetic analysis of mechanistic pathways, *Catal. Today* 45 (1998) 299–305.
- [199]. S. Glisic, PhD dissertation “Catalytic and non-catalytic methanolysis of triglycerides: Reaction kinetic and process simulation“, Faculty of Technology and Metallurgy, University of Belgrade, Belgrade 2009.
- [200]. Peng, D., Robinson, D., A New Two-Constant Equation of State. *Ind. Eng. Chem. Fund.* 15 (1976) 59-64.
- [201]. ASPEN Plus 11.1, Aspen Physical Property System. Methods and Models 11.1.3-32. (2006).
- [202]. Sandra Glišić, Oscar Montoya, Aleksandar Orlović, Dejan Skala, Vapor-liquid equilibria of triglycerides - methanol mixture and its influence on the biodiesel synthesis under supercritical conditions of methanol, *Journal of the Serbian Chemical Society*, 72 (1) 2007, 13-27.
- [203]. Sandra B. Glisic, Dejan U. Skala, Phase transition at subcritical and supercritical conditions of triglycerides methanolysis, *The Journal of Supercritical Fluids* 54 (2010) 71-80.

## REFERENCES

---

- [204]. Abdualnaser Muftah Almagrbi, Sandra B. Glisic, Aleksandar M. Orlovic, The phase equilibrium of triglycerides and ethanol at high pressure and temperature: The influence on kinetics of ethanolysis, *The Journal of Supercritical Fluids*, 61 (2012) 2-8.
- [205]. Sandra Glisic, Dejan Skala, The prediction of critical parameters for triolein, diolein, monoolein and methyl esters, 9th International Symposium on SuperCritical Fluids 2009, New Trends in Supercritical Fluids: Energy, Materials, Processing, Archon (France), May, 2009, Full text: Topic: Properties: P018 (6 pages) N° ISBN: 978-2-9511591-7-4.
- [206]. L. Constantinou, R. Gani, New group contribution method for estimating properties of pure compounds, *AIChE Journal* 40 (1994) 1697-1710.
- [207]. L. Constantinou, R. Gani, R.J.P. O'Connell, Estimation of the acentric factor and the liquid molar volume at 298 K through a new group contribution method, *Fluid Phase Equilibria* 103 (1995) 11-22.
- [208]. D. Ambrose, Correlation and estimation of vapour-liquid critical properties. I. Critical temperatures of organic compounds", National Physical Laboratory, Teddington, NPL Rep. Chem. 92, (1980)
- [209]. K.G. Joback, R.C. Reid, Estimation of pure-component properties from group-contributions, *Chemical Engineering Communications* 57 (1987) 233 – 243.
- [210]. A.L. Horvath, *Molecular Design*, Elsevier, Amsterdam, 1992.
- [211]. K.M. Klincewicz, R.C. Reid, Estimation of critical properties with group contribution methods, *AIChE Journal* 30 (1984) 137-142.
- [212]. A. L. Lydersen, Estimation of critical properties of organic compounds, Univ. Wisconsin Coll. Eng., Eng. Exp. Stn. rept. 3, Madison, WI, April 1955.
- [213]. W.J. Lyman, W.F. Reehl, D.H. Rosenblatt, *Handbook of Chemical Property Estimation Methods*, American Chemical Society, Washington, DC, 1990.
- [214]. R. Gani, L. Constantinou, Molecular structure based estimation of properties for process design, *Fluid Phase Equilibria*, 116 (1996) 75-86.
- [215]. R. Gani, B. Nielsen, A. Fredenslund, A group contribution approach to computer-aided molecular design, *AIChE Journal* 37 (1991) 1318–1332.
- [216]. D. Ambrose, R.C. Reid, J.M. Prausnitz, B.E. Poling *The properties of gases & liquids*, Monograph, McGraw-Hill, 4th Ed., 1987, 12 – 22.



- [217]. L. Vázquez, A. M. Hurtado-Benavides<sup>b</sup>, G. Regleroa, T. Fornaria, E. Ibáñezc, F.J. Señoránsa, Deacidification of olive oil by counter-current supercritical carbon dioxide extraction: Experimental and thermodynamic modelling, *Journal of Food Engineering*, 90 (2009) 463-470.
- [218]. Dukanović, Z., Glišić, S.B., Čobanin, V.J., Nićiforović, M., Georgiou, C.A., Orlović, A.M., „Hydrotreating of straight-run gas oil blended with FCC naphtha and light cycle oil“, *Fuel Processing Technology* 106 (2013) 160–165.
- [219]. S.Glisic, A.Orlovic, Modelling of non-catalytic biodiesel synthesis under sub and supercritical conditions: The influence of phase distribution, *J. of Supercritical Fluids* 65 (2012) 61-70.
- [220]. GF.Froment, The kinetics of complex catalytic reactions, *Chem. Eng. Sci.*, 42 (1987) 1073-1087.
- [221]. T-Y.Park, GF.Froment, A hybrid genetic algorithm for the estimation of parameters in detailed kinetic models, *Comput. Chem. Eng.*, 22 (1998) Suppl., S103-S110.
- [222]. G.Pontikakis, C.Papadimitriou, A. Stamatelos. Kinetic parameter estimation by standard optimization methods in catalytic converter modeling, *Chem. Eng. Comm.*, 191 (2004) 1473-1501.
- [223]. WH.Press, SA.Teukolsky, WT.Vetterling, BP. Flannery, *Numerical Recipes in C*, Cambridge, U.K: Cambridge University Press; 1992.
- [224]. A.Neumaier, *Complete Search in Continuous Global Optimization and Constraint Satisfaction in Acta Numerica* (A. Iserles, ed.), Cambridge, U.K: Cambridge University Press; 2004
- [225]. T.Bäck, *Evolutionary algorithms in theory and practice*. Oxford, U.K: Oxford University Press; 1996.
- [226]. K.De Jong, *An analysis of the behaviour of a class of genetic adaptive systems PhD thesis*, The University of Michigan 1975.
- [227]. LJ.Fogel, AJ.Owens, MJ.Walsh, *Artificial intelligence through simulated evolution* John Wiley; 1966.
- [228]. JH.Holland, *Adaptation in natural and artificial systems*. Ann Arbor, MI: The University of Michigan Press; 1975.

## REFERENCES

---

- [229]. A. Corana, C. Marchesi, S. Ridella, Minimizing multimodal functions of continuous variables with the simulated annealing algorithm, *ACM Trans. Math. Softw.* 13 (1987) 262-280.
- [230]. S. Kirkpatrick, C. D. Gelatt, M. P. Vecchi, Optimization by simulated annealing, *Science* (1983) 671-680.
- [231]. K. Levenberg, A method for the solution of certain nonlinear problems in least squares. *Quart. Appl. Math* 2 (1944) 164-168.
- [232]. D. W. Marquardt, An algorithm for least squares estimation of nonlinear parameters. *SIAM J.* 11 (1963) 431-441.
- [233]. L. H. Hosten, A comparative study of short cut procedures for parameter estimation in differential equations, *Computers Chem Engng* 3 (1979) 117-126.
- [234]. J. Glowinski, J. Stocki, Estimation of kinetic parameters — initial guess generation method, *AIChE J* 27 (1981) 1041-1043.
- [235]. S. Rajasekaran, G. V. Pai, *Neural Networks, Fuzzy Logic, and Genetic Algorithms*, India: Prentice-Hall; 2007.
- [236]. S. N. Sivanandam, S. N. Deepa, *Introduction to Genetic Algorithms*, Springer, Berlin, Heidelberg, N.Y., 2008.
- [237]. M. Mitchell, *An Introduction to Genetic Algorithms*. Cambridge, MA: MIT Press; 1996.
- [238]. I. Rechenberg, *Evolutionsstrategie: Optimierung technischer systeme nach prinzipien der biologischen evolution*. Stuttgart: Frommann-Holzboog Verlag; 1973.
- [239]. H. P. Schwefel, *Evolutionsstrategie und numerische optimierung*. Ph.D. Thesis, Technische Universität Berlin; 1975.
- [240]. T. Hatami, S. B. Glisic, A. M. Orlovic, Modelling and optimization of supercritical CO<sub>2</sub> extraction of St. John's Wort (*Hypericum perforatum* L.) using genetic algorithm, *J. of Supercritical Fluids* 62 (2012) 102-108.
- [241]. H. S. Fogler, *Elements of chemical reaction engineering*, 4th edition, Prentice Hall, 2006, USA
- [242]. F. Jiménez, V. Kafarov, M. Nuñez, *Chemical Engineering Journal*, 134, 2007, 200-208.
- [243]. <http://webbook.nist.gov/cgi/cbook.cgi?ID=C1333740&Type=JANAFG&Plot=on>
- [244]. <http://lorien.ncl.ac.uk/ming/webnotes/therm2/prop/prop.swf>

## REFERENCES

---

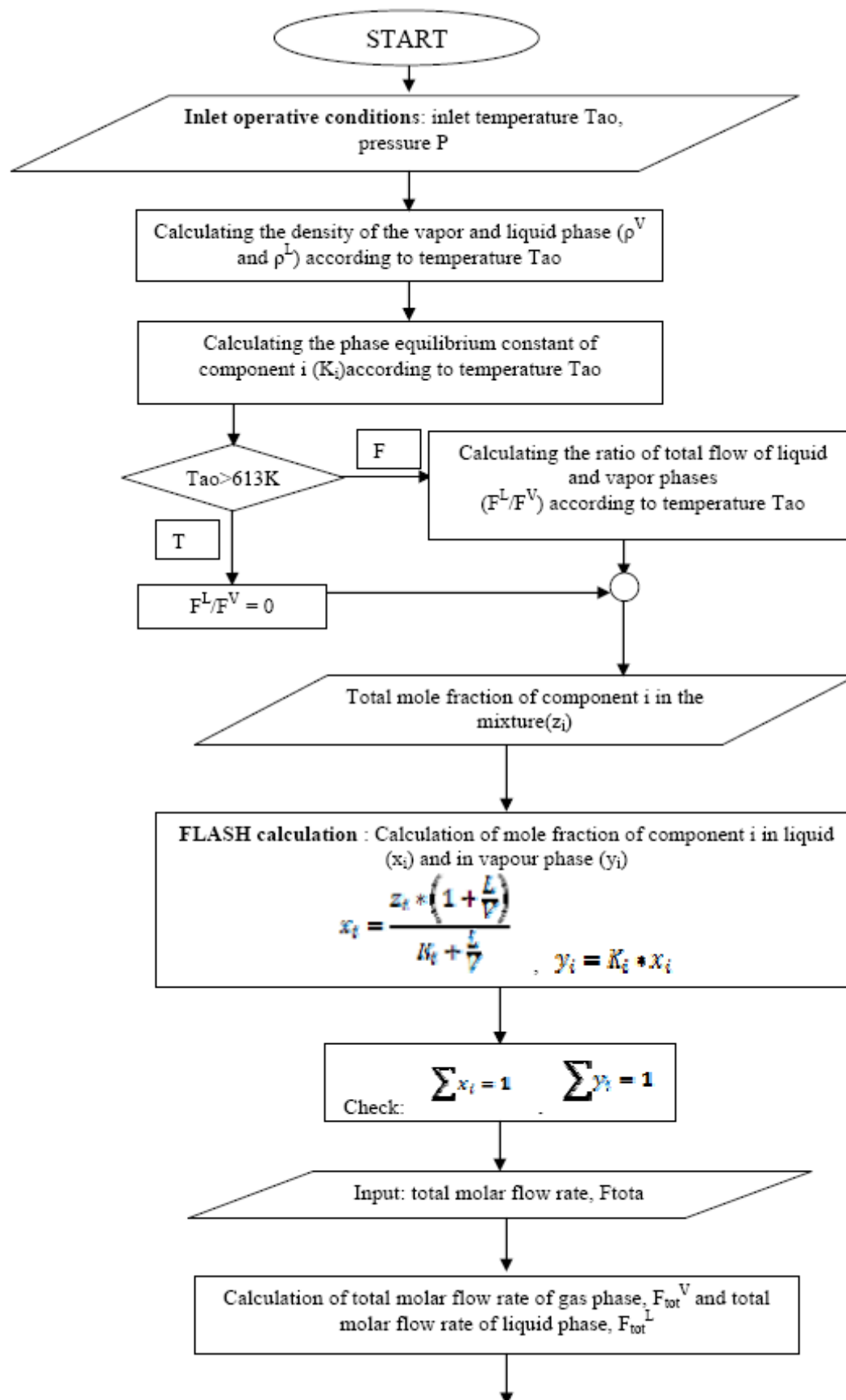
- [245]. <http://www.fiz-chemie.de/infotherm/>
- [246]. <http://chemeo.com/cid/59-086-2>
- [247]. <http://www.chemeo.com/cid/27-250-4>
- [248]. M. H. Al-Dahhan, M.P. Dudukovic, *Chemical Engineering Science*, 50 (15), 1995, 2377 – 2389.
- [249]. V.Anikeev, D.Stepanov, A.Yermakova, *Thermodynamics of Phase and Chemical Equilibrium in the Process of Biodiesel Fuel Synthesis in Subcritical and Supercritical Methanol*, *Ind. Eng. Chem. Res.* 51(2012) 4783 – 4796.
- [250]. Y.Asakuma, K.Maeda, H.Kuramochi K.Fukui, *Theoretical study of the transesterification of triglycerides to biodiesel fuel*, *Fuel* 88 (2009) 786–791.
- [251]. Y.Asakuma, O.Kawanami, K.Maeda, H.Kuramochi, K.Fukui, *Theoretical study of the transesterification of triglycerides to biodiesel fuel under various conditions*, *Int. J. of Thermodynamics* 14 (2011) 193-196.
- [252]. C.West, M.Mengue Metogo, E.Lesellier, *Investigations on the measurement of pH of supercritical mobile phases*, France: ICOA communications; 2009. <http://www.icoa.fr/communications/com2009/west1.pdf>
- [253]. Demirbas A., *Recent developments in biodiesel fuels*, *International Journal of Green Energy* 4 (2007) 15–26.
- [254]. Kusdiana D., Saka S., *Effects of water on biodiesel fuel production by supercritical methanol treatment*, *Bioresource Technology* 91 (2004) 289–295.
- [255]. Demirbas, A., *Studies on cottonseed oil biodiesel prepared in non-catalytic SCF conditions*, *Bioresource Technology* 99 (2008) 1125–1130.
- [256]. Demirbas, A., *Production of biodiesel fuels from linseed oil using methanol and ethanol in non-catalytic SCF conditions*, *Biomass and Bioenergy* 33 (2009)113–118.
- [257]. Warabi, Y., Kusdiana, D., Saka, S., *Reactivity of triglycerides and fatty acids of rapeseed oil in supercritical alcohols*, *Bioresource Technology* 91 (2004) 283–287.
- [258]. Gui, M.M., Lee, K.T., Bhatia, S., *Supercritical ethanol technology for the production of biodiesel: Process optimization studies*, *Journal of Supercritical Fluids* 49 (2009) 286–292.
- [259]. Madras, G., Kolluru, C., Kumar, R., *Synthesis of biodiesel in supercritical fluids*, *Fuel* 83 (2004) 2029–2033.

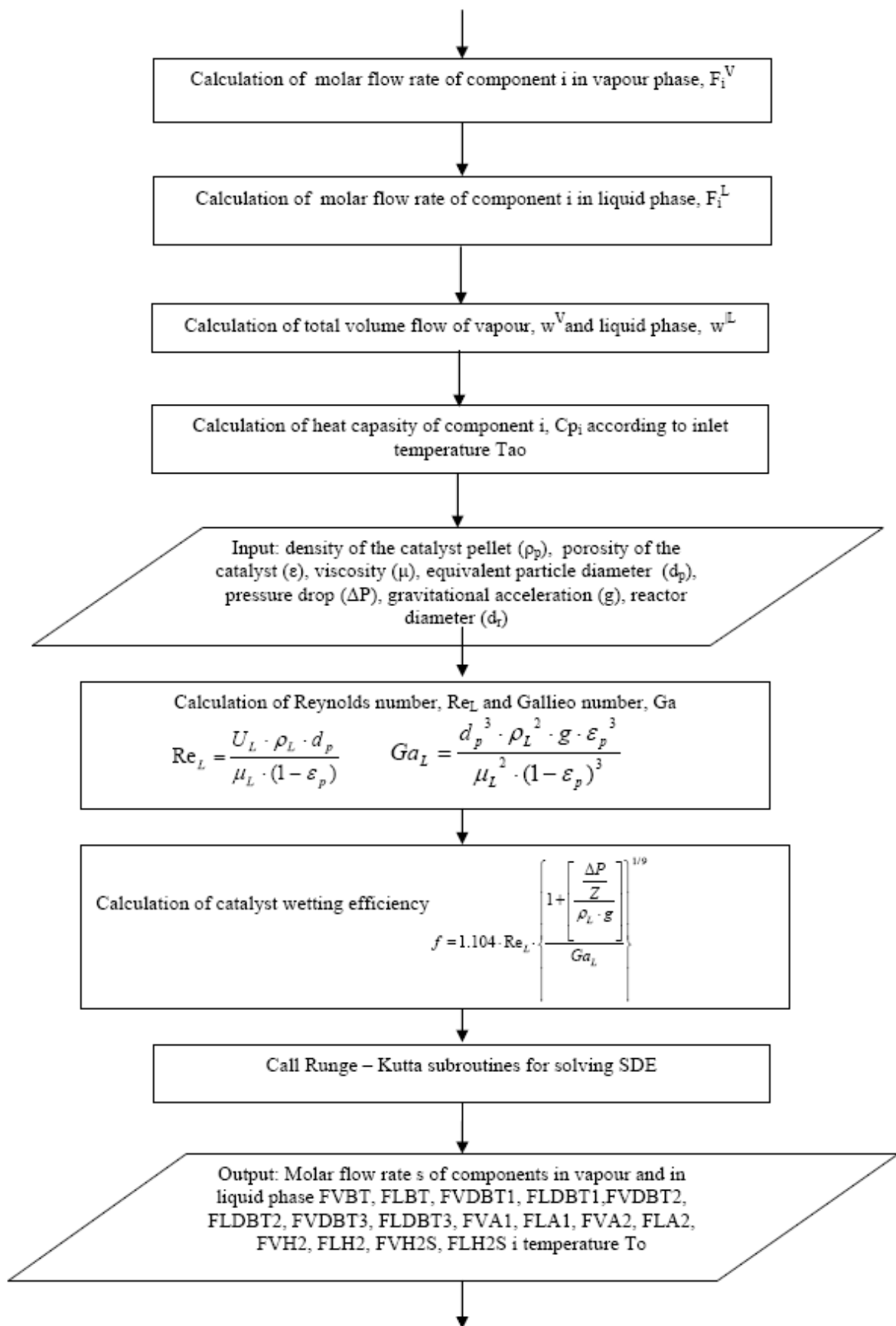
## REFERENCES

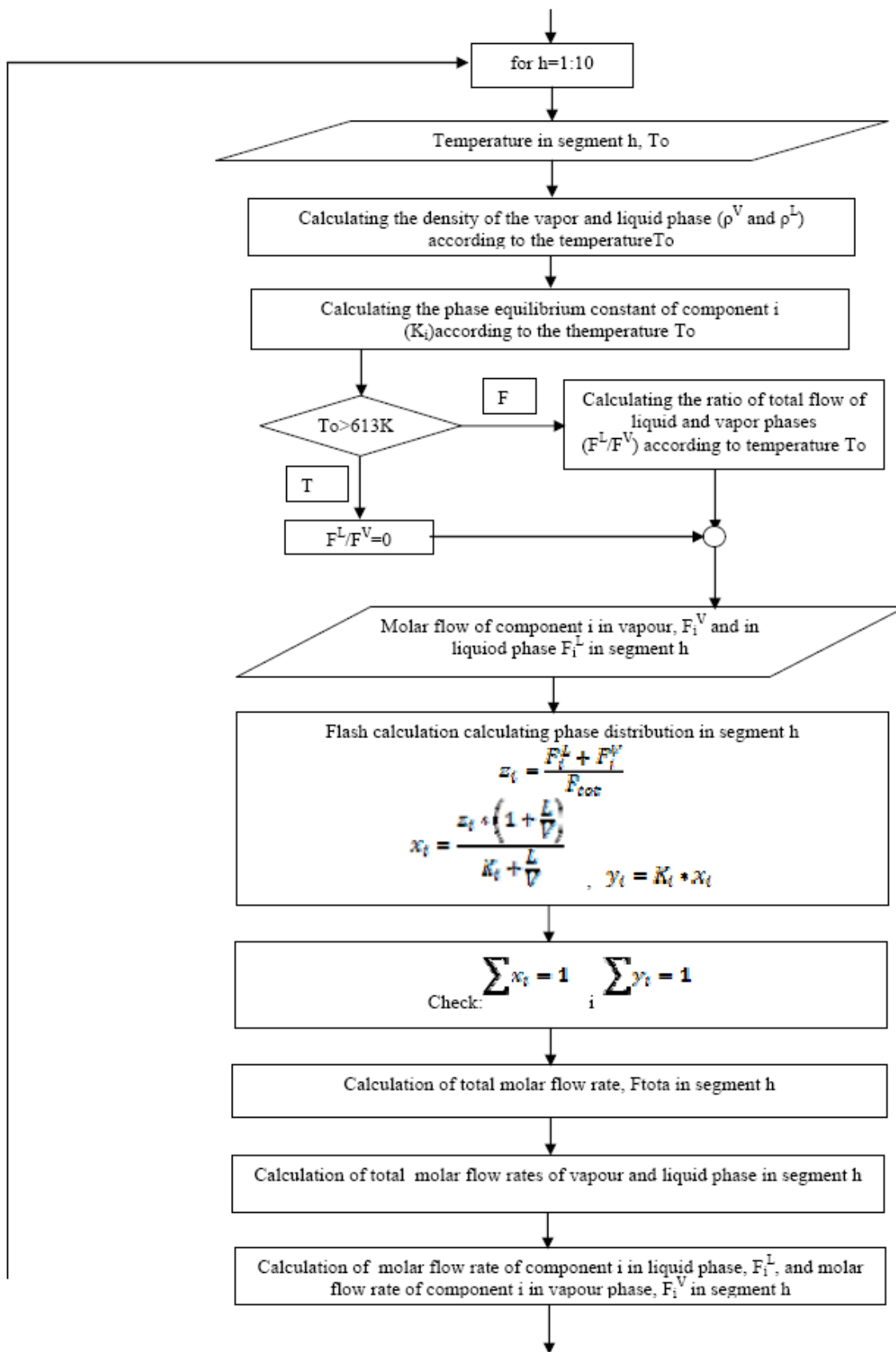
---

- [260]. Varma, M.N., and Madras, G., Synthesis of Biodiesel from Castor Oil and Linseed Oil in Supercritical Fluids, *Industrial & Engineering Chemistry Research* 46 (2007) 1–6.
- [261]. Vieitez, I., Da Silva, C., Borges, G.R., Corazza, F.C., Oliveira, J.V., Grompone, M.A., Jachmanian, I., production of soybean biodiesel in supercritical ethanol–water mixtures, *Energy Fuels* 22 (2008) 2805–2809.
- [262]. Valle, P., Velez, A., Hegel, P., Mabe, G., Brignole, E.A., Biodiesel production using supercritical alcohols with a non-edible vegetable oil in a batch reactor, *Journal of Supercritical Fluids* 54 (2010) 61-70.
- [263]. Barton AFM. *Handbook of Solubility and Other Cohesion Parameters*, Florida: CRC Press; 1985.

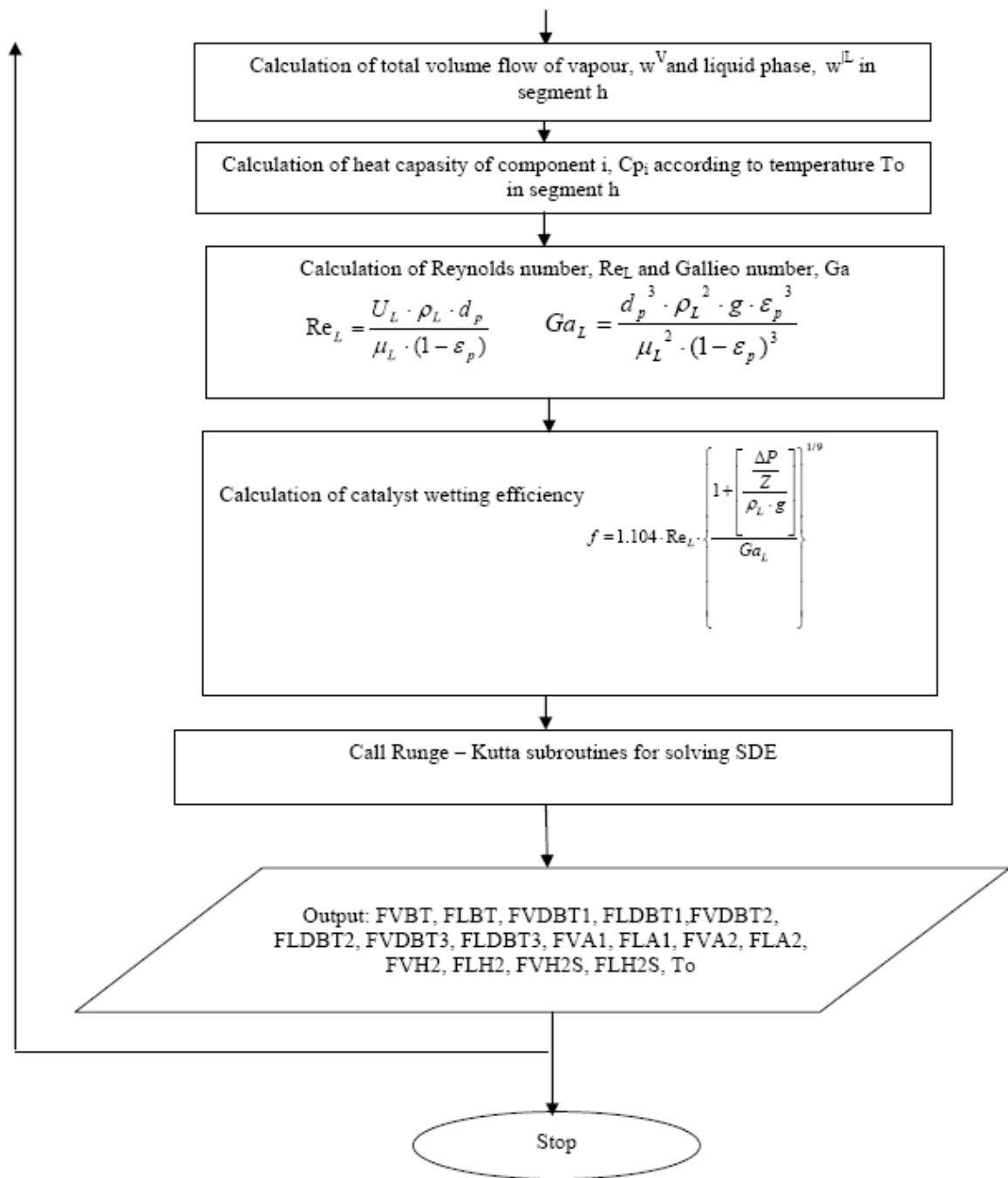
**APPENDIX I**



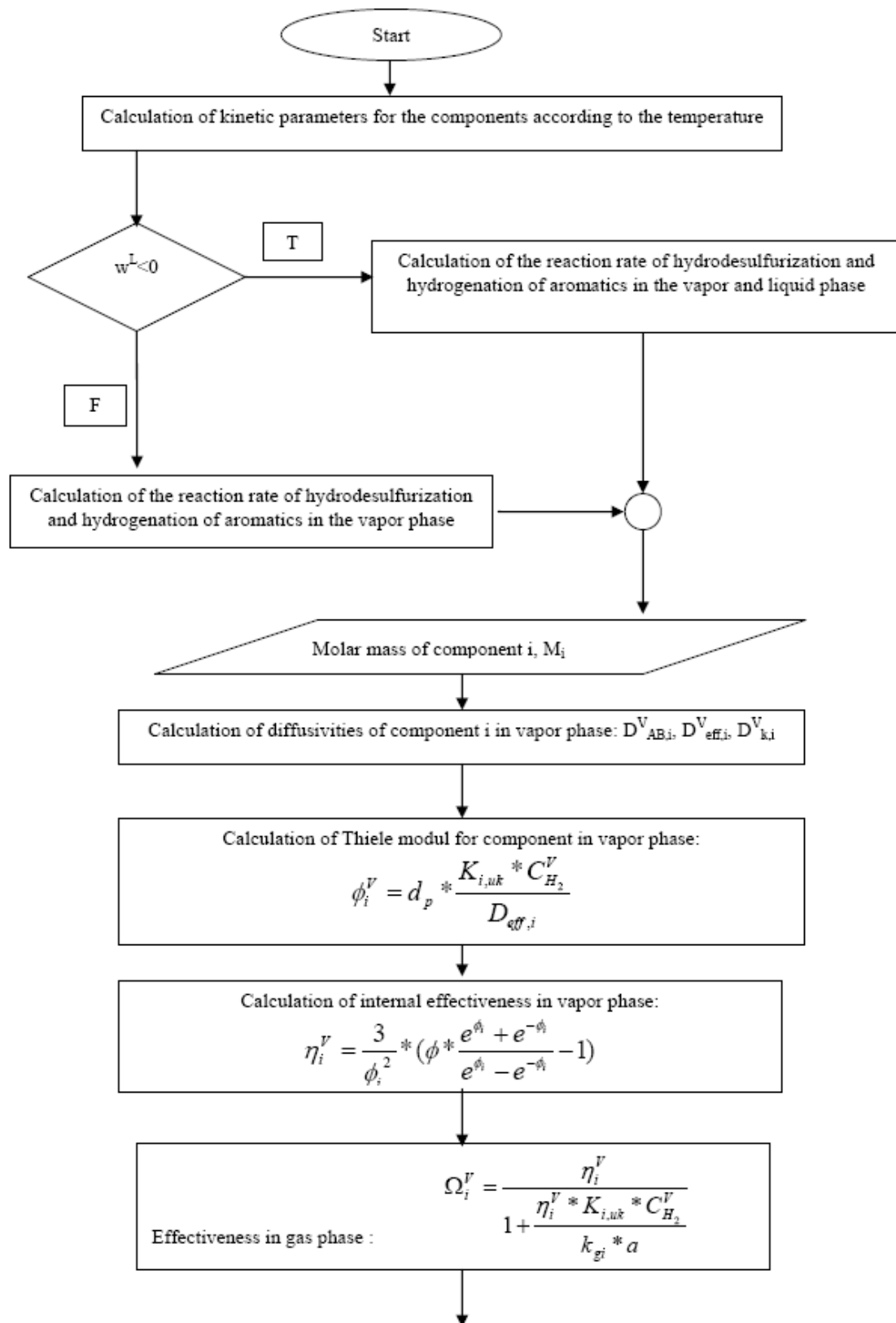


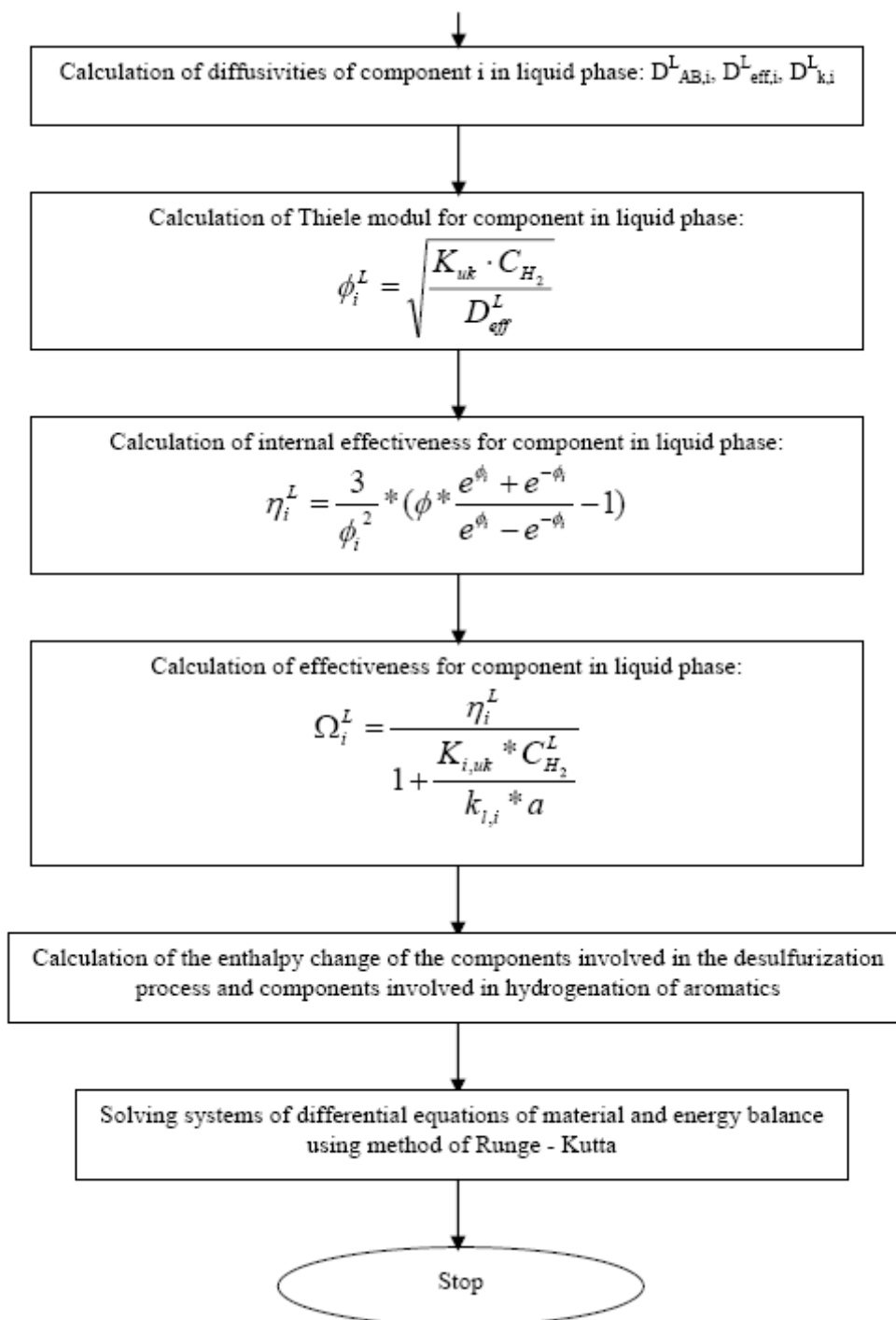






Subroutine:





**APPENDIX II**

**NOMENCLATURE***Symbols*

$C$  = concentration ( $\text{kmol dm}^{-3}$ )

$E_A$  = activation energy ( $\text{kJ kmol}^{-1}$ )

$K$  = equilibrium constant

$k$  = kinetic constant of reaction ( $\text{kmol dm}^{-3} \text{s}^{-1}$ )

$P$  = pressure (MPa or bar)

$T$  = temperature ( $^{\circ}\text{C}$  or  $\text{K}$ )

$t$  = time (minute or second)

$V$  = volume ( $\text{dm}^3$ )

$T_0$  = inlet temperature [ $\text{K}$ ]

$\rho^V$  = density for vapour phase [ $\text{kmol/m}^3$ ]

$\rho^L$  = density for liquid phase [ $\text{kmol/m}^3$ ]

$K_i$  = phase equilibrium constant of component  $i$

$F^L/F^V$  = the ratio of total flow of liquid and vapor phases

$z_i$  = mole fraction of component  $i$  (total)

$x_i$  = mole fraction of component  $i$  in liquid phase

$y_i$  = mole fraction of component  $i$  in vapour phase

$F_i^V$  = molar flow rate of component  $i$  in vapour phase [ $\text{kmol/h}$ ]

$F_i^L$  = molar flow rate of component  $i$  in liquid phase [ $\text{kmol/h}$ ]

$F_{\text{tot}}^V$  = total molar flow rate of gas phase [ $\text{kmol/h}$ ]

$F_{\text{tot}}^L$  = total molar flow rate of liquid phase [ $\text{kmol/h}$ ]

$w^V$  = total volume flow of vapour phase [ $\text{m}^3/\text{h}$ ]

$w^L$  = total volume flow of liquid phase [ $\text{m}^3/\text{h}$ ]

$C_{p_i}$  = heat capacity of component  $i$  [ $\text{kJ/mol/K}$ ]

$\rho_p$  = density of the catalyst pellet [ $\text{kg/m}^3$ ]

$R$  = universal gas constant [ $\text{kJ/kmol/K}$ ]

$\mu_L$  = liquid viscosity [ $\text{Pas}$ ]

$\mu_V$  = gas viscosity

$\varepsilon$  = porosity of the catalyst

$d_p$  = equivalent particle diameter [m]

$d_r$  = reactor diameter [m]

$\Delta P$  = pressure drop [Pa/m]

$A_p$  = cross section area [m<sup>2</sup>]

$U^L$  = superficial velocity of the liquid phase [m/s]

$U^V$  = superficial velocity of the vapour phase [m/s]

$g$  = gravitational acceleration [m/s<sup>2</sup>]

$Re^L$  = Reynolds number for liquid phase

$Re^V$  = Reynolds number for vapour phase

$Ga^L$  = Galileo number

$f$  = catalyst wetting efficiency

$C_j^V$  = molar concentration of component j in liquid phase

$C_j^V$  = molar concentration of component j in vapour phase

$r_{i,HDS}^V$  = reaction rate in vapour phase for hydrodesulfurization of component i [kmol/kg<sub>cat</sub>/h]

$r_{i,HDS}^L$  = reaction rate in liquid phase for hydrodesulfurization component i [kmol/kg<sub>cat</sub>/h]

$r_{i,ARM}^V$  = reaction rate in vapour phase for hydrodearomatization of component i  
[kmol/kg<sub>cat</sub>/h]

$r_{i,ARM}^L$  = reaction rate in liquid phase for hydrodearomatization component i [kmol/kg<sub>cat</sub>/h]

$k_{j,\sigma}$  = kinetic parameter for component j, [kmol/kg<sub>cat</sub>/h]

$k_{j,\tau}$  = kinetic parameter for component j, [kmol/kg<sub>cat</sub>/h]

$K_{j,\sigma}$  = kinetic parameter for component j, [m<sup>3</sup>/kmol]

$K_{j,\tau}$  = kinetic parameter for component j, [m<sup>3</sup>/kmol]

$\sigma$  = with respect to the hydrogenolysis function

$\tau$  = with respect to the hydrogenation function

### **Abbreviations**

TG            triglycerides

DG            diglycerides

MG            monoglycerides

FAME        fatty acid methyl esters

## APPENDIX

---

FAEE	fatty acid ethyl esters
MeOH	methanol
EtOH	ethanol
Gly	glycerol

### *Subscripts*

$n1$	$n=1,2,3$ , index for the forward reaction
$n2$	$n=1,2,3$ , index for the reverse reaction

$i$  = component index (BT, DBT1, DBT2, DBT3, A1, A2, H<sub>2</sub>, H<sub>2</sub>S)

Mr Abdualnaser Muftah Almagrbi, chem.eng. was born in Libya during 1976. He completed his undergraduate studies of chemical engineering in 1999 at Al-Mergheb University in Al-Khoms Libya. At the same University he completed his MSc studies in year 2004. His MSc thesis was dedicated to investigations of heat transfer and temperature gradients in fixed bed catalytic reactors. From 2004 till 2008 he was associated with Chemical Engineering department of Al-Mergheb University as research fellow and lecturer. During this period he was also involved in teaching at Polytechnics at Tripoli and Mesalata.

Mr Almagrbi spent one year at University of Newcastle in United Kingdom during 2008 and 2009 where he was involved in research dedicated to packed bed reactors.

He started work on his PhD thesis at University of Belgrade in 2010. His research was in the area of multiphase reactions occurring in processing of renewable (biodiesel) and mineral diesel fuels. The following papers resulting from research in this thesis have been published prior to defense:

Leading international scientific journal in chemical engineering:

1. Abdualnaser M. Almagrbi, Sandra B. Glisic, Aleksandar M. Orlovic, "The phase equilibrium of triglycerides and ethanol at high pressure and temperature: The influence on kinetics of ethanolysis", *The Journal of Supercritical Fluids*, 61 (2012) 2-8. IF(2012)=2.732; ISSN 0896-8446

International scientific journal in chemical engineering:

1. Abdualnaser M. Almagrbi, Tahmasb Hatami, Sandra B. Glišić, Aleksandar M. Orlović, "Determination of kinetic parameters for complex transesterification reaction by standard optimisation methods", *Hemijska industrija*, DOI:10.2298/HEMIND130118037A. IF(2012)=0.463; ISSN 0367-598X

Presentations at international scientific conference:

1. Abdualnaser M. Almagrbi, Ivana Mijatović, Sandra B. Glisic, Aleksandar M. Orlović, "Kinetic parameters of non-catalytic biodiesel synthesis under elevated pressure: Determination by standard optimisation methods", ICOSSECS 8, Belgrade, June 27-29, CD ROM P06
2. Abdualnaser M. Almagrbi, Ivana Mijatović, Sandra B. Glisic, Aleksandar M. Orlović, "Phase equilibrium of ethanolysis of triglycerides at high pressure and temperature", ICOSSECS 8, Belgrade, June 27-29, CD ROM P04



Прилог 1.

## Изјава о ауторству

Потписани-а Abdualnaser Muftah Almagrbi

број индекса \_\_\_\_\_

### Изјављујем

да је докторска дисертација под насловом

**MATHEMATICAL MODELLING OF MULTIPHASE REACTION PROCESSES  
FOR PRODUCTION OF RENEWABLE AND MINERAL DIESEL FUELS**

---

**MATEMATIČKO MODELOVANJE VIŠEFAZNIH REAKCIONIH PROCESA U  
PROIZVODNJI OBNOVLJIVIH I MINERALNIH DIZEL GORIVA**

---

- резултат сопственог истраживачког рада,
- да предложена дисертација у целини ни у деловима није била предложена за добијање било које дипломе према студијским програмима других високошколских установа,
- да су резултати коректно наведени и
- да нисам кршио/ла ауторска права и користио интелектуалну својину других лица.

**Потпис докторанда**

У Београду, 09.09.2013.

\_\_\_\_\_

Прилог 2.

**Изјава о истоветности штампане и електронске верзије  
докторског рада**

Име и презиме аутора Abdualnaser Muftah Almagrbi

Број индекса \_\_\_\_\_

Студијски програм hemijsko inženjerstvo

Наслов рада

**MATHEMATICAL MODELLING OF MULTIPHASE REACTION PROCESSES**

**FOR PRODUCTION OF RENEWABLE AND MINERAL DIESEL FUELS**

**MATEMATIČKO MODELOVANJE VIŠEFAZNIH REAKCIONIH PROCESA U**

**PROIZVODNJI OBNOVLJIVIH I MINERALNIH DIZEL GORIVA**

Ментор Dr Aleksandar Orlović komentor Dr Sandra Glišić komentor

Потписани/а Abdualnaser Muftah Almagrbi

Изјављујем да је штампана верзија мог докторског рада истоветна електронској верзији коју сам предао/ла за објављивање на порталу **Дигиталног репозиторијума Универзитета у Београду**.

Дозвољавам да се објаве моји лични подаци везани за добијање академског звања доктора наука, као што су име и презиме, година и место рођења и датум одбране рада.

Ови лични подаци могу се објавити на мрежним страницама дигиталне библиотеке, у електронском каталогу и у публикацијама Универзитета у Београду.

**Потпис докторанда**

У Београду, 09.09.2013.

\_\_\_\_\_

### Прилог 3.

## Изјава о коришћењу

Овлашћујем Универзитетску библиотеку „Светозар Марковић“ да у Дигитални репозиторијум Универзитета у Београду унесе моју докторску дисертацију под насловом:

**MATHEMATICAL MODELLING OF MULTIPHASE REACTION PROCESSES  
FOR PRODUCTION OF RENEWABLE AND MINERAL DIESEL FUELS  
МАТЕМАТИЧКО MODELOVANJE VIŠEFAZNIH REAKCIONIH PROCESA U  
PROIZVODNJI OBNOVLJIVIH I MINERALNIH DIZEL GORIVA**

која је моје ауторско дело.

Дисертацију са свим прилозима предао/ла сам у електронском формату погодном за трајно архивирање.

Моју докторску дисертацију похрањену у Дигитални репозиторијум Универзитета у Београду могу да користе сви који поштују одредбе садржане у одабраном типу лиценце Креативне заједнице (Creative Commons) за коју сам се одлучио/ла.

1. Ауторство
2. Ауторство - некомерцијално
- 3. Ауторство – некомерцијално – без прераде**
4. Ауторство – некомерцијално – делити под истим условима
5. Ауторство – без прераде
6. Ауторство – делити под истим условима

(Молимо да заокружите само једну од шест понуђених лиценци, кратак опис лиценци дат је на полеђини листа).

**Потпис докторанда**

У Београду, \_\_\_\_\_ 09.09.2013. \_\_\_\_\_

\_\_\_\_\_

1. Ауторство - Дозвољаваате умножавање, дистрибуцију и јавно саопштавање дела, и прераде, ако се наведе име аутора на начин одређен од стране аутора или даваоца лиценце, чак и у комерцијалне сврхе. Ово је најслободнија од свих лиценци.
2. Ауторство – некомерцијално. Дозвољаваате умножавање, дистрибуцију и јавно саопштавање дела, и прераде, ако се наведе име аутора на начин одређен од стране аутора или даваоца лиценце. Ова лиценца не дозвољава комерцијалну употребу дела.
3. Ауторство - некомерцијално – без прераде. Дозвољаваате умножавање, дистрибуцију и јавно саопштавање дела, без промена, преобликовања или употребе дела у свом делу, ако се наведе име аутора на начин одређен од стране аутора или даваоца лиценце. Ова лиценца не дозвољава комерцијалну употребу дела. У односу на све остале лиценце, овом лиценцом се ограничава највећи обим права коришћења дела.
4. Ауторство - некомерцијално – делити под истим условима. Дозвољаваате умножавање, дистрибуцију и јавно саопштавање дела, и прераде, ако се наведе име аутора на начин одређен од стране аутора или даваоца лиценце и ако се прерада дистрибуира под истом или сличном лиценцом. Ова лиценца не дозвољава комерцијалну употребу дела и прерада.
5. Ауторство – без прераде. Дозвољаваате умножавање, дистрибуцију и јавно саопштавање дела, без промена, преобликовања или употребе дела у свом делу, ако се наведе име аутора на начин одређен од стране аутора или даваоца лиценце. Ова лиценца дозвољава комерцијалну употребу дела.
6. Ауторство - делити под истим условима. Дозвољаваате умножавање, дистрибуцију и јавно саопштавање дела, и прераде, ако се наведе име аутора на начин одређен од стране аутора или даваоца лиценце и ако се прерада дистрибуира под истом или сличном лиценцом. Ова лиценца дозвољава комерцијалну употребу дела и прерада. Слична је софтверским лиценцама, односно лиценцама отвореног кода.